Interactions of metal complexes with DNA

Jihan Talib
University of Wollongong

Interactions of Metal Complexes With DNA

A thesis submitted in (partial) fulfilment of the requirements for the award of the degree

Doctor of Philosophy

from

University of Wollongong

by

Jihan Talib

Bachelor of Medicinal Chemistry Advanced (Honours)

School of Chemistry

November 2008

DECLARATION

I, Jihan Talib, declare that this thesis, submitted in partial fulfilment of the requirements for the award of Doctor of Philosophy, in the School of Chemistry, University of Wollongong, is wholly my own work unless otherwise referenced or acknowledged. The work has not been submitted for qualification at any other academic institution.

Jihan Talib

4th November 2008

ACKNOWLEDGEMENTS

This thesis would not have been possible without the support, encouragement and guidance from the people listed below, of whom I would like to send them my deepest gratitude and appreciation.

- My supervisors Dr Stephen Ralph and Dr Jennifer Beck, thank you for giving me the opportunity to accomplish this work under your supervision here at the University of Wollongong. Your support and guidance during the course of this project has been a constant source of motivation and inspiration. Your advice has not only helped carry me through my postgraduate research but will always be remembered as I continue my scientific career. Steve your positive energy and enthusiasm encouraged me to continue to persevere especially during the more challenging times. Jenny, thank you for your knowledge and patience. I deeply appreciated your guidance, advice and direction.

- The past and present members of the Mass Spectrometry group. Thank you for your friendships and for contributing to an enjoyable and pleasant working environment. Thankyou to Thitima Urathamakul, Stephen Watt and Raj Gupta for teaching me how to use the instruments and essential lab skills.

- Larry Hick, thank you for knowledge and assistance with the mass spectrometers. I am immensely grateful for your willingness and dedication to help me with the instruments. I will never forget your warm presence and infectious chuckle.

- Dr Janice Aldrich-Wright (School of Science, Food and Horticulture, University of Western Sydney) for the ruthenium and platinum drugs used in this work.

- Dr Joel McKay (School of Molecular and Microbial Biosciences, The University of Sydney, Australia) for providing the transcription factor used in this study.

- David Harman, thank you for your guidance during the synthesis of the organic ligands.

- Jemise, Kate, Louise, Emma, Cameron, and Jess, thank you for your friendships and encouragement.

- David, thank you so much for your patience and understanding. Your inspiration, encouragement, advice and willingness to listen, has helped me enormously through the last stages of this work. I cherish you and all your qualities.

Finally, I would especially like to thank my parents, without your support and love, I would have never been able to achieve this. Every day I remind myself how lucky I am to have you as my parents. I am truly gracious for the life you have given me.

PUBLICATIONS

Gornall, K. C., Samosorn, S., **Talib, J.,** Bremner, J. B. and Beck, J.L. (2007) Selectivity of an Indolyl Berberine Derivative for Tetrameric G-quadruplex DNA. *Rapid Commun. Mass Spectrom.* 11, 1759-1766.

Talib, J., Green, C. Davis, K. J., Urathamakul, T., Beck, J. L., Aldrich-Wright, J. R and Ralph, S. F. (2008) A Comparison of the Binding of Metal Complexes to Duplex and Quadruplex DNA. *Dalton Trans.* **8**, 1018-1026

Talib, J., Harman, D., Dillon, C., Beck, J. L., Aldrich-Wright, J. R and Ralph, S. F. (2009) Does the Metal Influence the Non-covalent Binding of Complexes to DNA? *Dalton Trans.* DOI: 10.1039/B814156H.

ABSTRACT

Electrospray ionisation mass spectrometry (ESI-MS), absorption spectrophotometry and circular dichroism spectroscopy were used to investigate the non-covalent binding interactions of the nickel complexes $[Ni(phen)_2(L)]Cl_2$, (L = phen, dpq ,dpqc and dppz) with the 16mer oligonucleotide D2, which has the following base sequence: (GCTGCCAAATACCTCC/GGAGGTATTTGGCAGC). In addition, the extent of unwinding of the negatively supercoiled plasmid pUC9 caused by the nickel complexes, and the extent to which they inhibit *in vitro* synthesis of mRNA, were investigated using gel electrophoresis. The results of these studies showed that DNA binding strengthened as the size of the unique ligand was increased. Comparison of each of the above sets of results with those obtained from identical experiments performed using the analogous ruthenium complexes $[Ru(phen)_2(L)]^{2+}$ (L = phen, dpq, dpqc, dppz) showed that varying the metal ion had a measurable effect on DNA binding affinity, with the nickel complexes generally interacting more weakly with D2 than the corresponding ruthenium complexes.

ESI-MS/MS and in-source collision-induced dissociation experiments were performed using the tetrameric quadruplex DNA molecule Q5 $(TTGGGGGT)_4$ and antiparallel dimeric quadruplex Q2 $(GGGGTTTTGGGG)_2$ in order to determine their gas-phase dissociation profiles. It was found that the gas phase stability of the quadruplex DNA was dependent on its charge state, the number of oligonucleotide strands that make up the quadruplex, and the number of consecutive G-tetrads that it contains. ESI-MS and circular dichroism spectroscopy were also used to examine the non-covalent binding interactions of the octahedral nickel and ruthenium complexes stated above, as well as several square planar platinum complexes with Q5. The platinum complexes studied were

$[Pt(en)(phen)]^{2+}$, $[Pt(en)(3,4,7,8\text{-}Me_4phen)]^{2+}$, $[Pt(en)(4,7\text{-}Me_2phen)]^{2+}$ and $[Pt(5,6\text{-}Me_2phen)(S,S\text{-}dach)]^{2+}$. The results obtained from these experiments showed that each of the three groups of metal complexes were able to bind to Q5. In contrast to what was found in experiments involving the duplex DNA molecule D2, the presence of the intercalating dppz ligand in the coordination sphere of both the nickel and ruthenium complexes did not greatly increase their binding affinity towards quadruplex DNA. This observation suggests that intercalative binding interactions may not play as important a role in the binding of metal complexes to quadruplex DNA. ESI-MS was used to analyse mixtures containing the organic drug daunomycin, Q5, and either $[Ru(phen)_2(dppz)]^{2+}$ or $[Pt(en)(4,7\text{-}Me_2phen)]^{2+}$, in order to obtain information about the qDNA binding modes of these metal complexes. The affinity of the above two metal complexes towards parallel tetrameric quadruplexes with different lengths was also compared using ESI-MS in an attempt to shed light on whether they bind to the ends of the quadruplexes or in grooves along their lengths.

The optimal conditions required to obtain ESI mass spectra of the non-covalent adduct formed between the DNA binding domain of mouse transcription factor PU.1, and a short 10mer DNA molecule containing its 5'-GGAA-3' consensus sequence, were determined. ESI-MS was then used to probe the extent of inhibition of formation of this non-covalent complex caused by addition of $[Ru(phen)_2(dppz)]^{2+}$ or $[Pt(5,6\text{-}Me_2phen)(S,S\text{-}dach)]^{2+}$. Both metal complexes were shown to inhibit binding of the transcription factor to its DNA recognition site, demonstrating the potential of these complexes for transcription therapy.

ABBREVIATIONS

A	adenine
AML	acute myeloid leukemia
bip	biphenyl
Bqdi	1,2-benzoquinone diimine
Bpy	bipyridine
C	cytosine
CD	circular dichroism
CI	chemical ionisation
CID	collision induced dissociation
CT-DNA	calf thymus DNA
Dach	1,2-diaminocyclohexane
DCM	dichloromethane
DMB	4,4'-dimethyl-2,2'-bipyridine
DNA	deoxyribonucleic acid
dppm	1,2-bis(diphenylphosphino)methane
dppz	dipyrido[3,2-*a*:2',3'-c]phenazine
dpq	dipyrido[3,2-*d*-2',3'-*f*]quinoxaline
dpqc	dipyrido[3,2-*a*:2',3'-c](6,7,8,9-tetrahydrophenazine)
dsDNA	double-stranded DNA
DTC	diethylthiocarbocyanide
EDTA	ethylenediaminetetraacetic acid
EGR1	early growth response factor 1

EI	electron ionisation
en	(1,2-diaminoethane)
ESI	electrospray ionisation
FAB	fast atom bombardment
FD	field desorption
FDA	food and drug administration
G	guanine
GSH	glutathione
GST	glutathione-S-transferase
HAT	1,4,5,8,9,12-hexaazatriphenylene
HIF-1	hypoxia inducible factor 1α
IκB	inhibitor of κB
ICD	induced circular dichroism
MALDI	matrix assisted laser desorption ionisation
MGP	4-(guanidylmethyl)-1-10-phenanthroline
MOPS	3-(*N*-morpholino)propanesulfonic acid
MS	mass spectrometry
m/z	mass-to-charge
NF-κB	nuclear factor-κB
NH_4OAc	ammonium acetate
NMR	nuclear magnetic resonance
PD	plasma desorption
phi	9,10-phenanthrenequinone diimine
phen	1,10-phenanthroline

Q-TOF	quadrupole time-of-flight
qDNA	quadruplex DNA
RNA	ribonucleic acid
R,R-Me_2trien	2R,9R-diamino-4,7-diazadecane
Sp1	Specficity Protein 1
Stat3	Signal transducer and activator of transcription
T	thymine
TBACl	tetrabutylammonium chloride
terpy	2,2:6'2''-terpyridine
TFOs	triplex forming oligonucleotides
TMPyP4	[tetra(*N*-methyl-4-pyridyl-porphine)]
tpphz	tetrapyridophenazine
yAP-1	yeast Activator Protein 1

TABLE OF CONTENTS

LIST OF FIGURES

LIST OF TABLES

Chapter 1
General Introduction

1.1 DNA as a Drug Target for Metal Complexes

Nucleic acids are fundamental components within living cells, and occur in two forms: DNA (deoxyribonucleic acid) and RNA (ribonucleic acid). The structure of DNA contains genetic information, which through the processes of transcription and translation is used to direct the synthesis of proteins that perform numerous essential functions and contribute to the physical and chemical development of an organism.[1] Many diseases, including cancer, occur because of aberrant gene expression, which makes DNA an attractive target site for the development of therapeutic agents. In fact a range of diseases including AIDS,[2] malaria,[3,4] herpes,[5] hepatitis[5] and cancer,[6,7] as well as bacterial[8] and fungal[9] infections are often treated with drugs that bind to DNA and/or interfere with its biological functions (**Table 1.1**). Unfortunately, toxic side effects always accompany treatment using DNA-binding drugs owing to their poor selectivity towards disease affected cells, and consequent damage to healthy cells. Difficulties in minimizing these side effects also arise as a result of uncertainties over the exact mode of action of these drugs.[10]

During the last 25 years there has been growing interest in transition metal complexes as DNA-interactive compounds and potential therapeutics.[11] This stems partially from the fortuitous discovery of the anticancer activity of cisplatin (cis-diamminedichloroplatinum(II), **Figure 1.1a**) following an experiment in which platinum electrodes were used to examine the effects of an electric field on the growth of *E. coli*.[12] The components of the medium used to grow the *E. coli* reacted with the electrodes to

produce a mixture of platinum complexes that caused inhibition of cell division, which is a characteristic often associated with anticancer agents. Subsequent testing of the anticancer activity of a variety of platinum compounds including cisplatin, showed the latter to be effective against a range of tumours whereas the corresponding trans isomer (**Figure 1.1b**) was totally ineffective. Cisplatin was approved by the United States FDA (Food and Drug Administration) in 1978 as a treatment for genitourinary tumours. It is now known that the anticancer activity of cisplatin is due to its ability to bind covalently to DNA in a way that produces specific structural alterations.[12] Although transplatin is also able to bind to DNA, it does so in a different fashion which does not produce the same structural alterations. Unfortunately cisplatin therapy is associated with numerous side-effects including nausea, vomiting, neurotoxicity and nephrotoxicity. However, research has led to the development of several second generation platinum drugs including carboplatin (*cis*-diammine(1,1-cyclobutanedicarboxylato)platinum(II), **Figure 1.1c**), which has similar anticancer activity to cisplatin, but produces less severe side effects.

Table 1.1: Examples of clinically used drugs whose mechanisms of action involve interference with DNA chemistry.

Disease	Drugs	Mechanism of action
AIDS	3'-azido-3'-deoxythymidine (AZT)	Blocks the nucleoside binding site of the viral reverse transcriptase.[2]
Malaria	Chloroquine and cryptolepine	Drugs form a complex with DNA by intercalating with the base pairs.
Herpes and hepatitis	Lamivudine and adefovir dipivoxil	Lamivudine competitively inhibits the binding of DNA polymerase to DNA. Adefovir dipivoxil is a nucleotide analogue that targets reverse transcriptase and causes chain termination.
Bacterial and fungal infections	Flucytosine and auinolones	Flucytosine inhibits fungal DNA synthesis. Quinolones inhibit DNA gyrase and topoisomerase.
Cancer	Bleomycin, cisplatin, carboplatin and oxaliplatin	Bleomycin induces oxidative damage to DNA causing single and double strand breaks. Platinum drugs bind to guanine and adenine N-7 atoms.

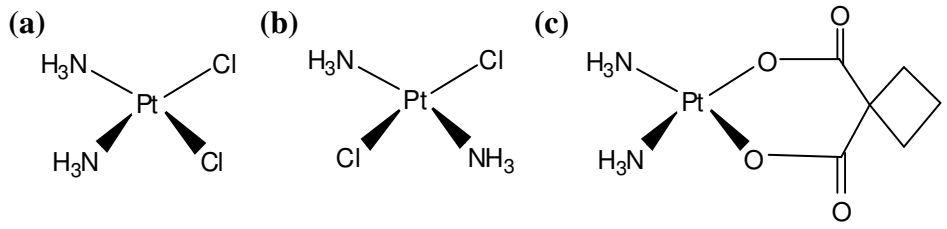

Figure 1.1: Structures of some platinum complexes known to bind to DNA: (a) cisplatin, (b) transplatin and (c) carboplatin**.**

Over the past decades there has also been increasing attention given to the DNA binding properties of square planar and octahedral complexes containing two or three bidentate heterocyclic ligands such as bpy (bipyridine) or phen (phenanthroline). Many of these complexes contain inert metal ions such as Ru(II), Rh(III) and Pt(II), which ensures that they cannot bind covalently to DNA. However, they are able to bind non-covalently by one or more mechanisms that depend on their 3-dimensional structure and the presence of DNA-binding and recognition elements in their organic ligand framework. The photophysical and electrochemical properties of these transition metal complexes have been utilised to show how they could be used in a wide range of capacities from DNA footprinting agents to fluorescent markers of specific DNA structures.[11] As a consequence, there is a large amount of ongoing research effort that aims to gain greater insight into the binding mechanisms of transition metal complexes with DNA in order to further the development of new therapeutic and diagnostic agents. Many different biochemical and analytical techniques have been used to gain insight into the mechanisms by which these molecules interact with DNA. These include NMR (nuclear magnetic resonance) spectroscopy, absorption spectrophotometry, X-ray crystallography, gel electrophoresis, molecular modelling, fluorescence spectroscopy, isothermal titration calorimetry and circular dichroism (CD) spectroscopy.[13,14,15,16,17]

1.2 Double-Stranded DNA

DNA is a polymer made from thousands or even millions of four different repeating units called nucleotides. Each nucleotide is made up of three components: a nitrogenous base, a pentose sugar (deoxyribose) and a phosphate group. The nucleotides are linked through a phosphodiester bond between the 3'-carbon of one pentose sugar and the 5'-carbon of the next, resulting in a polymeric chain consisting of alternating phosphate and sugar residues, from which the bases project (**Figure 1.2**). The nitrogenous bases are the purines adenine (A) and guanine (G), which are comprised of two heterocyclic ring systems, and the pyrimidines thymine (T) and cytosine (C), each having a structure consisting of a single heterocyclic ring.[18]

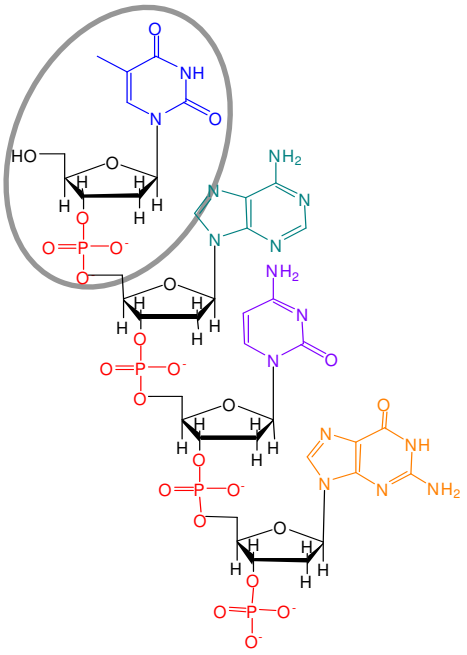

Figure 1.2: A single polymer chain of DNA is made up of nucleotides (circled), each comprised of a phosphate group (red), nitrogenous base (T, A, C or G, coloured blue, green, purple and orange, respectively) and a deoxyribose sugar (black). The nucleotides are linked together through phosphodiester bonds, resulting in a backbone of alternating phosphate and sugar residues.

In the early 1950s James Watson and Francis Crick deduced the three dimensional structure of DNA using the results of X-ray crystallographic studies.[19] They showed that DNA is made up of two antiparallel polynucleotide strands held together by hydrogen bonding interactions involving the nitrogenous bases (**Figure 1.3**). The two strands form a double helix in which the hydrophobic heterocyclic bases are on the inside stacked 0.34 nm apart from each other, and away from the surrounding aqueous medium. In contrast the phosphate and deoxyribose units which form the backbone of the double helix are on its outside and directly exposed to solvent molecules.[19] The structure can be described as a spiral staircase, with the base pairs forming the steps. The diameter of the helix is approximately 2 nm, and one full turn is made every 3.4 nm along its length with 10 bases in each turn. Two kinds of grooves are present in the Watson and Crick DNA structure. These are called the major groove (12 Å wide) and the minor groove (6 Å wide). Watson and Crick proposed that the nitrogenous bases on opposite DNA strands were always paired together in two specific combinations; A was always found to be joined to T by means of two hydrogen bonds, while G and C were bonded *via* three hydrogen bonds. Since the width of GC and AT base pairs are almost the same, this arrangement ensures that the width of a DNA molecule is constant along its entire length. Another important feature of the structure of the DNA double helix is that it is not a constrained, rigid structure. Instead it can be bent or supercoiled causing little change to its basic molecular structure. This flexibility allows DNA to wrap around proteins in the nucleus of eukaryotic cells, and circular DNA molecules to be formed.[20]

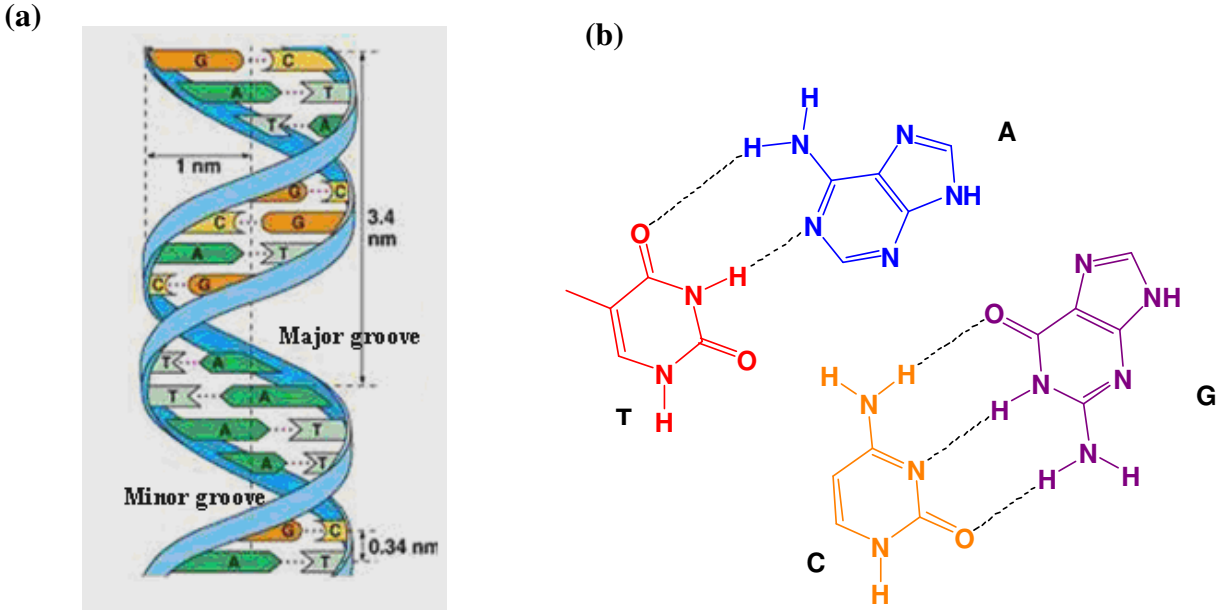

Figure 1.3: (a) The double helical structure of DNA contains a sugar phosphate backbone (illustrated as the blue ribbon) on the outside of the molecule, while the heterocyclic bases (T, A, G and C) stack together on the inside and are involved in specific hydrogen bonding interactions (dotted lines).[18] (b) Close up of the hydrogen bonding interactions between complementary (AT and GC) base pairs.

It is now known that the structure proposed by Watson and Crick is just one of three conformations for double-stranded DNA; namely A-DNA, B-DNA and Z-DNA (**Figure 1.4**).[20] The model proposed by Watson and Crick is B-DNA, which is the most common form found in solution. A-DNA was discovered during X-ray diffraction studies of dehydrated DNA, and forms when the surrounding humidity is reduced to below 75%. Like B-DNA it is also a right-handed double helical molecule. However, it is shorter and wider than B-DNA, with a diameter of ~ 26 Å , a pitch of ~ 28 Å, and 11 base pairs which are tilted towards the helix axis per helical turn. The stability of A-DNA within a dehydrated environment is a result of the phosphate groups binding fewer water molecules than in B-DNA. Nucleic acid conformations very similar to that in A-DNA have been found in double-stranded regions of RNA and RNA-DNA hybrids.[20]

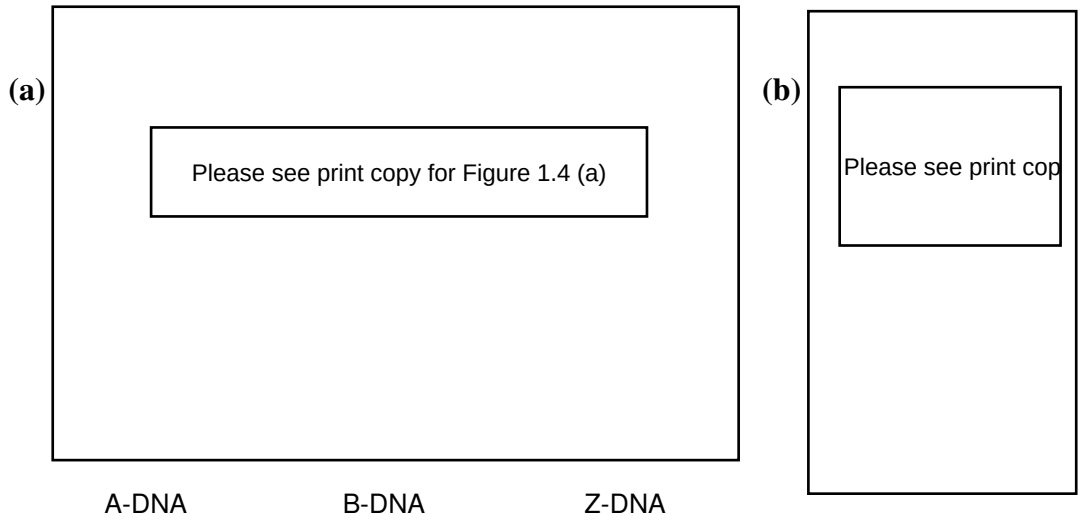

Figure 1.4: Comparison of the structures of A-DNA, B-DNA, and Z-DNA: (a) Views perpendicular to the helix axis.[21] (b) Views down the helix axis.[21,22]

The structure of Z-DNA consists of a left handed double helix in which the repeating subunits are dinucleotides, as opposed to the mononucleotides present in A-DNA and B-DNA. These repeating dinucleotide subunits cause the backbone phosphates to adopt a zigzag conformation. In addition, the phosphate groups on opposite strands in Z-DNA are 8 Å apart, which is much smaller than the 12 Å minimum distance apart in B-DNA. This shorter distance means that electrostatic repulsions between phosphate groups are stronger in Z-DNA than in B-DNA. The structure of Z-DNA has 12 base pairs per turn, a pitch of ~ 45 Å and a diameter of ~18 Å. It also has a 60^{o} rotation per base pair, a flat major groove and a deep minor groove. B-DNA can convert to Z-DNA by flipping its base pairs 180^{o} and rotating the sugars bound to the purine residues. The formation of Z-DNA is thermodynamically unfavourable, however, the transition from B-DNA to Z-DNA can be induced by methylation of cytosine residues as well as by negative supercoiling.[20] In

addition, at low ionic strengths the addition of divalent transition metal ions such as Zn^{2+}, Cu^{2+}, Mn^{2+}, Co^{2+} and Ni^{2+} has been shown to induce a B to Z transition in poly(dGdC).[23]

The left-handed Z-DNA molecule has been proposed to have biological roles during the regulation of gene expression, DNA processing, and in some instances, the development of human diseases. For example, several studies have found a close relationship between Z-DNA structures and chromosomal breakage and translocation events that are often associated with blood cell cancers such as leukaemia, lymphoma and myeloma.[24,25,26,27] Z-DNA formation has also been identified in the hippocampus of patients with Alzheimer's disease. However, its role in the development of this disease has yet to be elucidated.[28] Z-DNA has also been found in the promoter region of the NHRAMP1 gene, which plays an important role in determining human susceptibility to autoimmune diseases (e.g. rheumatoid arthritis, juvenile rheumatoid arthritis, type 1 diabetes, Crohnn's disease) and infectious diseases (e.g. tuberculosis, leprosy). Polymorphism in this region has been found to contribute directly to disease susceptibility.[29] As the biological roles of Z-DNA and its association with some human diseases becomes better understood there is a growing interest in developing small molecules that can specifically target Z-DNA to either enhance or inhibit its biological functions, and thereby prevent or treat some human diseases.[24] For example, the Z-DNA binding protein E3L has been found in pox viruses including the vaccinia virus, and is necessary for pathogenicity in mice. Kim *et al.* found that mutations of the Z-DNA binding domain of the protein reduced viral pathogenicity in mice. However, if the Z-DNA binding domain was substituted by other Z-DNA binding sequences the virus retained its lethality towards mice. Since the vaccinia E3L protein is almost identical to that

found in the variola virus, which is the cause of smallpox, these findings provide impetus for the design of small antiviral agents that act by inhibiting binding of E3L to Z-DNA.[30]

1.3 Quadruplex DNA

In addition to the forms discussed in the previous section, DNA is also known to form a variety of other structures including DNA triplexes and quadruplexes.[31] DNA triplexes can occur when a third DNA strand becomes associated with the major groove of a DNA duplex through Hoogsteen hydrogen bonds.[31] The use of triplex forming oligonucleotides (TFOs) that can modulate gene activity *in vivo,* by targeting regulatory regions on duplex DNA, is currently being explored as an avenue for the development of new therapeutic agents.[31,32] Quadruplex DNA can be formed from cytosine rich (C-quadruplex) or guanine rich (G-quadruplex) sequences such as those found within telomeres. Telomeres are stretches of DNA found at the ends of all eukaryotic chromosomes, and are comprised of repetitive C-rich base sequences and single stranded G-rich overhangs. Their biological role includes controlling cell age and death, maintaining the structural integrity of chromosomes, and establishing the three dimensional architecture of the nucleus and chromosome pairing. During each DNA replication cycle telomeres shorten, leading eventually to the onset of apoptotic pathways. In 80% of cancer cells the ribonucleoprotein complex telomerase is found at elevated levels and acts to elongate the ends of telomeres, thereby helping to confer immortality on these cells. The formation of quadruplex DNA structures within telomeres has attracted considerable interest as a potential drug target in the treatment of cancer.[33]

C-quadruplex DNA adopts an *i*-motif structure comprising from two parallel duplexes containing cytosine-cytosine base pairs in which one of the cytosines is protonated.[34,35] The crystal structure of a cytosine rich strand d(TAACCC) corresponding to the metazoan telomeric repeat unit has been determined,[36] and shows the parallel cytosine duplexes to be intercalated into each other, with the 5'-terminal d(TAA) sequences forming intermolecular loops held together by A-T base pairing. G-quadruplex DNA is made from G-rich DNA sequences arranged to form "G-tetrads". A G-tetrad is comprised of four guanine bases held together in a square planar arrangement that is stabilized by eight Hoogsteen hydrogen bonds (**Figure 1.5a**). Individual G-tetrads are stacked on top of one another to form the G-quadruplex DNA structure, which is often stabilized by monovalent cations such as potassium ions. These coordinate to the electronegative carbonyl groups of guanines on adjacent G-tetrads, which are directed towards the interior of the structure (**Figure 1.5b**).

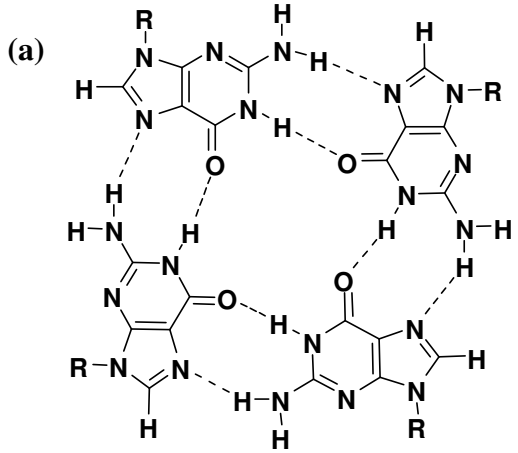

(b)

Please see print copy for Figure 1.5(b)

Figure 1.5: (a) Structure of a G-tetrad. (b) Schematic illustration of the structure of G-quadruplex DNA formed by stacking of G-tetrads, with orange dots representing the stabilising monovalent cations.[37]

G-quadruplex DNA has been shown to be highly polymorphic in solution, with the exact structure observed dependent on a number of factors including the orientation and number

of DNA strands involved in forming the G-tetrads, their loop connectivity, and the identity of anions present in the surrounding environment.[38-40] **Figure 1.6** shows that G-quadruplex DNA structures can be formed from one, two or four DNA strands in a variety of strand orientations. For example, several different monomeric quadruplexes can be formed from the folding of a single DNA strand that contains four or more G-rich sequences (**Figure 1.6a**). The length and identity of the bases in the loops connecting the G-rich sequences determines the way the single DNA strand folds (parallel or antiparallel conformation) and the stability of the resulting monomeric G-quadruplex DNA structure.[41]

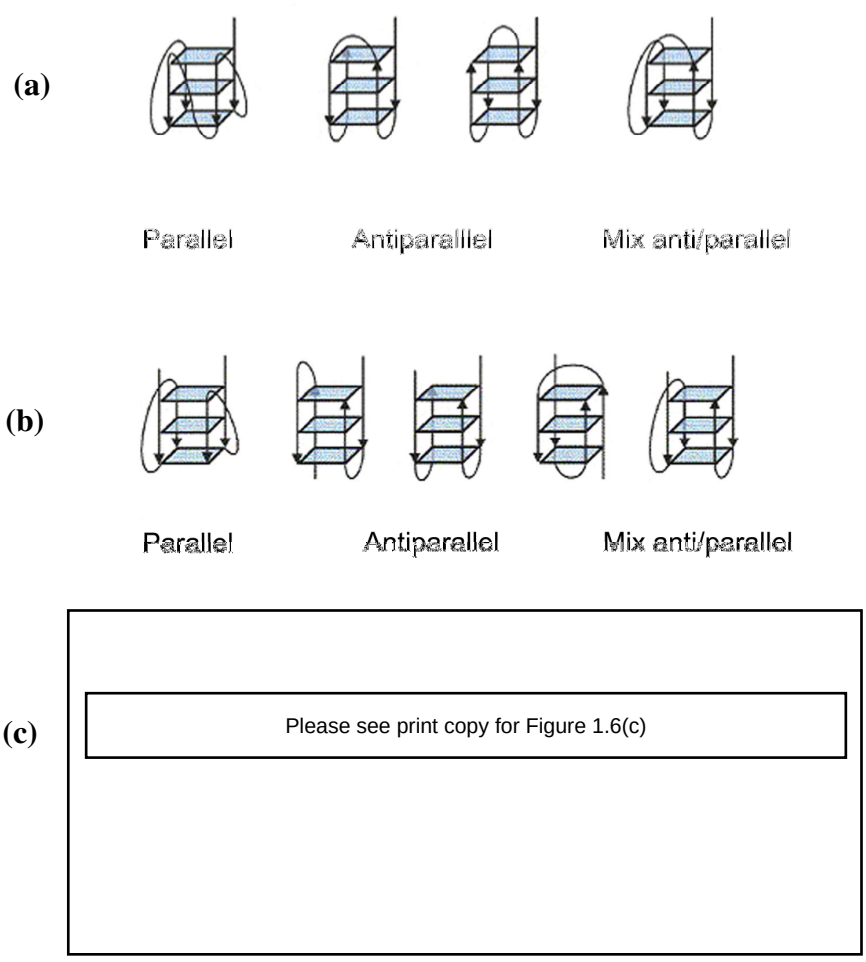

Figure 1.6: Different conformers for G-quadruplex DNA. (a) 1-strand intramolecular G-quadruplexes. (b) 2-strand intermolecular G-quadruplexes. (c) 4-strand intermolecular G-quadruplexes.[37]

In solution, dimeric and tetrameric G-quadruplex DNA structures have been shown to predominantly exist in their more energetically favoured anti-parallel and parallel forms, respectively.[37,39] Tetrameric G-quadruplex DNA structures, however, can theoretically exist in four different strand orientations (**Figure 1.6c**). These are four parallel DNA strands, three parallel and one antiparallel DNA strands, two pairs of adjacent parallel DNA strands and alternating antiparallel DNA strands.[37] Until recently, only parallel tetrameric G-quadruplex DNA had been found in solution. The first antiparallel tetrameric G-quadruplex DNA structure was identified to be formed from a double repeat of the human telomeric DNA sequence d(TTAGGGTTAGGG) using CD spectroscopy and gel electrophoresis. In the proposed model the G-quadruplex DNA structure is stabilized by Watson-Crick hydrogen bonding between the TTA base sequences separating the G-tetrads (**Figure 1.7**).[42]

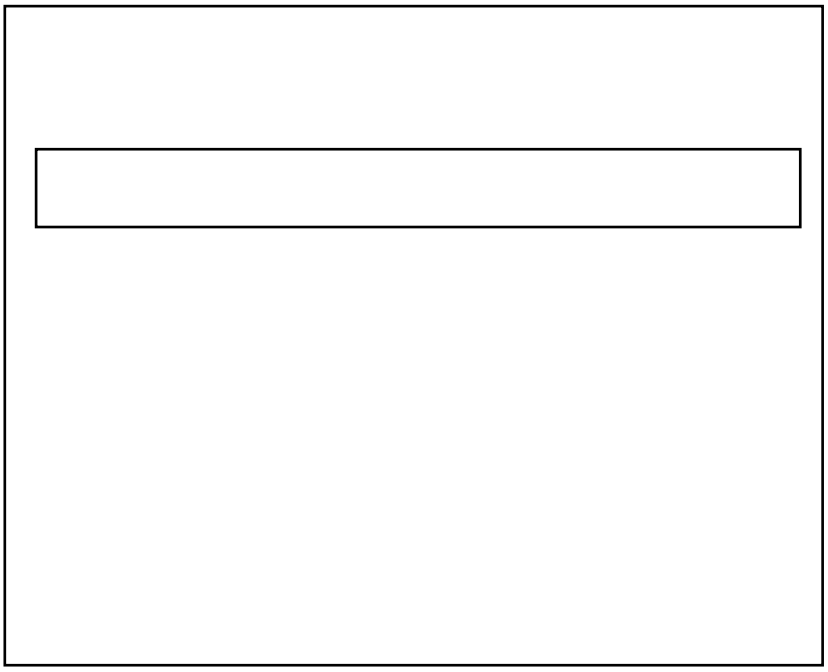

Figure 1.7: Proposed model for the anti-parallel G-quadruplex DNA structure formed from the human telomere DNA sequence d(TTAGGGTTAGGG).[42]

The identity of the cations present in the surrounding environment can also play a role in determining the conformation adopted in a G-quadruplex DNA structure. This is because differences in the size of monovalent cations can influence whether they bind to one or two G-tetrads and how the resulting G-quadruplex DNA structure will be folded. For example, sodium cations are found in the centre of a single G-tetrad, whereas potassium ions are positioned between the planes of two G-tetrads.[39] CD spectra of the double repeat of the human telomere sequence d(TTGGGTTAGGG) suggested it is able to form either a parallel or antiparallel G-quadruplex DNA structure, depending on what cation is present.[43] There have been a number of studies that investigated the structures in the presence of the different metal ions. In the presence of K^+ it can form a tetrameric antiparallel quadruplex structure as well as a dimeric parallel quadruplex, whilst Na^+ only facilitates the formation of an antiparallel dimeric G-quadruplex structure.[43] ^{125}I radioprobing experiments using the human telomere sequence dTAGGG$(TTAGGG)_3$ found that it predominantly formed a basket type antiparallel quadruplex structure in a sodium ion environment, whereas the presence of potassium ions favoured the chair-type antiparallel quadruplex strucutre.[44] The topology of crystal structures of two human telomere quadruplexes containing 12-nucleotide and 22-nucleotide repeat sequences, grown at a K^+ concentration that approximates its intracellular concentration, were fundamentally different from the previously published structure containing sodium cations.[45-48] The crystal structure of the dimeric (12-mer) and the 22-mer intramolecular quadruplex comprised of four strands in a parallel arrangement and TTA loops positioned on the exterior of the quadruplex core, in a propeller like arrangement. In contrast, an NMR analysis of a Na^+ containing human four-repeat 22-mer sequence showed four strands alternating between parallel and antiparallel orientations, with the TTA loops connecting G-quartets.[48] Subsequently, biophysical

experiments in solution and computational studies characterising the structure of the same 22-mer intramolecular quadruplex indicated that the structure of the human telomere quadruplex was not the major conformation that is present in solution.[49] It was found that the solution structure is hydrodynamically more compact than the crystal structure. However, the computational studies did find that a conformational change occurred for the 22-mer in both Na^+ and K^+ solutions, which primarily involves an alteration in loop structures, and also noted that the K^+ form is hydrodynamically more compact.[49]

Guanine-rich DNA sequences that have the propensity to fold into G-quadruplex DNA structures are found in a number of places besides telomeric regions, including human and chicken β-globin genes, retinoblastoma susceptibility genes, the *c-myc* gene and the human insulin gene.[50,51] Drugs that stabilize G-quadruplex structures in these regions may interfere with DNA replication, transcription or recombination of DNA strands. However, the majority of research into G-quadruplex DNA structures has focused on their formation and stabilisation within the G-rich sequences belonging to telomeres.[38,40,49,52] In 1991 Zahler and co-workers demonstrated that K^+-stabilised G-quadruplex DNA structures were able to inhibit telomerase activity. Since this discovery there has been considerable interest in developing small molecules that can inhibit telomerase activity *via* stabilisation of G-quadruplex DNA structures.

1.4 Non-covalent Binding of Small Molecules to B-DNA

Non-covalent binding of small molecules to B-DNA can be achieved through one or more of the following principal binding modes:

(i) Electrostatic interactions with the anionic sugar-phosphate backbone;

(ii) Intercalation; and

(iii) Groove binding.

The binding mechanism or mechanisms used by a small molecule to bind to DNA depend on the exact base sequence of the latter and the structural features of the small molecule.[53,54] In the following sections the main characteristics of the three principal non-covalent binding modes will be described.

1.4.1 Electrostatic Interactions

Electrostatic interactions with B-DNA are generally non-specific and occur along the exterior of the double helix. Counterion condensation is the non-specific interaction of DNA with metal cations in solution (e.g. Na^+ or Mg^{2+}) that assists in the stabilisation of folded DNA conformations. Condensed counterions can be released by neutralisation of the charge of the phosphate backbone by specific electrostatic interactions with organic cations which cause a favourable entropic contribution to the binding free energy.[54] This entropically driven counterion release also makes a favourable contribution to the binding free energy of highly charged molecules such as DNA-binding proteins.[53] In addition, complex organic cations that bind to DNA by specific groove or intercalative mechanisms at equilibrium, may initially be involved in electrostatic interactions with the negatively charged phosphate groups.

1.4.2 Groove Binding

Most small molecules that act as DNA groove binding drugs prefer to interact with the minor groove, while proteins and oligonucleotides are generally involved in binding to the major groove.[6] The reasons for this include differences in chemical properties between the grooves, such as variations in electrostatic potential, hydrogen bonding characteristics, steric effects and extent of hydration.

Minor groove binding drugs are typically made of several aromatic heterocycles linked by amide or vinyl groups, and possess a characteristic crescent shape that is isohelical to the shape of the DNA minor groove. Classical minor groove binders include distamycin A, netropsin and Hoechst 33258 (**Figure 1.8**). The torsional freedom of the bonds within the ring systems also allows the molecules to adjust to a conformation that mimics the shape of the minor groove, without inducing structural rearrangement of the DNA molecule. Minor groove binders have a preference for interacting with AT rich sequences, as the minor groove has a deeper electrostatic potential and less steric hindrance in such regions. The interactions of minor groove binding agents with DNA are stabilised by van der Waals interactions with functional groups on the walls and floor of the groove, and through hydrogen bonding with the AT base pairs. Although similar functional groups are present in GC base-pairs, the hydrogen bond between the amino group of guanine and the carbonyl oxygen of cytosine sterically inhibits penetration of small molecules into the minor groove where GC rich regions occur.[54]

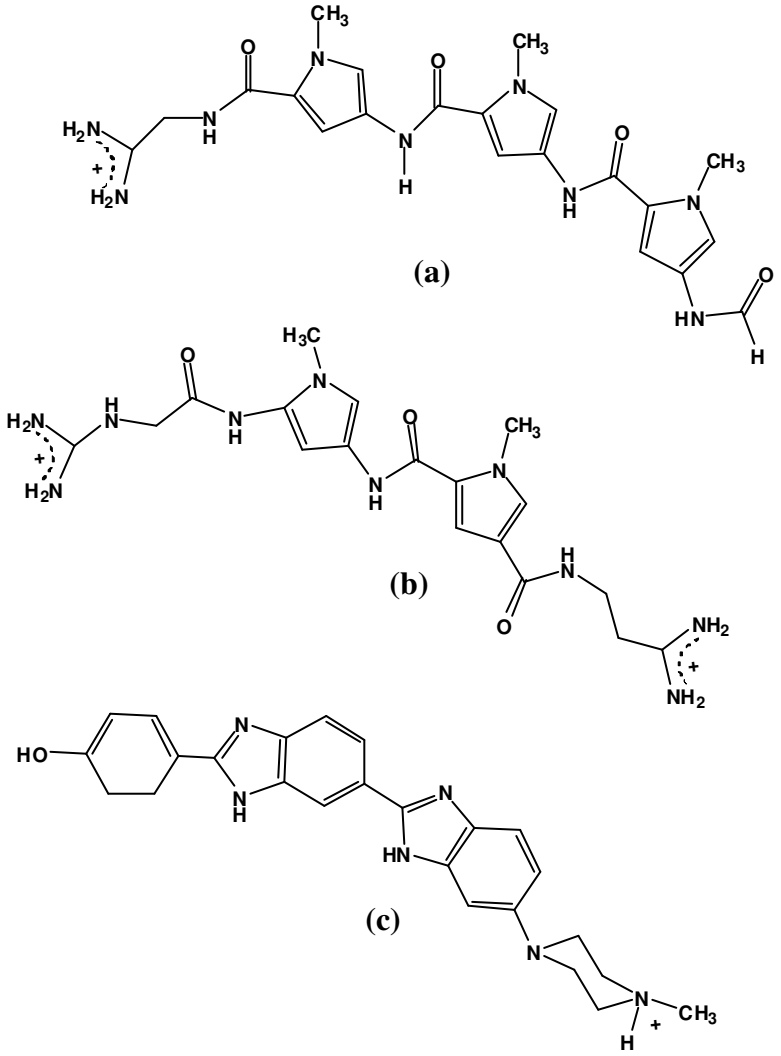

Figure 1.8: Examples of DNA minor groove binders: (a) distamycin, (b) netropsin and (c) Hoechst 33258.

Distamycin A and netropsin are comprised of three and two pyrrole units, respectively, connected by amide bonds, and contain one or more positively charged nitrogen atoms at their ends. Distamycin and netropsin act like typical minor groove binders, preferring to bind to AT rich base sequences, and forming complexes that are stabilised *via* hydrogen bonding and electrostatic interactions involving the amide groups and protonated amines, respectively.[55] Analogues of distamycin that contain more pyrrole units have a greater specificity for longer AT tracts due to increased hydrogen bonding and van der Waals

contacts.[55] Depending on the DNA sequence distamycin can bind to DNA with a 1:1 or 2:1 stoichiometry. The stronger electrostatic repulsion between netropsin molecules prevents more then one molecule binding to similar DNA sequences.[54-56] For example, an X-ray crystal structure of netropsin binding to the minor groove of d(CGCAAATTTGCG) is shown in **Figure 1.9**.[57] In this structure netropsin can be seen to bind to the AATT centre, causing a small conformational change including widening of the minor groove and tilting of the helix axis away from the site of binding.

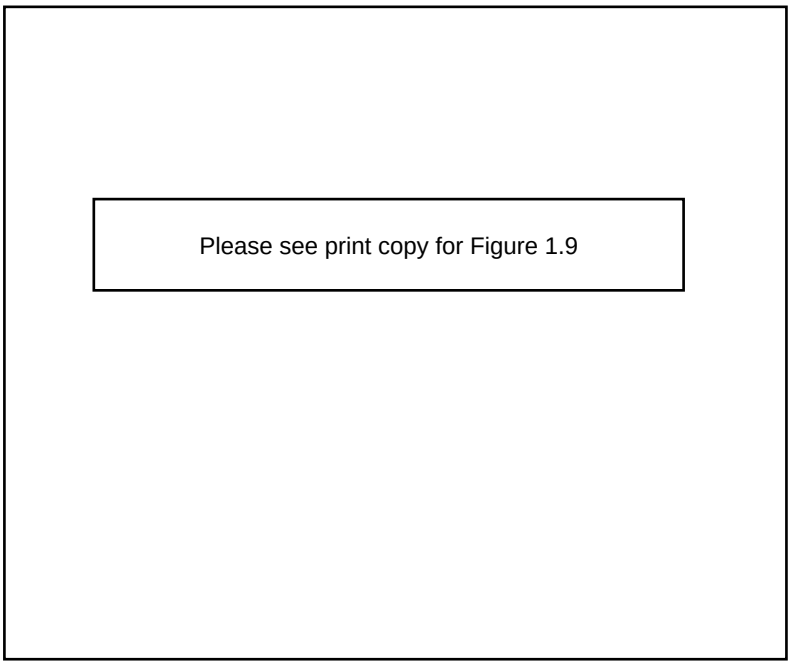

Figure 1.9: Crystal structure of netropsin binding to the minor groove of d(CGCAAATTTGCG).[52]

By acting as minor groove binders, distamycin and netropsin have been shown to affect the interactions of DNA with a range of proteins that facilitate transcriptional processes, including helicases (Werner and Bloom syndrome helicases), and topoisomerases I and II.[58,59] Analogues of distamycin and netropsin which show greater cytotoxicity include brostallicin and tallimustine (**Figure 1.10**).[60,61] Tallimustine demonstrated promising initial

results in murine cancer model systems, but unfortunately clinical trials with the drug were cut short due to its association with severe myelotoxicity.[62] Nevertheless tallimustine has proven to be an important model compound for the design of new minor groove alkylating agents.[60] Brostallicin has demonstrated more promising results as it has a much higher therapeutic index against bone marrow cancer *in vitro* compared to other distamycin derivatives,[63] and is also effective against cancer cells that are resistant to alkylating agents and topoisomerase inhibitors.[63] Brostallicin has also demonstrated cytotoxicity against tumour cells that have defective DNA mismatch repair systems.[64] Loss of DNA mismatch repair by a tumour cell often results in resistance to a variety of anticancer drugs including tallimustine. However, the α-bromoacrylic moiety of brostallicin reacts with glutathione (GSH) in a reaction catalysed by glutathione-*S*-transferase (GST) forming a GSH complex that can covalently bind to DNA.[65] Since the *in vitro* and *in vivo* activity of brostallicin is increased in the presence of GSH and/or GST, and increased levels of GST/GSH are often found in human tumours cells, this could represent an advantage for the therapeutic application of brostallicin.[63]

Hoechst 33258 (pibenzimol) is a bis(benzimidazole) that is widely used as a DNA stain.[54] It has been assessed in a phase 1 clinical trial as an anticancer agent, however its high cytotoxicity and low potency limited its potential and hence ended its clinical evaluation.[55] Hoechst 33258 exerts its cytotoxicity by inhibiting the binding of helicases and topoisomerases to DNA as a result of its ability to bind to the minor groove of DNA, particularly in regions where there are four or five consecutive AT-base pairs.[55] Modifications of the terminal piperazine ring of Hoechst 33258 with an amidinium, imidazoline or a tetrahydropyridinium group reinforces significantly the affinity of the drug

for AT-stretches,[55] as does the addition of one or more benzimidazole units.[66] Analogues of Hoechst 33258 that contain a nitrogen mustard moiety added to the benzimidazole ring demonstrated improved cytotoxicity compared to Hoechst 33258.[67] This has led to the Hoechst 33258 derivative in **Figure 1.11a** being evaluated clinically in phase I and II trials as an anticancer agent.[66] **Figure 1.11** also shows the structure of two other compounds derived from Hoeschst 33258 (**Figure 1.11b** and **c**) which show higher DNA sequence selectivity and structural selectivity compared to the parent compound. Both compounds contain two ortho bisubstituted phenyl rings, as this has been shown to increase the electron density at the nitrogen atoms on the imidazole ring, and thereby improve the ability of the compound to form hydrogen bonds with DNA.[68]

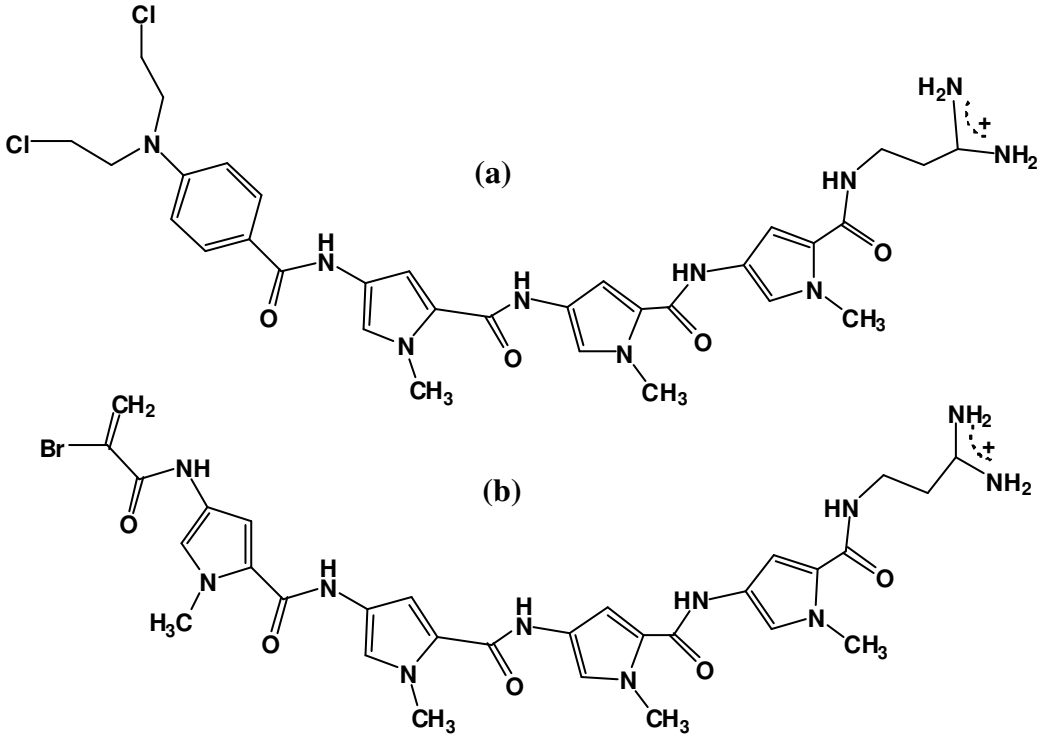

Figure 1.10: Derivatives of the minor groove binder distamycin which have shown greater therapeutic potential: (a) brostallicin and (b) tallimustine.

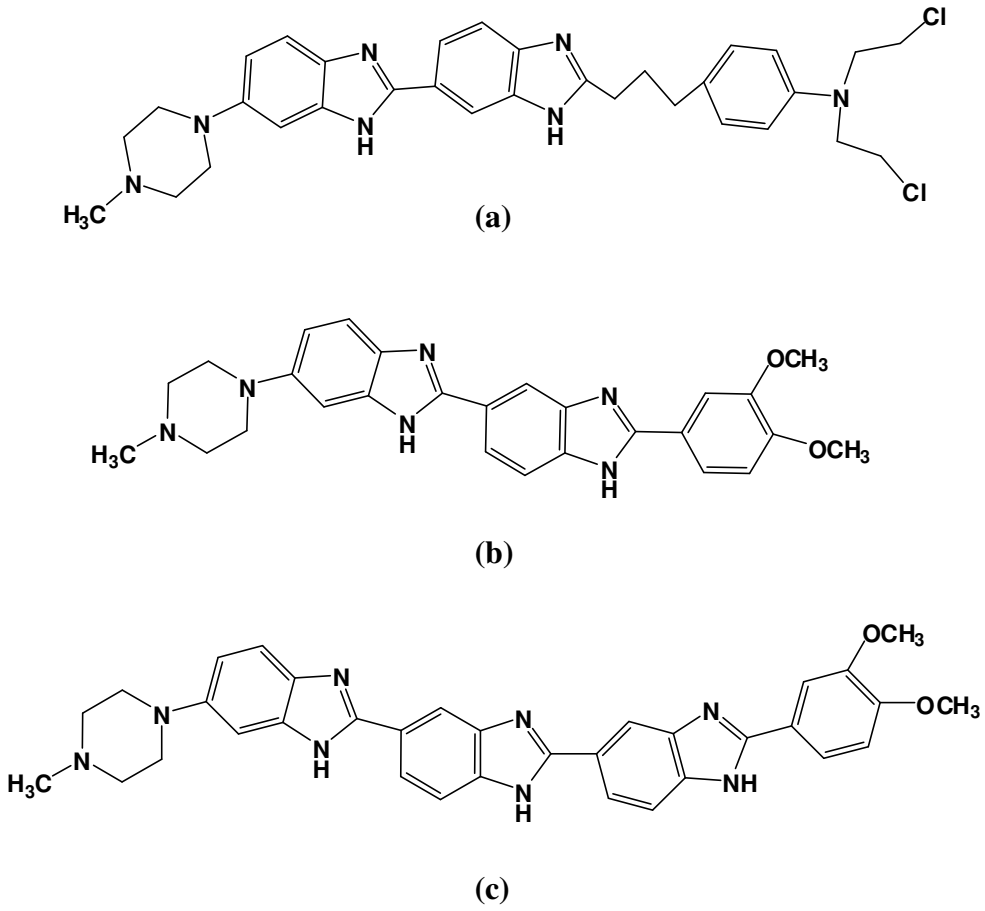

Figure 1.11: Structures of some analogues of Hoechst 33258

1.4.3 Intercalation

Classical intercalators are planar polycyclic aromatic cations that are able to insert themselves at right angles to the DNA double helix and stack between the base pairs.[54] Hydrophobic attractions between aromatic intercalator molecules and the interior environment of the DNA base stack play a major role in determining the stability of these systems. However, hydrogen bonding, electrostatic and charge transfer interactions also contribute to the stability of the stacking of the drug within the DNA molecule. Intercalative interactions induce lengthening of the double helix by approximately 3.4 Å for

every intercalator involved, which equates roughly to the thickness of a typical aromatic ring system. In addition, intercalation also leads to unwinding and bending of the DNA helix. These drug induced architectural changes can be detected by several methods including measurement of viscosity changes and linear dichroism spectroscopy, and prevent DNA from participation in its normal regulatory processes such as transcription and replication.[53,54]

Figure 1.12 shows the structures of some classical intercalators. Ethidium bromide is the paradigm for DNA intercalating agents, as its biological activity has been established for more than half a century, and it is commonly used as a fluorescent dye for staining DNA in gel electrophoresis experiments. Daunomycin (daunorubicin) and adriamycin (doxorubicin) are clinically used DNA intercalating anticancer drugs that belong to the family of anthracycline antibiotics.[54] However, despite being proven as effective anticancer drugs, therapy with these compounds elicits significant side effects including cardiotoxicity and drug resistance in some cancer cells. The chemical structures of daunomycin and adriamycin include an aglycone chromophore with four fused rings and an amino sugar called daunosamine. The differences between the binding interactions of daunomycin and adriamycin with DNA are very small. A high resolution crystal structure analysis by Wang *et al.* of a 2:1 complex of daunomycin bound to $d(CGTACG)_2$ showed that the drugs intercalate their aglycone chromophore into the DNA double helix, and the daunosamine group lies in the minor groove where it participates in other non-covalent interactions.[69] The specific binding of daunomycin to DNA is directed by hydrogen bonding between the hydroxyl group of the daunomycin aglycone ring and the N2 and N3 positions of a guanine base located adjacent to the aglycone ring.[70] These hydrogen bonds are important for the

biological activity of daunomycin, since anthracycline derivatives without the hydroxyl group on the aglycone ring are not biologically active.[70]

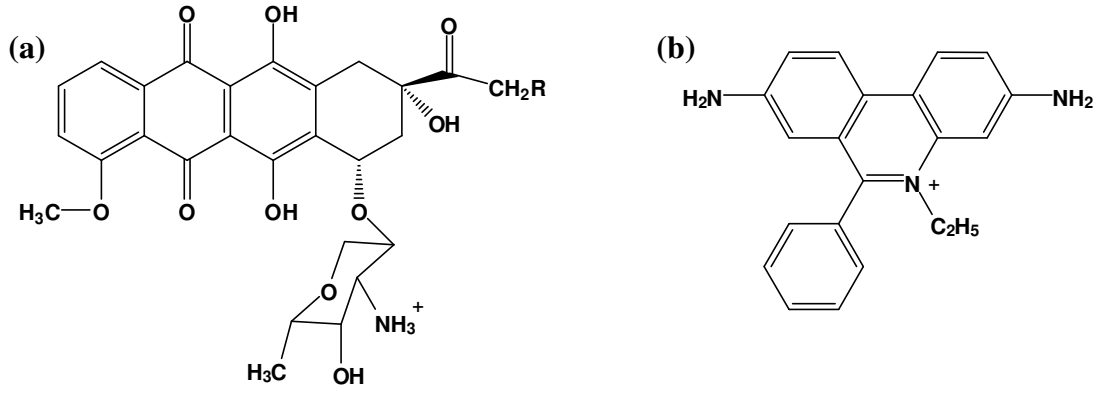

Figure 1.12: Examples of classical intercalators: (a) daunomycin (R = H), adriamycin (R = OH), (b) ethidium.

In addition to causing separation of the base pairs, daunomycin binding produces other conformational changes to the structure of B-DNA including a lateral shift of the GC base pairs towards the major groove. While base pairs at the actual intercalative site were found not to be unwound, those at adjacent sites were unwound by 8^{o}.[54] DNA footprinting data and theoretical studies show daunomycin has a preference for binding to 5'-(A/T)GC-3'[*] and 5'-(A/T)CG-3' sequences over those containing GC base pairs alone.

1.5 Non-covalent Binding of Transition Metal Complexes to B-DNA

There are now many examples of square planar and octahedral complexes containing d^8 and d^6 transition metal ions, respectively which act as non-covalent DNA binding agents. In each case, the metal ion serves as a central scaffold for an array of chelating ligands that

[*] A/T indicates either A or T may occupy that position.

can possess recognition elements for binding to DNA. Some of these transition metal complexes also possess useful photochemical or photophysical properties that can be used to probe DNA structure and function for a spectrum of potential biophysical applications.[11,71,72]

The interaction of $[Cu(phen)_2]^+$ (**Figure 1.13a**) with the minor groove of DNA was first studied by the Sigman group in the late 1970's and early 1980's, and was probably one of the first investigations of the non-covalent binding of a transition metal complex to DNA.[73,74] Also during this time Lippard and co-workers synthesised the square planar complex $[Pt(terpy)(SCH_2CH_2OH)]^+$ (terpy = 2,2:6',2''-terpyridine) (**Figure 1.13b**), which became the progenitor of a large number of metal complexes that can intercalate into DNA now often referred to as *metallointercalators*. Evidence for intercalation of $[Pt(terpy)(SCH_2CH_2OH)]^+$ into calf thymus DNA was obtained from X-ray diffraction patterns which revealed platinum atoms distributed at 10.2 Å intervals at inter base pair sites, and partial unwinding of the sugar phosphate backbone.[75] They later expanded their research to investigate the intercalation of other platinum complexes possessing heterocyclic rings including $[Pt(phen)(en)]^{2+}$ (en = 1,2-diaminoethane) and $[Pt(bpy)(en)]^{2+}$ (**Figures 1.13c and d**). It was deduced that the DNA binding interaction was dependent on the structural characteristics of the intercalating complex, as well as the composition of the DNA and the ionic strength of the medium. Therefore these factors must be taken into consideration when attempting to compare intercalative abilities of different metal complexes.[76]

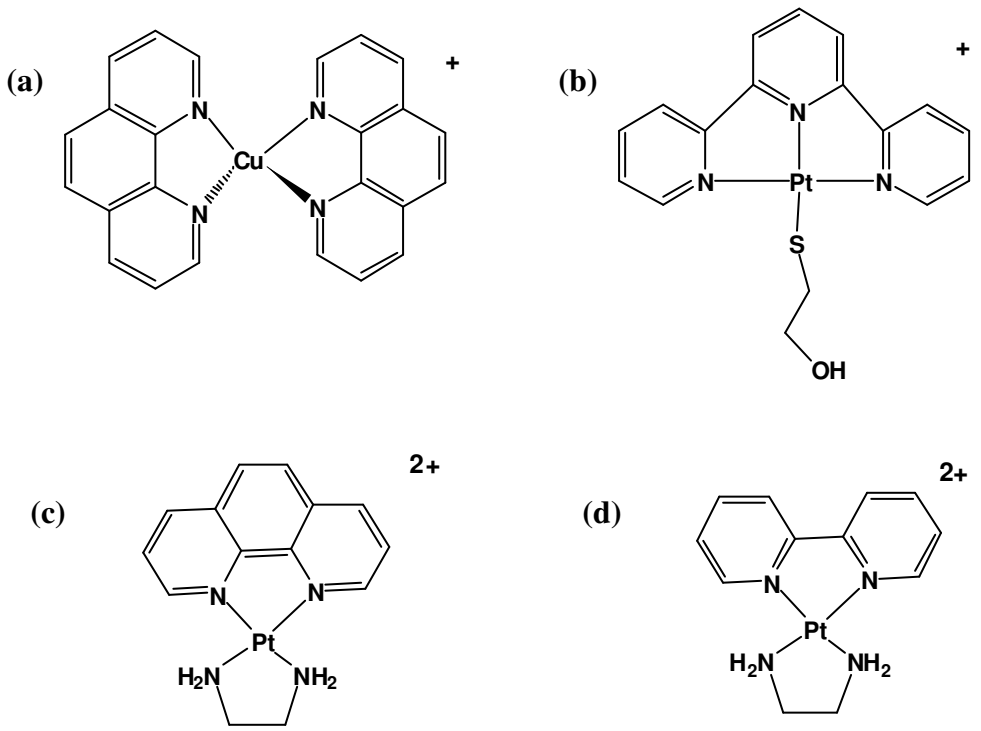

Figure 1.13: Structures of some transition metal complexes used in early studies of non-covalent binding to DNA: (a) $[Cu(phen)_2]^+$, (b) $[Pt(terpy)(SCH_2CH_2OH)]^+$, (c) $[Pt(phen)(en)]^{2+}$ and (d) $[Pt(bpy)(en)]^{2+}$.

Today metallointercalators encompass a large family of metal complexes usually containing an inert transition metal centre, and bearing at least one planar intercalating ligand which can readily π-stack in the major groove of DNA parallel to the base pairs. The intercalating ligand acts as an anchor point within the major groove, directing the orientation of the ancillary ligands with respect to the DNA duplex. Examples of other metallointercalators containing octahedral transition metal ions are shown in **Figure 1.14.**

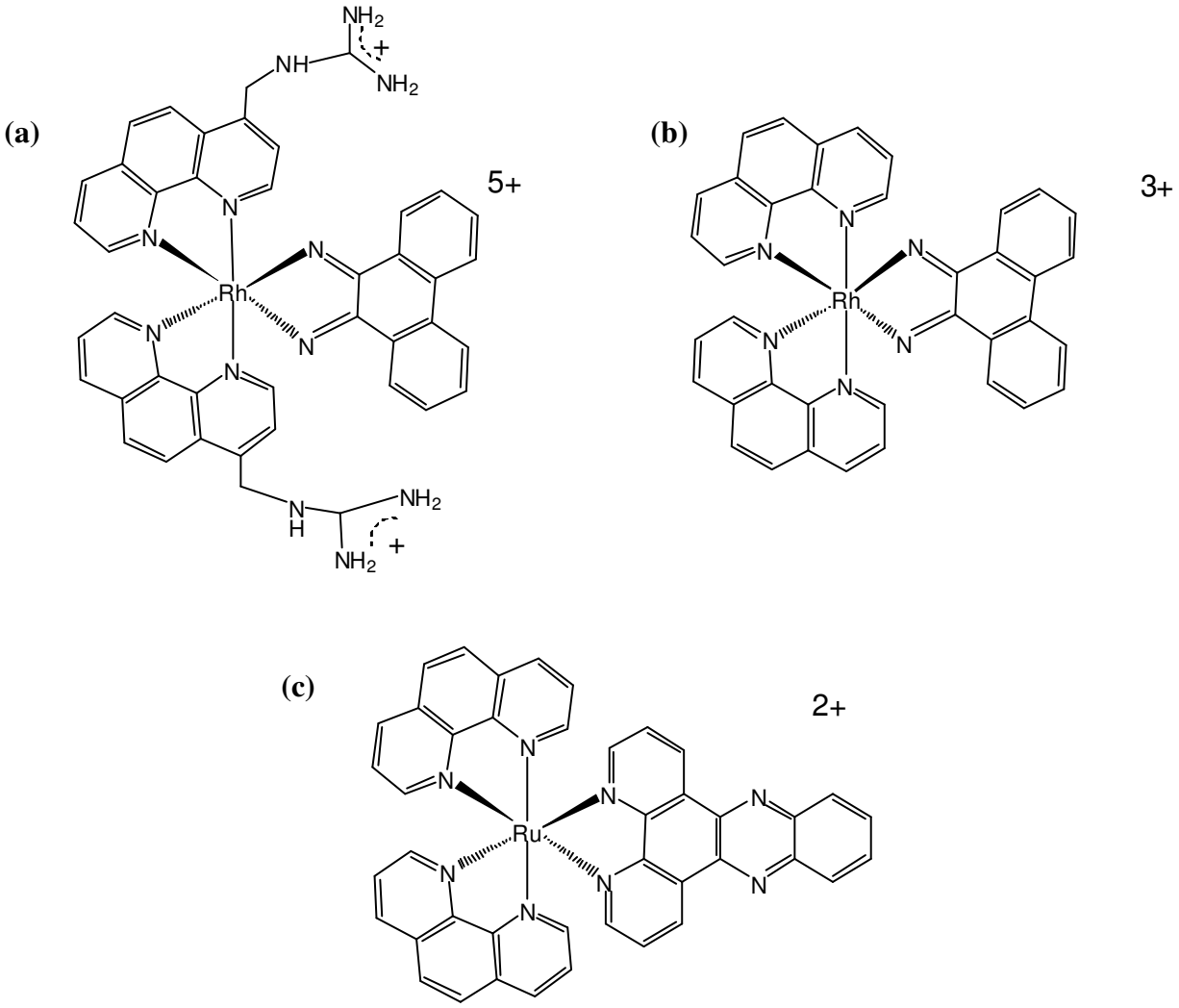

Figure 1.14: Examples of octahedral metallointercalators (a) Λ-1-$[Rh(MGP)_2(phi)]^{5+}$ (phi = 9,10-phenanthrenequinone diimine and MGP = 4-(guanidylmethyl)-1,10-phenanthroline) (b) $[Rh(phen)_2(phi)]^{3+}$ and (c) $[Ru(phen)_2(dppz)]^{2+}$ (dppz = dipyrido[3,2-a:2,3'-c]phenazine).

Both the intercalative and ancillary ligands of metallointercalators can be altered to provide new structural features in order to enhance DNA affinity and sequence selectivity. For example, DNA binding affinity can be enhanced substantially by including the highly intercalative dppz ligand in the coordination sphere of the metal complex instead of phenanthroline or bipyridine.[72,77,78] On the other hand the metallointercalator Λ-1-$[Rh(MGP)_2(phi)]^{3+}$ (**Figure 1.14a**), which was derived from $[Rh(phen)_2(phi)]^{3+}$ (**Figure 1.14b**) by the addition of pendant guanidinium groups to the ancillary ligands, shows

significantly higher DNA sequence selectivity than its parent compound. The latter modification was made in order to enable the compound to specifically bind to 5'-pyrimidine-pyrimidine-purine-3' triplet sequences flanked by two GC base pairs, through the formation of hydrogen bonds between the guanidinium groups of the metal complex and the O6 atoms of the guanines.[79] It was subsequently found that the Δ enantiomer demonstrated high binding specificity to the DNA sequence 5'-CATCTG-3', while the Λ isomer binds preferentially to the sequence 5'-CATATG-3'.[80]

Another example of a metallointercalator that was purposefully designed to exhibit DNA binding selectivity is Δ-α-[Rh[(R,R)-Me_2trien]phi]$^{3+}$ (*R,R*-Me_2trien = 2*R*,9*R*-diamino-4,7-diazadecane) (**Figure 1.15a**), which was constructed to target the DNA sequence 5'-TGCA-3'.[81] Photocleavage data indicated that the metal complex binds to the target site with a binding constant of 9×10^7 M^{-1}.[81] The complex targets the above sequence from the major groove where it intercalates between the DNA base pairs. At the same time the axial amines of the (R,R)-Me_2trien ligand form hydrogen bonds to the O6 atom of guanine, and van der Waals interactions exist between the pendant methyl groups of the same ligand and those on the flanking thymine.[81] The crystal structure of the metallointercalator Δ-α-[Rh[(*R,R*)-Me_2trien](phi)]$^{3+}$ bound to its target sequence 5'-TGCA-3' is illustrated in **Figure 1.15b.** The structure shows that 60% of the surface area of the phi ligand is deeply inserted into the DNA base stack, which is similar to the degree of stacking of consecutive base pairs in a free B-DNA duplex.

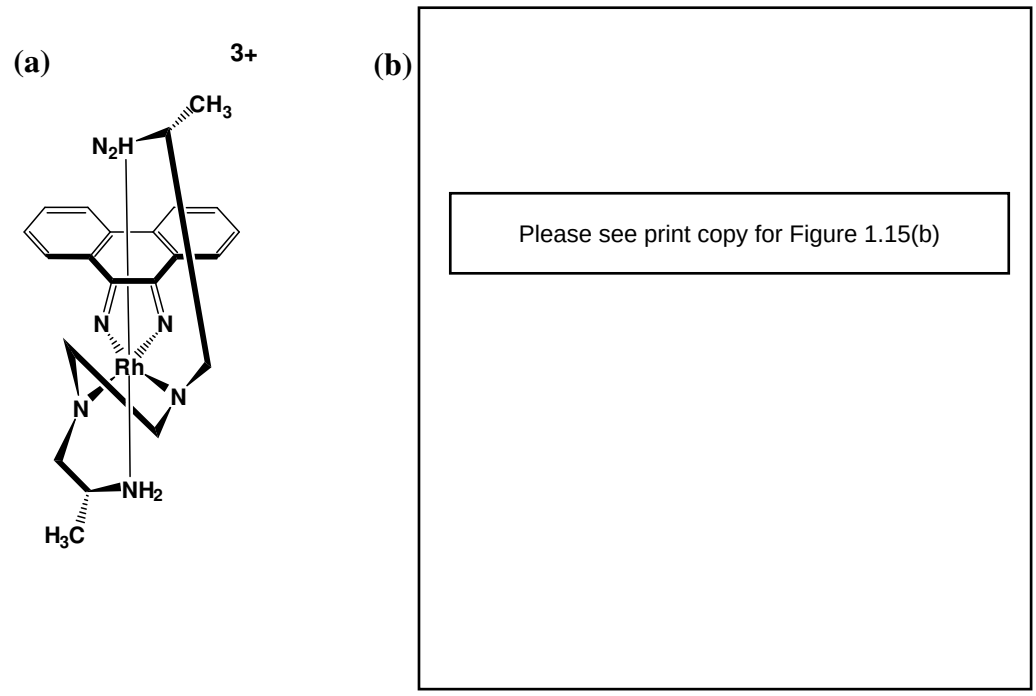

Figure 1.15: (a) Structure of Δ-α-[Rh[(*R,R*)-Me_2trien](phi)]$^{3+}$. (b) Crystal structure of Δ-α-[Rh(*R,R*)-Me_2trien](phi)]$^{3+}$ (in red) bound to the DNA sequence 5′-TGCA-3′ (in green and yellow).[82]

The continuing interest in metallointercalators stems partially from the possibility that their chemical and physical properties may be able to be exploited for applications including DNA structure probes and repair agents.[11,71,72] In this context one of most potentially useful properties of some metallointercalators is their ability to luminesce in organic solvents. For, example, compounds containing the dppz ligand such as [Ru(bpy)$_2$dppz]$^{2+}$ and [Ru(phen)$_2$dppz]$^{2+}$ display solvatochromic luminescence.[72,11,83,84,85] In aqueous solution water molecules deactivate the excited state of these complexes by forming hydrogen bonds with the endocyclic nitrogen atoms of the dppz ligand. When these metal complexes are bound to DNA in aqueous solution the water molecules are shielded from the dppz ligand, allowing the complexes to display considerably enhanced luminescence lifetimes. This effect has led to these complexes being dubbed "molecular light switches".[83] The molecular

light switch effect has been used to discriminate between the binding mechanisms of Δ-$[Ru(phen)_2(dppz)]^{2+}$ and Λ-$[Ru(phen)_2(dppz)]^{2+}$ with B-DNA.[86,87]

In another demonstration of the potential use of metallointercalators, the photooxidative properties of some rhodium complexes were harnessed to directly promote the repair of thymine dimers incorporated into a 16 base pair duplex DNA molecule. [88] Thymine dimers are formed as a result of a [2 + 2] cycloaddition reaction between neighbouring thymines on the same DNA strand, usually as a result of exposure to UV radiation. When the compound $[Rh(phi)_2(DMB)]^{3+}$ (DMB = 4,4'-dimethyl-2,2'-bipyridine) was covalently tethered to one end of the damaged DNA molecule and then irradiated with 400 nm light, it was able to mediate repair of the thymine dimer. Interestingly, when the $[Rh(phi)_2(DMB)]^{3+}$ complex was allowed to simply bind non-covalently to the damaged DNA molecule it produced a higher repair efficiency than when covalently tethered.

In another demonstration of a potential application for metallointercalators, the complex $[Rh(phi)_2(bpy)]^{3+}$ was covalently attached to a metallopeptide bearing a hydrolytic zinc ion (**Figure 1.16**).[89] The resulting metallointercalator-peptide conjugate was shown to mimic a restriction enzyme by hydrolysing DNA at low concentrations and under mild conditions. Intercalation of the phi ligand into the DNA structure was believed to position the peptide chain so that the zinc ion was in the correct position to perform the hydrolytic cleavage.

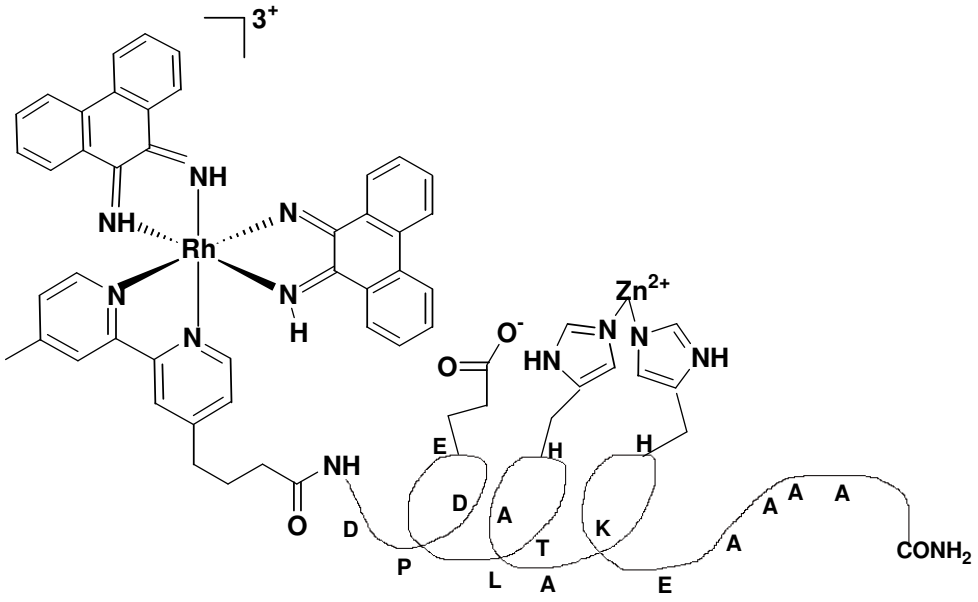

Figure 1.16: Structure of a synthetic restriction enzyme based on the complex $[Rh(phi)_2(bpy)]^{3+}$.

Until recently most, or at least many, studies involving metallointercalators have examined ruthenium(II) or rhodium(III) complexes coordinated to three bidentate ligands, at least one of which was capable of being inserted deeply into the DNA base stack. Whilst other transition metal ions can also accommodate these ligands in a similar fashion to ruthenium(II) and rhodium(III), binding studies using such compounds have until recently attracted much less attention. Further investigations involving such complexes, however, would allow an evaluation of the effects of subtle variations in metallointercalator structure on duplex DNA and G-quadruplex DNA binding interactions.

One of the few studies to have directly compared the DNA binding properties of closely related metallointercalators containing different metal ions is that of Arounaguiri and co-workers, who examined the ability of the complexes $[M(phen)_2(dppz)]^{n+}$ (M=Co(III), Ni(II)

and Ru(II), n = 2 or 3) to bind to CT-DNA (calf thymus DNA).[78,90] Binding constants were determined using an absorption titration method and found to be > 10^6, 5.05×10^5 and 1.51×10^5 M^{-1} for the ruthenium, cobalt and nickel complexes, respectively. In contrast to these results, thermal denaturation studies indicated that addition of the three different metal complexes produced similar shifts in DNA melting temperature, suggesting that they all produced a similar degree of stabilisation when bound to DNA.[78] Unlike the other metal compounds, $[Ni(phen)_2(dppz)]^{2+}$ was found to not be able to cleave supercoiled DNA upon irradiation using 350 nm light. This result was attributed to the paramagnetic nature of the nickel compound.[78,90] Barton *et al.* compared the binding of $[Ni(phen)_2(L)]^{2+}$ where L= dppz, phi or dpq (dipyrido[3,2-d:2'3'-f]quinozaline) to the oligonucleotides $d(GTCGAC)_2$ and $d(GTGCAC)_2$ using ^1H NMR spectroscopy.[91] They found that subtle differences in the DNA sequence caused significant changes in the binding location of the metal complex on the oligonucleotide.

1.6 Non-covalent Binding to G-quadruplex DNA

The possibility of inhibiting telomerase activity by stabilising G-quadruplex DNA structures within telomeres using small molecules has attracted growing research interest. For example, over the past few years a wide range of heteroaromatic molecules have been investigated for their ability to act as G-quadruplex DNA binders.The majority of reports have proposed small molecules to inteact with G-qaudruplex DNA through stacking interactions with the terminal G-qaurtet, however there have a been a small number of reports suggesting binding of small molecules by intercalation between G-tetrad layers.[92-95] Several anthraquinone analogues have been shown to interact with G-quadruplexes and

inhibit telomerase activity. The first compound to do so was a 2,6-diamidoanthraquinone (**Figure 1.17a**), which was shown by NMR spectroscopy to bind by an intercalative mode to a parallel 7mer G-quadruplex DNA molecule.[96]

The planar arrangement of aromatic rings in porphyrins has led researchers to propose that these compounds may bind to G-quadruplexes by stacking between the G-tetrads.[50] For example, Wheelhouse and co-workers used absorption spectrophotometry, as well as NMR and CD spectroscopy to show that the porphyrin TMPyP4 [tetra-(*N*-methyl-4-pyridyl)-porphine] (**Figure 1.17b**) was able to stabilise both parallel and anti-parallel G-quadruplex DNA.[97,98] In addition, these workers showed that TMPyP4 was able to inhibit telomerase activity.[97] Today more than 150 porphyrin compounds have been screened for their ability to interact with G-quadruplex DNA. These studies have shown that the overall charge, the length of the side-chains, and the presence of hydrogen bonding substituents, all play a role in determining the overall ability of the compound to bind to G-quadruplex DNA.[96]

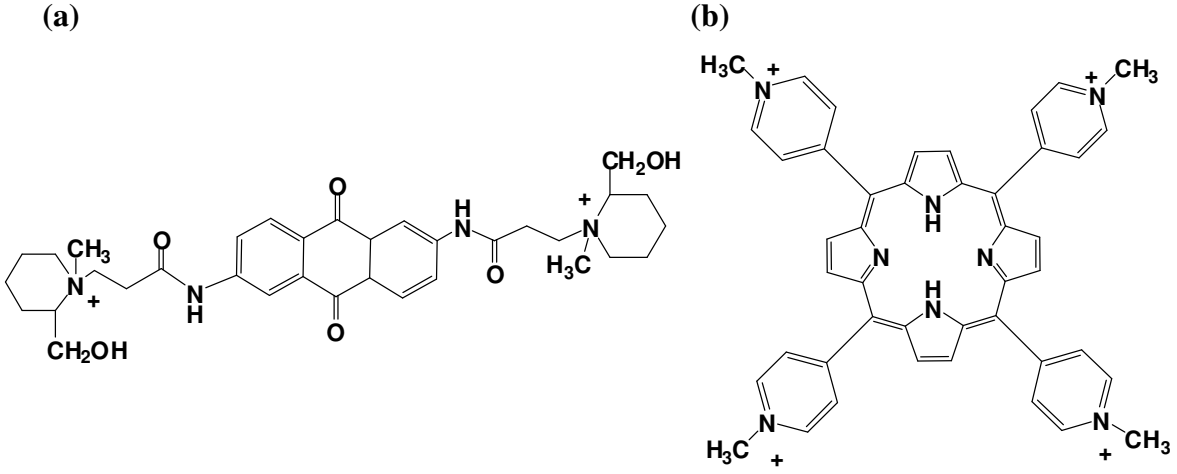

Figure 1.17: Examples of G-quadruplex DNA binding molecules: (a) 2,6-diamidoanthraquinone and (b) TMPyP4 [tetra-(*N*-methyl-4-pyridyl)-porphine].

Several well known duplex DNA binding compounds such as distamycin and Hoechst 33258, have also been demonstrated to bind to G-quadruplex DNA. For example, distamycin binds to parallel G-quadruplex DNA structures by stacking on the terminal G-tetrads and interacting with the flanking bases. Hoechst 33258 was shown to bind to G-quadruplex DNA formed in the promoter region of the human *c-myc* gene with a binding constant of ~10^6 M^{-1}.[99] However, it is not clear from this study how Hoechst 33258 interacts with the DNA. The intercalators daunomycin and ethidium bromide have also been shown to bind to G-quadruplex DNA. In the case of the former compound, X-ray crystallography showed that it prefers to stack onto a terminal G-tetrad rather than intercalate between the layers.[100] Different mechanisms have been proposed for the binding of ethidium bromide to G-quadruplex DNA. Whilst earlier studies reported ethidium bromide to interact with G-quadruplex DNA by intercalating between the G-tetrads,[101-104] more recent studies suggested that this is not correct and that instead alternative binding modes occur. [105-107]

1.7 Interactions of Transition Metal Complexes with G-Quadruplex DNA

The binding interactions between transition metal complexes and G-quadruplex DNA have not yet been fully investigated despite it being possible to prepare complexes with structural features that make them ideal for this purpose. This includes the ability of the metal centre to distribute ligands in a square planar arrangement ideal for optimising π-π stacking interactions with the G-tetrads. In addition, the binding of transition metal complexes to G-quadruplex DNA often occurs in such a way that the electropositive metal ion is positioned above the centre of a G-tetrad, enabling it to form stabilising electrostatic

interactions with the carbonyl groups of the guanines after replacing the potassium ion or other cation that normally occupies that site.[108] Reed and co-workers showed that several nickel(II) complexes of derivatised salphen ligands were able to inhibit telomerase by binding to and stabilising a parallel intramolecular G-quadruplex formed from four repeats of human telomeric DNA (**Figure 1.18a**).[108] Qualitative molecular modelling studies showed that the nickel complexes possessed structural and electrostatic properties which make them ideal for G-quadruplex DNA binding. This included the planar arrangement of aromatic rings in the salphen ligands, and the protonated piperidine substituents, which interact with functional groups in the grooves and loops of the quadruplex (**Figure 1.18b**). In addition, the Ni^{2+} ion was found to lie directly above the central ion channel of the quadruplex, allowing it to participate in electrostatic interactions that contributed to stabilising the metal/quadruplex complex. These compounds were found in telomerase inhibition assays to show $^{tel}EC_{50}$ values of ~ 0.1 μM.[108]

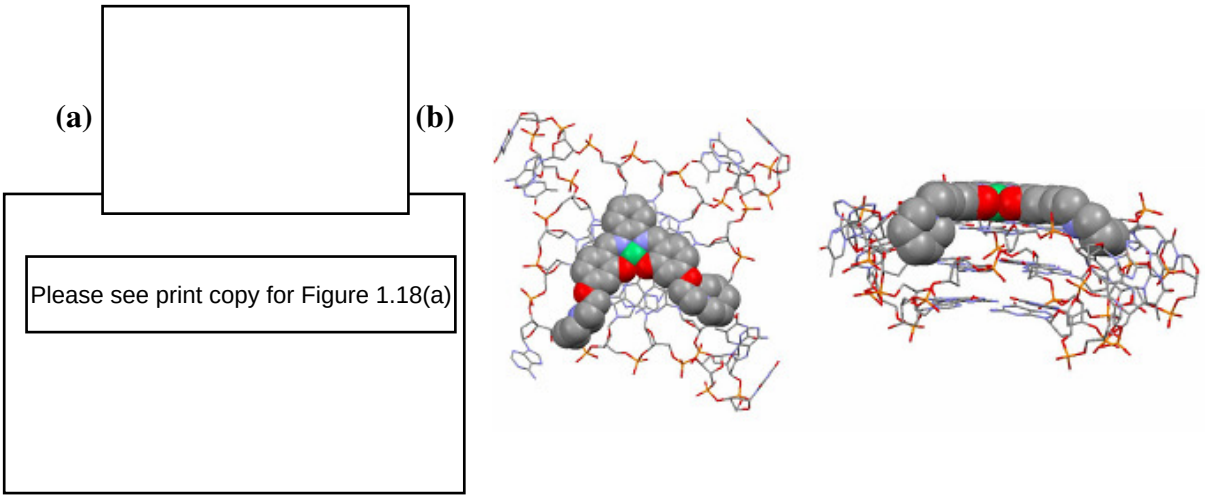

Figure 1.18: (a) Structure of the nickel(II) complexes studied by Reed and co-workers. (R=H or F).[108] (b) Two views of a complex formed by interaction of a nickel(II)-salphen complex (R= H) with a parallel intermolecular G-quadruplex formed from four repeats of human telomeric DNA.

Bertrand and co-workers examined the affinity and selectivity for G-quadruplex DNA of terpyridine complexes of several different metal ions.[93] The results of this study indicated that the copper and platinum complexes studied were much more potent G-quadruplex DNA binders compared to those containing zinc and ruthenium. It was proposed that this difference may originate from the different geometries of the metal complexes. Both the square planar platinum and square pyramidal copper complexes feature at least one flat face that can form favourable π-π interactions with G-tetrads. In contrast the trigonal bipyramidal and octahedral geometries of the zinc and ruthenium complexes are sterically hindered from forming similar suitable stacking interactions.[93]

In another recent study the dinuclear ruthenium compounds shown in **Figure 1.19** were found to display more favourable binding interactions to G-quadruplex DNA than duplex DNA.[109] Luminescence studies demonstrated that binding was accompanied by a "quadruplex light switch effect", which resulted in luminescence enhancements 2.5 times larger than those observed in analogous studies involving duplex DNA. It was suggested that the complexes either bind to the terminal ends of the DNA molecule, or alternatively thread through the loops on the sides of the G-quadruplex.

1.8 Techniques used to Investigate Binding of Metal Complexes to DNA

There are numerous techniques and methods which have been used to investigate the binding of metallointercalators to duplex and G-quadruplex DNA. In the following sections

the basic principles behind the techniques most widely used in this project are discussed, together with how they can be used to better understand metal/DNA interactions.

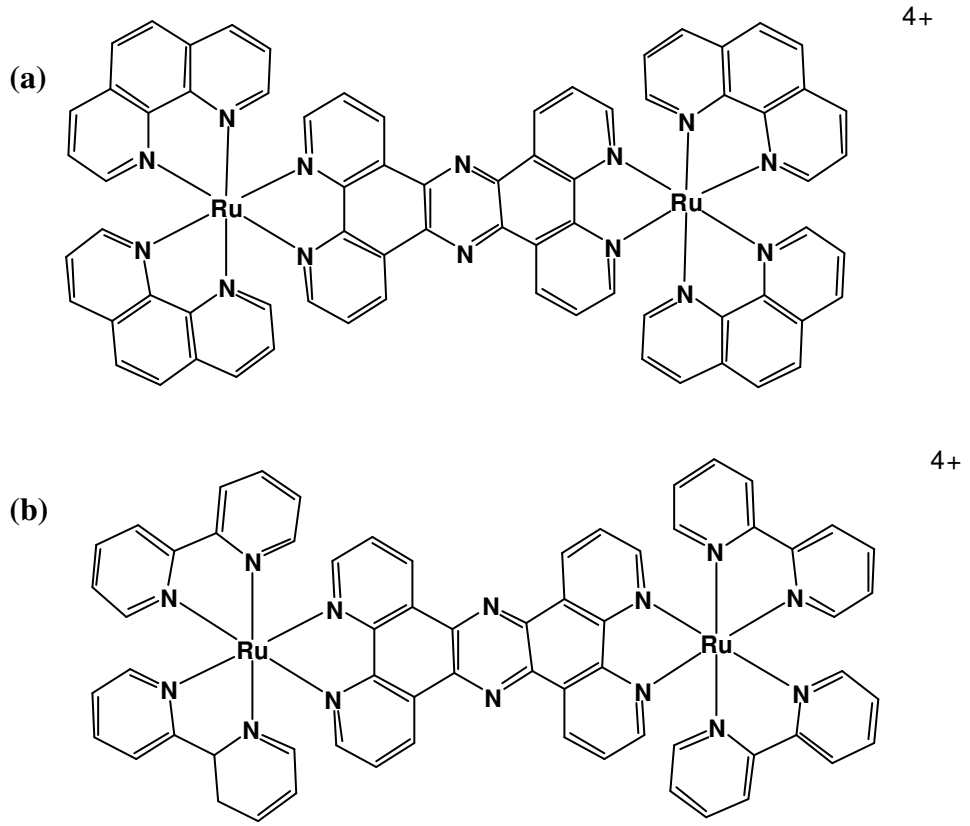

Figure 1.19: Structures of dinuclear ruthenium(II) complexes shown to bind selectivity to G-quadruplex DNA: (a) Δ,Δ-$[(phen)_2Ru(tpphz)Ru(phen)_2]^{4+}$ (tpphz = tetrapyridophenazine) and (b) $[(bpy)_2Ru(tpphz)Ru(bpy)_2]^{4+}$.

1.8.1 Circular Dichroism Spectroscopy

Circular dichroism (CD) is the difference in absorption of left and right circularly polarised light by asymmetric molecules. Nucleic acids exhibit CD signals owing to the helicity of their secondary structures and the presence of chiral carbon atoms in their nucleotides. There are many applications of CD spectroscopy for the study of nucleic acids including:[110]

- Characterisation of secondary structure;
- Detecting changes in conformation (e.g. B-DNA to Z-DNA);
- Analysis of interactions with small molecules.

The first two applications take advantage of the significant differences in appearance of CD spectra of the three types of duplex DNA. In the case of the most common form of DNA, B-DNA, the spectrum contains a postive band centred at approximately 275 nm, a negative band at 240 nm and another large positive band at 180-190 nm. Interconversion of B-DNA into one of the other two forms can be readily detected owing to significant changes in appearance of the CD spectra. For example, the CD-spectrum of Z-DNA displays a negative band at 290 nm and a positive band at 260 nm. In addition, it also displays a large negative signal in the 195-200 nm region, whereas the CD spectrum of B-DNA exhibits a large, positive signal in this region.

Octahedral metal complexes containing three bidentate ligands are typically prepared as racemic mixtures of Λ and Δ enantiomers, which can subsequently be resolved into the individual optical isomers that display mirror image CD spectra. Upon addition of either isomer to DNA, both the CD spectrum of the DNA and the metal complex are changed in a way that depends on the strength and geometry of the binding interaction.[111] In addition, when small achiral molecules bind to DNA, the former can exhibit induced CD signals (ICD) as a result of the interaction. Identification of an induced CD signal confirms that a small molecule does indeed bind to DNA. Furthermore, by monitoring changes in the CD spectrum of DNA caused by addition of increasing amounts of small molecules, it is possible to obtain additional information about the DNA binding mode of the latter.[110] For

example, if there is a change in intensity of the CD signal, but the shape of the spectrum remains the same, then it can be concluded that the mode of binding does not change even though the amount of small molecule bound may have changed. If however there is a change in the shape of the CD spectrum it can be concluded that there is a change in the nature of the DNA-small molecule interaction. This may occur, for example, as a result of the small molecule binding to a second binding site at high drug:DNA ratios. In addition to determining whether a small molecule binds to DNA by one or more binding modes, it is also possible to use CD spectroscopy to provide information about the actual nature of the binding event itself. Based on numerous studies of such systems it is generally now accepted that classical intercalation of small molecules into B-DNA results in enhancement of the CD signals of the latter at 275 nm and 240 nm due to strengthening of base stacking interactions and stabilisation of the right-handed helical conformation. In contrast, groove binding results in little perturbation of the base-stacking and therefore has little effect on the ellipticity of the CD bands.[112-118]

1.8.2 Absorption Spectral Studies

The absorption spectra of metal complexes contain a variety of features arising from d-d and charge transfer electronic transitions. Many studies have shown that the addition of DNA to metal complexes results in perturbations to these absorption bands, which most typically result in hypochromism (decrease in peak intensity) and bathochromism (shift in wavelength to lower energy).[78,109,119-125] While the magnitudes of both effects are believed to reflect the overall strength of the binding interaction, it is only the extent of hypochromism that is used to afford quantitative information in the form of binding constants. A variety of methods have been developed for accomplishing this task, including

procedures developed by Scatchard,[126] McGee and von Hippel,[127] Norden and Tjerneld,[128] Rodger,[129] Rodger and Norden,[110] Kumar and Asuncion,[130] and Stoutman and co-workers.[131] Another method which has been widely used to obtain binding constants is that originally developed by Benesi and Hidlebrand,[132] and more recently adapted by Meehan and co-workers,[133] to analyse the binding of polycyclic aromatic hydrocarbons to DNA. This method relies on the use of the following equation (1.1):

$$[DNA]/(\varepsilon_A-\varepsilon_F) = [DNA]/ (\varepsilon_B-\varepsilon_F) + 1/ K_b(\varepsilon_B- \varepsilon_F) \qquad \text{Eqn 1.1}$$

where [DNA], ε_A, ε_F and ε_B correspond to the concentration of DNA in base pairs, the observed extinction ((A_{obsd})/[drug]), the extinction coefficient for the free complex, and the extinction coefficient of the complex when saturated with DNA, respectively. Using this approach K_b can be obtained from a plot of $[DNA]/(\varepsilon_a-\varepsilon_f)$ vs [DNA], by dividing the slope of the line of best fit by the y-intercept. Many workers have used this facile approach to provide an overall binding constant for the interactions of a wide variety of metal complexes with CT-DNA.[78,109,119-125]

1.8.3 Gel Electrophoresis

Gel electrophoresis can be used to separate DNA molecules with different sizes, flexibility or charge. It involves applying an electric field across a gel matrix containing the biopolymers, which are negatively charged at p.H 7.0. The applied field causes the charged DNA molecules to migrate from the cathode towards the oppositely charged anode at a rate which are dependent on their size and conformation. The distance moved by the DNA is then measured under UV light after the gels have been stained using ethidium bromide. Supercoiled plasmid DNA moves towards the anode at a much faster rate than its relaxed

form, as the former is tightly compacted by forming left-handed superhelical twists. However, when supercoiled DNA is relaxed into its open circular form, the decrease in superhelical density causes a reduction in the rate of migration.[1]

The binding of small molecules to DNA affects its size and/or conformation and therefore its electrophoretic mobility. For example, the binding of metallointercalators can induce unwinding of the supercoiled DNA in order to accommodate the intercalative stacking of these molecules, and cause a reduction in electrophoretic mobility. At higher ratios of metallointercalator to DNA, binding can induce right handed superhelical twists into the DNA structure, which is accompanied by an increase in the rate of migration.[13] This is illustrated by the results shown in **Figure 1.20**.

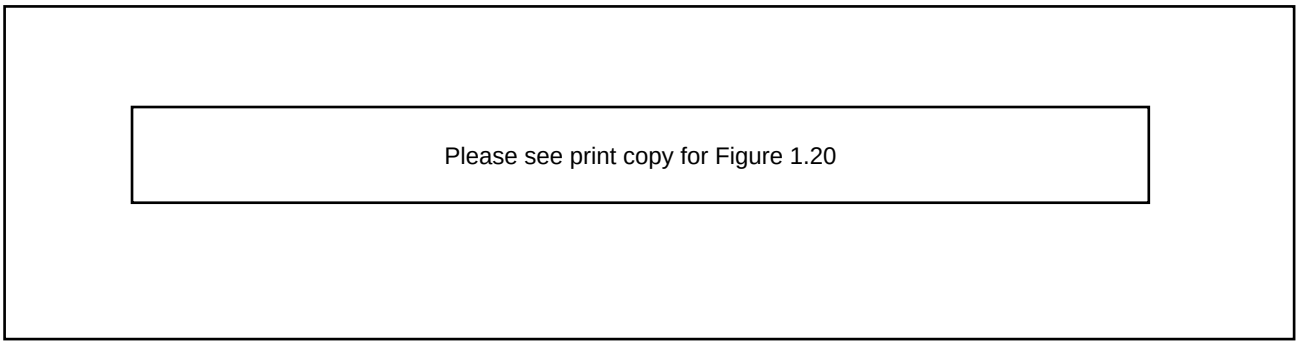

Figure 1.20: Gel electropherogram of plasmid DNA in the presence of different amounts of $[(\eta^6\text{-bip})RuCl(Et\text{-}en)]^{2+}$ (bip = biphenyl, Et-en = $Et(H)NCH_2CH_2NH_2$). Lanes 2-9 correspond to drug to nucleotide ratios of 0.004, 0.008, 0.017, 0.036, 0.05, 0.067, 0.076 and 0.084 to 1. Lanes 1 and 10 are controls corresponding to free DNA which has been partially relaxed. [134]

By comparing the extent of migration of supercoiled plasmid DNA in the presence of different metal complexes it is possible to first of all say something about the likely binding mode and, secondly, in the case of metallointercalators compare relative binding affinities. The former can be accomplished by estimating the intercalative unwinding angle induced

by the metal compound. Lippard and co-workers estimated an unwinding angle for supercoiled plasmid DNA in the presence of a variety of platinum complexes using the following equation 1.2:[135]

$$Ø = 18\sigma/r_b(c) \qquad \text{Eqn 1.2}$$

where Ø is the unwinding angle, σ the superhelical density and $r_b(c)$ the drug to nucleotide ratio corresponding to the point at which all negative supercoils from the DNA are removed. Beyond this point, the migration rate begins to increase again as positive supercoils are induced. For example, in **Figure 1.20** $r_b(c)$ would correspond to the drug nucleotide ratio for lane 5. It was found that the magnitude of the unwinding angle observed reflected the binding mode used by the platinum complexes and increased in the following order: monofunctional covalent binding < bifunctional covalent binding < monofunctional covalent binding plus intercalative binding < bifunctional covalent binding plus intercalative binding. In general, intercalative binding by a metal complexes has been found to produce significantly higher unwinding angles compared to monofunctional or bifunctional covalent binding.[13]

1.9 Electrospray Ionisation Mass Spectrometry of Small Molecule Binding Interactions with B-DNA

Mass spectrometry (MS) is an analytical technique that can be used to study molecules of different sizes ranging from small organic molecules to polymers such as proteins and nucleic acids. It can provide structural information as well as insight into reaction mechanisms. For analysis by MS, molecules must be converted to gas-phase ions that can be separated according to their mass-to-charge ratios (*m/z*).[136-141] Earlier ionisation

techniques such as electron ionisation (EI)[142] and chemical ionisation (CI)[143] were limited to analysis of volatile compounds with low molecular masses (≤ 1000 Da). For EI and CI, ionisation of volatile molecules is accomplished by direct exposure to a beam of electrons or through collision with the ions of a reagent gas, respectively. Softer ionisation techniques such as field desorption (FD),[144,145] plasma desorption (PD),[146] and fast atom bombardment (FAB),[147] were later introduced during the late 1960s and early 1980s to enable the ionisation of thermally labile non-volatile compounds. Relatively recent and highly useful ionisation methods used for the mass spectrometric analysis of large biomolecules include matrix assisted laser desorption ionisation (MALDI)[148,149] and electrospray ionisation (ESI).[150,151] Both methods allow not only the transfer of large biomolecules from the solution phase to the gas phase, but also can maintain non-covalent complexes with minimal dissociation.[138]

The utilisation of ESI-MS for the study of non-covalent binding interactions of biomolecules has been described comprehensively in several reviews.[136-141] The ESI process itself can be divided into 3 steps: droplet formation, droplet fission and the production of desolvated ions (**Figure 1.21**). Droplet formation occurs at the capillary that contains the solution to be ionised. A strong electric field is applied to the capillary that causes an electrophoretic movement of ions inside the liquid followed by the release of charged droplets at the tip. The droplets are charged because they contain excess ions of one polarity, which depends on the sign of the applied potential. For example, positive ions such as $[M + nH]^{n+}$ are formed when a positive voltage is applied to the capillary and negative ions such as $[M - nH]^{n-}$ are formed when a negative voltage is applied. For DNA a negative potential is applied because nucleic acids are negatively charged in solution at

natural pH levels due to their phosphodiester backbone being fully deprotonated.

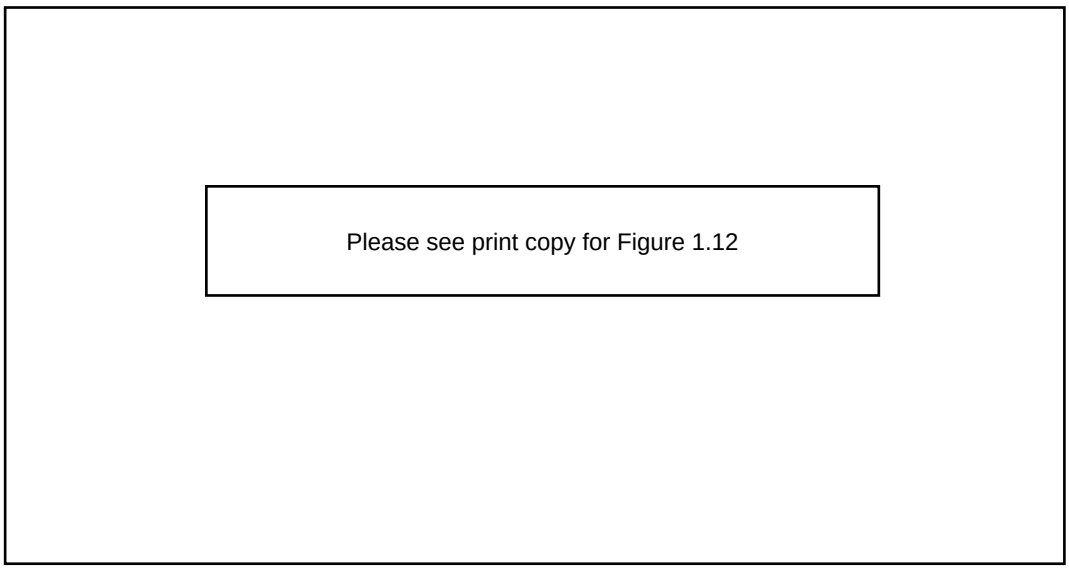

Figure 1..21: A schematic representation of ion formation in ESI.[152]

During droplet fission droplets travel from the capillary to the cone of the mass spectrometer. There the droplets shrink as solvent evaporation occurs due to collisions with ambient gas molecules. When the surface tension of the droplets can no longer sustain the charge (Rayleigh limit), the droplets explode (Coulombic explosion) producing a series of smaller daughter droplets. The daughter droplets undergo evaporation and fission themselves to the point where the droplets are free of solvent and consist of isolated ions. The mechanism by which final formation of the lone desolvated ions occurs is still under debate, with models based on ion evaporation (ion-evaporation model)[153] and complete solvent removal (charged-residue model) being proposed.[154] The solvent free ions are then transported through a pressure gradient to a high vacuum environment required for mass analysis. There the ions are separated according to their *m/z* ratio using one of several types

of mass analysers including ion trap, quadrupole (or triple quadrupole), time-of-flight (TOF), or quadrupole time-of-flight (Q-TOF) mass analysers.[136,140,155]

Electrospray ionisation mass spectrometry (ESI-MS) enables a considerable amount of data to be acquired in a short period of time (less than one minute) using only picomole to femtomole quantities of sample. Other techniques including NMR spectroscopy, CD spectroscopy and X-ray crystallography in general require longer sample preparation and data acquisition times, and also require larger amounts of sample (micromoles) for analysis. Another significant advantage of ESI-MS for the analysis of biomolecular interactions is its specificity. ESI-MS allows for comparison of different binding interactions between DNA and small molecules based on differences in their structural and/or energetic properties. This includes determination of the stoichiometry of non-covalent complexes present in complex reaction mixtures.

The first observation of intact oligonucleotide duplexes by ESI-MS was in 1993 by Ganem *et al.*[156] and Light-Wahl *et al.*[157] The stability of duplex DNA during ESI-MS has enabled this technique to be extensively used for studying non-covalent DNA binding interactions. Gale and co-workers were the first to report the observation of DNA-drug non-covalent complexes by ESI-MS.[158] They detected complexes formed between the minor groove binders distamycin, Hoechst 33258, and pentamidine, and the DNA sequence $d(CGAAATTTGCG)_2$. Distamycin was shown to bind in both a 1:1 and 2:1 ratio, consistent with NMR results obtained for the same DNA sequence and identical distamycin to DNA ratios.[158]

By comparing the relative abundances of ions corresponding to different DNA-drug species in a mass spectrum, ESI-MS can be used as a screening method for developing a binding affinity profile for different drugs with a particular DNA sequence, as well as for evaluating the DNA sequence selectivity of the drug.[136,159-162] Competitive binding of drugs to DNA is also readily analysed by ESI-MS, and is another method of obtaining information about relative binding affinities and specificities.[162-164] The preferential binding of classical minor groove binders to AT-rich DNA sequences, and of classical intercalators to GC-rich DNA sequences has also been confirmed using ESI-MS.[136,159-162] Gabelica and co-workers showed that ESI-MS was able to detect the selective binding of Hoechst 33342 and Hoechst 33258 to DNA molecules containing subtle differences in their sequences.[159] By using the 12mer DNA strands dGGGG(A/T)4GGGG it was shown that the binding affinity of both drugs was dependent on the central four base sequence, and increased in the order: AAAA < ATAT < AATT.

Most mass spectrometers can also be used to perform tandem mass spectrometry (MS/MS) experiments. In these experiments, ions of a given mass are isolated and fragmented in a process called collision-induced dissociation (CID).The resulting fragments are subsequently analysed. MS/MS experiments can provide information about the structure and stability of non-covalent DNA complexes, and the gas phase stability of such complexes can be compared with that in solution to seek correlations and insights about intrinsic binding events. Gale and Smith used MS/MS experiments to show that 1:1 complexes formed between distamycin and dsDNA were less stable than 2:1 complexes.[164] The increased stability of the 2:1 complexes was attributed to additional stacking interactions between the two distamycin molecules in the DNA minor groove. Importantly

the above observation was also in agreement with what had been observed in solution studies. Gabelica, De Pauw and Rosu performed MS/MS experiments on non-covalent complexes formed between DNA and either netropsin or Hoechst 33325, which suggested that the DNA-drug complexes were more stable than the duplex alone.[165] This result correlates with what is known from solution phase studies, namely that minor groove binders can stabilise the double helical structure of DNA by forming hydrogen bonds and van der Waals interactions with both strands.[139] They also observed that the Hoechst 33258/DNA complex dissociated at lower collision energies than the netropsin/DNA complex. This result is in accord with a recent crystallographic study, which suggested that netropsin forms a more stable DNA complex than Hoechst 33258 because it forms more hydrogen bonds with the duplex.[165] During a MS/MS study of the stability of non-covalent complexes formed by a range of drugs with self complementary 6-12mer DNA duplexes, Gross and co-workers showed that the collision energy at which half the non-covalent complexes underwent dissociation correlated with the number of hydrogen bonds involved in stabilising the complex.[160] This experiment therefore provides further evidence that ESI-MS can be used to obtain information about the relative stability of non-covalent complexes in solution.

Studies of the binding interactions of metal complexes with DNA using ESI-MS have been limited, despite its great potential as an analytical tool.[77,139,160] One of the first such studies was by Urathamakul and co-workers, who investigated the DNA affinity and sequence selectivity of ruthenium metallointercalators with the formula $[Ru(phen)_2(L)]^{2+}$ (L = dppz, phen, dpqc and dpq; (dpqc = dipyrido[3,2-*a*:2',3'-c](6,7,8,9-tetrahydrophenazine) and dpq = dipyrido[3,2-*d*-2',3'-*f*]quinoxaline).[77,166] Competition experiments performed using pairs of

the ruthenium complexes and a DNA duplex were used to confirm the order of relative binding affinities determined by preliminary experiments in which increasing amounts of metal complex were added to the DNA. Other competition experiments were performed in which the ruthenium complexes competed for binding sites on the DNA molecule with the well characterised DNA binding drugs daunomycin and distamycin, in order to provide further information on the DNA binding modes of the metal complexes.

1.10 Electrospray Ionisation Mass Spectrometry of Small Molecule Binding Interactions with G-quadruplex DNA

One of the earliest observations of G-quadruplex DNA by ESI-MS was reported by Goodlett *et al*. who examined the stability of the G-quadruplex formed by $d(CGCGGGGGGCG)_2$ in a sodiated solution.[158] When the sample was desalted and analysed by ESI-MS, only ions corresponding to single-stranded DNA species were observed. This observation agrees with other experimental evidence that shows that G-quadruplex formation is only possible in the presence of suitable cations. Rosu and co-workers later reported an ESI-MS study of three different quadruplexes: a four stranded parallel quadruplex $[d(TGGGGT)]_4$, an antiparallel dimer $[d(GGGGTTTTGGGG)]_2$, and a intramolecular monomeric folded quadruplex with the sequence $d((GGG(TTAGGG)_3)$ that mimics the human telomere sequence.[167] These experiments were performed in solutions containing relatively high (150 mM) concentrations of ammonium acetate, which has proved to be an excellent electrolyte for ESI-MS studies of nucleic acids. This is because the two components of the electrolyte form volatile products upon undergoing proton exchange reactions with other components of the sample. Mass spectra of the first two types of G-quadruplex DNA molecules showed ions containing n-1 ammonium cations,

where n is the number of consecutive G-tetrads in the quadruplex. This provides strong evidence that the observed ions are in fact from quadruplex DNA, with the ammonium ions playing an integral role in stabilising the quadruplex structure. CD data were also obtained showing that the mimic of the human telomere DNA sequence also formed a stable quadruplex structure in solution. However, the absence of ions containing the expected number of ammonium ions bound to DNA in its mass spectrum made it impossible to determine unambiguously whether or not it had in fact formed. By using ion-mobility mass spectrometry in combination with molecular dynamics calculations, Bowers and co-workers were later able to confirm that single-stranded intramolecular G-quadruplexes do maintain their structural integrity in the mass spectrometer after the evaporation of the solvent, either with or without the presence of non-covalently bonded ammonium ions.[37] Based on their findings they proposed that ionic stabilisation of intramolecular G-quadruplexes is not required for these structures to survive in the gas phase.

A small number of reports have described the use of ESI-MS for examining the binding interactions of small molecules to G-quadruplexes.[159,168-171] The first such study was that of Brodbelt and co-workers, who compared the binding of the organic compounds Tel01, distamycin A and diethylthiocarbocyanine iodide (DTC), to doubled-stranded DNA and a parallel DNA quadruplex $[d(TTGGGGGT)]_4$.[169] By examining dissociation patterns of ions arising from non-covalent complexes in MS/MS experiments, evidence was obtained that supported the results of previous solution studies that suggested Tel01 interacts with G-quadruplex DNA by end-stacking with a guanine tetrad, whereas distamycin A and DTC interacted by binding to the grooves of the quadruplex.

1.11 Transcription of DNA

The transfer of genetic information from DNA to proteins occurs in two major stages: transcription and translation.[1,18] Transcription is the synthesis of specific mRNA molecules using the nucleotide sequence of DNA as a template, in a reaction catalysed by the enzyme RNA polymerase. Translation occurs at the ribosome, and results in the genetic information encoded in the newly synthesised mRNA molecule being used to correctly assemble amino acids into a polypeptide chain that will eventually form a specific protein.[18] For prokaryotes and eukaryotes the basic mechanisms of transcription and translation are similar; however there are specific differences (**Figure 1.22**). Many diseases, in particularly cancer, are associated with aberrant transcription and/or translational behaviour within cells.[172-175] Actinomycin, cisplatin and many anthracycline antibiotics are chemotherapeutic drugs whose mode of action involves modifying specific steps during DNA transcription.

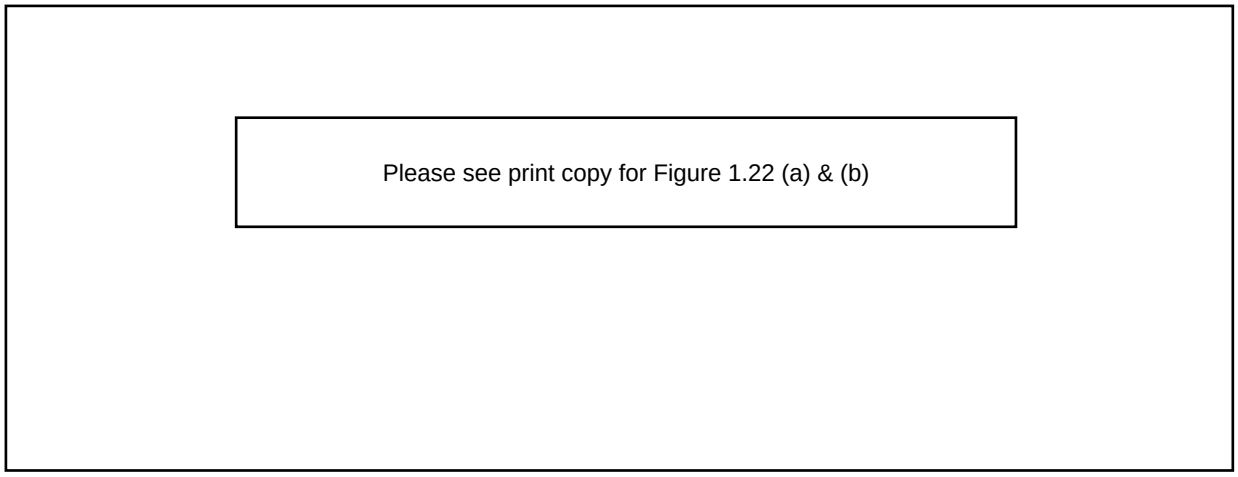

Figure 1.22: Schematic illustration of the general flow of genetic information within: (a) a prokaryotic cell and (b) a eukaryotic cell. In prokaryotic cells, mRNA is sent to ribosome for translation without additional processing. In a eukaryotic cell transcription and translation occur in the nucleus and cytoplasm, respectively, and the original RNA transcript (pre-mRNA) is processed in various ways by enzymes before leaving the nucleus.[176]

1.11.1 Transcription Factors

Within eukaryotic cells, transcription factors are proteins that mediate the attachment of the DNA template to RNA polymerase. Irregular transcription factor behaviour has been recognised to contribute to the onset of oncogenic transformation and cancer development. For example, the transcription factor nuclear factor-κB (NF-κB) assists in regulating the expression of numerous immune specific genes and cytokines, and also in controlling expression of genes involved in cellular proliferation and suppression of apoptosis.[177] Irregular NF-κB activity has been associated with a wide variety of cancers including those of the prostate,[178] breast[179] and lung.[180] Overexpression of the transcription factor c-myc is one of the most common alterations in human cancers, yet it is not clear how this transcription factor acts to promote malignant transformation.[181] The c-myc transcription factor is a primary regulator of cell cycling and has been found to be deregulated in hematopoietic (blood cell) malignancies, Burkitt's lymphoma, melanoma and various other carcinomas.[182-186] Other transcription factors for which irregular activity has been associated with the onset of cancer are listed in **Table 1.2**.

PU.1 (also known as SPi-1) is a haematopoietic ETS family transcription factor that is required for the development of macrophages and granulocytes as well as B and T lymphocytes.[187] The ETS family is comprised of more than 45 transcription factors that share a unique 85 amino acid DNA binding domain, the ETS domain. This binding domain is a winged helix-turn-helix motif that recognises a 5'-GGAA/T-3' core sequence and binds to dsDNA with a 1:1 stoichiometry.[174,188] PU.1 is made up of 261 amino acids, and contains a terminal protein/protein interaction domain and a C-terminal DNA-binding ETS domain.

Table 1.2: Transcription factors associated with cancer development.

Please see print copy for Table 1.2

The co-crystal structure of a PU.1/DNA complex shows that the protein binds to DNA over a 10 base pair region by inserting its recognition helix into the major groove at the core consensus sequence where two arginine residues make direct and water-mediated base-specific contacts.[212] Regions of the ETS domain flanking the recognition helix interact with phosphates along the minor groove both upstream and downstream from the DNA binding site, further stabilising the complex and bending the DNA around the protein.[212] Beyond the critical requirement of a central 5'-GGAA/T-3' binding region, PU.1 tolerates a large number of DNA sequences with a diverse combination of bases on both sides. Despite this, PU.1 shows considerable DNA selectivity due to differential protein/DNA contacts in the

flanking sequences that modulate the orientation of the ETS recognition sequence and the stability of the ETS/DNA complex.[213-215] Deregulation of PU.1 during haemotopoiesis has been related to the occurrence of erythroid and acute myeloid leukemias (AML).[216-218]

1.11.2 Transcription Therapy

There is currently considerable research effort focused on the development of therapies that will antagonise anomalous activity of transcription factors.[172,175,219,220] For example, small molecules may be able to inhibit oncogenic transcription factor activity by non-covalently binding either to the transcription factor or its DNA recognition sequence, thereby inhibiting interactions between the two.[220] Minor groove binding drugs such as distamycin A, netropsin and Hoechst 33258 have been shown to competitively inhibit binding of the TATA box binding protein (TBP) to its A/T rich target sequence, thereby providing evidence towards proof of concept of this approach.[221] The binding of TBP to its DNA recognition site is also inhibited by structural distortions to the latter caused by intercalators such as nogalamycin and hedamycin.[221] These drugs have also been shown to inhibit growth response factor 1 (EGR1) binding to its GC rich consensus sequence.[221]

Covalent modification of specific DNA sequences can create new binding sites for transcription factors, thus hijacking them from their normal functions. For example, DNA modified by cisplatin is able to lure TBP away from its normal promoter sequence. This hijacking mechanism has been proposed as a possible explanation for the anticancer activity of platinum drugs.[222]

Polyamides are a promising class of potential therapeutics which bind specifically to the minor groove of dsDNA and inhibit transcription both *in vitro* and *in vivo*.[223,224] A DNA-binding polyamide has been shown to antagonise Androgen Receptor (AR) mediated gene expression.[225] The AR is a transcription factor involved in the development of prostate cancer in both hormone-sensitive and hormone-refractory disease. The polyamide inhibited androgen-induced expression of PSA (prostate specific antigen) and several other AR-regulated genes in cultured prostate cancer cells. Inhibition occurred as a result of interactions between the polyamide and the consensus Androgen Response elements, which prevents the latter being able to bind to the Androgen Receptor.

Whilst transcription factors target the major groove of DNA in their binding interactions, polyamides disrupt transcription factor binding to DNA by disrupting minor groove contacts. Surprisingly there are only a few strategies that use the major groove to inhibit the initiation of transcription.[80] The greater functionality of the DNA major groove versus the minor groove, combined with the former being the principle transcription factor binding region, makes it an attractive target for therapeutic design. Metal complexes that can intercalate into the DNA major groove are therefore potentially useful for transcription therapy.[72,166,226,227] Whilst there have been many thorough studies investigating the binding interactions and mechanisms by which metal complexes interact with DNA, only a few have investigated what effects the metal complexes have on DNA transcription.[80,228-231]

Turro and co-workers used transcription inhibition assays to show that the rhodium metal complexes $[Rh(phen)_{3-n}(L)_n]^{3+}$ (L = phi, bqdi = 1,2-benzoquinone diimine n = 0, 1, 2) and $[Ru(phen)_{3-n}(phi)_2]^{2+}$ (n = 0, 1, 2) were capable of inhibiting DNA transcription.[229,231] It was found that the concentration required to cause 50% inhibition of transcription varied from

one metal complex to another, and that complexes possessing two quinone diimine ligands in their coordination sphere displayed a greater degree of inhibition than complexes possessing a single such ligand (e.g. $[Ru(phen)_2(phi)]^{2+}$) or complexes containing no quinone diimine ligands (e.g. $[Ru(phen)_3]^{2+}$).

Further evidence that metal complexes can selectively inhibit binding of a transcription factor to DNA was provided by Odom *et al.*, who used gel mobility shift assays, to monitor the ability of Λ-1-$[Rh(MGP)(phi)]^{5+}$ (**Figure 1.14a**) to inhibit the binding of the transcription factor yeast Activator Protein 1 (yAP-1), to a modified activator recognition region that included both the yAP-1 binding region and a Λ-[1-$Rh(MGP)(phi)]^{5+}$ binding site.[80] The results of the study showed that the rhodium complex was able to produce 50% inhibition of binding by the transcription factor to its DNA recognition sequence at a concentration of 120 nM. Similar experiments performed using the parent complex $[Rh(phen)_2(phi)]^{3+}$ required much higher concentrations to afford the same degree of inhibition of DNA/protein binding.[80] The greater degree of inhibition of transcription factor binding by Λ-1-$[Rh(MGP)(phi)]^{5+}$ was attributed to the greater DNA sequence specificity of the former complex. Whilst $[Rh(phen)_2(phi)]^{3+}$ displays shape selectivity towards 5'-pyrimidine-purine-3' sequences within the major groove, it displays only a small degree of sequence selectivity.[232] The pendant guanidinium arms present in Λ-1-$[Rh(MGP)(phi)]^{5+}$, however, enable strong and site-selective binding to the sequence 5'CATATG-3' present in the modified activation region. The above findings demonstrate the potential of metal complexes as therapeutic agents that act by modulating transcriptional activity.

Despite the above promising results, only one transcription factor targeting agent (Oncomyc-NG/Resten-NG, AVI Biopharma) has to date made it to clinical trials, and there

are only a small number of ongoing preclinical studies using similar therapeutic agents with animal models.[175] This is partially because there are a number of challenges to developing a successful cancer therapy based on antagonising transcription factor activity, including finding an ideal transcription factor to target. The ideal target would be a transcription factor that is over-expressed in cancer cells and the main promoter of cell malignancy. It should also have specificity, so that there is a low risk of cross reactivity with off-target genes or proteins. Furthermore, the ideal transcription factor target would be easily accessible to drugs present in the circulatory system.[175]

1.12 Thesis Synopsis

It is now generally accepted that ESI-MS can be used to accurately analyse non-covalent binding interactions between small organic molecules and DNA.[139,158,161,164,165,233] However, while there have been many investigations into the non-covalent binding of metal complexes to DNA, only a small number of these studies have used ESI-MS.[77,166,170,234]

Chapter 3 of this thesis presents results obtained from ESI-MS studies into the binding interactions between the nickel complexes $[Ni(phen)_2(L)]^{2+}$ (L = phen, dpq, dpqc, dppz), and a hexadecamer duplex DNA molecule. These results were used to derive an order of relative binding affinity for the nickel complexes, which was then compared to similar series obtained using several other spectroscopic and biochemical techniques in order to further validate the use of ESI-MS for examining these types of systems. The results of these studies were also compared to those obtained in an identical series of experiments performed using the analogous ruthenium complexes $[Ru(phen)_2(L)]^{2+}$ (L = phen, dpq, dpqc, dppz). This study was conducted in order to determine what effect, if any, changing

the central metal ion from ruthenium(II) to nickel(II) has on the binding interactions of these types of metal complexes with dsDNA.

In chapter 4 the best conditions for acquiring ESI mass spectra of the quadruplexes $(GGGGTTTTGGGG)_2$ (Q2) and $(TTGGGGGT)_4$ (Q5) are described. The MS/MS profiles of the above quadruplexes were also investigated, in order to observe what effect the number of strands and number of G-tetrads that make up the quadruplex molecule have on the gas phase stability of its ions in different charge states. Chapter 4 also describes experiments performed to determine if ESI-MS can be used to characterise non-covalent complexes formed between metal complexes and quadruplex DNA. In addition, by performing these studies with the same complexes used previously in binding studies with duplex DNA, information about the relative affinities of the metal complexes towards dsDNA and qDNA was obtained, as well as whether similar binding modes were involved.

One of the potential applications that has been proposed for metal complexes such as those discussed throughout this thesis is as anticancer agents. For example, it might eventually be possible to prevent the onset of tumour formation by using metal complexes similar to $[Ru(phen)_2(dppz)]^{2+}$ or $[Pt(5,6\text{-}Me_2phen)(S,S\text{-}dach)]^{2+}$ to block key binding interactions between transcription factors and their DNA binding partners. Chapter 5 highlight this possibility, by describing the application of ESI-MS for monitoring the effect of the above metal complexes on interactions between the DNA-binding domain of the transcription factor PU.1 and DNA molecules containing its consensus sequence.

Chapter 2
Materials and Methods

2.1 Materials

All chemical solvents and reagents used were of the highest grade commercially available. MilliQ^{TM} water from Millipore (Molsheim, France) was used in all experiments. **Table 2.1** lists the metal complexes that were used in this study. Most ruthenium and platinum compounds were kind gifts from Assoc. Prof. Janice Aldrich-Wright (School of Science, Food and Horticulture, University of Western Sydney, Australia). The ETS domain of mouse transcription factor PU.1 (PU.1-DBD, 113 amino acids from 158 - 270) was a kind gift from Dr Joel Mackay (School of Molecular and Microbial Biosciences, The University of Sydney, Australia).

Table 2.1: Metal complexes that were used in this study.

Metal complex	Mass (Da)
Mononuclear Ruthenium Complexes	
$[Ru(phen)_3]Cl_2$	712.6
$[Ru(phen)_2(dpq)]Cl_2$	764.6
$[Ru(phen)_2(dpqc)]Cl_2$	814.7
$[Ru(phen)_2(dppz)]Cl_2$	818.7
Mononuclear Nickel Complexes	
$[Ni(phen)_3]Cl_2$	670.2
$[Ni(phen)_2(dpq)]Cl_2$	722.2
$[Ni(phen)_2(dpqc)]Cl_2$	776.3
$[Ni(phen)_2(dppz)]Cl_2$	772.3
Mononuclear Platinum Complexes	
$[Pt(en)(phen)]Cl_2$	506.3
$[Pt(en)(4,7\text{-}Me_2phen)]Cl_2$	534.4
$[Pt(en)(3,4,7,8\text{-}Me_4phen)]Cl_2$	562.4
$[Pt(5,6\text{-}Me_2phen)(S,S\text{-dach})]Cl_2$*	586.4

* dach = 1,2-diaminocyclohexane

$[Ru(phen)_3]Cl_2$, boric acid, chloroform, daunomycin, 1,2-diaminocyclohexane (mixture of cis and trans isomers), ethylenediaminetetraacetic acid (EDTA, free acid form), formamide, sodium hydroxide, sucrose, tetrabutylammonium hexafluorophosphate, tetrabutylammonium chloride (TBACl), 3-(*N*-morpholino)propanesulfonic acid (MOPS), nickel(II) chloride hexahydrate, 1,10-phenanthroline-5,6-dione, 1,10-phenanthroline, 1,2-phenylenediamine, sodium bromide and sodium sulfate (anhydrous) were purchased from Sigma-Aldrich (St Louis, USA). Cesium iodide, ethylenediamine and glycerol were obtained from Fluka (Buchs, Switzerland). Ammonium acetate (NH_4OAc), acetic acid, acetonitrile, methanol, nitric acid (70% *w/v*), ethanol, dichloromethane (DCM), diethyl ether (anhydrous), sodium chloride, sulfuric acid (98%) and toluene were purchased from Ajax Finechem (Seven Hills, Australia). Bromophenol blue and tris(hydroxymethyl)aminomethane (Tris base) were purchased from ICN Biomedicals (now MP Biomedicals, Aurora, USA). $ZnSO_4.7H_2O$ was obtained from Standard Laboratories Pty. Ltd (Melbourne, Australia) and $FeSO_4.7H_2O$ from BDH chemicals Ltd (Poole, England).

Ribomax™ large scale RNA production system and pGEM® express positive control template were obtained from Promega (Madison, USA). Dialysis tubing (3,500 molecular weight cut-off) was purchased from Crown Scientific (Moorebank, Australia). Ethidium bromide and agarose were obtained from Bio-Rad (Hercules, USA). Nanospray capillaries (Au/Pd coated, medium size) were purchased from Proxeon (Odense, Denmark). $CDCl_3$ and CD_3OD were obtained form Cambridge Isotope Laboratories Inc. (Andover, Massachusetts, USA). All oligonucleotides (deprotected) were obtained from Geneworks (Adelaide, South Australia).

2.2 Synthesis of Nickel Complexes

2.2.1 Synthesis of Phendione

1,10-Phenanthroline-5,6-dione (phendione) was synthesised following a method adapted from Hiort *et al*.[87] In a 100 ml round bottom flask equipped with a reflux condenser, 1,10-phenanthroline (5.0 g, 27.8 mmol) was dissolved in portions during stirring in 30 ml of concentrated sulfuric acid. Sodium bromide (2.5 g, 24.3 mmol) was then added followed by 70% nitric acid (15 ml). The mixture was brought to reflux for 40 min, the heat reduced and the reflux condenser removed. The mixture was boiled gently for 15 min to ensure that all the bromine vapours had escaped.

After the solution had cooled to room temperature it was poured onto 400 g of ice. Approximately 120 ml of 10 M sodium hydroxide was slowly added to the solution to bring the pH to 10.0 - 10.5 and then the solution was allowed to stand for 40 min. The turbid orange solution was heated to ensure that all the solids had dissolved. After the solution had cooled to room temperature, ~ 2 g of sodium chloride was added and the solution was left to stand. After 1 hour the solution was extracted using 6 × 100 ml DCM, and the combined organic phase was washed with 2 × 50 ml of water and then dried over anhydrous sodium sulfate, filtered and evaporated under reduced pressure. The resulting orange crystals were recrystallised using a minimum amount of toluene giving fine orange needles of phendione (yield 2.2 g, 44%). ^{1}H NMR (300 MHz, $CDCl_3$): δ (ppm) 9.10 (dd, J = 4.8, 1.8 Hz, 2H); 8.51 (dd, J = 8.1, 1.8 Hz, 2H); 7.59 (dd, J = 8.1, 4.8 Hz, 2H).

2.2.2 Synthesis of Quinoxaline and Phenazine Ligands

The preparation of the dppz ligand was adapted from the method described by Dupureur and Barton.[235] A mixture of phendione (520 mg, 3 mmol) and ethanol (20 ml) was refluxed until all the phendione had dissolved (~20 min). To the mixture, 1,2-phenylenediamine (405 mg, 3.75 mmol) was added and the reaction mixture refluxed for a further 20 min. The solution was cooled to room temperature then placed on ice where it yielded a yellow crystalline solid. The crude product was isolated by filtration and subsequently recrystallised from chloroform (yield 590 mg, 84%). ^{1}H NMR (300 MHz, CD_3OD): δ (ppm) 9.46 (dd, *J* = 8.1, 1.5 Hz, 2H); 9.08 (dd, *J* = 4.5, 1.5 Hz, 2H); 8.24 (d, *J* = 6.3 Hz, 2H); 7.94 (d, *J* = 6.3 Hz, 2H); 7.80 (dd, *J* = 8.1, 4.5 Hz, 2H).

The dpqc and dpq ligands were synthesised using methods adapted from those described by Collins *et al.*[236] The dpqc ligand was prepared by refluxing phendione (870 mg, 4.80 mmol) and 1,2-diaminocyclohexane (mixture of *cis* and *trans* isomers) (602 mg, 5.3 mmol) in ethanol (60 ml) for 2 hr. The resulting yellow solution was reduced in volume and refrigerated overnight, yielding a pale yellow solid. The crude product was filtered and recrystallised from methanol. (yield 480 mg, 35%). ^{1}H NMR (300 MHz, CD_3OD): δ (ppm) 9.30 (dd, *J* = 11.0, 6.4 Hz, 2H); 9.57 (dd, *J* = 8.0, 1.4 Hz, 2H); 7.8 (dd, *J* = 11.0, 8.0 Hz, 2H); 3.3 (m, 4H); 2.1 (m, 4H).

The dpq ligand was prepared by stirring a mixture of 1,10-phenanthroline-5,6-dione (1.0 g, 4.84 mmol) and ethylenediamine (0.4 g, 6.89 mmol) in ethanol (350 ml) for 2 h at 40 ^{o}C and subsequently at room temperature overnight. The resulting solution was reduced in volume by rotary evaporation at 50 ^{o}C, yielding a cream-coloured product and left to stand

overnight. The crude product was then filtered and washed with 100 ml of methanol/water (10/90) and 50 ml of acetone followed by recrystallisation from methanol (yield 320 mg, 30%). ^{1}H NMR (300 MHz, CD_3OD): δ (ppm) 9.45 (dd, *J* = 8.1, 1.5 Hz, 2H); 9.18 (dd, *J* = 5.2, 1.5 Hz, 2H); 9.01 (d, *J* = 5.8 Hz, 2H); 7.90 (dd, *J* = 8.1, 4.5 Hz, 2H).

2.2.3 Synthesis of $[Ni(phen)_2(H_2O)Cl]Cl.H_2O.CH_3CN$

This compound was prepared using an adaptation of the method of Zhong *et al.*[237] $NiCl_2.6H_2O$ (1.19 g, 0.005 mol) and 1,10-phenanthroline monohydrate (1.80 g, 0.01 mol) were homogenised using a mortar and pestle forming a pale blue coloured compound. The crude product was recrystallised using approximately 100 ml of acetonitrile, resulting in the formation of light blue crystals over approximately 3 days. The final product was isolated by filtration, washed with ethanol and ether and dried under vacuum, (yield 184 mg, 65%).

2.2.4 Synthesis of $[Ni(phen)_3]Cl_2$

$NiCl_2.6H_2O$ (1.19 g, 0.005 mol) was dissolved in 40 ml of water. 1,10-Phenanthroline monohydrate (2.7 g, 0.015 mol) was added slowly with constant stirring at room temperature. After 1 hour of stirring, 3.0 g of $NaClO_4$ was added to the solution and stirred until precipitation was complete. The solid was filtered off, washed with a small quantity of water, then ethanol, and finally ether, and dried in air for approximately 2 hours. The perchlorate salt was dissolved in a minimum amount of acetone, and a saturated solution of TBACl added dropwise until precipitation was complete. The resulting $[Ni(phen)_3]Cl_2$ was isolated and washed with acetone, then dried under vacuum (yield 2.41 g, 72%).

2.2.5 Synthesis of $[Ni(phen)_2(L)]Cl_2$, L = dppz, dpqc and dpq

Method 1

Initial attempts at synthesising $[Ni(phen)_2(dppz)]Cl_2$ followed the procedure described by Arounaguiri and Maiya.[90] A stoichiometric amount of dppz was added to an ethanolic solution of $[Ni(phen)_2(H_2O)Cl]Cl.H_2O.CH_3CN$ and the mixture refluxed for 1 hour under nitrogen, and then stirred for a further 4 - 5 hours at room temperature whilst maintaining an inert atmosphere. The solution was filtered by gravity and the complex precipitated from the filtrate by the addition of a saturated ethanolic solution of ammonium hexafluorophosphate. The hexafluorophosphate salt of the complex was isolated by filtration and then dried under vacuum. It was subsequently recrystallised from acetone/ether, and then converted to the corresponding chloride salt by dissolving in a minimum amount of acetone and subsequently adding TBACl dropwise until precipitation was complete. The $[Ni(phen)_2(dppz)]Cl_2$ was isolated by filtration, washed with acetone and then dried under vacuum. This procedure afforded $[Ni(phen)_2(dppz)]^{2+}$ that was generally contaminated with small but significant amounts of $[Ni(phen)_3]^{2+}$ and $[Ni(phen)(dppz)_2]^{2+}$, and was therefore not used any further.

Method 2

Dppz (141 mg, 0.5 mmol) was added to a 25 ml ethanolic solution of $[Ni(phen)_2(H_2O)Cl]Cl.H_2O.CH_3CN$ (266 mg, 0.5 mmol). The resulting solution was stirred at room temperature for 30 minutes, and the crude product precipitated by addition of a saturated ethanolic solution of ammonium hexafluorophosphate. After isolation the solid was dissolved in a minimum amount of acetone, and a saturated solution of TBACl added dropwise until precipitation was complete. The resulting $[Ni(phen)_2(dppz)]Cl_2$ was isolated

by filtration, washed with acetone, and dried under vacuum (yield 2.04 g, 53%). This procedure was also used to obtain the analogous dpq and dpqc compounds. In each case the purity of the resulting materials (as judged by ESI-MS) was found to be significantly greater than that of the products obtained by method 1.

2.2.6 Synthesis of $[M(phen)_3](ClO_4)_2$ M = Fe^{2+} or Zn^{2+}

$MSO_4.7H_2O$ (3.5 mmol) and 1,10-phenanthroline monohydrate (11.2 mmol) were dissolved in a minimum amount of water and ethanol, respectively. The ethanolic solution of 1,10-phenanthroline monohydrate was slowly added to the $MSO_4.7H_2O$ solution and subsequently stirred for 10 mins. The $[M(phen)_3](ClO_4)_2$ product precipitated upon addition of a 5 M aqueous sodium perchlorate solution. The resulting solids were then isolated by filtration, washed with acetone and dried under vacuum.

2.3 Oligonucleotides

2.3.1 Purification of Single Stranded Oligonucleotides

Freeze-dried single stranded (ss) oligonucleotides were purchased from Geneworks, Adelaide, South Australia as 'trityl-off' derivatives and purified using a procedure previously described employing a Beckman high performance liquid chromatograph (HPLC) and C18 octadecylsilyl column (8 × 100 mm Waters Delta Pak Radial Pak Cartridge).[238] Prior to purification the oligonucleotides were dissolved in 1 ml of 10 mM ammonium acetate (NH_4OAc). A linear gradient of 0 - 60% acetonitrile in 10 mM NH_4OAc (35 min; 1 ml/min flow rate) was used to elute the ssDNA, which had a retention time of 10 minutes. Approximately 4 ml of purified DNA was collected in 1.5 ml Eppendorf tubes, freeze-dried and redissolved in 300 µl of MilliQ™ water. The concentrations of the

resulting oligonucleotide solutions were determined using the Beer-Lambert Law by measuring their UV absorbance at 260 nm. The extinction coefficients for the sequences were determined by using ε_{260} values for adenine, guanine, cytosine and thymine of 15200, 12010, 7050 and 8400 $M^{-1}cm^{-1}$, respectively obtained from the *Oligonucleotide Properties Calculator*.[239]

2.3.2 Preparation of 16mer dsDNA and qDNA

The base sequences of the oligonucleotides used in this study are shown in **Table 2.2**. In order to prepare dsDNA and qDNA, appropriate quantities of the component single stranded oligonucleotides were measured out and dissolved in either 100 mM NH_4OAc, pH 7.4 (dsDNA), or 150 mM NH_4OAc, pH 7.0 (qDNA), to give a final DNA concentration of 1 mM. The DNA was then annealed by heating the oligonucleotide solution to 20 ^oC above the melting temperature of the target dsDNA or qDNA molecule.* The solution was then allowed to cool slowly to room temperature overnight.[239]

Table 2.2: Base sequences of the dsDNA and qDNA molecules used in this study.

Oligonucleotide Sequence (5′ → 3′)	**Label**	**Mass (Da)**
dsDNA		
GCTGCCAAATACCTCC/GGAGGTATTTGGCAGC	D2	9763.5
CTGGTTTCACTTCCTCTCGCG/GCGGAGAGGAAGTGAAACCAG	P1	12853.5
TTGGTTTCACTTCCTTTTATT/AATAAAAGGAAGTGAAACCAA		
CACTTCCGCT/AGCGGAAGTG	P2	12847.6
	P3	6056.1
Four-stranded G-quadruplex DNA		
$(TTGGGGT)_4$	Q4	8670.0
$(TTGGGGGT)_4$	Q5	9986.8
$(TTGGGGGGGT)_4$	Q7	12620.4
Two-stranded G-quadruplex DNA		
$(GGGGTTTTGGGG)_2$	Q2	2576.2

* determined using the Oligonucleotide Properties Calculator.[224]

2.4 Reactions of Oligonucleotides with Metal Complexes

2.4.1 ESI-MS Experiments

Titration of DNA with metal complexes

ESI-MS was used to analyse the composition of solutions containing either dsDNA or qDNA and various ratios of nickel, platinum or ruthenium complexes. Stock solutions of metal complexes (1 mM) were prepared in 100 mM NH_4OAc, pH 7.4 for reactions with dsDNA while for studies involving qDNA the metal solutions were prepared in 150 mM NH_4OAc, pH 7.0. Reaction mixtures containing various metal complex:DNA ratios were prepared with the final concentration of DNA in each case being 10 μM. Reaction mixtures were allowed to equilibrate for approximately 10 minutes at room temperature prior to analysis using mass spectrometry.

Mass spectrometry conditions

Mass spectra were acquired using a Waters Q-ToF Ultima^{TM} (Wyntheshawe, UK) ESI mass spectrometer equipped with a Z-spray probe and mass analyser with a *m/z* range of 32000. Reaction mixtures were injected into the source of the mass spectrometer using a Harvard model 22 syringe pump (Natick, MA, USA) at a flow rate of 20 μl/min. The instrument was calibrated using cesium iodide (1 mg/ml) over the same mass range used to acquire spectra. **Table 2.3** lists the different parameters used in order to obtain optimal spectra for the four different types of DNA molecules most widely investigated in this thesis.

Table 2.3: ESI-MS conditions used for the analysis of duplex and quadruplex DNA.

MS Parameter	D2 or P3	Q5	Q2
Ion mode	-ve	-ve	-ve
Capillary (V)	2500	2500	2500
Cone (V)	100	150	70
RF lens 1 energy (V)	70	70	50
Desolvation temperature (^{o}C)	100	200	120
Collision energy (V)	2	2	2
Transport/Aperture (V)	5/5	5/5	5/5
Acquisition mass range (m/z)	500 - 4500	500 - 4500	500 - 4500
Number of acquisitions	30	30	30
Ion optic region pressure (mbar)	3.6×10^{-3}	3.6×10^{-3}	3.6×10^{-3}

Electrospray ionisation tandem mass spectrometry (ESI-MS/MS)

Tandem mass spectrometry experiments (ESI-MS/MS) were used to examine the fragmentation of Q5, Q2 and non-covalent complexes formed between Q5 and metal complexes. For tandem mass spectra, collision energy was varied between 2 - 16 V and the collision gas (argon) pressure was 17 psi.

Competition experiments

Competition experiments were performed to compare the relative binding affinites of daunomycin, $[Ru(phen)_2(dppz)]^{2+}$ and $[Pt(en)(4,7\text{-}Me_2phen)]^{2+}$ for Q5. Reaction mixtures were prepared by first adding 1 μl of 1 mM Q5 to a predetermined quantity of the first DNA-binding compound (typically 10 - 20 μl). After allowing the solution to stand for 10 mins at room temperature, a predetermined amount of the second compound was added to the reaction mixture, which was then allowed to stand for another 10 min prior to being made up to a total volume of 100 μl using 150 mM NH_4OAc, pH 7.0. The final concentration of DNA in these experiments was 10 μM. The different drug 1: drug 2: Q5

ratios used in these experiments are given later in the relevant sections of this thesis. The composition of the reaction mixtures were determined using ESI-MS.

2.4.2 CD Experiments: Titration of DNA with Metal Complexes

CD spectra (200 – 320 nm) were obtained using a Jasco J-810 spectropolarimeter and a 0.1 cm pathlength quartz cell. For experiments involving dsDNA, a CD spectrum was initially obtained using a solution of 20 μM D2 in 100 mM NH_4OAc, pH 7.4. Aliquots of a stock solution containing both 500 μM metal complex and 20 μM D2 in 100 mM NH_4OAc, pH 7.4 were then added to give reaction mixtures containing 0:1, 1:1, 3:1, 6:1 and 10:1 ratios of metal complex to D2. All solutions were allowed to stand for 10 min at room temperature prior to CD spectra being obtained. Experiments involving Q5 were performed in a similar fashion using reaction mixtures containing metal:DNA ratios of 0:1, 1:1, 4:1, 10:1, 20:1 and 40:1. However, the concentration of Q5 in each mixture was 5 μM and the solvent used was 150 mM NH_4OAc, pH 7.0. Details of the final concentrations of DNA and metal complexes appear in the relevant chapters of this thesis.

2.4.3 Absorption Spectrophotometry

Absorption spectrophotometry was used to monitor changes in the absorption spectra of nickel compounds upon the addition of increasing amounts of DNA. In a typical experiment, the absorption spectrum (320 – 400 nm) of a 2.5 ml solution of the nickel complex to be examined (50 μM) in 100 mM NH_4OAc, pH 7.4 was first obtained. Aliquots (1 - 2 μl) of 1.25 mM D2 (in 100 mM NH_4OAc, pH 7.4) were added to the nickel solution and the mixture was allowed to equilibrate at room temperature for 10 min prior to obtaining additional spectra. This process was repeated until there were no further

significant changes in the appearance of the absorption spectrum. These experiments were performed using a Shimadzu UV 1700 PharmaSpec spectrophotometer and 1 cm quartz pathlength cells.

2.4.4 Gel electrophoresis: Gel Mobility Shift Assays

Gel electrophoresis was used to observe the changes in the migration behaviour, and therefore the degree of unwinding, of negatively supercoiled plasmid DNA caused by addition of increasing amounts of nickel and ruthenium complexes. Stock solutions containing 50 μg/ml of supercoiled plasmid DNA (pUC9) and stock metal solutions were prepared in 50 mM NH_4OAc, pH 7.4. Reaction mixtures were prepared on ice and contained the following ratios of metal to nucleotides: 0:1, 0.02:1, 0.04:1, 0.06:1, 0.08:1, 0.1:1, 0.2:1, 0.3:1, 0.4:1, 0.5:1, 0.7:1, 0.9:1, 1:1 and 1.5:1. They were subsequently equilibrated at 36 ^{o}C for 30 min. Prior to loading samples on the gel, 2.5 μl of a loading solution consisting of 0.25% (w/v) bromophenol blue and 40% (w/v) sucrose was added to the reaction mixtures. Samples (10 μl) were then loaded onto a 1% agarose gel using a TBE (45 mM Tris base, 45 mM boric acid, 1 mM EDTA) running buffer solution. Gel electrophoresis experiments were performed at 30 volts for 3.5 hours using a Cleaver Scientific Multisub midi horizontal electrophoresis system. The resulting gels were soaked in the TBE buffer for 24 hours, then stained using a 0.5 μg/ml ethidium bromide solution for 45 minutes, and finally soaked in water for 20 minutes. All gels were visualised under UV light and photographed using a Bio-Rad Gel Doc^{TM} XR.

2.5 Inhibition of Transcription Factor Binding to DNA

The ETS domain of mouse transcription factor PU.1 purified as previously described was kindly provided by Dr Joel Mackay, University of Sydney.[240] The protein (220 μM) was provided in a 10 mM phosphate buffer pH 7, and was stored at -20 ^{o}C prior to use. Protein concentration was determined by measuring the A_{280} of solutions using a Shimadzu UV 1700 PharmaSpec spectrophotometer and using an extinction coefficient for the protein of 22460 $M^{-1}cm^{-1}$.[241] Prior to mass spectral experiments, aliquots of the protein were diluted to a final volume of 300 μl using 400 mM NH_4OAc, pH 7.2. The resulting protein solution (~ 3.6 μM) was dialysed against 2 litres of the same solvent at 4 ^{o}C (3 changes). Reaction mixtures containing PU.1-DBD, the dsDNA molecule P3 (**Table 2.2**) and either $[Ru(phen)_2(dppz)]Cl_2$ or $[Pt(5,6\text{-}Me_2phen)(S,S\text{-dach})]Cl_2$ were prepared as described below. The base sequence of P3 contains the recognition sequence 5'-GGAA-3' for PU.1-DBD. All reagents used in reaction mixtures were prepared in 400 mM NH_4OAc, pH 7.2. Reaction mixtures were prepared at room temperature by first adding 1 μl of 29 μM P3 to 8 μl of 3.6 μM PU.1-DBD, and allowing the solution to stand for 10 min at room temperature. Then 1 μl of 29 μM, 86.4 μM, 173 μM, 288 μM or 576 μM stock metal solution was added, and the reaction mixture allowed to stand for another 10 minutes. This gave a final dsDNA concentration of 2.9 μM and PU.1-DBD:P3:metal ratios of 1:1:1, 1:1:3, 1:1:6 and 1:1:10 respectively. Reaction mixtures were also prepared in which P3 and the metal complexes were first mixed together and allowed to stand for 10 minutes at room temperature prior to the addition of PU.1-DBD. The conditions used for ESI-MS analysis of the PU.1-DBD/P3 complexes are shown in **Table 2.4**.

Table 2.4: ESI-MS conditions used for the analysis of reaction mixtures containing PU.1-DBD, P3 and metal complexes.

MS Parameter	
Ion mode	+
Capillary (V)	1500
Cone (V)	150
RF lens 1 energy (V)	70
Collision energy (V)	2
Transport/Aperture (V)	13/5
Acquisition mass range (m/z)	500 - 4500
Number of acquisitions	30
Ion optic region pressure (mbar)	3.6×10^{-3}

2.6 Transcription inhibition assays

These experiments were performed to determine the degree of inhibition of mRNA synthesis caused by mononuclear platinum, ruthenium and nickel complexes. All assays used a Promega pGEM linear express positive control template and the Ribomax Large Scale RNA production System with T7 RNA polymerase. Further details of the reagents used in these experiments are provided in **Table 2.5**.

All reaction mixtures were prepared by adding the reagents in the following order: T7 transcription buffer, 5 × (2 μl) rNTPs (3 μl, made up of an equimolar mixture of ATP, CTP, GTP and UTP), DNA template (3 μl, dissolved in nuclease free H_2O), metal complexes (1 μl made up in 50 mM NH_4OAc, pH 7.4) and enzyme mix (1 μl). The transcription reaction was allowed to proceed for 1 h at 37 ^oC, and then the reaction mixture was diluted with 75 μl of RNA sample buffer solution and 15 μl of RNA loading buffer solution, prior to analysis by gel electrophoresis. The reaction mixtures (5 μl) were loaded onto a 1% agarose gel using a TAE (65% Tris base, 33% glacial acetic acid and 2% EDTA)

running buffer solution. Gel electrophoresis experiments were performed at 30 volts for 2 hours using a Cleaver Scientific Multisub midi horizontal electrophoresis system, and then stained and visualised as previously described in section 2.4. The intensities of the bands present in the gel electropherograms were integrated and plotted as a function of metal ion concentration.

Table 2.5: Reagents used in transcription inhibition assays.

Reagents	Composition
rATP (Adenosine 5′-triphosphate) rCTP (Cytidine 5'-triphosphate) rGTP (Guanosine 5'-triphosphate) rUTP (Uridine 5'-triphosphate	All rNTPs are 100 mM in water
T7 Transcription Buffer	400 mM HEPES-KOH (pH 7.5) 120 mM $MgCl_2$, 200 mM DTT, 10 mM spermidine
Enzyme mix T7	RNA polymerase, Recombinant RNasin®, Ribonuclease Inhibitor, Recombinant Inorganic Pyrophosphate
Nuclease free water	
pGEM® express postive control DNA template	1 mg/ml in 10 mM Tris-HCl (pH 7.4)
RNA sample buffer	10 ml deionised formamide, 3.5 ml 37% formaldehyde, 2 ml MOPs buffer
RNA loading buffer	50% glycerol, 1 mM EDTA, 0.4% bromophenol blue

Chapter 3
Analysing the Effect of the Metal Ion on Non-covalent Binding of Metal Complexes to DNA

3.1 Scope of this Chapter

Characterisation of the binding interactions of different metal complexes with dsDNA is often conducted using a variety of analytical techniques.[13,113,115,116,134,234,242] These include absorption spectrophotometry, circular dichroism spectroscopy, isothermal titration calorimetry, NMR spectroscopy, gel electrophoresis, viscosity measurements, fluorescence spectroscopy and molecular modelling. In addition, previous work has demonstrated the capability and effectiveness of ESI-MS as an analytical technique for examining the non-covalent binding interactions of ruthenium metal complexes with dsDNA.[77,166,234] ESI-MS was able to provide information regarding differences in dsDNA binding affinity between ruthenium complexes, as well as the number, stoichiometry, and relative amounts of non-covalent complexes present in solutions containing ruthenium molecules and dsDNA. Information concerning the DNA sequence selectivity of the ruthenium complexes was also obtained by comparing the extent of binding of a specific metal complex with several oligonucleotides having different base sequences.[166]

Most investigations of metal complexes/dsDNA interactions have focussed on octahedral complexes of transition metals such as ruthenium(II) and rhodium(III). This may be attributed partially to the extremely slow rates of substitution reactions of tris chelate complexes of these metals, as well as their interesting and potentially useful redox and photophysical properties. Our understanding of the non-covalent DNA binding chemistry

of complexes of these and other metals now has a firm platform to build upon, and has been reviewed recently.[11,13] For example, it has been well established that in order for a mononuclear metal complex to display high binding affinity towards dsDNA, it must contain at least one ligand such as dppz, which is capable of intercalating strongly with the DNA base stack.[11,72] It has also been possible to engineer the structure of metal complexes to display a high degree of selectivity in their DNA binding chemistry. For example, $[Rh(bpy)_2(chyrsi)]^{3+}$ (chrysi = 5,6-chrysenequinone diimine) displays a profound ability to bind to DNA only at regions where base mismatches are present.[243] Despite this, there still remains a great deal to be learnt, particularly about the factors which govern binding specificity towards duplex DNA sequences that are correctly base paired, before it may become possible to tailor-make metal complexes for specific applications.

There have been comparatively few studies of the DNA binding chemistry of tris chelate complexes of first row transition metal ions. This is somewhat surprising, as metal ions such as chromium(III), cobalt(III) and nickel(II) form stable complexes with bidentate ligands, and display spectroscopic and redox properties that can be used to provide information about their DNA binding interactions. In addition, subtle differences in size and shape of complexes of these metal ions, compared to those of ruthenium(II) and rhodium(III) with the same ligands, may produce significant changes in DNA affinity and selectivity. It is therefore of interest to compare the DNA binding chemistry of related series of complexes such as those of the type $[M(phen)_2(L)]^{2+}$, where L is either 1,10-phenanthroline (phen) or one of several other bidentate aromatic diimine ligands, and M is different metal ions.

In this chapter the synthesis and dsDNA binding properties of the nickel(II) metal complexes shown in **Figure 3.1** are described. The techniques used to investigate their binding interactions were ESI-MS, absorption spectrophotometry, circular dichrosim spectroscopy, gel electrophoresis and transcription inhibition assays. The results obtained from these experiments are also compared to those obtained previously, or reported within this chapter for the first time, for the corresponding ruthenium(II) complexes. This comparative study was performed in order to reveal what, if any, effect varying the metal ion in complexes featuring identical ligand environments has on their binding interactions with duplex DNA.

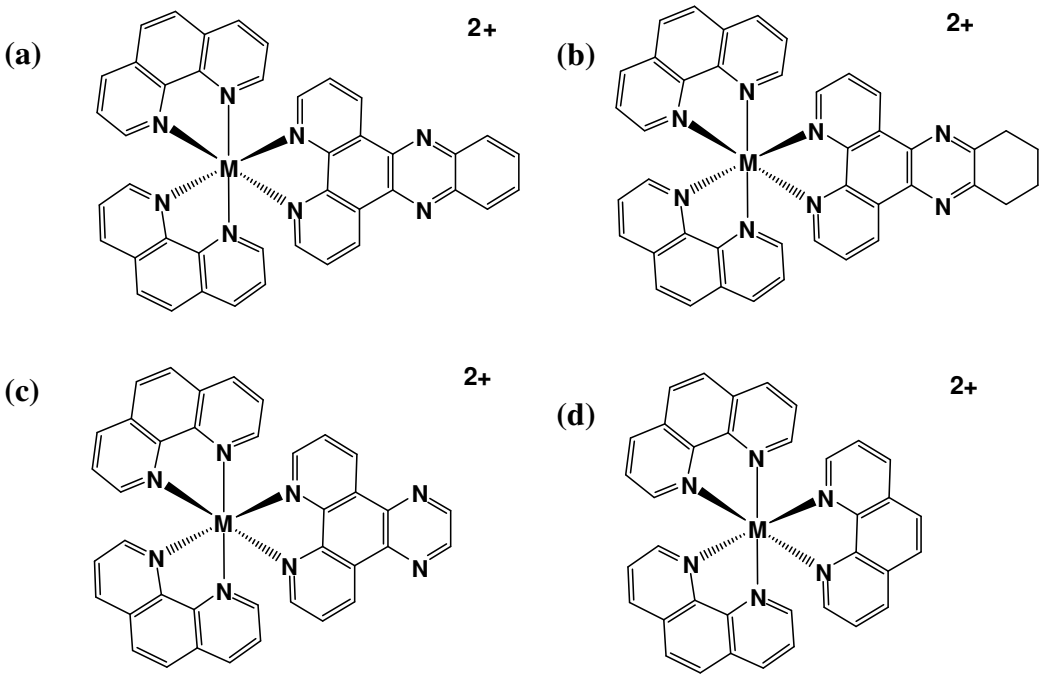

Figure 3.1: Structures of metal complexes used in this study. (a) $[M(phen)_2(dppz)]^{2+}$, (b) $[M(phen)_2(dpqc)]^{2+}$, (c) $[M(phen)_2(dpq)]^{2+}$ and (d) $[M(phen)_3]^{2+}$. (M = Ni^{2+}or Ru^{2+}).

3.2 Synthesis of Nickel Complexes

While the synthesis of $[Ni(phen)_3]^{2+}$ according to the procedure described in section 2.2 proved straightforward, problems were surprisingly encountered during preparation of the complexes $[Ni(phen)_2(L)]^{2+}$ (L = dpq, dpqc, dppz). Previously the complexes where L = dpq and dppz have been prepared by the method of Harris and McKenzie,[244] using $[Ni(phen)_2Cl_2]$ as the starting material. Mass spectrometric analysis of samples of $[Ni(phen)_2Cl_2]$ prepared using this method showed that that they were invariably contaminated with significant amounts of $[Ni(phen)_3]^{2+}$ (**Figure 3.2a**). We therefore decided to investigate other methods for preparing suitable nickel precursor compounds. Liu and co-workers[237] reported the X-ray crystal structure of $[Ni(phen)_2(H_2O)Cl]Cl.H_2O.CH_3CN$ prepared by a procedure which involves initially grinding together $NiCl_2.2H_2O$ and phenanthroline using a mortar and pestle, and recrystallising the resulting powder from acetonitrile. **Figure 3.2b** shows the ESI mass spectrum of a typical sample of $[Ni(phen)_2(H_2O)Cl]Cl.H_2O.CH_3CN$ prepared by this procedure after it had been recrystallised twice. It is immediately evident that there is far less $[Ni(phen)_3]^{2+}$ and other impurities in this sample compared to the $[Ni(phen)_2Cl_2]$ described above. The dominant ion in the mass spectrum (at *m/z* 209.3) is not surprisingly due to the fragment $[Ni(phen)_2]^{2+}$, as the weakly bound unidentate chloro and aqua ligands in the $[Ni(phen)_2Cl(H_2O)]^+$ cation would be expected to readily dissociate during the ionisation process or subsequent stages of mass analysis. It was therefore decided to prepare the three members of the $[Ni(phen)_2(L)]^{2+}$ series using $[Ni(phen)_2(H_2O)Cl]Cl.H_2O.CH_3CN$ instead of $[Ni(phen)_2Cl_2]$ as the starting material.

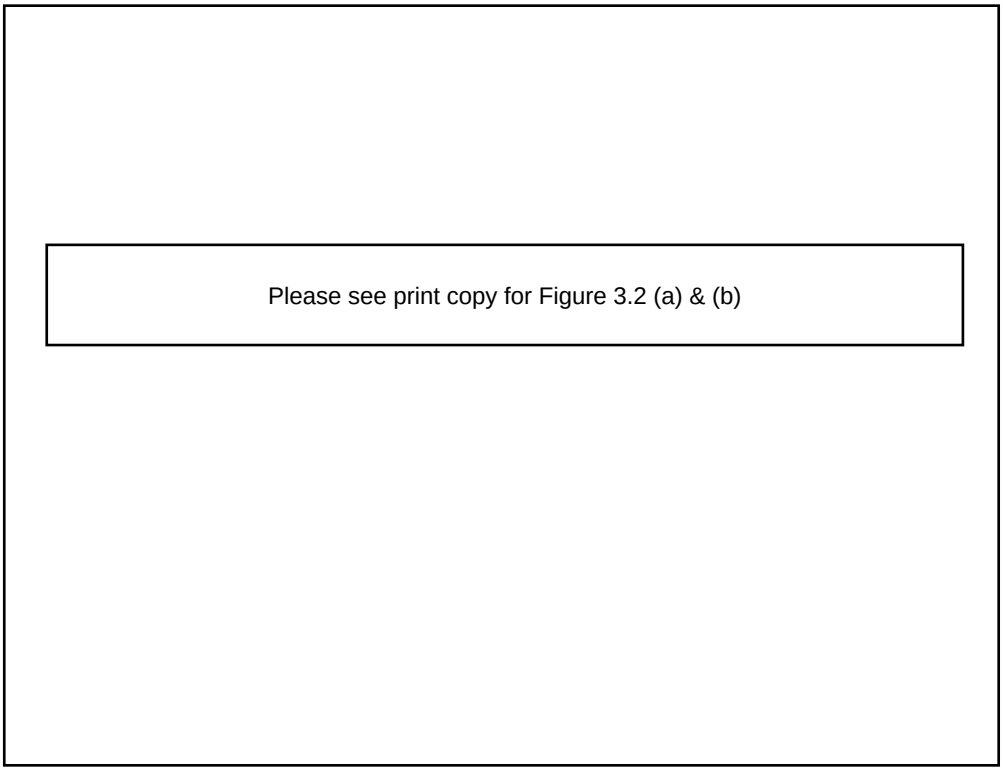

Figure 3.2: Positive ion ESI mass spectra of: (a) $[Ni(phen)_2Cl_2]$ prepared using the method of Harris and McKenzie,[244] and (b) $[Ni(phen)_2(H_2O)Cl]Cl.H_2O.CH_3CN$ prepared using the method of Liu and co-workers.[237] ● $[Ni(phen)_2]^{2+}$; ■ $[Ni(phen)_3]^{2+}$.

Literature methods for preparing $[Ni(phen)_2(dpq)]^{2+}$ and $[Ni(phen)(dppz)]^{2+}$ require $[Ni(phen)_2Cl_2]$ to be refluxed with 1.5 equivalents of dpq and dppz, respectively, for 1 h and subsequently stirred at room temperature for a further 4 – 5 h.[78,91] When this procedure was followed, but with $[Ni(phen)_2(H_2O)Cl]Cl.H_2O.CH_3CN$ instead of $[Ni(phen)_2Cl_2]$ as a reactant, the products obtained were shown by ESI-MS to contain significant amounts of impurities, most notably $[Ni(phen)_3]^{2+}$. Changing the length of time the solution was held under reflux, and recrystallisation of the mixture of compounds obtained after precipitation using ammonium hexafluorophosphate, failed to yield a product with a satisfactory level of purity. For example, **Figure 3.3a** shows the positive ion ESI mass spectrum of a sample of $[Ni(phen)_2(dppz)]^{2+}$ prepared using the standard literature conditions and

$[Ni(phen)_2(H_2O)Cl]Cl.H_2O.CH_3CN$ as the starting nickel complex. The most abundant ion present (at *m/z* 350.3) is from the desired complex. However, there are also ions of low abundance at *m/z* 299.3 that indicate a small, but significant amount of $[Ni(phen)_3]^{2+}$ is also present in the product, as well as ions of very low abundance at *m/z* 405.3 that reveal the presence of trace amounts of $[Ni(phen)(dppz)_2]^{2+}$. Similar results were obtained in reactions between $[Ni(phen)_2(H_2O)Cl]Cl.H_2O.CH_3CN$ and either dpq or dpqc carried out under the same conditions.

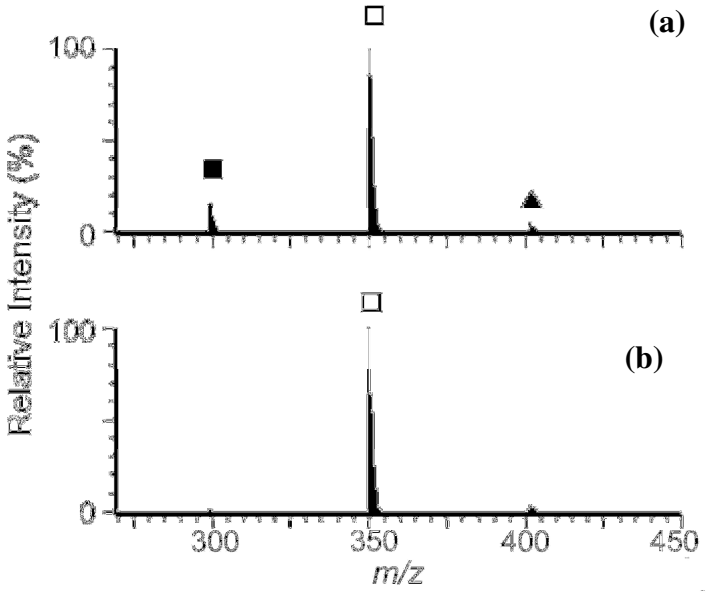

Figure 3.3: Positive ion ESI mass spectra of: (a) the product obtained after refluxing $[Ni(phen)_2(H_2O)Cl]Cl.H_2O.CH_3CN$ with 1.5 equivalents of dppz for 1 h and subsequently stirring at R.T. for 4 h, and (b) the product obtained after stirring equimolar amounts of $[Ni(phen)_2(H_2O)Cl]Cl.H_2O.CH_3CN$ and dppz at R.T. for 30 min. ■ $[Ni(phen)_3]^{2+}$; □ $[Ni(phen)_2(dppz)]^{2+}$; ▲ $[Ni(phen)(dppz)_2]^{2+}$.

It was therefore decided to see if products with a higher level of purity could be obtained by simply stirring reaction mixtures containing a 1:1 ratio of $[Ni(phen)_2(H_2O)Cl]Cl.H_2O.CH_3CN$ and dpq, dpqc or dppz at room temperature. **Figure**

3.3b shows the ESI mass spectrum of a typical product obtained by addition of ammonium hexafluorophosphate to a reaction mixture containing dppz and $[Ni(phen)_2(H_2O)Cl]Cl.H_2O.CH_3CN$ that had been stirred for only 30 min. The spectrum is dominated by ions of high abundance attributable to the desired $[Ni(phen)_2(dppz)]^{2+}$ product, demonstrating that this method does not suffer from the side reactions that occur when similar solutions are heated. This method was therefore also used to prepare the corresponding complexes containing the dpq and dpqc ligands.

3.3 ESI-MS Studies of the Binding Interactions of Nickel Complexes with dsDNA

ESI-MS studies of the binding interactions of the nickel complexes shown in **Figure 3.1** with dsDNA were performed using the hexadecamer oligonucleotide D2 (GCTGCCAAATACCTCC/GGAGGTATTTGGCAGC). This particular DNA sequence had been used previously in ESI-MS investigations of binding by a related series of ruthenium(II) complexes.[77,166,234] Therefore by investigating solutions containing ratios of Ni:D2 identical to those used in the earlier study involving the ruthenium complexes, it would be possible to directly compare the dsDNA binding affinity of metal complexes differing only in the identity of the metal ion.

Figure 3.4 shows the ESI mass spectra obtained following preparation of solutions containing different ratios of $[Ni(phen)_2(dppz)]^{2+}$ and D2. The spectrum of a solution containing D2 alone, (**Figure 3.4a**), contains ions at *m/z* 1626.4 and 1951.8, which are assigned to $[D2\text{-}6H]^{6-}$ and $[D2–5H]^{5-}$, respectively. Addition of increasing amounts of $[Ni(phen)_2(dppz)]^{2+}$ to this solution resulted in the appearance of new ions with 5- and 6-

overall charges, that indicate the presence of non-covalent complexes in solution containing one or more intact nickel molecules bound to D2. For example, addition of 1 equivalent of $[Ni(phen)_2(dppz)]^{2+}$ resulted in the appearance of new ions of low abundance, at *m/z* 1743.2 and 2092.2 (**Figure 3.4b**), which are assigned to $[D2 + [Ni(phen)_2(dppz)]^{2+} - 8H]^{6-}$ and $[D2 + [Ni(phen)_2(dppz)]^{2+} - 7H]^{5-}$, respectively. Both ions arise from a non-covalent complex consisting of a single intact nickel molecule bound to double-stranded D2. The abundances of these ions increased when the Ni:D2 ratio was increased to 3:1 (**Figure 3.4c**). This spectrum also contained ions at *m/z* 1859.9 and 2232.1 arising from non-covalent complexes containing two $[Ni(phen)_2(dppz)]^{2+}$ molecules bound to D2. In addition, ions of low abundance were also detected at *m/z* 2372.0, which are consistent with assignment to non-covalent complexes containing three $[Ni(phen)_2(dppz)]^{2+}$ molecules bound to D2. Further increasing the Ni:D2 ratio resulted in the appearance of additional ions attributable to DNA molecules containing greater numbers of bound $[Ni(phen)_2(dppz)]^{2+}$ molecules (**Figures 3.4d** and **3.4e**). At the same time the abundances of ions attributable to free D2 decreased.

Similar trends were observed in titration experiments performed with the remaining three nickel(II) complexes, and have been noted previously in studies using both octahedral ruthenium(II) complexes and square planar platinum(II) complexes.[77,166,234] Assignments for ions observed in ESI mass spectra of solutions containing different nickel complexes and D2 are presented in **Table 3.1**. In all cases there was excellent agreement between the calculated and observed *m/z* values for a particular ion. It is important to note that all ions attributable to non-covalent complexes consisted of one or more intact nickel molecules bound to D2. Therefore both the nickel complexes themselves and the non-covalent

complexes they formed with D2 were stable under the conditions employed in these mass spectrometric studies.

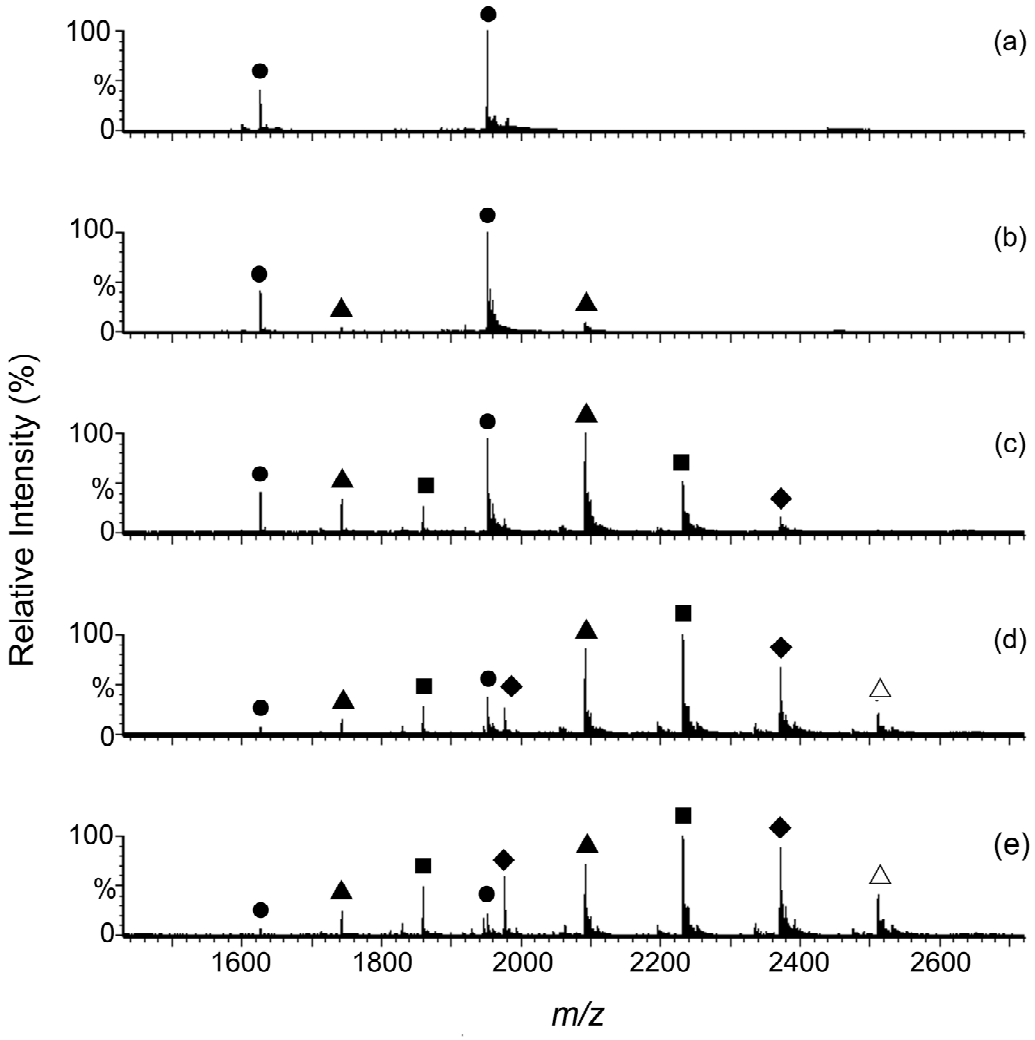

Figure 3.4: Negative ion ESI mass spectra of solutions containing different $[Ni(phen)_2(dppz)]^{2+}$:D2 ratios: (a) Ni:D2 = 0:1; (b) Ni:D2 = 1:1; (c) Ni:D2 = 3:1; (d) Ni:D2 = 6:1; (e) Ni:D2 = 10:1. The concentration of D2 was 10 μM in each case. ● D2; ▲ D2 + $[Ni(phen)_2(dppz)]^{2+}$; ■ D2 + 2 $[Ni(phen)_2(dppz)]^{2+}$; ◆ D2 + 3 $[Ni(phen)_2(dppz)]^{2+}$; Δ D2 + 4 $[Ni(phen)_2(dppz)]^{2+}$.

Table 3.1: Assignments for ions observed in ESI mass spectra of solutions containing nickel complexes and D2.

Assignment	Observed *m/z*	Calculated *m/z*
$[Ni(phen)_3 + D2 - 8H]^{6-}$	1726.3	1725.9
$[Ni(phen)_3 + D2 - 7H]^{5-}$	2071.8	2071.3
$[2Ni(phen)_3 + D2 - 10H]^{6-}$	1825.8	1825.4
$[2Ni(phen)_3 + D2 - 9H]^{5-}$	2191.3	2190.7
$[Ni(phen)_2(dpq) + D2 - 8H]^{6-}$	1735.0	1734.6
$[Ni(phen)_2(dpq) + D2 - 7H]^{5-}$	2082.2	2081.7
$[2Ni(phen)_2(dpq) + D2 - 10H]^{6-}$	1843.3	1842.7
$[2Ni(phen)_2(dpq) + D2 - 9H]^{5-}$	2212.2	2211.5
$[3Ni(phen)_2(dpq) + D2 - 12H]^{6-}$	1951.4	1950.9
$[3Ni(phen)_2(dpq) + D2 - 11H]^{5-}$	2342.0	2341.3
$[4Ni(phen)_2(dpq) + D2 - 13H]^{5-}$	2471.8	2471.1
$[Ni(phen)_2(dpqc) + D2 - 8H]^{6-}$	1744.0	1743.6
$[Ni(phen)_2(dpqc) + D2 - 7H]^{5-}$	2093.1	2092.5
$[2Ni(phen)_2(dpqc) + D2 - 10H]^{6-}$	1861.2	1860.7
$[2Ni(phen)_2(dpqc) + D2 - 9H]^{5-}$	2233.7	2233.1
$[3Ni(phen)_2(dpqc) + D2 - 12H]^{6-}$	1978.3	1977.9
$[3Ni(phen)_2(dpqc) + D2 - 11H]^{5-}$	2374.4	2373.7
$[4Ni(phen)_2(dpqc) + D2 - 13H]^{5-}$	2515.0	2514.3
$[Ni(phen)_2(dppz) + D2 - 8H]^{6-}$	1743.4	1742.9
$[Ni(phen)_2(dppz) + D2 - 7H]^{5-}$	2092.4	2091.7
$[2Ni(phen)_2(dpqc) + D2 - 10H]^{6-}$	1859.9	1859.4
$[2Ni(phen)_2(dppz) + D2 - 9H]^{5-}$	2232.2	2231.5
$[3Ni(phen)_2(dppz) + D2 - 12H]^{6-}$	1976.6	1975.9
$[3Ni(phen)_2(dppz) + D2 - 11H]^{5-}$	2372.1	2371.3
$[4Ni(phen)_2(dppz) + D2 - 14H]^{6-}$	2092.4	2092.4
$[4Ni(phen)_2(dppz) + D2 - 13H]^{5-}$	2512.0	2511.1

The relative binding affinities of the four different nickel complexes towards D2 was determined by comparing the spectra shown in **Figure 3.5**, which were obtained using solutions containing a single nickel complex and D2 in a 6:1 ratio. Despite the relatively high Ni:D2 ratios used, the dominant ions in the spectrum of the solution containing $[Ni(phen)_3]^{2+}$ (**Figure 3.5a**) were still those attributable to unbound DNA. Several other ions were also present at low to medium abundance at *m/z* 1726.3, 2071.8 and 2191.3,

which may be attributed to the presence of very small amounts of non-covalent complexes containing one or two nickel molecules bound to D2. The abundance of analogous ions in the other spectra shown in **Figure 3.5** was significantly greater, indicating that the relative binding affinity of $[Ni(phen)_3]^{2+}$ towards D2 was measurably less than that of the other three nickel complexes. For example, when the nickel complex was $[Ni(phen)_2(dpq)]^{2+}$, ions attributable to non-covalent complexes containing one, two and three nickel molecules bound to D2 were observed, with the latter ions (at *m/z* 2342.0) only of low abundance (**Figure 3.5b**). However, when the nickel complex used was $[Ni(phen)_2(dpqc)]^{2+}$, the abundance of ions at *m/z* 2374.3 from non-covalent complexes containing three nickel molecules bound to D2 was significantly greater (**Figure 3.5c**), indicating that this nickel complex has a higher binding affinity. This view is further reinforced by the observation of ions of very low abundance at *m/z* 2515.3 in **Figure 3.5c** from non-covalent DNA complexes containing four nickel molecules. Comparison of **Figures 3.5c** and **3.5d** show that the spectra obtained using $[Ni(phen)_2(dpqc)]^{2+}$ and $[Ni(phen)_2(dppz)]^{2+}$ were very similar in overall appearance, indicating that the number, relative amounts and stoichiometry of the non-covalent complexes present in solution were similar. However, the abundances of ions at *m/z* 2372.0 and 2512.0 in **Figure 3.5d**, assigned to non-covalent complexes containing three and four molecules of $[Ni(phen)_2(dppz)]^{2+}$ bound to D2, were noticeably greater than that of analogous ions containing $[Ni(phen)_2(dpqc)]^{2+}$ in **Figure 3.5c**. This therefore suggests that the former nickel complex has a slightly greater affinity towards D2 than $[Ni(phen)_2(dpqc)]^{2+}$, and the greatest DNA affinity of the four nickel complexes examined.

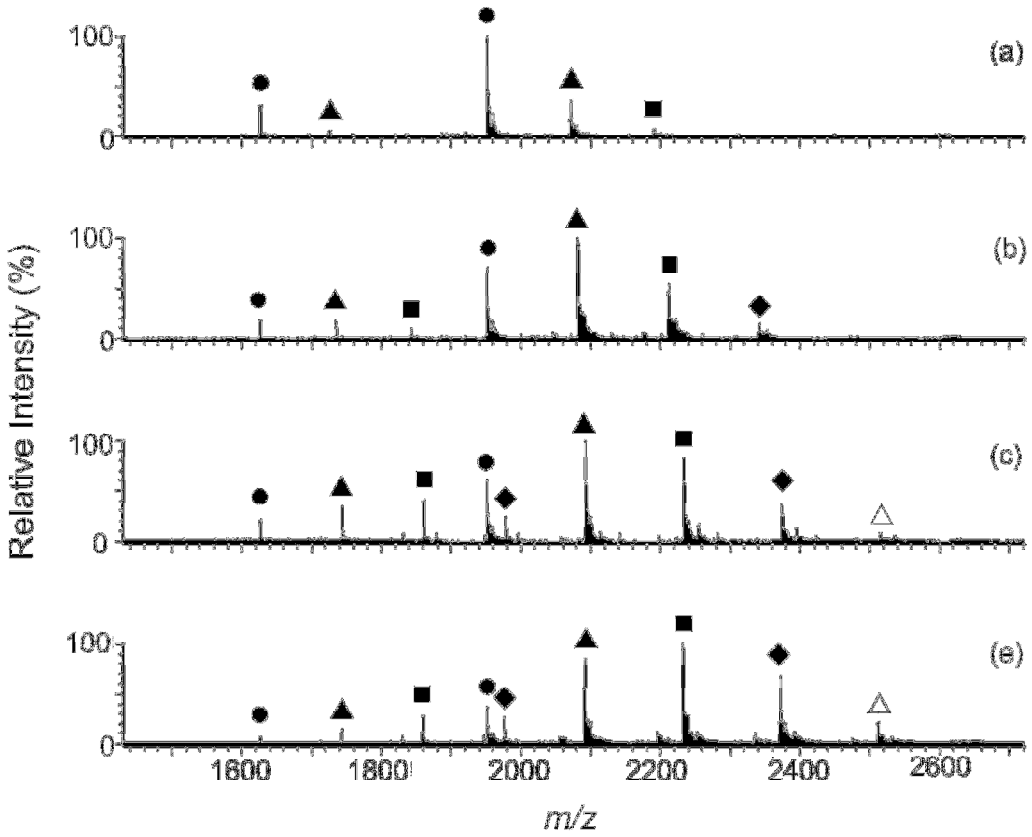

Figure 3.5: Negative ion ESI mass spectra of solutions containing a 6:1 ratio of nickel complex and duplex D2: (a) $[Ni(phen)_3]^{2+}$; (b) $[Ni(phen)_2(dpq)]^{2+}$; (c) $[Ni(phen)_2(dpqc)]^{2+}$; (d) $[Ni(phen)_2(dppz)]^{2+}$. ● dsDNA; ▲ dsDNA + 1 $[Ni(phen)_2(L)]^{2+}$; ■ dsDNA + 2 $[Ni(phen)_2(L)]^{2+}$; ◆ dsDNA + 3 $[Ni(phen)_2(L)]^{2+}$; Δ dsDNA + 4 $[Ni(phen)_2(L)]^{2+}$.

The differences in binding affinity towards D2 displayed by the different nickel complexes can be more readily seen by comparing the relative abundances of ions assigned to different non-covalent complexes. These were determined using spectra of solutions containing a 6:1 ratio of the different nickel complexes and D2. Relative abundances were obtained by adding together the individual intensities for all 5- and 6- ions assigned to a specific non-covalent complex containing D2 and one or more nickel molecules, and then dividing by the total intensity of all ions in the spectrum and expressing the result as a percentage. **Figure 3.6** presents graphically the relative abundances obtained using this method and

data from **Figure 3.5**. It can be clearly seen that the relative abundance of non-covalent complexes comprised of D2 with 3 or 4 $[Ni(phen)_2(dppz)]^{2+}$ bound is significantly greater than that for analogous ions containing the other three nickel complexes. This further demonstrates that $[Ni(phen)_2(dppz)]^{2+}$ has the highest binding affinity towards D2 of the nickel complexes studied. The greater binding affinity of $[Ni(phen)_2(dppz)]^{2+}$ is attributable to the extended and completely planar dppz ligand, which enables stronger intercalative interactions with the DNA base stack compared to the other ligands present in these complexes. **Figure 3.6** also reveals that $[Ni(phen)_2(dpqc)]^{2+}$ has a slightly higher binding affinity towards D2 compared to $[Ni(phen)_2(dpq)]^{2+}$, as the relative abundances of non-covalent complexes containing between 2 and 4 nickel molecules bound to D2 are slightly higher for the former complex. **Figure 3.6** also clearly shows that $[Ni(phen)_3]^{2+}$ has the lowest binding affinity of the four nickel complexes examined.

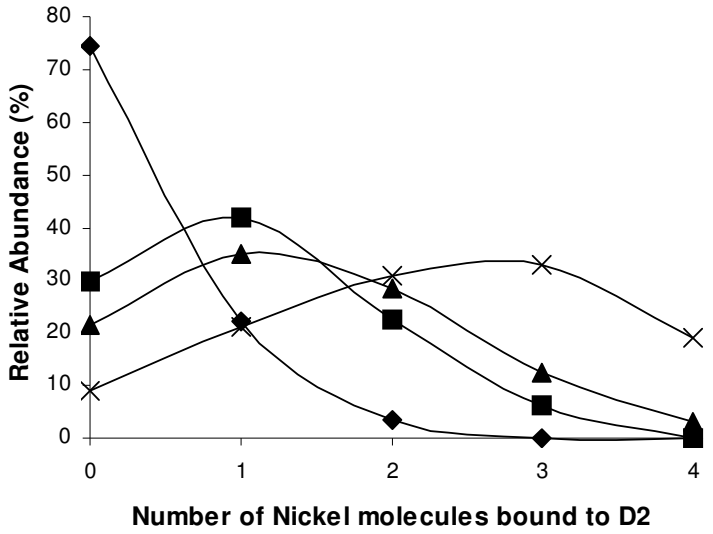

Figure 3.6: Relative abundances of non-covalent complexes present in solutions containing a 6:1 ratio of different nickel complexes and D2. ◆ $[Ni(phen)_3]^{2+}$; ■ $[Ni(phen)_2(dpq)]^{2+}$, ▲ $[Ni(phen)_2(dpqc)]^{2+}$; × $[Ni(phen)_2(dppz)]^{2+}$.

Analysis of the results presented in **Figures 3.5** and **3.6** affords the following overall order of binding affinity towards D2: $[Ni(phen)_3]^{2+}$ < $[Ni(phen)_2(dpq)]^{2+}$ < $[Ni(phen)_2(dpqc)]^{2+}$ < $[Ni(phen)_2(dppz)]^{2+}$. It is also interesting to note that this series bears a strong resemblance to that determined by ESI-MS in an earlier study using the four analogous ruthenium(II) complexes and D2, namely $[Ru(phen)_3]^{2+}$ < $[Ru(phen)_2(dpq)]^{2+}$ < $[Ru(phen)_2(dpqc)]^{2+}$ < $[Ru(phen)_2(dppz)]^{2+}$.[77,166] This suggests that the relative ability of the different ligands (phen, dpq, dpqc, dppz) to enhance overall DNA binding affinity of metal complexes remains constant, and is independent of the identity of the metal ion present. A further question that remains, however, is whether the identity of the metal ion has a significant effect on DNA binding. In order to probe this aspect, a comparison was made of the ESI mass spectra of solutions containing a 6:1 ratio of specific nickel complexes and D2, with those obtained previously using solutions containing the same ratio of the corresponding ruthenium complexes and D2.[77,166] In the case of the two tris phenanthroline complexes, $[Ni(phen)_3]^{2+}$ and $[Ru(phen)_3]^{2+}$, it proved impossible to determine which had the greater affinity towards D2 owing to relatively low extents of complexation. In both cases ESI-MS showed that ions assigned to unbound D2 were the most abundant in solution, while ions attributable to non-covalent complexes containing a single metal complex bound to DNA were of very low abundance. It also proved impossible to distinguish whether $[Ni(phen)_2(dpq)]^{2+}$ or $[Ru(phen)_2(dpq)]^{2+}$ had the higher affinity towards D2, as spectra of solutions containing these complexes showed ions assigned to unbound D2, and non-covalent complexes containing one and two metal complexes bound to DNA, with comparable abundances.

The comparison of mass spectal results did, however, provide evidence that indicated $[Ru(phen)_2(dpqc)]^{2+}$ and $[Ru(phen)_2(dppz)]^{2+}$ had significantly greater affinities towards D2 than $[Ni(phen)_2(dpqc)]^{2+}$ and $[Ni(phen)_2(dppz)]^{2+}$, respectively. In the case of $[Ru(phen)_2(dpqc)]^{2+}$, it had been previously reported that the ESI mass spectrum of a solution containing a 6:1 ratio of metal complex and D2 showed ions attributable to non-covalent DNA complexes containing up to four ruthenium molecules, with those containing two and three ruthenium molecules the most abundant.[77,166] When the ruthenium complex examined was $[Ru(phen)_2(dppz)]^{2+}$, ESI-MS showed that the most abundant ions present in a spectrum of a solution containing a 6:1 ratio of Ru:D2 were those attributable to non-covalent complexes containing four ruthenium molecules bound to D2, with other ions attributable to non-covalent complexes containing five ruthenium molecules also evident.[77,166] In contrast to the above results, **Figure 3.5c** showed that the most abundant ions attributable to non-covalent complexes in solutions containing a 6:1 ratio of $[Ni(phen)_2(dpqc)]^{2+}$ and D2 were those containing just one and two nickel molecules. **Figure 3.5d** reveals that the most abundant ions in the corresponding solution containing $[Ni(phen)_2(dppz)]^{2+}$ were those attributable to non-covalent complexes of D2 with only two nickel molecules bound. These results therefore suggest that the ruthenium(II) complexes may have a significantly greater affinity towards D2 than analogous nickel(II) complexes. In describing these observations the term "greater affinity" is used to indicate that under the same experimental conditions a greater number of a particular molecule binds to a given DNA sequence compared to another molecule. These results cannot provide information on the magnitude of the binding constant for a single binding site. For example, the ESI mass spectra show that a maximum of 5 $[Ru(phen)_2(dppz)]^{2+}$ can bind to D2, however it cannot be ruled out that the binding constant for an individual binding site is not higher than for

one of the other binding sites. Similarly, the results cannot confirm whether the binding constant of the bound nickel complexes for individual sites on D2 is lower compared to the binding for ruthenium complexes. At low concentrations of metal complex, a greater percentage of D2 is bound to ruthenium than nickel complexes, suggesting that the binding affinity for the first binding site is greater for the ruthenium than the nickel complexes. At high concentrations of metal complex, it cannot be excluded that some non-specific binding occurs. The spectra do, however, clearly indicate that a greater number of molecules of a specific ruthenium complex bind to this particular DNA sequence compared to the corresponding nickel complex. Interpretation of the spectra therefore suggests that the identity of the metal ion may significantly affect the ability of a metal complex to form non-covalent complexes with D2, particularly when large, intercalating ligands such as dpqc or dppz are present. This proposal is further explored in the following sections.

3.4 Circular Dichroism Studies of the Binding Interactions of Nickel Complexes With D2

B-form DNA is a left-handed helical molecule that gives a characteristic circular dichroism (CD) spectrum in the ultraviolet region. It has been well documented that the non-covalent binding of metal complexes to DNA results in the perturbation of these CD signals.[234,111,245-248] In addition, it is possible for the chiral DNA molecule to induce circular dichroism into both d-d and charge transfer absorption bands of an achiral metal complex, resulting in additional bands in the ultraviolet and sometimes the visible region of the spectrum. These spectroscopic changes can be used to qualitatively probe the extent and mechanism of binding of small molecules to DNA, as well as to provide quantitative data in the form of binding constants. Most previous CD studies of the binding of metal

complexes to DNA have used calf thymus DNA. Here CD spectroscopy was used to examine the binding of the nickel complexes to D2, in order to provide a better comparison with the results of binding studies performed using D2 and both ESI-MS and absorption spectrophotometry.

Figure 3.7 illustrates the effect of adding increasing amounts of the four different nickel complexes on the circular dichroism spectrum of D2. The spectrum of a solution containing D2 alone contains a positive CD band centred at 269 nm and a negative CD band at 241 nm.

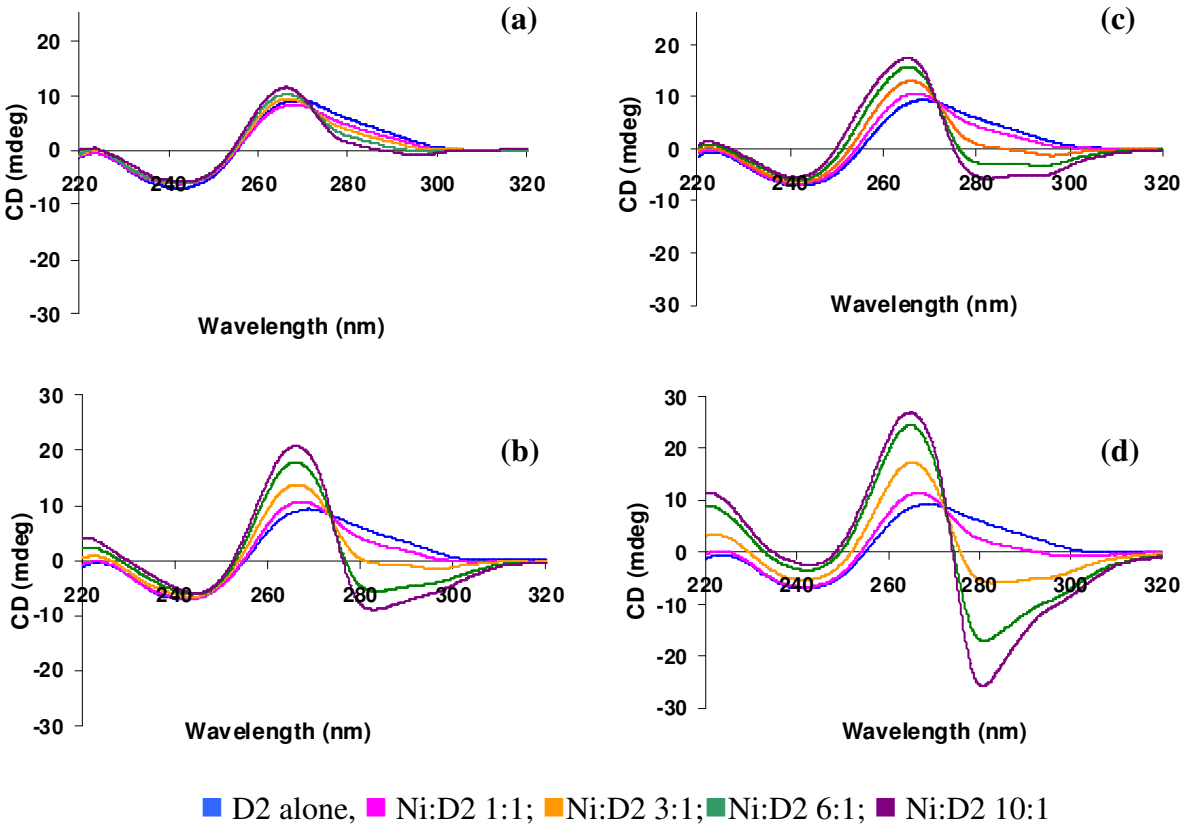

Figure 3.7: Circular dichroism spectra recorded over the wavelength range 220 – 320 nm for solutions containing different ratios of nickel complexes and D2: (a) $[Ni(phen)_3]^{2+}$; (b) $[Ni(phen)_2(dpq)]^{2+}$; (c) $[Ni(phen)_2(dpqc)]^{2+}$ and (d) $[Ni(phen)_2(dppz)]^{2+}$. The concentration of D2 in each solution was 20 μM.

At a Ni:D2 ratio of 10:1 all nickel complexes produced shifts to higher energy for the positive CD signal as well as an enhancement of CD ellipticity at 269 nm. This observation is consistent with previous reports that binding by small molecules to B-DNA via a classical intercalative mode results in enhancement of the positive CD signal of dsDNA due to strengthening of base stacking interactions and stabilisation of the right-handed helical conformation.[112-118]

The magnitudes of the shifts to higher energy for the positive CD signal, and enhancements of ellipticity at 269 nm, caused by addition of 10 equivalents of the different nickel(II) complexes to D2 are presented in **Table 3.2**. Also included are the corresponding spectroscopic changes observed in a previous CD study of the binding of the corresponding ruthenium(II) complexes $[Ru(phen)_2(L)]^{2+}$ (L = phen, dpq, dpqc, dppz) to D2.[234] On that occasion it was found that the change in ellipticity of the positive CD signal could be used to provide a relative order of DNA binding affinities that corresponded well with those obtained using several other spectroscopic techniques. Examination of **Table 3.2** shows that the magnitude of the increases in ellipticity at 269 nm changed in the following order: $[Ni(phen)_3]^{2+} < [Ni(phen)_2(dpq)]^{2+} < [Ni(phen)_2(dpqc)]^{2+} < [Ni(phen)_2(dppz)]^{2+}$, which is the order of relative binding affinities derived using ESI-MS, and similar to that based on binding constants obtained through absorption spectrophotometric titrations (section 3.4). Comparison of the data presented in **Table 3.2** also reveals that the shifts in position and enhancements of ellipticity elicited by each of the nickel(II) complexes is significantly smaller than what was observed previously with the corresponding ruthenium(II) complexes. This suggests that the nickel(II) complexes generally interact more weakly with

D2 than their ruthenium(II) analogues, a proposal that was also put forward earlier in this chapter on the basis of a comparison of ESI mass spectral data for solutions containing complexes with the dpqc and dppz ligands.

Nickel Complexes	CD $\Delta\lambda_{max}$ †	$\Delta\varepsilon$ ‡	Ruthenium Complexes	CD $\Delta\lambda_{max}$ †	$\Delta\varepsilon$ ‡
$[Ni(phen)_3]^{2+}$	-2	3	$[Ru(phen)_3]^{2+}$	-6	12
$[Ni(phen)_2(dpq)]^{2+}$	-4	9	$[Ru(phen)_2(dpq)]^{2+}$	-8	21
$[Ni(phen)_2(dpqc)]^{2+}$	-3	12	$[Ru(phen)_2(dpqc)]^{2+}$	-7	25
$[Ni(phen)_2(dppz)]^{2+}$	-4	18	$[Ru(phen)_2(dppz)]^{2+}$	-8	32

Table 3.2: Comparison of the effects of related nickel(II) and ruthenium(II) complexes on the CD spectrum of D2.*

* All values were calculated by comparing the CD spectra of solutions containing metal:D2 ratios of 10:1 with that of a solution containing free D2. Data for the ruthenium complexes was reported previously.[234]
† $\triangle\lambda$max is the shift in nm of the positive CD band at 269 nm
‡ $\triangle\varepsilon$ is the difference in ellipticity at 269 nm.

Each of the four nickel(II) complexes had relatively small effects on the negative CD signal at 241 nm, although a significant reduction in ellipticity was observed with both $[Ni(phen)_2(dpq)]^{2+}$ and $[Ni(phen)_2(dppz)]^{2+}$. **Figure 3.7** also reveals the growth of a new negative CD signal centred around 280 nm that was especially marked in the case of $[Ni(phen)_2(dppz)]^{2+}$, again suggesting that this nickel complex has the highest DNA affinity of the four investigated. While significant changes were observed in the CD spectra between 220 nm and 320 nm only 10 minutes after mixing of the nickel complexes with D2, no additional features appeared at longer wavelengths. For example, **Figure 3.8** shows the CD spectra between 200 and 600 nm for a solution of D2, and for a solution of D2 after it had been incubated with $[Ni(phen)_2(dpqc)]^{2+}$ for 10 minutes.

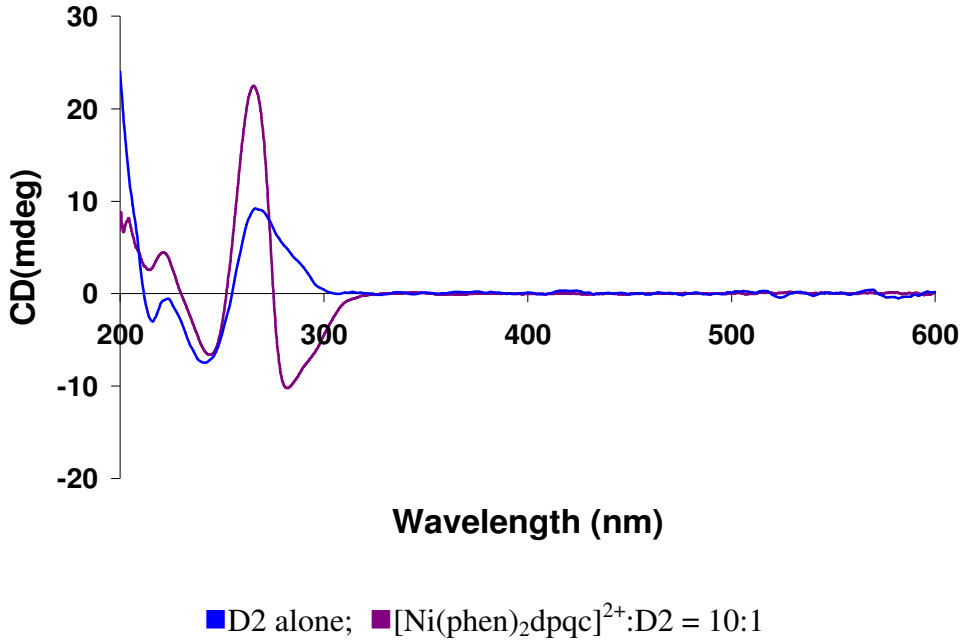

Figure 3.8: Circular dichroism spectra recorded over the wavelength range 200 – 600 nm for solutions containing either D2 alone, or a 10:1 ratio of $[Ni(phen)_2(dpqc)]^{2+}$ and D2. The concentrations of $[Ni(phen)_2(dpqc)]^{2+}$ and D2 were 200 μM and 20 μM, respectively.

The absence of new signals in the longer wavelength region of the CD spectrum mirrors results obtained previously using the analogous series of ruthenium complexes,[234] and suggests that both enantiomers of each of the nickel complexes bind to a similar extent to D2, and/or the DNA binding events result in similar perturbations to the CD signals of the enantiomers of the metal complexes.

3.5 Absorption Spectrophotometric Studies Of the Binding Interactions of Nickel Complexes with D2

The absorption spectra of $[Ni(phen)_3]^{2+}$ and $[Ni(phen)_2(dppz)]^{2+}$ have been measured previously.[78,90] In both cases several prominent bands were observed in the wavelength range between 200 and 400 nm and assigned to π-π* transitions of the ligands. The spectra of both $[Ni(phen)_2(dpq)]^{2+}$ and $[Ni(phen)_2(dpqc)]^{2+}$ on the other hand have not been

reported previously, but were also found to contain a number of similar electronic absorption bands that could be monitored after addition of D2 to determine if formation of non-covalent complexes took place. This includes absorption bands centred at 323 nm and 338 nm for $[Ni(phen)_2(dpq)]^{2+}$, and at 331 nm and 347 nm for $[Ni(phen)_2(dpqc)]^{2+}$.

Figure 3.9 shows the effect on the absorption spectra of each of the nickel complexes due to incremental additions of D2. In each case D2 was added until there were no further significant changes to the absorption spectrum, indicating that the DNA molecule was now fully complexed by nickel molecules. For example, **Figure 3.10a** shows a plot of absorbance at 379 nm as a function of the volume of D2 added for $[Ni(phen)_2(dppz)]^{2+}$, which clearly demonstrates that binding saturation was eventually achieved. For all complexes the addition of DNA was found to result in small (< 2 nm) bathochromic shifts for the main absorption bands, as well as significant hypochromism. The latter was analysed initially by measuring the decrease in absorbance for the lowest energy absorption bands of the nickel complexes caused by addition of 10 equivalents of D2. The resulting values of $\Delta Abs_{(\lambda max)}$ varied between 0.02 and 0.32, and increased in the same manner as the order of relative binding affinities derived from ESI-MS and CD studies, namely $[Ni(phen)_3]^{2+}$ ($\triangle Abs_{(\lambda max)}$ = 0.02) < $[Ni(phen)_2(dpq)]^{2+}$ ($\triangle Abs_{(\lambda max)}$ = 0.07) < $[Ni(phen)_2(dpqc)]^{2+}$ ($\triangle Abs_{(\lambda max)}$ = 0.24) < $[Ni(phen)_2(dppz)]^{2+}$ ($\triangle Abs_{(\lambda\text{-}max)}$ = 0.32).

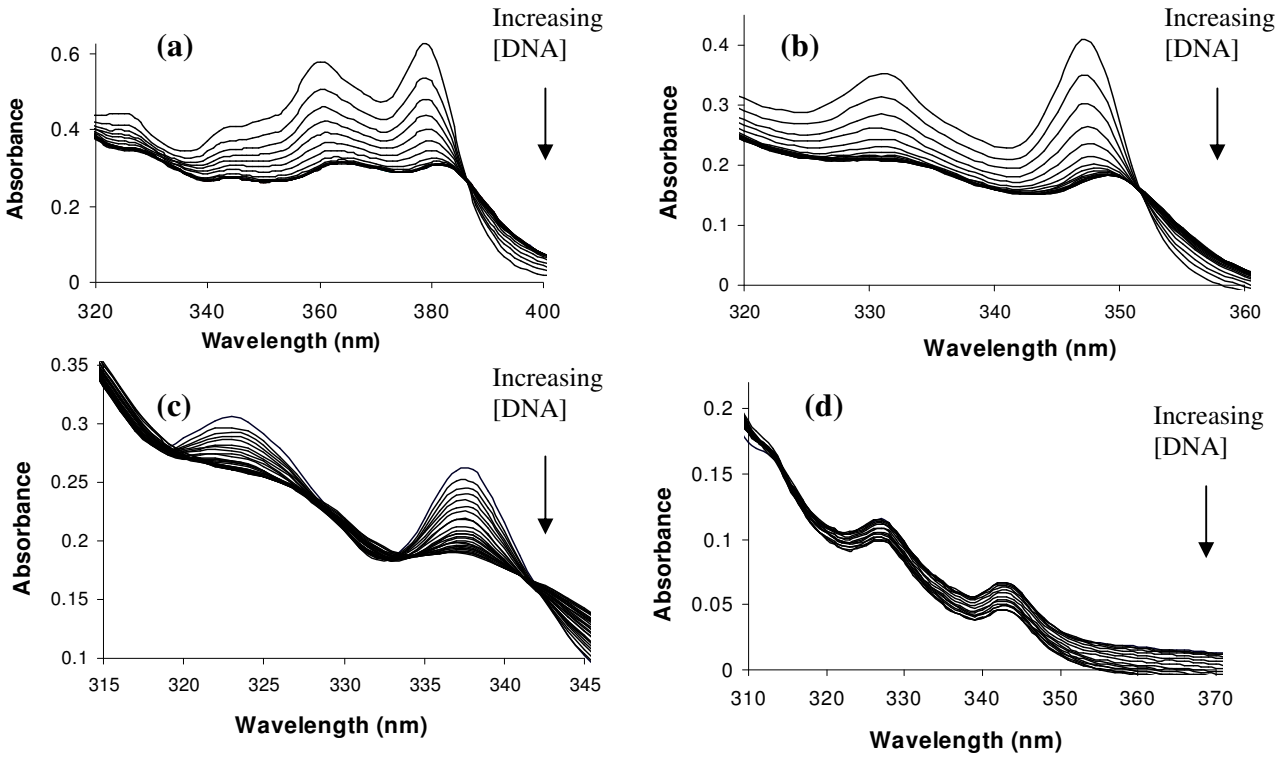

Figure 3.9: Visible absorption spectra of: (a) $[Ni(phen)_2(dppz)]^{2+}$, (b) $[Ni(phen)_2(dpqc)]^{2+}$, (c) $[Ni(phen)_2(dpq)]^{2+}$ and (d) $[Ni(phen)_3]^{2+}$ (all 10 μM) in the presence of increasing (0 – 40 μL) volumes of D2 (1.25 mM).

The changes in absorbance of the lowest energy absorption bands were then also analysed using equation 3.1 in order to afford an overall DNA binding constant for each nickel complex:

$$[DNA]/(\varepsilon_A - \varepsilon_F) = [DNA]/(\varepsilon_B - \varepsilon_F) + 1/K_b(\varepsilon_B - \varepsilon_F) \qquad \text{Eqn 3.1}$$

In this equation ε_A, ε_F and ε_B correspond to $A_{obsd}/[Ni]$, the extinction coefficient for the free nickel complex, and the extinction coefficient for the nickel complex when fully bound to DNA, respectively. The above equation was initially developed by Binesi and Hildebrand to determine equilibrium constants for the binding of iodine to aromatic hydrocarbons,[132] and was later used by Meehan and co-workers who examined the binding of polycyclic

aromatic hydrocarbons to CT-DNA.[133,249] Since then its use has been adopted by many others in order to afford a convenient estimate of the overall strength of binding of metallointercalators to DNA.[78,90,120,121,123,125,248,250-256]

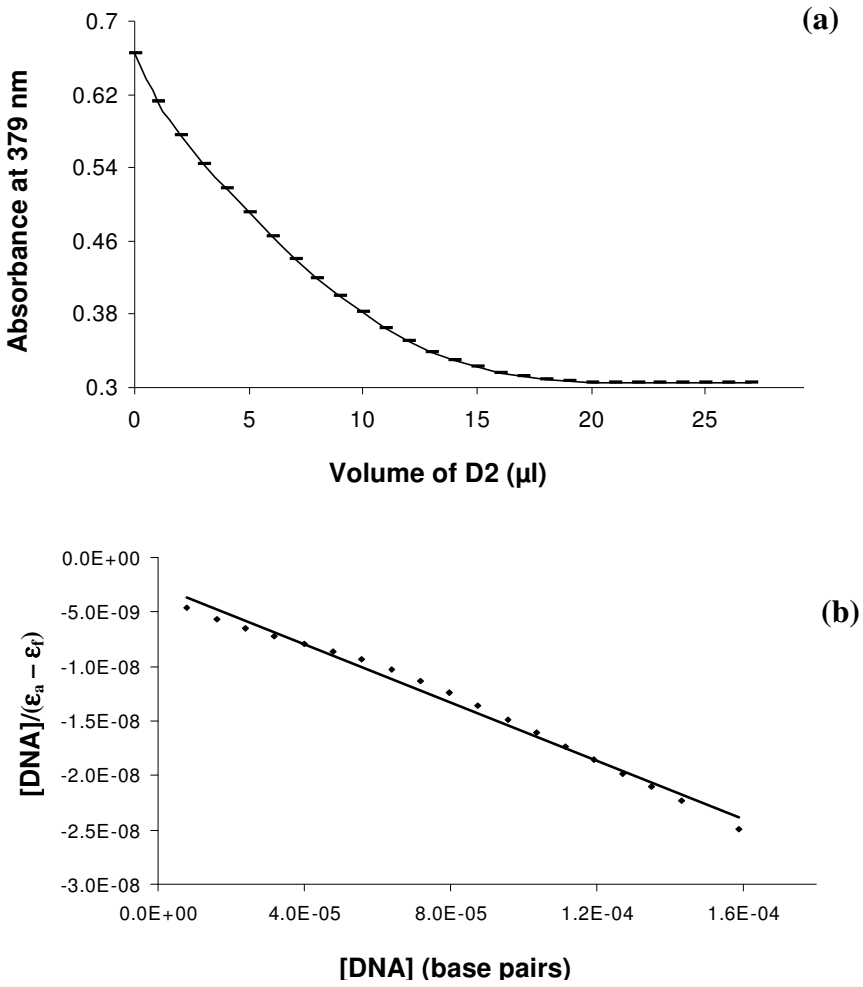

Figure 3.10: (a) Saturation curve for the binding of $[Ni(phen)_2(dppz)]^{2+}$ to D2. (b) Binding isotherm derived using absorption spectrophotometric titration data for $[Ni(phen)_2(dppz)]^{2+}$ and Equation 3.1.

Figure 3.10b shows a typical binding isotherm obtained by plotting the absorbance data shown in **Figure 3.10a** for $[Ni(phen)_2(dppz)]^{2+}$ in accordance with Equation 3.1. In all cases linear plots were obtained from which the binding constants shown in **Table 3.3** were derived. As expected, the binding constant for $[Ni(phen)_3]^{2+}$ was the lowest measured, with that determined for $[Ni(phen)_2(dpq)]^{2+}$ approximately two and a half times greater. The binding constants for both $[Ni(phen)_2(dpqc)]^{2+}$ and $[Ni(phen)_2(dppz)]^{2+}$ were larger than that for $[Ni(phen)_2(dpq)]^{2+}$, again as expected in view of the larger intercalating ligands present in the former two complexes. One surprising result, however, was that the binding constant for $[Ni(phen)_2(dpqc)]^{2+}$ was slightly larger than that for $[Ni(phen)_2(dppz)]^{2+}$. Although binding constants for $[Ni(phen)_2(dpq)]^{2+}$ and $[Ni(phen)_2(dpqc)]^{2+}$ have not been previously reported, values of $(9 \pm 2) \times 10^5$ M^{-1} and 1.5×10^5 M^{-1} have been reported previously for $[Ni(phen)_2(dppz)]^{2+}$ with CT-DNA.[78,90] Both values are significantly larger than that reported here (5.2×10^4 M^{-1}). While this may be attributed partially to the different DNA used in our study, it should be noted that other metal complexes containing the dppz ligand have been reported to have even larger binding constants.[78,83] Therefore it appears that our binding constant for $[Ni(phen)_2(dppz)]^{2+}$ may be anomalously low. In this regard the results here parallel those obtained in our previous study of the analogous ruthenium complexes, where binding constants determined by the absorption titration method for both $[Ru(phen)_2(dppz)]^{2+}$ and $[Ru(bpy)_2(dppz)]^{2+}$ were found to be 1 – 2 orders of magnitude smaller than values reported in the literature.[234] This was attributed to the relatively high concentration of salt (100 mM ammonium acetate) present in the absorption titration mixtures in order to closely mimic the conditions of ESI-MS experiments, compared to the lower salt concentration used in other studies (e.g. 5 mM tris, 55 mM NaCl). The use of 100 mM ammonium acetate in the current study may also account for the

relatively low binding constant for $[Ni(phen)_2(dppz)]^{2+}$, as well as the small range of binding constants observed for all the nickel complexes.

Table 3.3: Comparison of binding constants determined spectrophotometrically for binding of related ruthenium(II) and nickel(II) complexes to D2.*

Nickel Complexes	10^4 K_B ($M(base\ pair)^{-1}$)	**Ruthenium Complexes**	10^4 K_B ($M(base\ pair)^{-1}$)
$[Ni(phen)_3]^{2+}$	0.7	$[Ru(phen)_3]^{2+}$	0.3
$[Ni(phen)_2(dpq)]^{2+}$	1.8	$[Ru(phen)_2(dpq)]^{2+}$	1.4
$[Ni(phen)_2(dpqc)]^{2+}$	6.1	$[Ru(phen)_2(dpqc)]^{2+}$	6.1
$[Ni(phen)_2(dppz)]^{2+}$	5.2	$[Ru(phen)_2(dppz)]^{2+}$	6.4

*Values for ruthenium complexes reported previously in reference.[234]

Comparison of the binding constants for the nickel complexes with those obtained previously for their ruthenium analogues suggests that changing the metal ion has little effect on overall binding affinity. This conclusion contrasts with what was found using both ESI-MS and CD spectroscopy, although it must be remembered that both the spread and magnitude of individual binding constants obtained by the absorption titration method may have been significantly affected owing to the use of solutions with relatively high ionic strengths.

3.6 Gel Electrophoresis Studies of the Binding Interactions of Nickel and Ruthenium Complexes with Plasmid DNA

The ability of plasmid DNA to migrate through a gel in the presence of an electric field is known to be affected by factors that alter its size, shape or charge.[13] For example, the binding of either organic or inorganic molecules can cause unwinding of negatively supercoiled DNA, resulting in lengthening and changes to its shape that also reduces its electrophoretic mobility by an amount that reflects both the nature and extent of binding.

In the case of metal complexes that bind non-covalently to DNA, many researchers have used gel electrophoresis to provide evidence for or against an intercalative mode of interaction,[13,90,118,120,257,258] as well as to determine whether the complexes cleave DNA upon irradiation.[78,125,259-261] In one of the former studies, $[Ni(phen)_2(dppz)]^{2+}$ was reported to alter the mobility of pBR322 plasmid DNA, while $[Ni(phen)_3]^{2+}$ was found to have no effect.[90] However, previously there has not been a systematic study of the effect of binding of each of the four nickel complexes shown in **Figure 3.1** on the electrophoretic mobility of plasmid DNA, nor has there been a detailed comparison of the effects on DNA mobility of binding by related series of complexes containing different metal ions.**Figure 3.11** shows the gel electropherograms obtained after allowing the nickel complexes to interact with pUC9 plasmid DNA for 30 min. The addition of increasing amounts of both $[Ni(phen)_2(dppz)]^{2+}$ and $[Ni(phen)_2(dpqc)]^{2+}$ (**Figures 3.11a** and **b**) was found to result in significant retardation of the mobility of the closed, negatively supercoiled form of the plasmid, whereas $[Ni(phen)_2(dpq)]^{2+}$ and $[Ni(phen)_3]^{2+}$ (**Figures 3.11c** and **d**) had little, if any effect. This suggests that the former nickel complexes interact to a significantly greater extent with the DNA.

In the case of $[Ni(phen)_2(dppz)]^{2+}$, the closed, supercoiled form of the plasmid was found to co-migrate with the open, circular form when the nickel:nucleotide ratio was 0.06:1 (lane 5 in **Figure 3.11a**). Since co-migration did not occur on addition of $[Ni(phen)_2(dpqc)]^{2+}$ until a nickel:nucleotide ratio of 0.08:1 was used, these results lead to the same conclusion as that reached using ESI-MS and CD spectroscopy, which was that $[Ni(phen)_2(dppz)]^{2+}$ has the highest DNA binding affinity of all four nickel complexes. At $[Ni(phen)_2(dppz)]^{2+}$: nucleotide ratios greater than 0.06:1 the mobility of the closed supercoiled form of pUC9

increased to a small extent, indicating that this complex was also able to induce the formation of positive supercoils into the plasmid after it had been fully unwound.

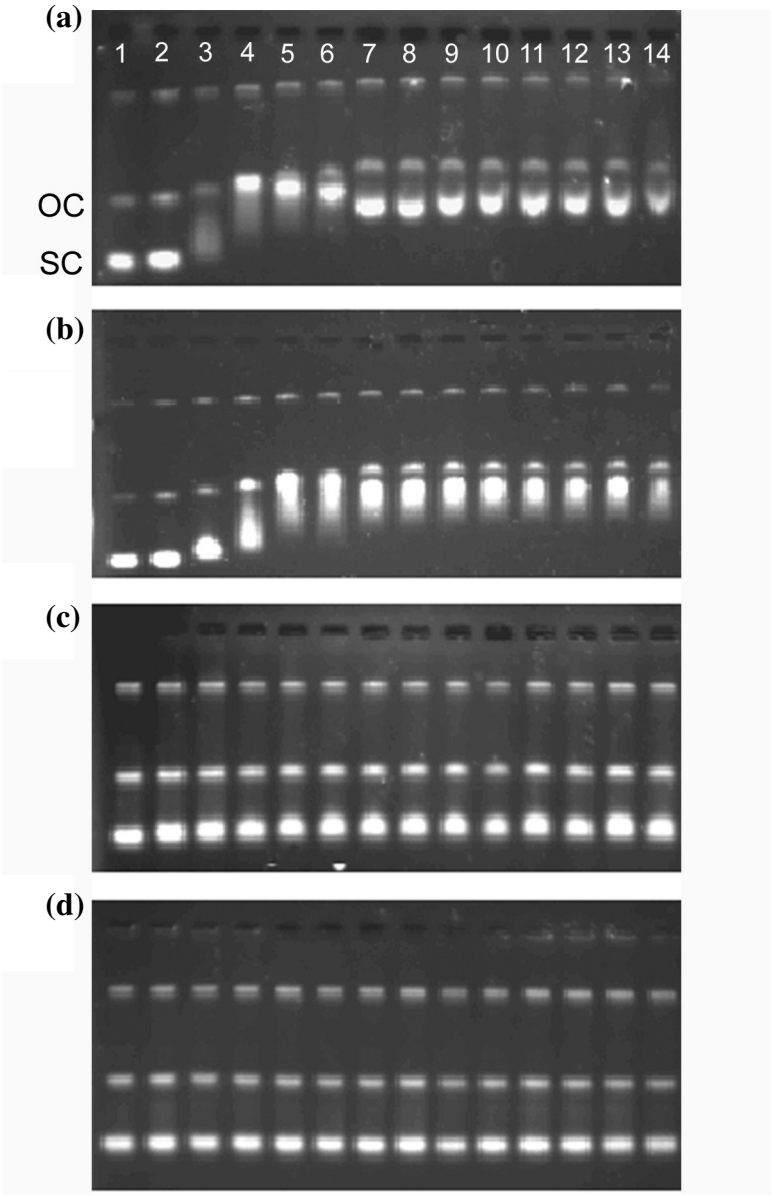

Figure 3.11: Gel electropherograms of the products obtained from reaction of pUC9 negatively supercoiled plasmid DNA with varying amounts of nickel complexes for 30 min at 36 ˚C, pH 7.0: (a) $[Ni(phen)_2(dppz)]^{2+}$; (b) $[Ni(phen)_2(dpqc)]^{2+}$; (c) $[Ni(phen)_2(dpq)]^{2+}$; (d) $[Ni(phen)_3]^{2+}$. The ratio of nickel to nucleotide in lanes 1 – 14 are: 0:1; 0.02:1; 0.04:1; 0.05:1; 0.06:1; 0.07:1; 0.08:1; 0.1:1; 0.2:1; 0.3:1; 0.4:1; 0.5:1; 0.7:1; 0.9:1; 1:1 and 1.5:1. OC = open circular form of DNA, SC = closed supercoiled form of DNA.

A very similar pattern of results was obtained from gel electrophoresis studies performed using the four analogous ruthenium complexes (**Figure 3.12**), which indicated that their order of increasing relative DNA binding affinities was $[Ru(phen)_3]^{2+}$ ~ $[Ru(phen)_2(dpq)]^{2+}$ < $[Ru(phen)_2(dpqc)]^{2+}$ < $[Ru(phen)_2(dppz)]^{2+}$. For both this and the nickel series it was impossible to determine with any certainty whether the tris(phen) or the dpq-containing complex had the lowest DNA affinity, as both failed to result in any significant changes to the mobility of the closed, negatively supercoiled form of the plasmid. This lack of mobility also prevents any meaningful comparison of the relative DNA binding affinities of nickel and ruthenium complexes containing an identical tris phen coordination sphere, or two phen and one dpq ligands. However, from **Figure 3.12** it is possible to determine that co-migration of bands due to the closed, supercoiled and open, circular forms of the plasmid occurred when the ratio of ruthenium to nucleotide was 0.05:1 in the case of $[Ru(phen)_2(dppz)]^{2+}$, and between 0.06:1 and 0.07:1 for $[Ru(phen)_2(dpqc)]^{2+}$. Both ratios are lower than those at which co-migration occurred with the analogous nickel complexes, suggesting once again that the ruthenium complexes containing dppz and dpqc ligands have DNA binding affinities that are greater than that of the related nickel complexes. This conclusion is therefore also consistent with those deduced from ESI-MS and CD spectroscopic studies.

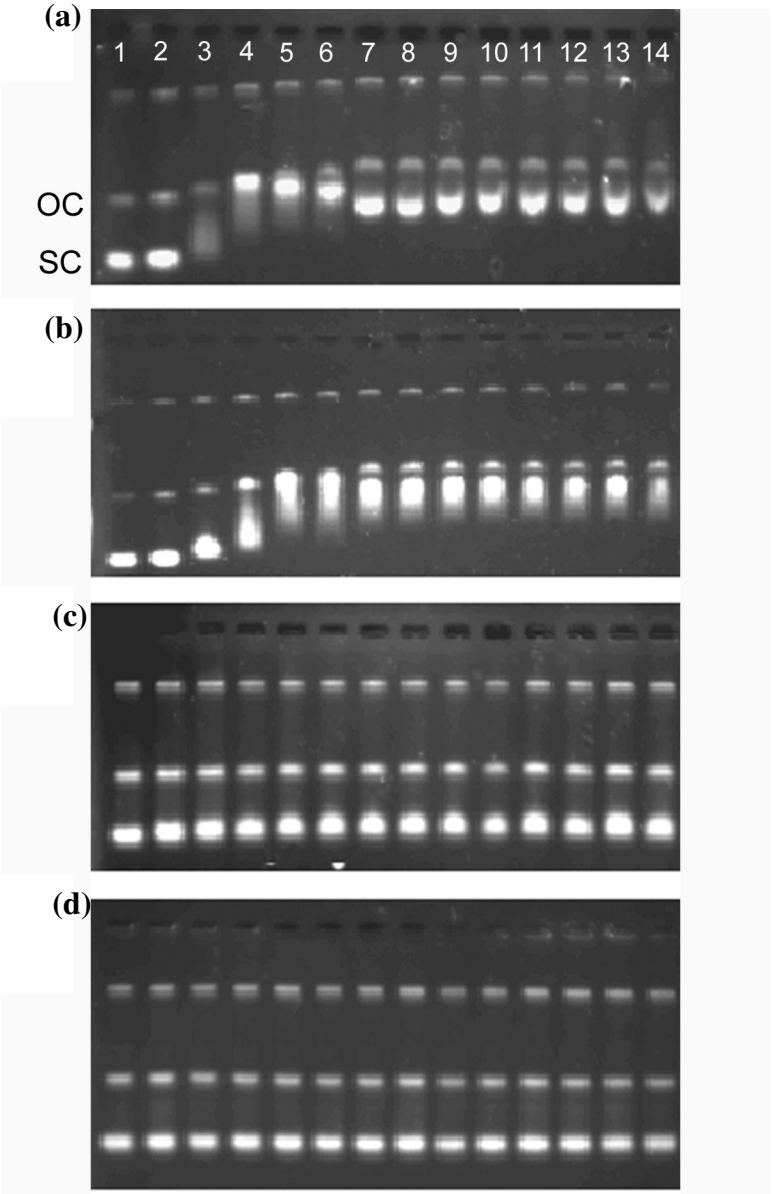

Figure 3.12: Gel electropherograms of the products obtained from reaction of pUC9 negatively supercoiled plasmid DNA with varying amounts of ruthenium complexes for 30 min at 36 ˚C, pH 7.0: (a) $[Ru(phen)_2(dppz)]^{2+}$; (b) $[Ru(phen)_2(dpqc)]^{2+}$; (c) $[Ru(phen)_2(dpq)]^{2+}$; (d) $[Ru(phen)_3]^{2+}$. The ratio of ruthenium to nucleotide in lanes 1 – 14 are: 0:1; 0.02:1; 0.04:1; 0.05:1; 0.06:1; 0.07:1; 0.08:1; 0.1:1; 0.2:1; 0.3:1; 0.4:1; 0.5:1; 0.7:1; 0.9:1; 1:1 and 1.5:1. OC = open circular form of DNA, SC = closed supercoiled form of DNA.

3.7 Transcription Inhibition Assays

Turro and co-workers showed that ruthenium and rhodium complexes containing phenanthroline and quinone diimine ligands are able to inhibit transcription to varying degrees as a result of their ability to bind to dsDNA.[229,231] The magnitude of transcription inhibition was conveniently monitored by using reagents readily available in kit form, and was found to correlate with the degree of duplex stabilisation revealed by increases in DNA melting temperature. In view of the chemical similarities between the metal complexes examined as part of the current study, and those studied by Turro and co-workers, it was decided to examine whether the transcription inhibition assay would reveal the same systematic differences in reactivity between ruthenium and nickel complexes containing identical ligand environments, that was found by the other methods discussed previously in this chapter.

In an initial experiment, the effect of a single concentration (40 μM) of the nickel and ruthenium complexes on the amount of DNA transcribed was examined. The results of this experiment, which was performed in triplicate, are shown in **Figure 3.13**. Two bands attributable to mRNA molecules with different lengths were observed (as expected) in all cases where the level of DNA transcription was above the detection limit. These two bands were, however, absent in lanes which correspond to solutions that contained 40 μM $[Ru(phen)_2(dppz)]^{2+}$, $[Ru(phen)_2(dpqc)]^{2+}$ (**Figure 3.13b**) or $[Ni(phen)_2(dppz)]^{2+}$ (**Figure 3.13a**). This indicates that these complexes produced the greatest degree of inhibition of mRNA synthesis. The fact that no bands corresponding to mRNA were observed when $[Ru(phen)_2(dpqc)]^{2+}$ was present in the reaction mixture, but were detected when $[Ni(phen)_2(dpqc)]^{2+}$ was added, suggests that the former complex has the greater ability of

the two to inhibit DNA transcription. Since the mechanism of transcription inhibition most likely involves binding of the metal complexes to DNA, and consequent inhibition of binding of RNA polymerase to the DNA template, this result is therefore additional evidence that $[Ru(phen)_2(dpqc)]^{2+}$ has a higher binding affinity towards dsDNA than the analogous nickel complex. By comparing the intensities of the bands in **Figure 3.13a** it is similarly possible to conclude the affinity of $[Ni(phen)_2(dpqc)]^{2+}$ toward dsDNA is greater than that of both $[Ni(phen)_3]^{2+}$ and $[Ni(phen)_2(dpq)]^{2+}$ (the bands in lanes 4, 8 and 12 are lower in intensity than those in 2, 6 and 10 or 3, 7 and 11). However, the lack of any bands due to mRNA in the case of solutions containing the two complexes containing the dppz ligand (Ni^{2+} or Ru^{2+}) made it impossible to use this experiment to determine which had the higher dsDNA binding affinity. Therefore a second set of experiments were performed in which the effect of increasing concentrations of metal complex on the amount of DNA transcribed were examined. The results of these experiments are shown in **Figures 3.14** and **3.15.**

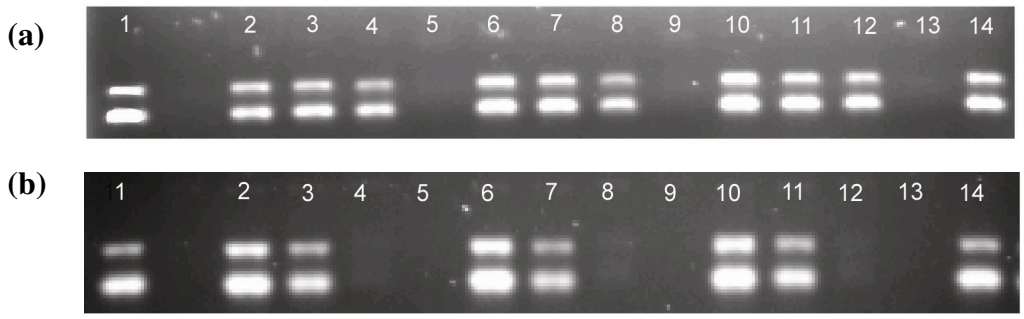

Figure 3.13: Ethidium bromide stained agarose gel (1%) of transcribed mRNA in the presence of 40 μM (a) nickel complexes and (b) ruthenium complexes. In part (a) lanes 1 and 14 = control, lanes 2, 6, and 10 = $[Ni(phen)_3]^{2+}$, lanes 3, 7 and 11 = $[Ni(phen)_2(dpq)]^{2+}$, lanes 4, 8 and 12 = $[Ni(phen)_2(dpqc)]^{2+}$ and lanes 5, 9 and 13 = $[Ni(phen)_2(dppz)]^{2+}$. In part (b) lanes 1 and 14 = control, lanes 2, 6 and 10 = $[Ru(phen)_3]^{2+}$, 3, 7 and 11 = $[[Ru(phen)_2(dpq)]^{2+}$, lanes 4, 8 and 12 = $[Ru(phen)_2(dpqc)]^{2+}$ and lanes 5, 9 and 13 = $[Ru(phen)_2(dppz)]^{2+}$.

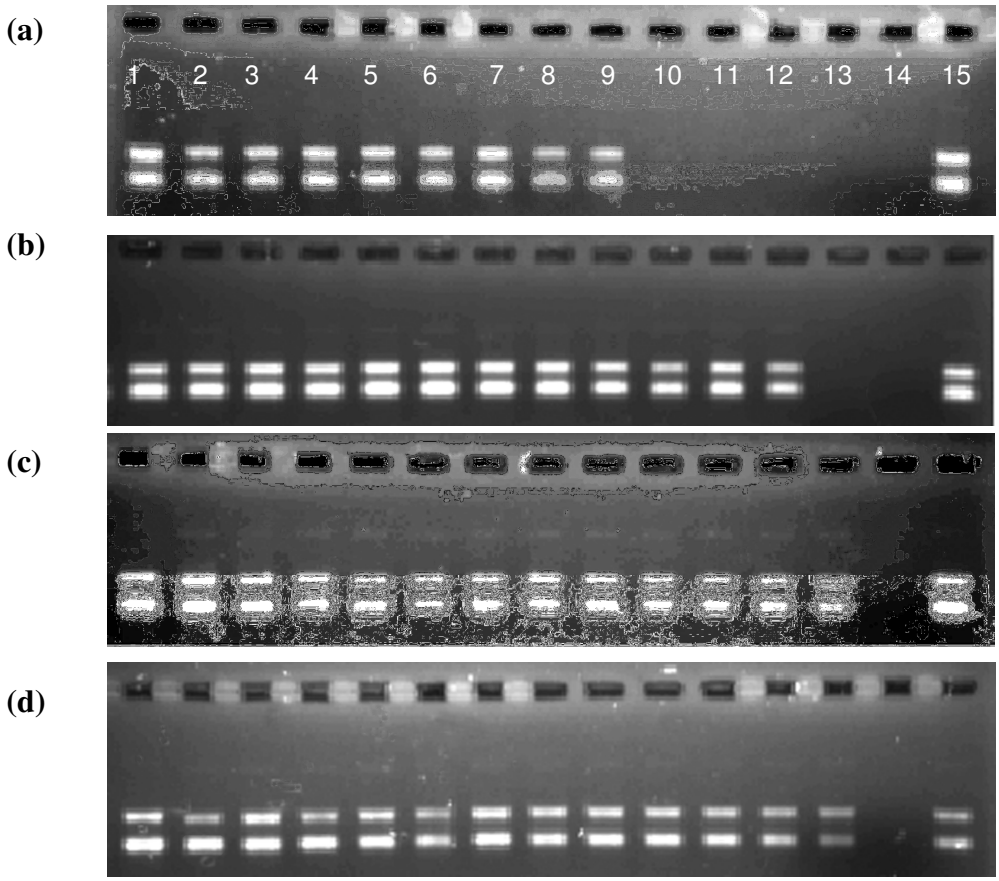

Figure 3.14: Ethidium bromide stained agarose gel (1%) of transcribed mRNA in the presence of increasing concentrations of: (a) $[Ni(phen)_2(dppz)]^{2+}$; (b) $[Ni(phen)_2(dpqC)]^{2+}$; (c) $[Ni(phen)_2(dpq)]^{2+}$; (d) $[Ni(phen)_3]^{2+}$. Both sets of bands imaged in each of the gels are due to mRNA. Lanes 1 – 15 correspond to: $[Ni^{2+}]$ = 0 μM, 2 μM, 4 μM, 6 μM, 8 μM, 10 μM, 15 μM, 20 μM, 25 μM, 30 μM, 35 μM, 40 μM, 50 μM, Blank, 0 μM.

Both figures show that increasing the concentration of the metal complexes resulted in smaller amounts of mRNA being produced (decreasing band intensity with increasing metal concentrations). **Figure 3.14** shows that the effect was most marked amongst the nickel complexes with $[Ni(phen)_2(dppz)]^{2+}$ (**Figure 3.14a**) and $[Ni(phen)_2(dpqc)]^{2+}$ (**Figure 3.14b**). In the case of the former compound, no bands attributable to mRNA were detected when its concentration was increased to 30 μM, while a higher concentration (50 μM) of

$[Ni(phen)_2(dpqC)]^{2+}$ was required to completely arrest DNA transcription. Although the results shown in **Figure 3.14** also demonstrate that $[Ni(phen)_2(dpq)]^{2+}$ and $[Ni(phen)_3]^{2+}$ inhibit DNA transcription, the extent to which this occurred was significantly less than with the previous two compounds. Subsequent experiments using higher concentrations of these nickel complexes showed that $[Ni(phen)_2(dpq)]^{2+}$ and $[Ni(phen)_3]^{2+}$ did not totally arrest DNA transcription when present at 250 μM concentration. Since the mechanism of transcription inhibition most likely involves binding of the nickel complexes to the DNA template, the results support the following order of increasing DNA binding affinity: $[Ni(phen)_3]^{2+}$ ~ $[Ni(phen)_2(dpq)]^{2+}$ < $[Ni(phen)_2(dpqc)]^{2+}$ < $[Ni(phen)_2(dppz)]^{2+}$, which is similar to those revealed by most of the other techniques discussed in this chapter.

The effect of increasing the concentration of the four analogous ruthenium complexes on mRNA synthesis is shown in **Figure 3.15**. Similar results to those obtained with the nickel(II) complexes were obtained, with complete inhibition of transcription in the presence of $[Ru(phen)_2(dppz)]^{2+}$ and $[Ru(phen)_2(dpqc)]^{2+}$ occurring when these metal complexes were present at 20 μM and 30 μM, respectively.

In order to compare the effect on DNA transcription of complexes containing the same set of ligands, but different metal ions, the intensities of bands present in the gel electropherograms were integrated and plotted as a function of metal ion concentration. The resulting curves were then used to determine values of $M_{50\%Inh}$, the concentration that resulted in 50% inhibition of DNA transcription. These values are presented in **Table 3.4**, and show that in most instances the ruthenium complexes are more effective at inhibiting DNA transcription than their nickel analogues. The only exception to this trend was for the

two tris phenanthroline complexes, neither of which produced 50% inhibition even when present at the highest concentration examined (250 μM). Overall, the results of the transcription inhibition assays support the conclusion that metal complexes containing a ruthenium(II) centre are more effective at binding to DNA than analogous nickel(II) complexes containing the same set of ligands.

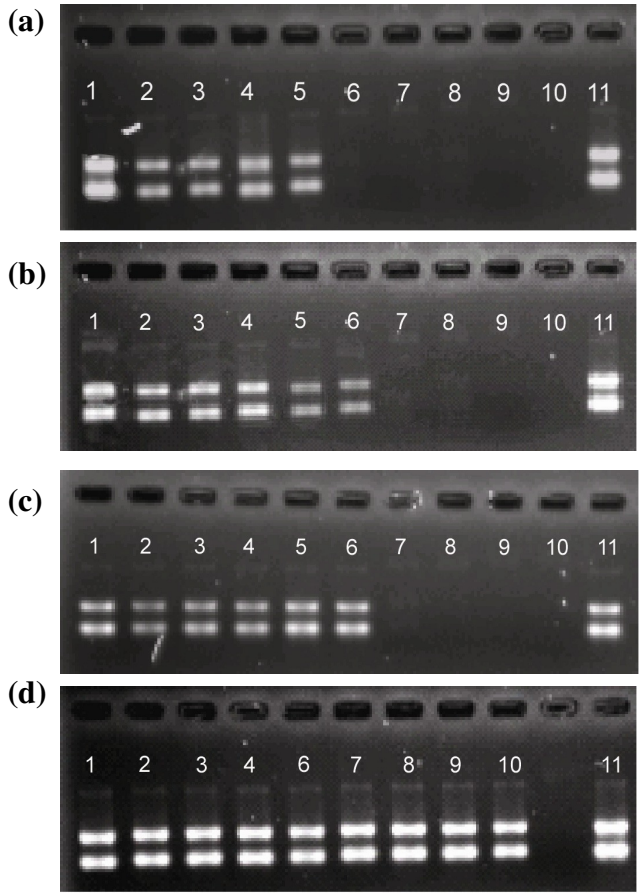

Figure 3.15: Ethidium bromide stained agarose gel (1%) of transcribed mRNA in the presence of increasing concentrations of: (a) $[Ru(phen)_2(dppz)]^{2+}$; (b) $[Ru(phen)_2(dpqC)]^{2+}$; (c) $[Ru(phen)_2(dpq)]^{2+}$ and (d) $[Ru(phen)_3]^{2+}$. Both sets of bands imaged in each of the gels are due to mRNA. In parts (a) and (b) lanes 1 – 11 correspond to: $[Ru^{2+}]$ = 0 μM, 4 μM, 8 μM, 10 μM, 15 μM, 20 μM, 30 μM, 40 μM, 50 μM, Blank, 0 μM. In parts (c) and (d) lanes 1 – 11 correspond to: $[Ru^{2+}]$ = 0 μM, 10 μM, 20 μM, 30 μM, 40 μM, 50 μM, 75 μM, 100 μM, 250 μM, Blank, 0 μM.

Table 3.4: Comparison of $M_{50\%inh}$ values, the concentration of metal complex required for 50% inhibition of DNA transcription, for related ruthenium(II) and nickel(II) complexes.

Nickel Complexes	$M_{50\%Inh}$ (μM)	Ruthenium Complexes	$M_{50\%Inh}$ (μM)
$[Ni(phen)_3]^{2+}$	> 250	$[Ru(phen)_3]^{2+}$	> 250
$[Ni(phen)_2(dpq)]^{2+}$	> 250	$[Ru(phen)_2(dpq)]^{2+}$	61
$[Ni(phen)_2(dpqc)]^{2+}$	43	$[Ru(phen)_2(dpqc)]^{2+}$	18
$[Ni(phen)_2(dppz)]^{2+}$	22	$[Ru(phen)_2(dppz)]^{2+}$	12

3.8 Conclusions

The results of ESI-MS and CD studies revealed the following order of increasing D2 binding affinity: $[Ni(phen)_3]^{2+}$ < $[Ni(phen)_2(dpq)]^{2+}$ < $[Ni(phen)_2(dpqc)]^{2+}$ < $[Ni(phen)_2(dppz)]^{2+}$. This sequence is similar to the order of binding affinity derived from absorption titration experiments involving D2, and is supported by the results of gel electrophoresis studies and transcription inhibition assays. Overall these results therefore provide a further demonstration of the potential of ESI-MS for analysis of binding interactions between metallointercalators and DNA, first revealed by studies involving the analogous ruthenium(II) complexes,[77,166] and more recently by experiments with square planar platinum(II) complexes.[18] In addition, ESI-MS proved to be a valuable tool for developing an improved method for the preparation of nickel(II) complexes.

Each of the techniques supported the conclusion that nickel(II) complexes generally interact more weakly with DNA than the corresponding ruthenium(II) complexes. This was most evident in the case of complexes containing dpqc and dppz ligands owing to their greater overall binding strengths. However, circular dichroism experiments and transcription inhibition assays also supported this conclusion in the case of the two complexes containing dpq ligands. One possible explanation for these observations is that

ruthenium and nickel complexes with identical ligand environments show systematic differences in metal-ligand bond distances, and therefore overall size. A survey of the crystallographic literature shows that the Ru-N(phen) bond distances in $[Ru(phen)_3](PF_6)_2$ (av. 2.063(4) Å),[262] $[Ru(phen)_2(bpy)]Cl_2.6H_2O$ (2.073(9) – 2.087(10) Å)[263] and $[Ru(phen)_2(dpq)](PF_6)_2$ (2.065(6) – 2.073(6) Å)[236] are slightly shorter than the Ni-N(phen) bond distances in complexes such as $[Ni(phen)_3](NO_3)_2$.thiourea monohydrate (2.0701(15) – 2.1060(16) Å),[264] $[Ni(phen)_3](ClO_4)_2.0.5H_2O$ (2.078(8) – 2.103(7) Å)[265] and $[Ni(phen)_2(H_2O)Cl]Cl.H_2O.CH_3CN$ (2.092(3) – 2.116(3) Å).[253] Unfortunately no crystallographic data exist for any of the other five complexes examined here. However, if the above data are representative of Ru-N(phen) and Ni-N(phen) bond distances, then it appears that the ruthenium complexes might be slightly smaller in size than their nickel analogues. This may enable the former complexes to participate in slightly stronger electrostatic interactions with the negatively charged DNA molecule. Alternatively, the smaller ruthenium molecules may fit more readily into the major or minor groove of DNA, and insert their dpq, dpqc and dppz ligands into the DNA base stack to a slightly greater extent. In a very recent study,[242] Ramakrishnan and Palaniandavar considered the effects of overall size and coordination geometry on the DNA binding of related series of zinc(II) and copper(II) complexes. These workers found the complex $[Cu(5,6\text{-dmp})_3](ClO_4)_2$ (5,6-dmp = 5,6-dimethyl-1,10-phenanthroline) binds more tightly to CT DNA than its zinc analogue $[Zn(5,6\text{-dmp})_3](ClO_4)_2$. This was suggested to be due to the smaller size of the former complex, which would favour stronger electrostatic interactions, as well as its more flexible coordination geometry.

An alternative explanation for the consistently stronger DNA binding exhibited by ruthenium complexes throughout the experiments described in this chapter, is that they bind to different DNA base sequences and/or interact using slightly different binding modes than the analogous nickel complexes. There has already been significant work in this area, primarily on the interactions of ruthenium complexes with CT-DNA. These studies have led to considerable debate as to the exact means by which complexes such as $[Ru(phen)_2(dppz)]^{2+}$ bind to DNA.[91,226,227,235,266,267] In the case of nickel complexes it has also been shown that a slight change in DNA base sequence could alter the exact binding location of the metal complex.[91] These studies all serve to highlight that more detailed structural data, especially information from X-ray studies on crystals containing the above metal complexes bound to the same DNA molecule, is required before it may be possible to assign the differences in binding affinity observed here between nickel and ruthenium complexes to variations in binding mode, or slight differences in size or shape of the metal complexes themselves.

Chapter 4
Investigation of the Binding of Metal Complexes to Quadruplex DNA

4.1 Scope of this Chapter

Today ESI-MS is widely recognised as a suitable technique for the analysis of non-covalent biological complexes with duplex DNA.[136,139,268] In contrast, the utilisation of ESI-MS to observe non-covalent complexes containing qDNA has only been recently reported.[162,167,171] The proven capability of ESI-MS for investigating binding interactions generally, as well as qDNA itself, will most likely see reports describing the use of ESI-MS for analysis of qDNA and qDNA/drug interactions increase dramatically. A survey of the literature also shows that whilst there have been many reports of organic compounds that can selectively bind to qDNA,[105,171,268-270] the number of studies examining the binding of metal complexes to qDNA has been limited.[93,108,109,170] This is surprising in view of the high binding affinity some metal complexes have displayed towards dsDNA, and the opportunities available to design octahedral or square planar metal complexes with ligands carefully selected to enhance binding to other types of nucleic acid structures.

In the first part of this chapter, the use of ESI-MS for determining the gas phase dissociation profile of the parallel tetrameric quadruplex Q5 $(TTGGGGGT)_4$ and the anti-parallel dimeric quadruplex Q2 $(GGGGTTTTGGGG)_2$ is described. These experiments were performed in order to assess the stability of different qDNA strucutures in the gas phase, prior to selecting one specific quadruplex for subsequent binding studies with metal complexes. In addition, the results of tandem MS studies on the qDNA structures are

compared to those obtained in the only two other studies of this type that have appeared in literature to date.[167,271]

The second part of this chapter describes results obtained using ESI-MS as a screening tool for determining the relative binding affinities of the metal complexes shown in **Figure 4.1** towards Q5. These complexes were selected to enable the effects of changing the identity of the central metal ion and the stereochemistry of the complex on qDNA binding interactions to be examined. Additional ESI-MS experiments were performed to obtain information about the binding modes of the ruthenium and platinum complexes. This included analysis of the results of competition experiments involving the metal complexes and the organic intercalator daunomycin, and an investigation of the effect of changing the length of the tetrameric qDNA used on the number of metal complexes or daunomycin molecules that it could bind.

Circular dichroism spectroscopy has proven to be a useful technique for analysing the binding interactions of dsDNA with metal complexes.[113,114,116,234] While there have been only a few reports of its use for studying the interactions of qDNA with metal complexes, it has been used to determine the conformation of qDNA in ammonium acetate solutions prior to analysis by ESI-MS.[37,167,271] In this chapter the potential of CD spectroscopy for investigation of qDNA/metal complex interactions is further demonstrated, by comparing results obtained from CD spectra and ESI mass spectra of identical solutions.

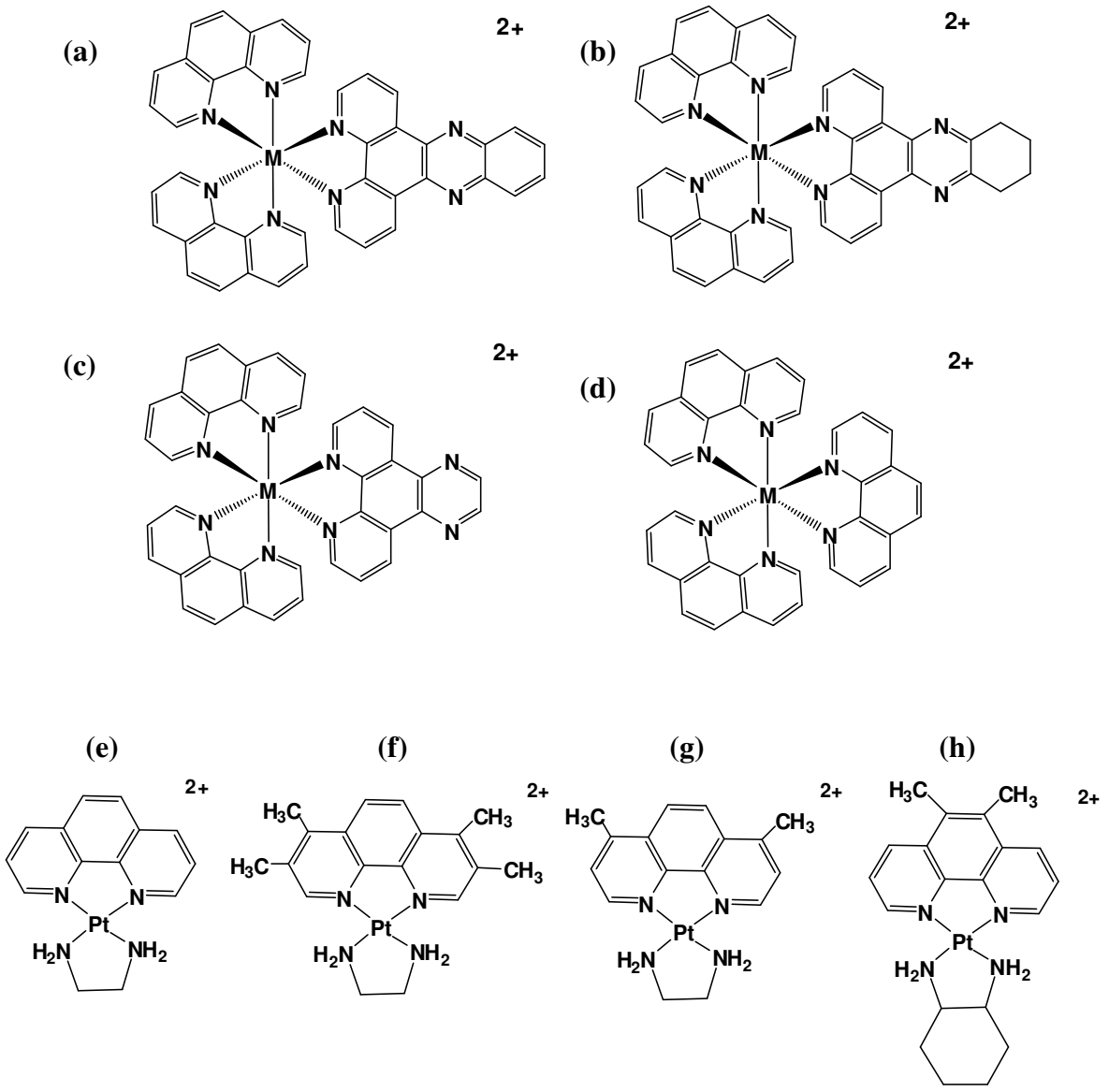

Figure 4.1: Structures of metal complexes used in studies with qDNA: (a) $[M(phen)_2(dppz)]^{2+}$, (b) $[M(phen)_2(dpqc)]^{2+}$, (c) $[M(phen)_2(dpq)]^{2+}$, (d) $[M(phen)_3]^{2+}$ (e) $[Pt(en)(phen)]^{2+}$, (f) $[Pt(en)(3,4,7,8\text{-}Me_4phen)]^{2+}$, (g) $[Pt(en)(4,7\text{-}Me_2phen)]^{2+}$ and (h) $[Pt(5,6\text{-}Me_2phen)(S,S\text{-dach})]^{2+}$ (M = Ni or Ru).

4.2 Conditions for Obtaining ESI-Mass Spectra of Quadruplex DNA

Negative ion ESI mass spectra of solutions containing qDNA (Q5 and Q2) were obtained when the DNA was annealed in, and sprayed from, 150 mM NH_4OAc, pH 7. Other researchers have obtained mass spectra of qDNA under similar conditions.[37,167,171] **Figure 4.2a** shows a negative ion ESI mass spectrum of $(TTGGGGGT)_4$ (Q5) obtained under these conditions. The spectrum contains contains ions at *m/z* 1675.3, 2010.6 and 2513.4 assigned to $[Q5 + 4NH_4^+ - 10H]^{6-}$, $[Q5 + 4NH_4^+ - 9H]^{5-}$ and $[Q5 + 4NH_4^+ - 8H]^{4-}$, respectively. Aqueous solutions containing NH_4OAc are commonly used in mass spectrometry, as it is a volatile salt. ESI-mass spectra of duplex DNA dissolved in aqueous NH_4OAc solution show no ions attributable to ammonium adducts of the oligonucleotide.[77,272] Therefore the presence of the above three ions all containing four ammonium ions bound to Q5, even after complete evaporation of the solvent and transfer through the mass spectrometer, strongly suggests that they are an intrinsic part of the qDNA structure. This is not unexpected since monovalent cations have been shown to stabilise qDNA structures by binding between the G-tetrad layers.[35] The observation that ESI mass spectra of Q5 consisted of ions containing $n-1 = 4$ ammonium ions, where $n = 5$ is the number of effective tetrads expected in the G-quadruplex structure, is therefore consistent with this.

The ESI mass spectrum of Q5 has previously been reported by David *et al.* [169] These workers used different instrumental and solution conditions (ThermoFinnigan LCQ ESI mass spectrometer, 3:1 55 mM aqueous NH_4OAc:methanol solutions) to those described in this thesis to obtain mass spectra. David *et al*. reported the observation of quadruplex ions with 6 and 7 Na^+ ions bound for the 7- charge state, but no quadruplex ions containing

bound ammonium ions. In contrast, other recent ESI-MS studies of G-quadruplex DNA performed using aqueous ammonium acetate did show the presence of *n-1* ammonium ions in quadruplex molecules having *n* G-tetrads.[37,136,167,171,273]

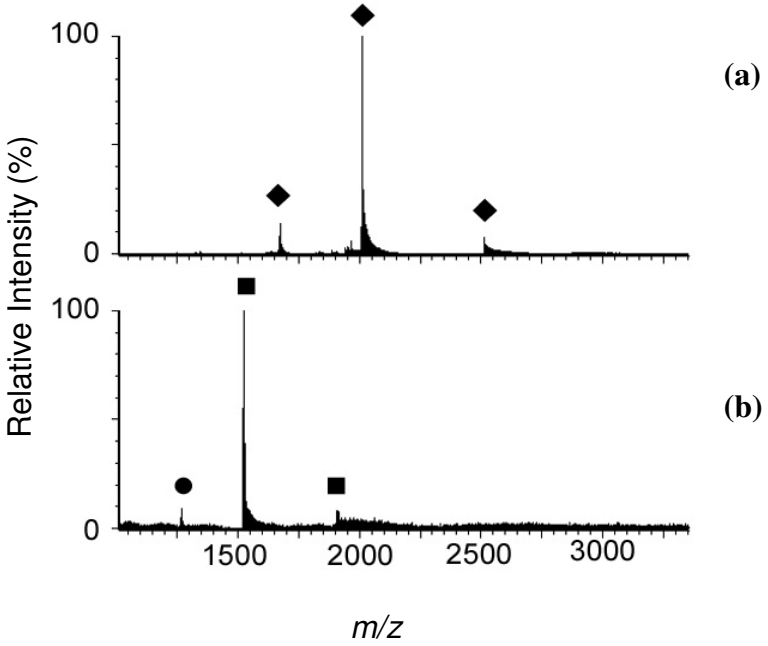

Figure 4.2: Negative ion ESI mass spectra of: (a) Q5 and (b) Q2. ◆ Q5 + $4NH_4^+$; ■ Q2 + $3NH_4^+$; and ● Q2 + $2NH_4^+$.

The ESI mass spectrum of Q2 shown in **Figure 4.2b** contains ions at *m/z* 1267.6, 1524.6 and 1906.2 corresponding to the two stranded structure $(GGGGTTTTGGGG)_2$ (Q2) with different numbers of bound ammonium ions. Specifically the ions of low abundance at *m/z* 1267.6 are assigned to $[Q2 + 2NH_4^+ - 8H]^{6-}$, while ions of high abundance at *m/z* 1524.6 and ions of low abundance at 1906.2 are assigned to $[Q2 + 3NH_4^+ - 8H]^{5-}$ and $[Q2 + 3NH_4^+ - 7H]^{4-}$, respectively.

Since this was the first time an ESI-MS spectrum of Q2 was obtained in our laboratory, experiments were performed in which ammonium acetate concentration and instrumental conditions (cone voltage, RF lens and desolvation temperature) were varied in order to

determine the best experimental conditions for acquiring a mass spectrum. The spectrum of Q2 shown in **Figure 4.2b** was obtained using a cone voltage of 70 V and a desolvation temperature of 120 ^{o}C. When the spectrum was acquired instead using the same experimental conditions found to be optimal for Q5 (cone voltage = 150 V, desolvation temperature = 200 ^{o}C), transformation of the spectrum only gave a mass of 7576 Da, which corresponds to the mass of Q2 without any bound ammonium ions. In the absence of ions attributable to ammonium adducts of Q2, it is not possible to confirm that the guanine tetrads are preserved in the solvent free environment of the mass spectrometer. However, when the source conditions were softened by reducing cone voltage and desolvation temperature, ions assigned to adducts of Q2 containing 3 ammonium ions were observed.

Rosu *et al.* have previously reported the ESI mass spectrum of Q2. They used 150 mM NH_4OAc, pH 7, and a Micromass Q-TOF2 instrument (similar to the instrument used in this work).[167] Immediately prior to injection of the sample a small amount of 15 % methanol was added. These workers also observed the 5- ion of Q2 with 3 ammonium ions bound, and showed that softer instrumental conditions (cone voltage and collision energy) were required to obtain this result than was necessary to observe the tetrameric qDNA molecule $(TGGGGT)_4$ containing three bound ammonium ions. They proposed that the stability of adducts containing ammonium cations bound between the tetrads was dependent on the conformational strain induced by the loops into the dimeric quadruplex molecule.[167]

4.3 Tandem Mass Spectrometry Studies Using Q5 and Q2

4.3.1 Studies performed using Q5

Tandem (MS/MS) mass spectrometry experiments allow ions of a given *m/z* to be selected, fragmented (or if a complex, dissociated) and the resulting product ions analysed. In a Q-TOF mass spectrometer the ions are selected in a quadrupole, and then accelerated in a hexapole where they undergo collisions with argon gas in a process called collision induced dissociation (CID). During this process, the relative kinetic energy produced when an ion collides with an argon atom is converted to vibrational energy of the ion (also called internal energy).[136] When these precursor ions have accumulated enough internal energy they fragment in the mass spectrometer.[160,272,274,275] In the present study, MS/MS experiments were used to assess the gas phase stabilities of 6-, 5- and 4- ions of Q5 and Q2, and to examine their fragmentation pattern. Only two other studies (Rosu *et al.* and Brodbelt *et al.*) [167,271] have examined the CID fragmentation pattern of qDNA. In both of these studies only the fragmentation pattern of 5- charge state ions was examined. In the current study MS/MS spectra of Q5 and Q2 were compared to those of similar quadruplexes used by Brodbelt and co-workers, and Rosu and co-workers.

Figure 4.3 shows the effect of increasing collision energy on the dissociation of the $[Q5 + 4NH_4^+ - 9H]^{5-}$ ion at *m/z* 2010.4. When a collision energy of 4 V was used, the precursor ion was still the most abundant. Ions of low abundance assigned to $[Q5 + 3NH_4^+ - 9H]^{5-}$ were also present at *m/z* 2006.3. Increasing the collision energy to 8 V resulted in ions assigned to $[Q5 + 3NH_4^+ - 8H]^{5-}$ and $[Q5 + 0NH_4^+ - 5H]^{5-}$ at *m/z* 2006.3 and 1996.2, respectively significantly increasing in abundance. In addition, ions assigned to $[Q5 + 1NH_4^+ - 6H]^{5-}$ and $[Q5 + 2NH_4^+ - 7H]^{5-}$ were now present in low to medium abundances.

Another ion of low abundance was now also observed at *m/z* 1966.5 that is attributable to the loss of a guanine and all four ammonium ions from the precursor ion. This is therefore the first occasion that ions arising from dissociation of a covalent bond were detected. When the collision energy was increased to 10 V and 14 V, ions corresponding to [Q5 + $0NH_4^+$ - 2G - 5H]$^{5-}$ and [Q5 + $0NH_4^+$– 3G - 5H]$^{5-}$ emerged and increased in relative abundance. In addition, at a collision energy of 14 V an ion at *m/z* 1247.7 (data not shown) appeared that is from single stranded DNA formed by dissociation of one or more strands of Q5. As no product ions corresponding to triple-stranded species were observed, it appears that at a collision energy of 14 V the complete dissociation of all four strands of qDNA was occurring.

The observation of ions arising from successive dissociation of guanine residues from Q5 contrasts with results reported from earlier MS/MS studies involving the 5- ion of tetrameric qDNA molecules. In these previous studies, the dissociation pathway involved initial loss of ammonium ions, followed by strand separation to produce a triplex ion, and finally guanine loss from the triplex species.[167,276] The tetrameric quadruplexes used containined 3 or 4 guanine tetrads ($(TGGGT)_4$ and $(TGGGGT)_4$), while the Q5 molecule used in the present study contains 5 guanine tetrads. The greater number of Hoogsteen hydrogen bonds holding the single strands together in Q5 would require greater energy to be applied in order for complete dissociation of a single strand to occur to form a triplex structure. Under these conditions it would most likely not be possible for triplex ions to persist, accounting for why they were not observed under our experimental conditions. A similar trend has also been observed with duplex DNA, where shorter duplexes first undergo dissociation of non-covalent bonds to give ssDNA, whereas longer duplexes

undergo extensive loss of DNA bases owing to cleavage of covalent bonds in addition to strand separation.[276]

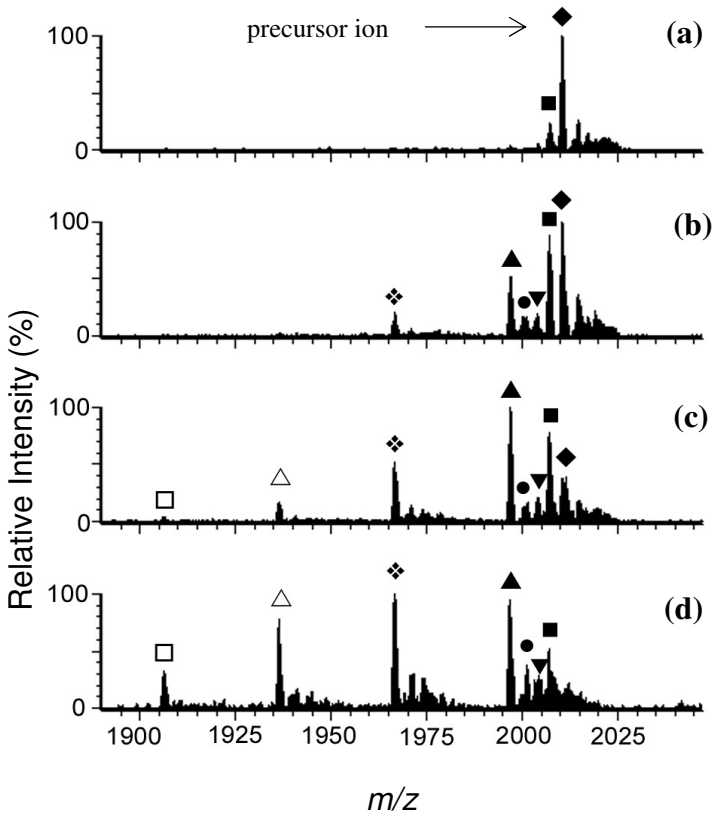

Figure 4.3: Negative ion MS/MS of $[Q5 + 4NH_4^+ - 9H]^{5-}$ at different collision energies: (a) 4 V, (b) 8 V, (c) 10 V and (d) 14 V. ◆$[Q5 + 4NH_4^+ - 9H]^{5-}$; ■ $[Q5 + 3NH_4^+ - 8H]^{5-}$; ● $[Q5 + 2NH_4^+ - 7H]^{5-}$; ▼ $[Q5 + 1NH_4^+ - 6H]^{5-}$; ▲ $[Q5 + 0NH_4^+ - 5H]^{5-}$; ❖ $[Q5 + 0NH_4^+ - 1G - 5H]^{5-}$; △ $[Q5 + 0NH_4^+ - 2G - 5H]^{5-}$; □ $[Q5 + 0NH_4^+ - 3G - 5H]^{5-}$. G is guanine.

Loss of thymine from Q5 did not occur under any of the conditions used in the experiments described here. Similar observations made in MS/MS studies of duplex DNA[276-279] have been accounted for by proposing that the lower proton affinity of thymine relative to the other DNA bases makes it a much less stable leaving group.[272,279]

The $[Q5 + 4NH_4^+ - 8H]^{4-}$ ion (*m/z* 2513.2) showed a similar dissociation profile (**Figures 4.4a-d)** to $[Q5 + 4NH_4^+ - 9H]^{5-}$. As the collision energy was increased from 4 V to 16 V,

ions arising from loss of ammonium ions were detected initially, while loss of guanine was observed at higher energies. Another interesting observation was that product ions attributable to Q5 with one or two bound NH_4^+ ions were absent from the dissociation profile for the 4- charge state, and observed only with low abundances in the dissociation profile for the 5- charge state. This indicates that these ions are not stable in the gas phase. The fragmentation pattern for the 6- ion ($[Q5 + 4NH_4^+ - 10H]^{6-}$; *m/z* 1675.6) is shown in **Figures 4.4e-h**, and is quite different to the dissociation profiles described above for the corresponding 5- and 4- ions. At a cone voltage of 4 V, $[Q5 + 4NH_4^+ - 10H]^{6-}$ is the predominant ion in the spectrum. Increasing the collision energy to 6 V results in an increase in abundance of ions assigned to $[Q5 + 3NH_4^+ - 9H]^{6-}$ and $[Q5 + 0NH_4^+ - 6H]^{6-}$. In addition, ions at *m/z* 1872.3 were observed that correspond to the triple-stranded species $[(TTGGGGGT)_3]^{4-}$. At collision energies of 8 V and 10 V (**Figures 4.4g** and **h,** respectively) ions corresponding to loss of one, two and three guanine bases from $[(TTGGGGGT)_3]^{4-}$ were observed. At collision energies of 6 and 8 V, an ion at *m/z* 1247.3 was present in the mass spectra with significant abundance (data not shown), that can be tentatively assigned to either the 2- charge state of single stranded TTGGGGGT or the 6- charge state of $(TTGGGGGT)_3$, as both species give the same *m/z* value. However, at 10 V an ion at *m/z* 1172.2 appears that is assignable only to $[TTGGGGGT - 1G - 2H]^{2-}$, suggesting that the ion at *m/z* 1247.3 is most likely attributable to $[TTGGGGGGT - 2H]^{2-}$. It is interesting to note that no 6- ions attributable to triplex or single stranded species were observed, and only ions with lower charge states (2- and 4-) attributable to these species were detected. A possible explanation for this observation is that the greater degree of charge repulsion present in the 6- charge state destabilises these complexes and hinders their ability to reach the detector. The fragmentation pathway for the 6- charge state ion

therefore occurs initially through loss of ammonium ions, followed by dissociation of a single strand. This results in the formation of a triple-stranded species which undergoes subsequent loss of guanine. In contrast, no loss of guanine from the tetrameric complex was observed. This overall pathway is similar to that observed previously in other studies involving $[(TGGGGT)_4]^{5-}$ and $[(TGGGT)_4]^{5-}$. [167,276] However, there is a clear difference between the fragmentation pathway for the 6- ion of Q5 + $4NH_4^+$, compared to the those for the corresponding 5- and 4- ions. This may be because the Hoogsteen hydrogen bonds in complexes carrying 6 negative charges may be sufficiently weakened compared to the less highly charged 4- and 5- ions to enable strand dissociation to occur prior to loss of a guanine residue.

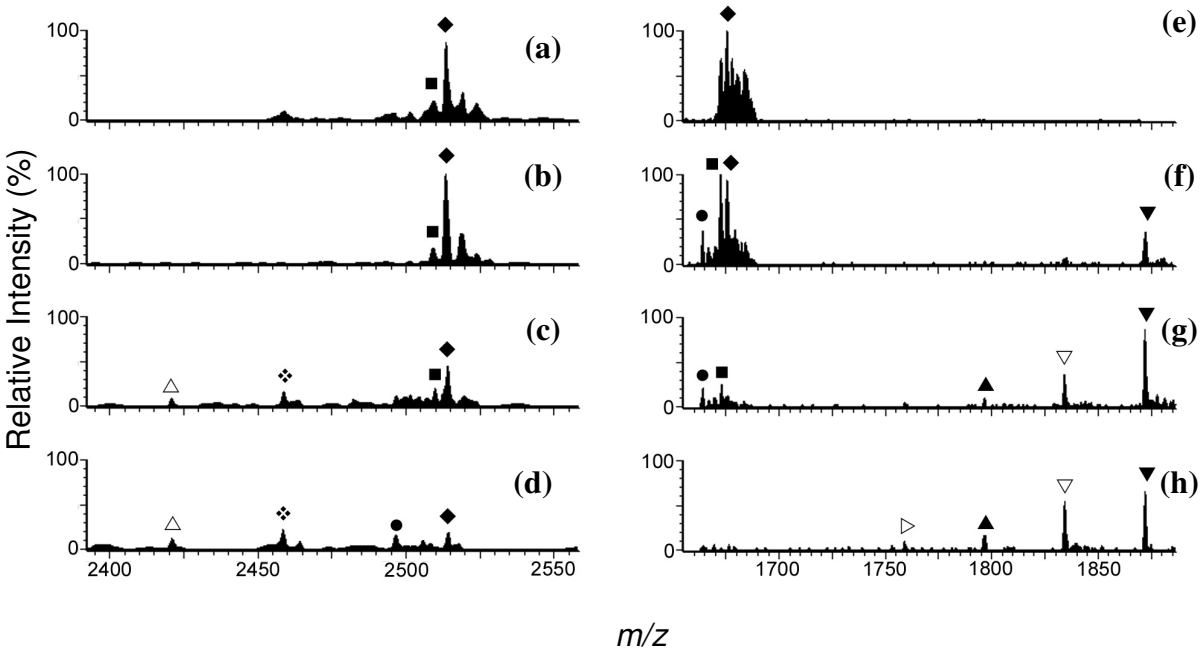

Figure 4.4: Negative ion MS/MS spectra of $[Q5 + 4NH_4^+ - 8H]^{4-}$ at: (a) 4 V (b) 10 V, (c) 14 V and (d) 16 V; and $[Q5 + 4NH_4^+ - 10H]^{6-}$ at: (e) 4 V, (f) 6 V, (g) 8 V and (h) 10 V .◆ Q5 + $4NH_4^+$, ■ Q5 + $3NH_4^+$, ● Q5 + $0NH_4^+$, ❖ Q5 + $0NH_4^+$ - 1G, △ Q5 + $0NH_4^+$ - 2G, ▼ $(TTGGGGGT)_3$, ▽ $(TTGGGGGT)_3$ - 1G, ▲ $(TTGGGGGT)_3$ – 2G and ▷ $(TTGGGGGT)_3$ – 3G.

Figure 4.5 show the relative abundances of the $[Q5 + 4NH_4^+ - 9H]^{5-}$ and $[Q5 + 4NH_4^+ - 8H]^{4-}$ ions at different collision energies. Increasing the collsion energy results in significant decreases in abundance of both types of ions. In addition, it is evident from **Figures 4.3** and **4.4** that the charge state plays a major role in determining the stability of Q5 ions the gas phase, with $[Q5 + 4NH_4^+ - 8H]^{4-}$ and $[Q5 + 4NH_4^+ - 9H]^{5-}$ showing greater stability than $[Q5 + 4NH_4^+ - 10H]^{6-}$. Similar results have also been observed with duplex DNA. For example, Wan *et al.* noted that as the charge on a DNA duplex increased from 3- to 5-, the collision energy required to reduce the relative abundance of the precursor ions to 50 % decreased significantly.[160] They proposed that the lower gas phase stability of duplex DNA ions with higher charge states is attributable to stronger Coulombic repulsion between the strands, which facilitates the dissociation of hydrogen bonds. [160]

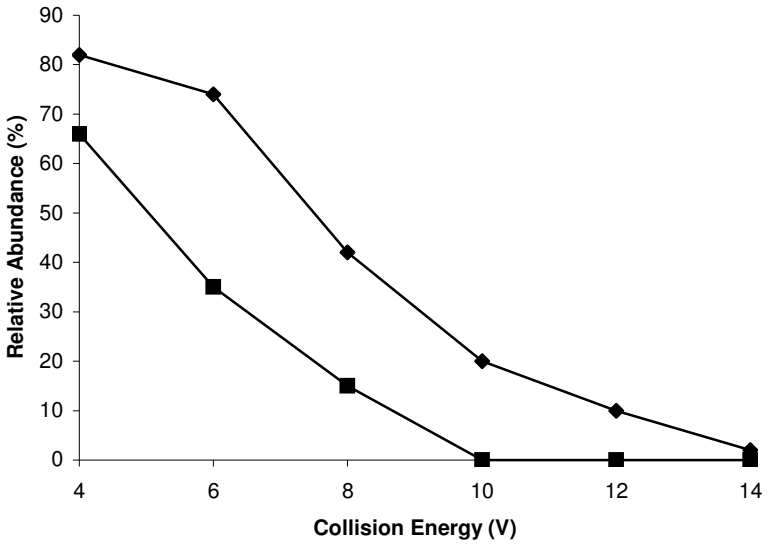

Figure 4.5: Effect of increasing collision energy on the relative abundance of the precursor ions ◆ $[Q5 + 4NH_4^+ - 9H]^{5-}$ and ■ $[Q5 + 4NH_4^+ - 8H]^{4-}$ in MS/MS experiments. Data for the $[Q5 + 4NH_4^+ + 10H]^{6-}$ ion are not shown here as it dissociates *via* a different pathway.

The monovalent cations that are often situated between the G-tetrads of qDNA are generally believed to be important contributors to the stability of quadruplex DNA

molecules. [40,280] Therefore the observation of product ions corresponding to Q5 + $0NH_4^+$ and Q5 + $0NH_4$ – G in MS/MS experiments raises the question whether these ions retain the quadruplex structure in the gas phase. Bowers and co-workers used ion-mobility mass spectrometry and molecular dynamics calculations to show that two-stranded and single-stranded quadruplexes maintain their structure in the gas phase in the absence of NH_4^+.[37] They proposed that ionic stabilisation of intramolecular qDNA is not required for the structure to survive. However, they could not confirm that four-stranded quadruplexes containing 3 and 4 G-tetrads retained a quadruplex structure in the absence of ammonium ion stabilisation in the gas phase. Future experiments using ion mobility mass spectrometry and molecular dynamics calculations are therefore required to determine if ions corresponding to four-stranded quadruplexes without bound ammonium ions maintain their structural integrity in the gas phase.

4.3.2 Studies performed using Q2

ESI-MS/MS experiments were also carried out to assess the stability of ions derived from Q2 in the gas phase. The dissociation profiles obtained from these experiments for the [Q2 + $2NH_4^+$ - 8H]$^{6-}$, [Q2 + $3NH_4^+$ - 8H]$^{5-}$ and [Q2 + $3NH_4^+$ - 7H]$^{4-}$ ions are shown in **Figures 4.6a, b** and **c**, respectively. **Figure 4.6a** (**part ii**) shows the product ion [Q2 + $0NH_4^+$ - 6H]$^{6-}$, formed by loss of two ammonium ions, is present in high abundance at a cone voltage of 4 V. As the collision energy was increased to 14 V (**Figure 4.6a parts (iii) - (v)**), no further dissociation ion was observed.

The ESI-MS/MS spectra shown in **Figure 4.6b** show that the complete loss of ammonium ions from [Q2 + $3NH_4^+$ - 8H]$^{5-}$ was observed only at a collision energy of 8 V. A further

point of contrast to the previous set of spectra shown in **Figure 4.6a** is that increasing the collision energy further did result in the appearance of ions at *m/z* 1484.5 and 1454.1, which can be attributed to the loss of guanine residues. This was also reported to occur in MS/MS experiments on the same two-stranded quadruplex by Brodbelt and co-workers.[271] The ESI-MS/MS spectra in **Figure 4.6c** (the 4- ion) do not show evidence of complete loss of ammonium ions until a cone voltage of 10 V was applied.

As previously mentioned, higher gas phase stability is often found with lower charge states for ions corresponding to DNA duplexes.[281] It was therefore expected that the stability of the precursor ions would follow the order: $[Q2 + 3NH_4^+ - 7H]^{4-} > [Q2 + 3NH_4^+ - 8H]^{5-} > [Q2 + 2NH_4^+ - 8H]^{6-}$. This order is evident when a comparison is made of the ESI-MS/MS spectra obtained using a collision energy of 4 V. **Figure 4.6a** (**part ii**) shows the ESI-MS/MS spectrum of $[Q2 + 2NH_4^+ - 8H]^{6-}$ at a collision energy of 4V. By far the most abundant ions present are those at *m/z* 1261.7 which are formed by loss of both ammonium ions. In contrast, **Figure 4.6b** (**part ii**) shows ions assigned to $[Q2 + 3NH_4^+ - 8H]^{5-}$ and the species produced by loss of all three ammonium ions are present in comparable abundances at a collision energy of 4V. The 4- ion $[Q2 + 3NH_4^+ - 7H]^{4-}$ proved to be even more stable under these conditions, as ESI-MS/MS experiments performed using a collision energy of 4V resulted in loss of only one ammonium ion (**Figure 4.6c** (**part ii**)).

It should be noted that Bowers and co-workers found using ion mobility mass spectrometry experiments that the higher charge states of single-stranded antiparallel intramolecular quadruplexes existed in different conformations in the gas phase.[37] It could therefore be possible that the higher Coulumbic repulsion likely to be present in the 6- charge state of

Q2 may contribute to dissociation of a G-tetrad, and adoption of a different conformation by the quadruplex that allows for the stable association of only two ammonium ions.

One way of conveniently comparing the stabilities of different precursor ions in ESI-MS/MS experiments is by determining their $E_{1/2}$ values. These values, which are presented in **Table 4.1** for some of the ions discussed above, are the calculated collision energies at which the relative abundance of the precursor ion is reduced to 50%.[163,271] The larger the $E_{1/2}$ value the more stable the quadruplex precursor ion is in the gas phase. Since the results in **Table 4.1** show that the $E_{1/2}$ values for different Q5 precursor ions are nearly twice as high as those for the corresponding charge states of Q2, it appears that ions arising from the tetrameric quadruplex Q5 have a higher gas phase stability compared to those arising from the dimeric Q2. These findings are consistent with those reported by Brodbelt and co-workers, who showed that precursor ions formed from the tetrameric quadruplexes $(TGGGGT)_4$ and $(TGGGT)_4$ had higher $E_{1/2}$ values compared to those formed from the dimeric quadruplex $(GGGGTTTTGGGG)_2$.[271]

Table 4.1: Summary of $E_{1/2}$ values for precursor ions formed from Q5 and Q2.

Precursor Ions	**$E_{1/2}$ value***
Q5	
$[Q5 + 4NH_4^+ - 10H]^{6-}$	5.0
$[Q5 + 4NH_4^+ - 9H]^{5-}$	7.5
$[Q5 + 4NH_4^+ - 8H]^{4-}$	12.6
Q2	
$[Q2 + 2NH_4^+ - 8H]^{6-}$	2.2
$[Q2 + 3NH_4^+ - 8H]^{5-}$	3.5
$[Q2 + 3NH_4^+ - 7H]^{4-}$	6.4

*Calculated collision energies at which the relative abundance of the precursor ion is reduced to 50 % during CID.

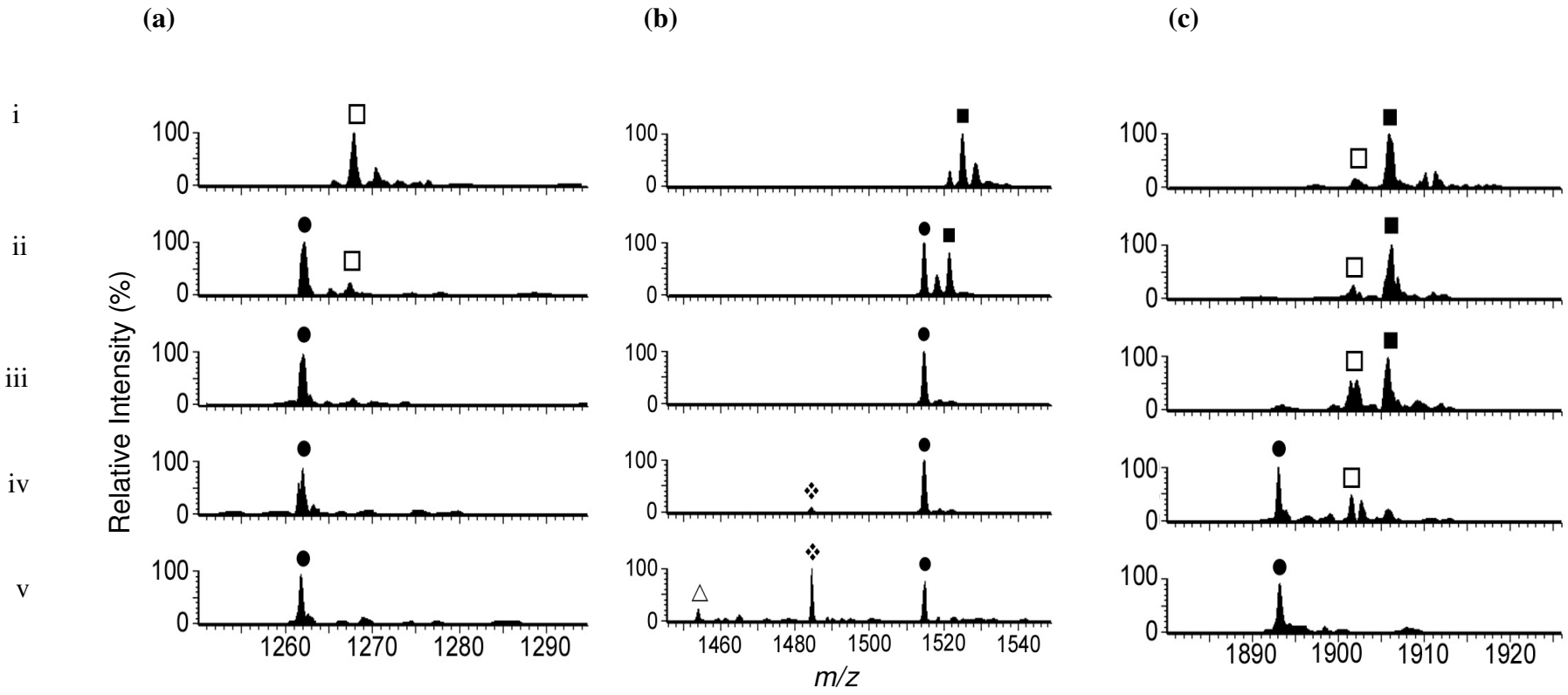

Figure 4.6: Negative ion ESI-MS/MS spectra of: (a) $[Q2 + 2NH_4^+ - 10H]^{6-}$ (b) $[Q2 + 3NH_4^+ - 8H]^{5-}$ and (c) $[Q2 + 3NH_4^+ - 7H]^{4-}$ at: (**i**) 2 V, (**ii**) 4 V, (**iii**) 8 V, (**iv**) 10 V and (**v**) 14 V. ■ $Q2 + 3NH_4^+$; □ $Q2 + 2NH_4^+$; ● $Q2 + 0NH_4^+$; ❖ $Q2 + 0NH_4^+ - 1G$; △ $Q2 + 0NH_4^+ - 2G$.

4.3.3 Effect of increasing cone voltage (in-source CID)

Another way of comparing the gas phase stability of different quadruplex ions is to perform in-source collision induced dissociation (CID) experiments. This is accomplished by increasing the cone voltage for the mass spectrometer, which raises the velocity of ions in the intermediate pressure region of the source. These energised ions undergo fragmentation upon collision with molecules of the bath gas (N_2) within the source.[86,282] By obtaining ESI mass spectra of Q5 and Q2 at several different cone voltages, the spectra shown in **Figure 4.7** were obtained. These reveal ion fragmentation patterns similar to the dissociation profiles obtained from MS/MS experiments (where energy is applied to one ion in the collision cell, rather than all ions in the source). For example, parts **(i)** and **(ii)** of **Figure 4.7a** show that when the cone voltage was 70 V or 150 V, the most abundant ions in the spectra were those at *m/z* 1674.9, 2010.0 and 2513.7, which are assigned to $[Q5 + 4NH_4^+ - 10H]^{6-}$, $[Q5 + 4NH_4^+ - 9H]^{5-}$ and $[Q5 + 4NH_4^+ - 8H]^{4-}$, respectively. Upon increasing the cone voltage further to 200V, and then to 250 V, new ions appeared as a result of loss of either one or all of the ammonium ions. In **Figure 4.7b** the spectrum of Q2 acquired using a cone voltage of 70 V shows ions of high abundance at *m/z* 1524.5 assigned to $[Q2 + 3NH_4^+ - 8H]^{5-}$. In addition, the spectrum contains ions of low abundance at *m/z* 1267.4 arising from $[Q2 + 3NH_4^+ - 9H]^{6-}$. Increasing the cone voltage from 70 V to 150 V resulted in a dramatic change in the spectrum. Most notably the most abundant ion in the spectrum was now that at *m/z* 1521.2, which was formed by loss of an ammonium ion from *m/z* 1524.5. In addition, the ions at *m/z* 1267.4 in part (i) of **Figure 4.7b** were now replaced by ions at *m/z* 1261.7 that contain no ammonium ions at all. These events involving loss of one or more ammonium ions occurred at a much lower cone voltage than that required for similar processes to occur with Q5. This is therefore further evidence that the

intermolecular 4-stranded quadruplex Q5 is more stable in the gas phase than the 2-stranded intermolecular quadruplex Q2.

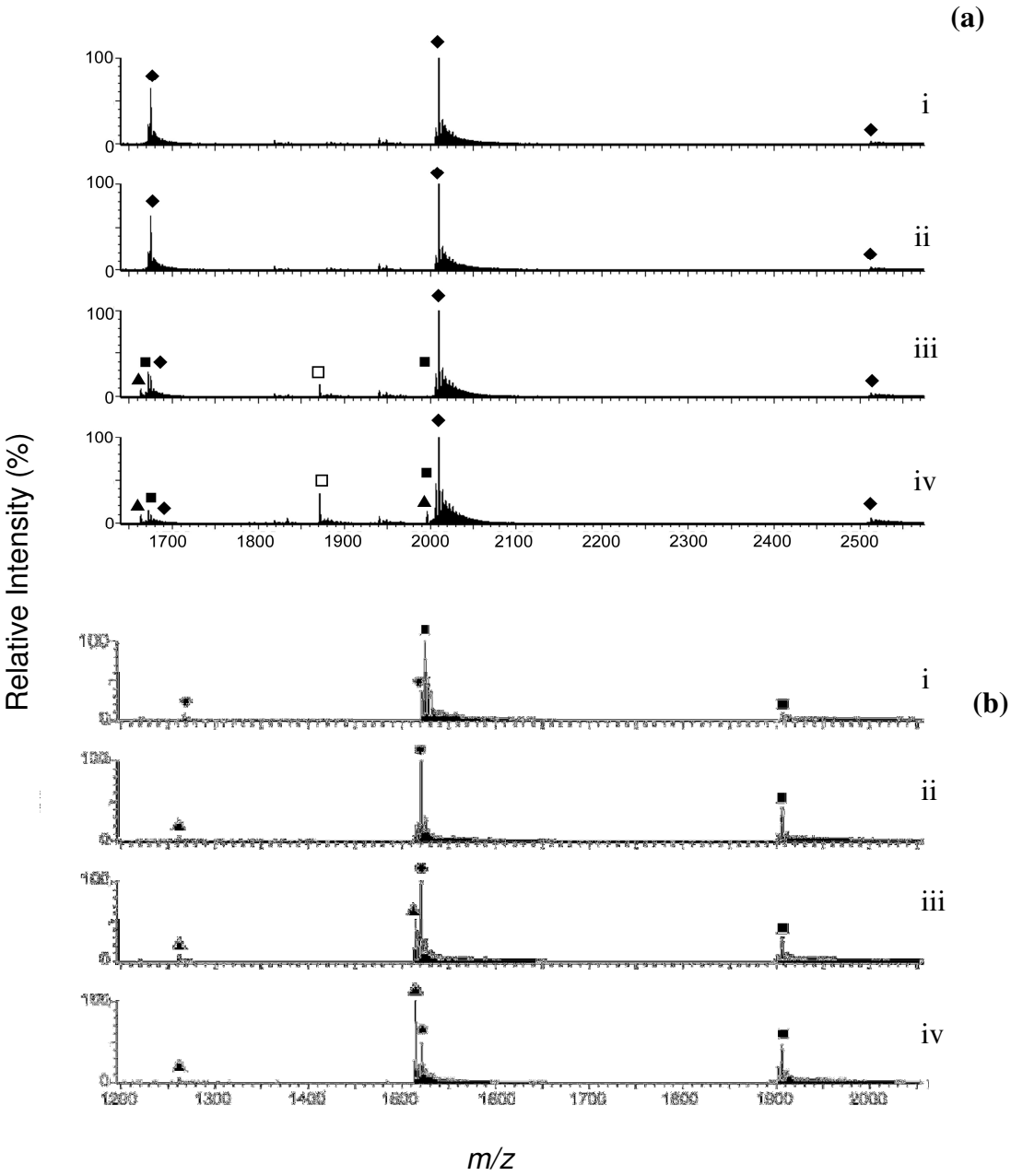

Figure 4.7: Effect of increasing cone voltage on negative ion ESI mass spectra of: (a) Q5 and (b) Q2 at: (i) 70V, (ii) 150V, (iii) 200V and (iv) 250V. ◆ quadruplex + $4NH_4^+$; ■ quadruplex + $3NH_4^+$; ● quadruplex + $2NH_4^+$; ▲ quadruplex + $0NH_4^+$.

4.4 ESI-MS Studies of the Binding Interactions of Metal Complexes with qDNA

4.4.1 Ruthenium Complexes and Q5

The use of ESI-MS for investigating the binding affinity, selectivity, and mode of interaction of $[Ru(phen)_3]^{2+}$, $[Ru(phen)_2(dpq)]^{2+}$, $[Ru(phen)_2(dpqc)]^{2+}$ and $[Ru(phen)_2(dppz)]^{2+}$ with the duplex DNA molecule D2 has been reported previously.[77,166] In these earlier studies it was found that the ruthenium complexes containing intercalating ligands with greater surface area ($[Ru(phen)_2(dpqc)]^{2+}$ and $[Ru(phen)_2(dppz)]^{2+}$) were the most avid DNA binders, and formed complexes containing up to 5 ruthenium molecules non-covalently bound to D2. In the present study, ESI-MS was used to investigate the binding of the ruthenium complexes to Q5. This was performed in order to see if the ruthenium complexes displayed greater or lesser binding affinity towards quadruplex DNA compared to duplex DNA, and to see if changing the third chelating ligand produced similar effects on quadruplex DNA binding to those noted above. These experiments were performed using Q5 because the results presented in the first part of this chapter showed it was more stable in the gas phase than Q2.

Figure 4.8 shows the negative ion ESI mass spectra of Q5 and solutions containing 10:1, 20:1, 30:1 and 40:1 ratios of $[Ru(phen)_2(dppz)]^{2+}$ and Q5. The spectrum of Q5 alone (**Figure 4.8a**) displays ions at *m/z* 1674.8 and 2009.9, assigned to $[Q5 + 4NH_4^+ - 10H]^{6-}$ and $[Q5 + 4NH_4 - 9H]^{5-}$, respectively. These ions were still present in the spectrum of the solution containing a 10:1 ratio of $[Ru(phen)_2(dppz)]^{2+}$ and Q5 (**Figure 4.8b**). In addition, this spectrum contains new ions at *m/z* 1798.6 and 2158.6 that can be assigned to non-covalent complexes containing one ruthenium molecule bound, and additional ions at *m/z*

1922.5 and 2307.0 that can be assigned to non-covalent complexes containing two ruthenium molecules bound to Q5. Increasing the ratio of Ru:Q5 further to 20:1 resulted in the abundance of these ions increasing so that they now dominated those attributable to free qDNA (**Figure 4.8c**). This spectrum also shows ions of low abundance at *m/z* 2455.2 that are assigned to a non-covalent complex of Q5 containing three intact $[Ru(phen)_2(dppz)]^{2+}$ molecules.

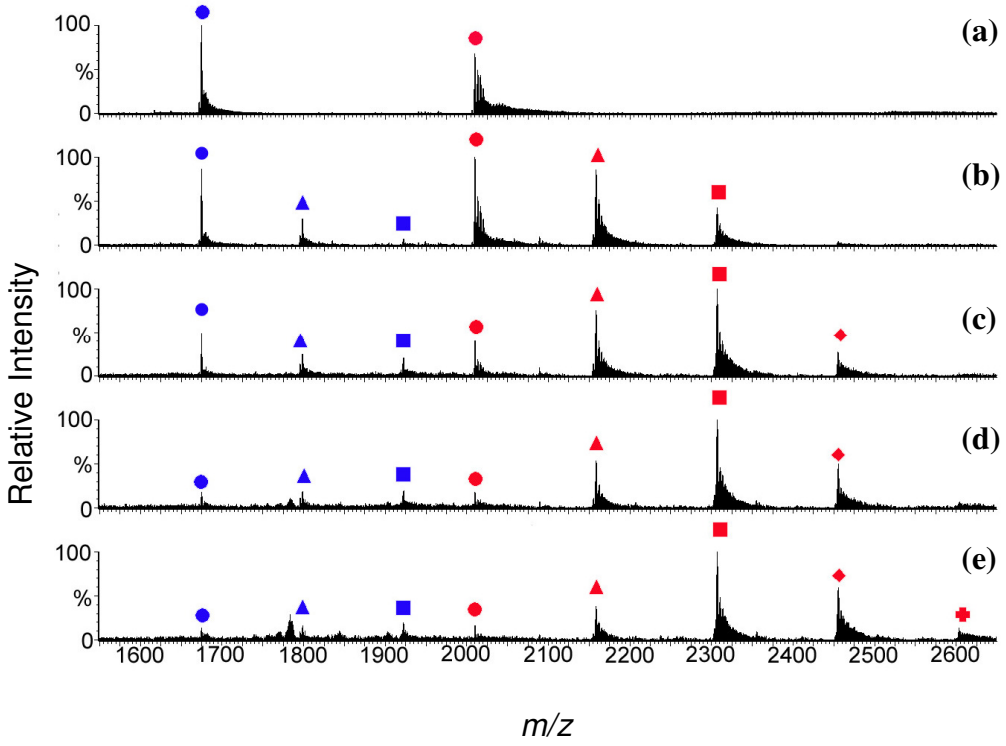

Figure 4.8: Negative ion ESI mass spectra of free Q5 and solutions containing different ratios of $[Ru(phen)_2(dppz)]^{2+}$ and Q5: (a) free Q5; (b) Ru:Q5 = 10:1; (c) Ru:Q5 = 20:1; (d) Ru:Q5 = 30:1; (e) Ru:Q5 = 40:1. ● free Q5; ▲ Q5 + 1$[Ru(phen)_2(dppz)]^{2+}$; ■ Q5 + 2$[Ru(phen)_2(dppz)]^{2+}$; ◆ Q5 + 3$[Ru(phen)_2(dppz)]^{2+}$; ✚ Q5 + 4$[Ru(phen)_2(dppz)]^{2+}$. Ions marked in red are 5- ions and ions marked in blue are 6- ions.

The spectra of solutions containing 30 and 40 equivalents of the ruthenium complex (**Figures 4.8d** and **e,** respectively) show that the relative abundance of ions assigned to free Q5 continued to decrease, while those assigned to more highly substituted non-covalent

complexes increased. The latter trend is particularly evident amongst ions with an overall charge of 5- (red), and was also observed in studies with each of the other ruthenium complexes. Whilst **Figure 4.8e** was the only spectrum to clearly show ions at *m/z* 2604.0 that may be assigned to non-covalent qDNA complexes containing four ruthenium molecules, there is overall very little difference between it and the spectrum in **Figure 4.8d**. This indicates that equilibrium was being approached in these solutions with high Ru:Q5 ratio.

The above results suggest that ESI-MS may be useful for analysing the composition of solutions containing metal complexes and qDNA. In addition, it appears that the binding affinity of $[Ru(phen)_2(dppz)]^{2+}$ towards Q5 is considerably less than that towards D2. This conclusion is supported by the following comparison. In the spectrum of a solution containing a 40:1 ratio of $[Ru(phen)_2(dppz)]^{2+}$ and Q5 (**Figure 4.8e**), the most abundant ions assigned to non-covalent complexes were those containing just two ruthenium molecules bound to Q5. In contrast, for reaction mixtures containing D2 and just 6 equivalents of $[Ru(phen)_2(dppz)]^{2+}$, the most abundant ions assigned to non-covalent complexes in the ESI mass spectrum contained four ruthenium molecules bound to the DNA duplex.[77,166] This suggests that there may be significant differences between the nature of the binding interactions between $[Ru(phen)_2(dppz)]^{2+}$ and the two types of DNA molecules, a proposal that is supported by the results obtained with the other ruthenium complexes (see below).

In order to directly compare binding affinities towards quadruplex DNA, negative ion ESI mass spectra were obtained of reaction mixtures containing a 40:1 ratio of the different ruthenium complexes and Q5. These spectra are shown in **Figure 4.9**, and are very similar

in appearance to each other. For example, in each case the abundance of ions attributable to free Q5 is very low, and the most abundant ions attributable to non-covalent complexes are 5- ions containing two ruthenium molecules bound to Q5. In addition, each spectrum shows ions assigned to non-covalent complexes containing one and three ruthenium molecules bound to Q5 that are of medium to high, and medium to low abundance, respectively. The similarity of the spectra suggests that these ruthenium complexes have very similar overall binding affinities towards Q5 and possibly similar binding mechanisms. The slightly greater abundance of ions attributable to Q5 with three $[Ru(phen)_2(dppz)]^{2+}$ bound suggests that this ruthenium complex may have a slightly higher binding affinity than the others. However, the differences in affinity are not as dramatic as that found previously in studies of the binding of the same complexes to dsDNA.[77,166]

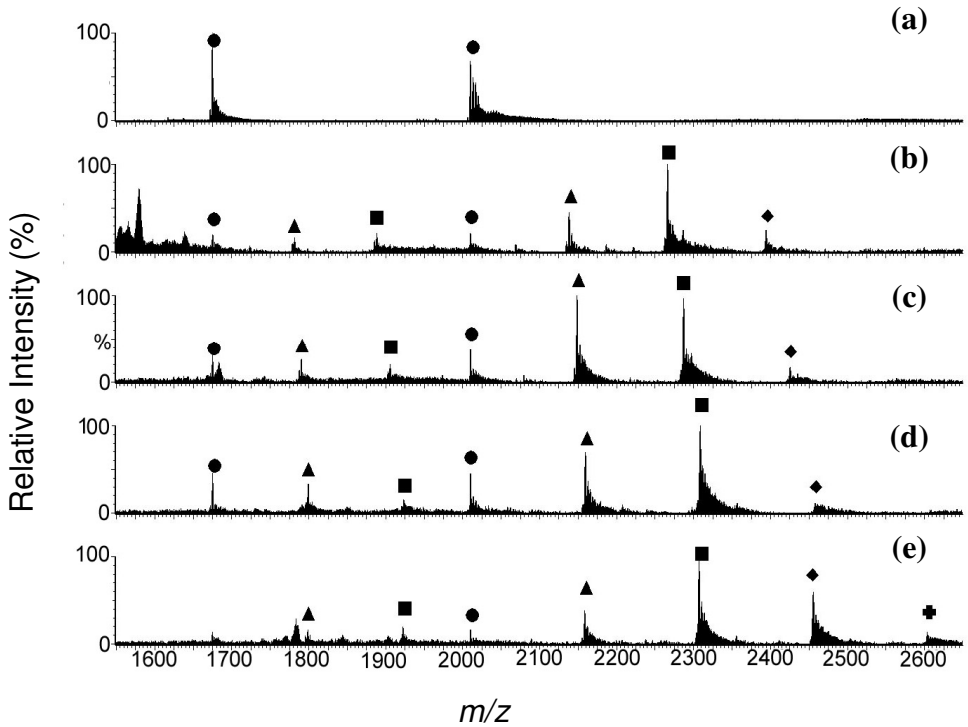

Figure 4.9: Negative ion ESI mass spectra of free Q5 and solutions containing a 40:1 ratio of different ruthenium complexes and Q5: (a) free Q5; (b) Q5 + $[Ru(phen)_3]^{2+}$; (c) Q5 + $[Ru(phen)_2(dpq)]^{2+}$; (d) Q5 + $[Ru(phen)_2(dpqc)]^{2+}$; (e) Q5 + $[Ru(phen)_2(dppz)]^{2+}$. ● free Q5; ▲ Q5 + 1$[Ru(phen)_2(L)]^{2+}$; ■ Q5 + 2$[Ru(phen)_2(L)]^{2+}$; ◆ Q5 + 3$[Ru(phen)_2(L)]^{2+}$; ✚ Q5 + 4$[Ru(phen)_2(L)]^{2+}$.

In the latter studies it was found that the order of binding affinity towards dsDNA was $[Ru(phen)_2(dppz)]^{2+} \geq [Ru(phen)_2(dpqc)]^{2+} > [Ru(phen)_2(dpq)]^{2+} > [Ru(phen)_3]^{2+}$. However, in the present study there appears to be only a small difference between the binding affinity of the complex with the lowest qDNA affinity ($[Ru(phen)_3]^{2+}$) and that of each of the other ruthenium complexes. It therefore appears that the presence of strongly intercalating ligands such as dppz in the coordination sphere of a metal ion does little, if anything, to enhance its overall binding affinity towards qDNA. This in turn suggests that classical intercalative interactions may not play as important a role in determining the strength of binding interactions between metal complexes and quadruplex DNA, as they do in non-covalent metal ion/dsDNA interactions. In most cases G-quadruplex binders have been reported to interact with DNA by "end stacking", which is stacking onto the external face of the terminal G-quartet [92-94,105,109] There are, however a small number of reports of small molecules that have displayed binding to G-quadruplex DNA through intercalation between adjacent G-tetrads.[92,95,283,284] Intercalative binding modes have been proposed for TMPyP4 derivatives, although this has been controversial as various other binding models have also been proposed[92,95,283,284] Intercalative binding modes towards G-quadruplex DNA have been proposed for TMPyP4 derivatives, although this has been controversial as various other binding models have also been proposed.[92,95,283,285] These other models include binding at a G-A interface [286] and end stacking.[287,288] Of these binding models, porphyrin intercalation between adjacent G-tetrads has appeared to be the least energetically favored.[286] Typically, the binding mode of a small molecule to G-quadruplex DNA is influenced by the topology and folding arrangement of the DNA strands of the quadruplex molecule. Exterior loops found in unimolecular and dimeric quadruplexes are expected to hinder intercalative binding by small molecules. In addition, intercalation into

four-stranded quadruplexes may possibly interfere with the ionic stabilisation of the quadruplex, potentially disrupting the quadruplex structure.[94,285]

4.4.2 Nickel Complexes and Q5

In order to determine the suitability of ESI-MS for analysing interactions of nickel complexes with quadruplex DNA, similar experiments to those described above were conducted with $[Ni(phen)(dppz)]^{2+}$, $[Ni(phen)_2(dpqc)]^{2+}$, $[Ni(phen)_2(dpq)]^{2+}$ and $[Ni(phen)_3]^{2+}$. ESI mass spectra were obtained of solutions containing Ni:Q5 ratios of 10:1, 20:1, 30:1 and 40:1. The results of these experiments were to be compared to those above obtained using the analogous series of ruthenium complexes, in order to ascertain the effects, if any, of varying the metal centre on the strength of qDNA binding. In addition, it was initially intended to compare the orders of relative binding affinity for the nickel complexes with both D2 and Q5, to see if the differences in behaviour exhibited by the ruthenium complexes also extended to those of nickel.

Surprising results were obtained, however, when solutions containing the above nickel complexes and Q5 were analysed by ESI-MS. For example, **Figure 4.10** shows the mass spectra of solutions containing a 10:1 ratio of $[Ni(phen)_2(dpq)]^{2+}$ or $[Ni(phen)_2(dpqc)]^{2+}$ and Q5. Neither spectrum contains ions of medium or high abundance attributable to non-covalent complexes containing Q5 with one or more intact nickel molecules bound. Instead the most abundant ions other than those assigned to free Q5, were attributable to Q5 + $[Ni(phen)(dpq)]^{2+}$ and Q5 + $[Ni(phen)(dpqc)]^{2+}$. These were almost certainly formed by loss of a phenanthroline ligand from non-covalent complexes containing intact $[Ni(phen)_2(dpq)]^{2+}$ or $[Ni(phen)_2(dpqc)]^{2+}$ molecules bound to Q5, which suggests that

significant levels of fragmentation had taken place in the mass spectrometer.

Further evidence for this was provided by the observation of other ions of low to medium abundance, such as Q5 + $[Ni(phen)]^{2+}$ and Q5 + $2[Ni(phen)]^{2+}$, in both spectra. Similar results were also obtained when ESI mass spectra were obtained of solutions containing $[Ni(phen)_3]^{2+}$ or $[Ni(phen)_2(dppz)]^{2+}$ and Q5, consistent with the conclusion that non-covalent complexes containing nickel molecules bound to qDNA were unstable in the mass spectrometer.

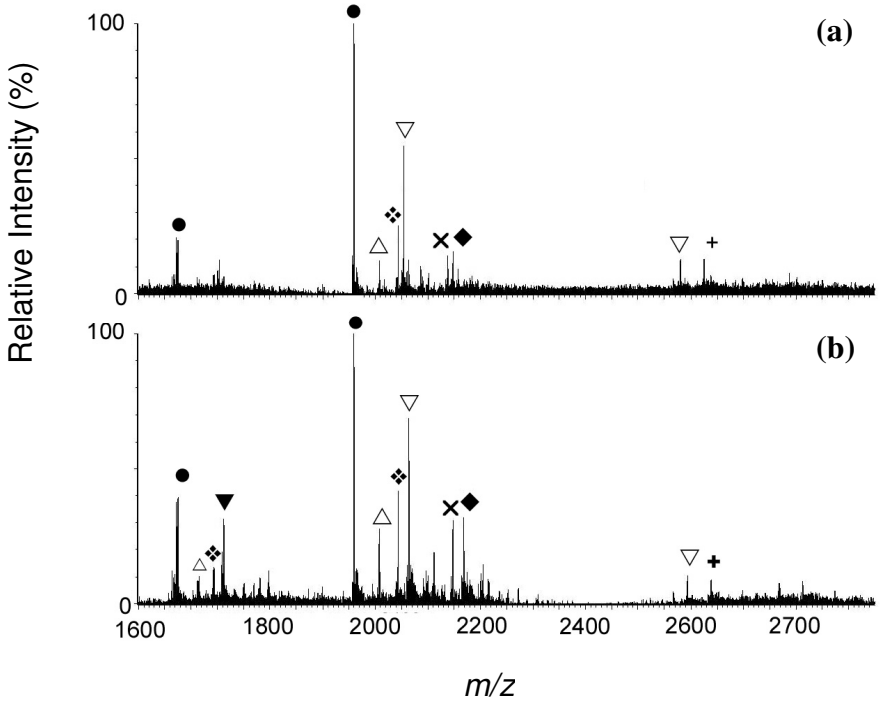

Figure 4.10: Negative ion ESI mass spectra of solutions containing: (a) a 10:1 ratio of $[Ni(phen)_2(dpq)]^{2+}$ and Q5; and (b) a 10:1 ratio of $[Ni(phen)_2(dpqc)]^{2+}$ and Q5: ● free Q5; △ Q5 + $[Ni(phen)]^{2+}$; △Q5 + $[Ni(phen)_2]^{2+}$, ❖ Q5 + $[Ni(phen)(L)]^{2+}$ (L = dpq or dpqc); ▽ Q5 + $[NI(phen)_2]^{2+}$ + $[Ni(phen)(L)]^{2+}$ (L = dpq or dpqc); ✖ Q5 + $2[Ni(phen)(L)]^{2+}$ (L = dpq or dpqc) ; ✚ Q5 + $[Ni(phen)_2(L)]^{2+}$ (L = dpq or dpqc).

The above results were unexpected in view of the absence of evidence for fragmentation occurring during mass spectral analysis of solutions containing either nickel or ruthenium

complexes and dsDNA, or solutions containing ruthenium complexes and qDNA. One possible explanation is that the slightly lower thermodynamic stability of the nickel complexes, combined with the slightly harsher instrumental conditions required to obtain mass spectra of qDNA (cone voltage = 150 V instead of 100 V, desolvation temperature = 150 ^{o}C instead of 100 ^{o}C), are sufficient for fragmentation of non-covalent complexes containing intact metal complexes bound to DNA to occur in the case of the nickel complexes. In order to obtain further evidence for this conclusion, a comparative tandem mass spectral analysis was performed on solutions containing Q5 and either $[Ni(phen)_3]^{2+}$ or $[[Ru(phen)_3]^{2+}$. The parent ions that were selected for MS/MS were $[Q5 + 4NH_4^+ + [Ru(phen)_3]^{2+} - 11H]^{5-}$ and $[Q5 + 4NH_4^+ + 2[Ni(phen)_2]^{2+} -13H]^{5-}$. The latter ion was selected instead of the $[Q5 + 4NH_4^+ + [Ni(phen)_3]^{2+} -11H]^{5-}$ because its greater stability resulted in better quality spectra that could be easily interpreted. The results of these experiments are shown in **Figure 4.11**, and reveal that ions attributable to $[Q5 + 4NH_4^+ + [Ru(phen)_3]^{2+} - 11H]^{5-}$ and $[Q5 + 4NH_4^+ + 2[Ni(phen)_2]^{2+} - 13H]^{5-}$ follow very different fragmentation pathways. For example, **Figure 4.11a** shows that the MS/MS profile of $[Q5 + 4NH_4^+ + [Ru(phen)_3]^{2+} - 11H]^{5-}$ involves initial loss of ammonium ions, followed by dissociation of a guanine nucleotide from the non-covalent DNA/metal complex. No evidence for loss of phenanthroline ligands was obtained, even at a colllsion energy of 12V. **Figure 4.11b** shows, instead, that loss of phenanthroline (180 Da) does occur from the $[Ni(phen)_2]^{2+}$/Q5 complex at a collsion energy of only 6 V. Similar results were obtained when tandem MS/MS experiments were performed using other ions present in these solutions or solutions containing different nickel and ruthenium complexes.

The above results therefore support the conclusion that it is the lower stability of Ni-N

bonds that results in fragmentation of non-covalent complexes containing intact nickel molecules bound to Q5. This conclusion has important implications concerning the analysis of non-covalent interactions between metal complexes and DNA, as it indicates that the initial coordination sphere of only the most thermodynamically stable metal ions may be able to survive the ESI process. Further evidence of this was obtained by examining the interactions of both $[Fe(phen)_3]^{2+}$ and $[Zn(phen)_3]^{2+}$with D2.

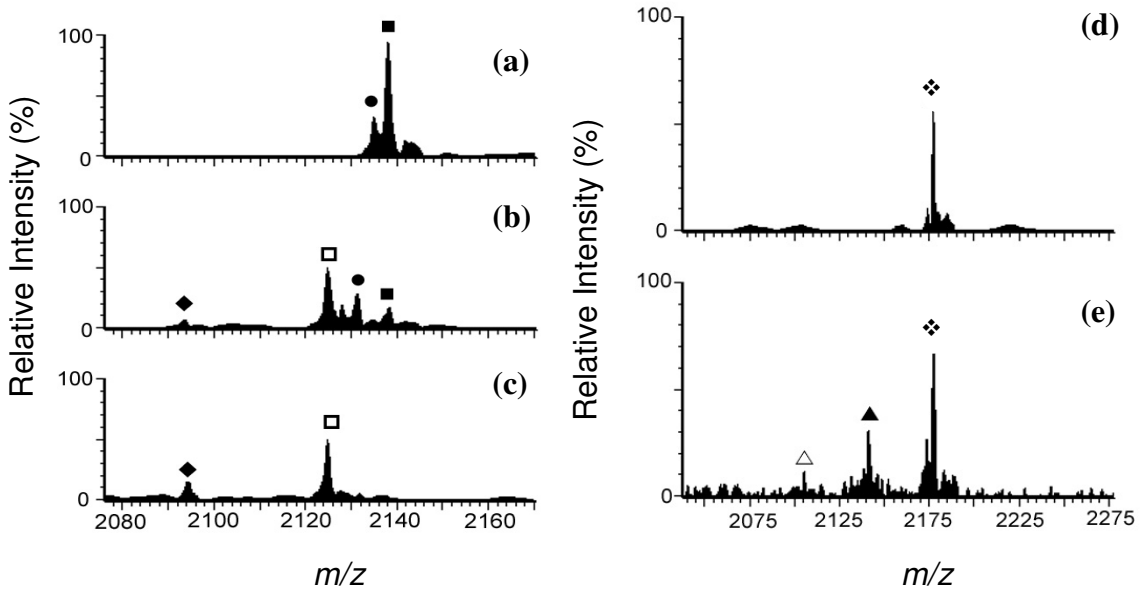

Figure 4.11: Negative ion MS/MS spectra of: $[Q5 + 4NH_4^+ + [Ru(phen)_3]^{2+} - 11H]^{5-}$ at different collision energies: (a) 4 V, (b) 8 V and (c) 12 V; and $[Q5 + 4NH_4^+ + 2[Ni(phen)_2]^{2+} - 8H]^{5-}$ at different collision energies: (d) 4 V and (e) 6 V. ■ $Q5 + 4NH_4^+ + [Ru(phen)_3]^{2+}$; ● $Q5 + 3NH_4^+ + [Ru(phen)_3]^{2+}$; □ $Q5 + [Ru(phen)_3]^{2+}$; ◆ $Q5 + [Ru(phen)_3]^{2+} - 1G$, ❖ $Q5 + 4NH_4^+ + 2[Ni(phen)_2]^{2+}$; ▲ $Q5 + 4NH_4^+ + [Ni(phen)_2]^{2+} + [Ni(phen)]^{2+}$; △ $Q5 + 4NH_4^+ + [Ni(phen)]^{2+}$.

Despite the gentler ESI conditions used to examine dsDNA, the mass spectra of both of the above systems showed that considerable fragmentation of non-covalent complexes had occurred. For example, **Figure 4.12** shows the ESI mass spectrum of a solution containing D2 and 40 equivalents of $[Fe(phen)_3]^{2+}$. The most abundant ions present, besides those

attributable to free D2, are assigned to [D2 + $[Fe(phen)_2]^{2+}$] and [D2 + $[Fe(phen)_3]^{2+}$]. Ions corresponding to [D2 + $[Fe(phen)_3]^{2+}$ + $[Fe(phen)_2]^{2+}$] and [D2 + $[Fe(phen)_3]^{2+}$ + $[Fe(phen)]^{2+}$] were also present in medium abundance. In the case of $[Zn(phen)_3]^{2+}$, the only ions that could be assigned to non-covalent complexes were those containing fragments of the initial zinc complex bound to D2.

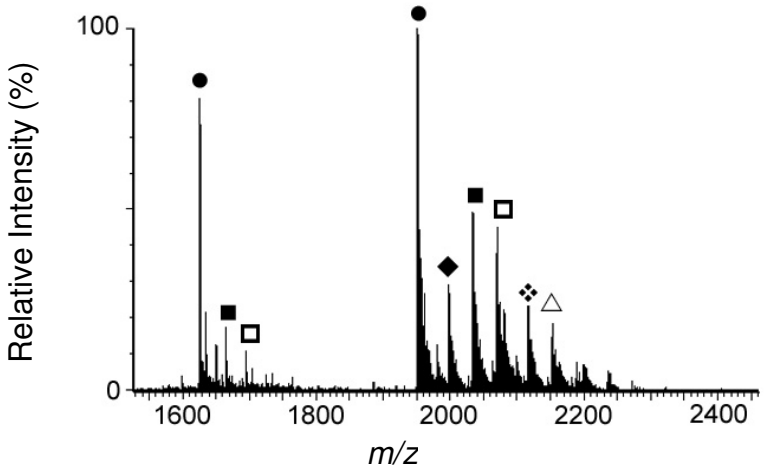

Figure 4.12: Negative ion ESI mass spectrum of a solution containing a 40:1 ratio of $[Fe(phen)_3]^{2+}$ and D2. ● Free D2; ◆ D2 + $[Fe(phen)]^{2+}$; ■ D2 + $[Fe(phen)_2]^{2+}$; □ D2 + $[Fe(phen)_3]^{2+}$; ❖ D2 + $[Fe(phen)_3]^{2+}$ + $[Fe(phen)]^{2+}$; △ D2 + $[Fe(phen)_3]^{2+}$ + $[Fe(phen)_2]^{2+}$.

4.4.3 Platinum Complexes with dsDNA and qDNA

The results in the previous section showed that significant fragmentation of nickel complexes occurred in the mass spectrometer under the conditions used to acquire ESI mass spectra of quadruplex DNA. This meant it was impossible to use ESI-MS to carry out a comparative mass spectral study of the binding of nickel and ruthenium complexes to Q5. Consequently it was decided to continue the study by examining the binding interactions of platinum(II) complexes with Q5, as it was expected that they might exhibit the requisite thermodynamic stability. Furthermore it was hoped that the square planar stereochemistry

of these complexes might facilitate intercalative or end stacking interactions with quadruplex DNA. As ESI-MS had not previously been used to examine the interactions of platinum(II) complexes with either duplex or quadruplex DNA, it was decided to investigate the binding of each of the platinum complexes shown in **Figure 4.1** with both Q5 and D2. There have been several previous studies which showed that complexes of the type $[Pt(en)(L)]^{2+}$, where L is either phenanthroline or one of several methylated phenanthroline ligands, display cytotoxicity towards murine leukaemia L1210 cells that was dependent on the number and position of the methyl substituents.[289,290] Circular dichroism spectroscopy was used to investigate the interactions of these complexes with calf thymus DNA, and provided binding constants which suggested that their affinities for DNA were comparable to that of complexes such as $[Ru(phen)_2(dppz)]^{2+}$. No simple correlation was found between the extent of methylation of the phenanthroline ligand and the binding constants, or between the binding constants and cytotoxicity. It was hoped that ESI-MS studies of their interactions with dsDNA and qDNA might shed further light on their mechanisms of toxicity.

Addition of an equimolar quantity of the platinum complexes shown in **Figure 4.1** to D2 resulted in the formation of significant amounts of non-covalent complexes containing one platinum molecule bound to DNA (results not shown). In the case of $[Pt(en)(4,7\text{-}Me_2phen)]^{2+}$, $[Pt(en)(3,4,7,8\text{-}Me_4phen)]^{2+}$ and $[Pt(5,6\text{-}Me_2phen)(\textit{S,S}\text{-dach})]^{2+}$, ions attributable to these complexes were the most abundant observed in the ESI mass spectra, which also showed ions assigned to non-covalent complexes containing two bound platinum molecules. Increasing the metal:D2 ratio resulted in the formation of non-covalent complexes containing even greater numbers of bound platinum molecules. For example,

Figures 4.13a-e show the spectra of solutions containing a 6:1 ratio of different platinum complexes and D2. The spectrum of the solution containing $[Pt(en)(phen)]^{2+}$ (**Figure 4.13b**) is dominated by ions attributable to non-covalent complexes containing one, two, three and four platinum molecules bound to DNA. **Figure 4.13c** shows that the addition of $[Pt(en)(3,4,7,8\text{-}Me_4phen)]^{2+}$ to D2 resulted in the formation of many analogous non-covalent complexes. On closer inspection it can be seen that the relative abundance of ions containing one platinum molecule bound to D2 is lower in **Figure 4.13c** than in **Figure 4.13b**. This result, together with the observation that **Figure 4.13c** also contains ions of low abundance assigned to non-covalent complexes containing five platinum molecules bound to D2, whereas **Figure 4.13b** does not contain analogous ions, suggests that the affinity of $[Pt(en)(3,4,7,8\text{-}Me_4phen)]^{2+}$ towards D2 is slightly greater than that of $[Pt(en)(phen)]^{2+}$.

ESI mass spectra of solutions containing the remaining two platinum complexes and D2 also showed ions assigned to non-covalent complexes consisting of up to five platinum molecules bound to DNA (**Figures 4.13d** and **e**). Overall the results indicate that the affinity of the platinum complexes towards duplex DNA is affected by both the extent of methylation of the phenanthroline ligand, as well as by the position of the methyl substituents. Furthermore the mass spectra also clearly demonstrate the tremendous affinity that each of the platinum complexes display towards D2, despite the absence of a strongly intercalating ligand such as dppz in their structures. In fact when the metal:D2 ratio was increased further to 10:1, the mass spectra of solutions containing $[Pt(en)(4,7\text{-}Me_2phen)]^{2+}$, $[Pt(5,6\text{-}Me_2phen)(S,S\text{-dach})]^{2+}$ and $[Pt(en)(3,4,7,8\text{-}Me_4phen)]^{2+}$ all contained ions of medium to high abundance attributable to non-covalent complexes containing six or seven platinum molecules bound to DNA (results not shown). This further illustrates the

favourable binding properties conferred on these metal complexes by their square planar geometry.

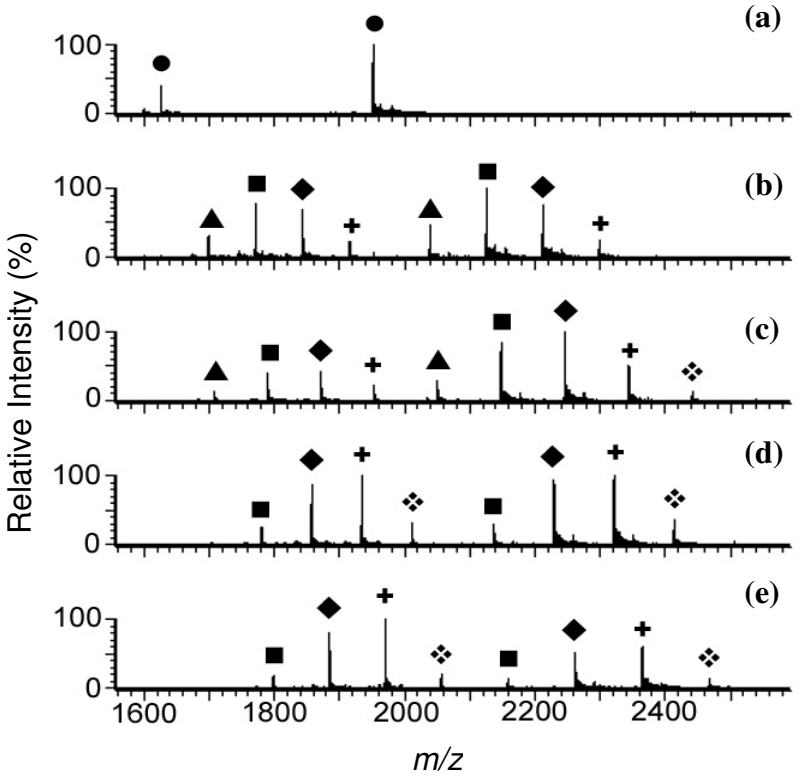

Figure 4.13: Negative ion ESI mass spectra of free D2 and solutions containing a 6:1 ratio of different platinum complexes and D2: (a) free D2; (b) D2 + $[Pt(en)(phen)]^{2+}$; (c) D2 + $[Pt(en)(3,4,7,8\text{-}Me_4phen)]^{2+}$; (d) D2 + $[Pt(en)(4,7\text{-}Me_2phen)]^{2+}$; (e) D2 + Pt(5,6-$Me_2$phen)(*S,S*-dach)]$^{2+}$; ● free DNA; ▲ DNA + 1$[Pt(L)L']^{2+}$; ■ DNA + 2$[Pt(L)L']^{2+}$; ◆ Q5 + 3$[Pt(L)L']^{2+}$; ✚ Q5 + 4$[Pt(L)L']^{2+}$; ❖ Q5 + 5$[Pt(L)L']^{2+}$. L = en or 5,6-$Me_2$phen; L' = *S,S*-dach, phen, or one of several other methylated phenanthroline ligands.

It was then decided to obtain ESI mass spectra of solutions containing different ratios of the platinum complexes and Q5, in order to determine whether these square planar molecules also have high binding affinities towards quadruplex DNA. **Figure 4.14** shows the spectra of solutions containing a 30:1 ratio of the different platinum complexes and Q5. The lowest binding affinity towards qDNA was exhibited by $[Pt(en)(phen)]^{2+}$, which formed non-

covalent complexes of high abundance containing one and two platinum molecules bound to Q5, and ions of low or medium abundance assigned to non-covalent complexes containing three platinum molecules (**Figure 4.14b**). Replacement of the phenanthroline ligand in this complex by one of the methylated derivatives resulted in the relative abundance of more highly substituted non-covalent complexes increasing, as well as the appearance of ions attributable to non-covalent complexes containing four and five bound platinum molecules in some instances. In the case of solutions containing [Pt(en)(3,4,7,8-Me_4phen)]$^{2+}$ (**Figure 4.14c**) and [Pt(en)(4,7-Me_2phen)]$^{2+}$ (**Figure 4.14d**), the most abundant ions observed were those attributable to non-covalent complexes containing three platinum molecules bound to Q5. It can therefore be concluded that at least some of the platinum molecules display a slightly higher binding affinity towards Q5 than the ruthenium complexes described in section 4.4.1, as the most abundant ions present in spectra of solutions containing a 40:1 ratio of the latter complexes and Q5 contained only two ruthenium molecules.

It is noteworthy that the least reactive platinum complex towards both duplex DNA and quadruplex DNA was [Pt(en)(phen)]$^{2+}$, while the most reactive was [Pt(5,6-Me_2phen)(*S,S*-dach)]$^{2+}$. This highlights the important role that hydrophobic interactions can play in determining overall binding affinities towards DNA.

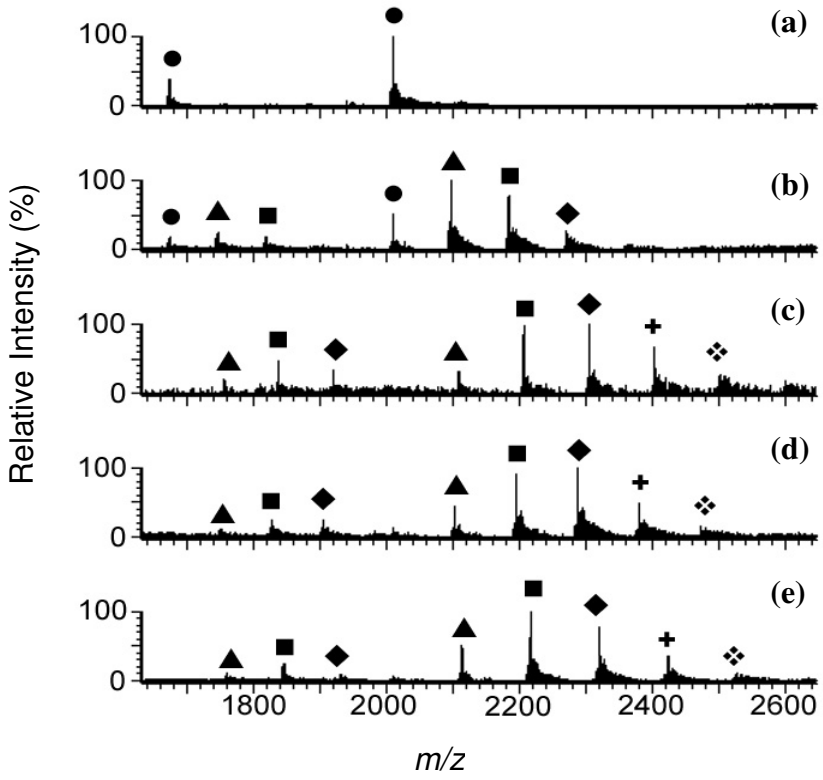

Figure 4.14: Negative ion ESI mass spectra of free Q5 and solutions containing 40:1 ratios of different platinum complexes and Q5: (a) free Q5; (b) Q5 + $[Pt(en)(phen)]^{2+}$; (c) Q5 + $[Pt(en)(3,4,7,8\text{-}Me_4phen)]^{2+}$; (d) Q5 + $[Pt(en)(4,7\text{-}Me_2phen)]^{2+}$; (e) Q5 + $[Pt(5,6\text{-}Me_2phen)(S,S\text{-dach})]^{2+}$; ● free DNA; ▲ DNA + 1$[Pt(L)L']^{2+}$; ■ DNA + 2$[Pt(L)L']^{2+}$; ◆ Q5 + 3$[Pt(L)L']^{2+}$; ✚ Q5 + 4$[Pt(L)L']^{2+}$; ❖ Q5 + 5$[Pt(L)L']^{2+}$. L = en or 5,6-$Me_2$phen; L' = *S,S*-dach, phen, or one of several other methylated phenanthroline ligands.

In order to more directly compare the relative affinities of the individual platinum complexes for dsDNA and qDNA, the graphs shown in **Figure 4.15** were prepared. These show the relative abundances of non-covalent complexes present in solutions containing identical (10:1) ratios of the same platinum complex and either D2 or Q5. Relative abundances were calculated by summing the intensities for 5- and 6- ions assigned to specific non-covalent complexes in a spectrum, and then dividing by the total intensity of all ions present, and expressing the result as a percentage.

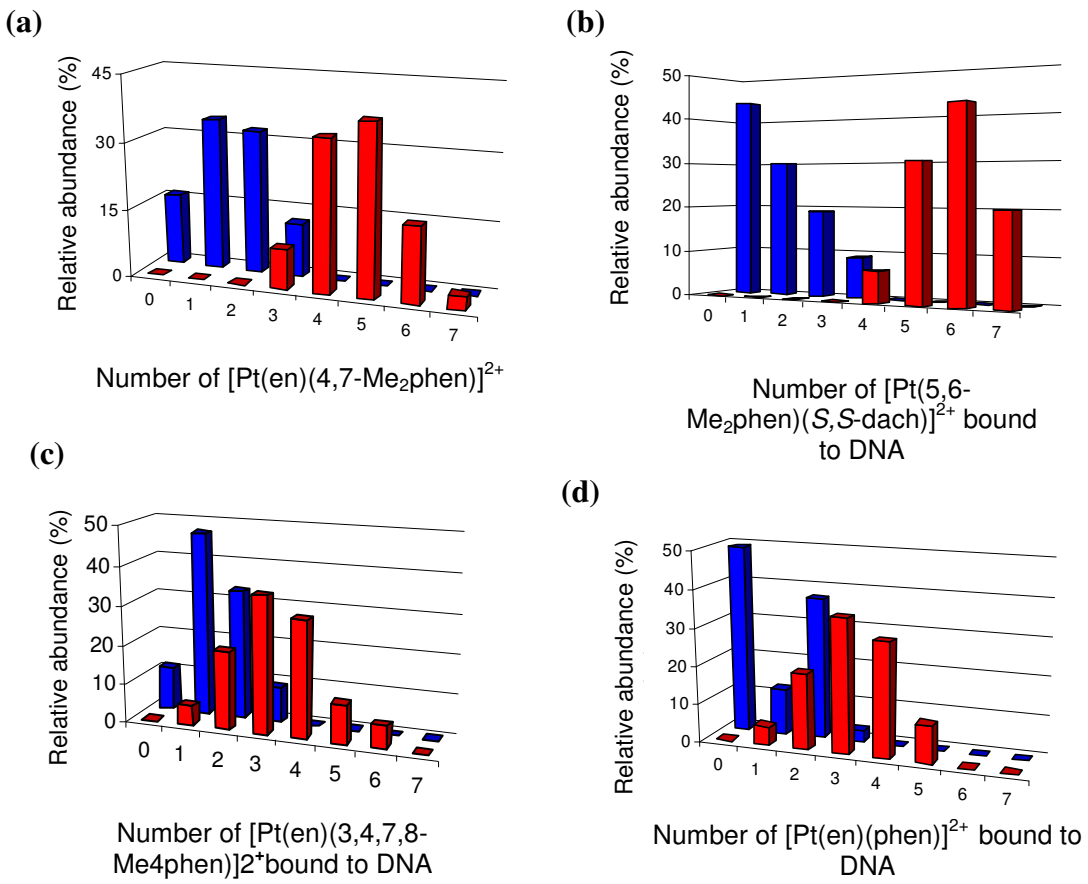

Figure 4.15: Relative abundances of non-covalent complexes present in solutions containing a 10:1 ratio of either $[Pt(en)(4,7\text{-}Me_2phen)]^{2+}$or $[Pt(5,6\text{-}Me_2phen)(S,S\text{-dach})]^{2+}$, and either Q5 (blue) or D2 (red).

The graphs show that each of the platinum complexes examined display a higher binding affinity towards D2 compared to Q5. This is particularly evident in **Figures 4.15a** and **b**, which present data for $[Pt(en)(4,7\text{-}Me_2phen)]^{2+}$ and $[Pt(5,6\text{-}Me_2phen)(S,S\text{-dach})]^{2+}$, respectively. Both of these complexes formed a high percentage of non-covalent complexes containing 4, 5, and 6 molecules bound to D2. In contrast, the most abundant non-covalent complexes present in solutions containing the same ratio of platinum complex and Q5 were those with just 1 and 3 platinum molecules bound.

4.4.4 Competition Between Daunomycin and Metal Complexes for Q5

In order to obtain information regarding the DNA binding modes of the metal complexes studied here, and their preferred binding sites, ESI-MS was used to analyse mixtures in which either $[Ru(phen)_2(dppz)]^{2+}$ or $[Pt(en)(4,7\text{-}Me_2phen)]^{2+}$ was present in solution with both Q5 and daunomycin. **Figure 4.16** shows the crystal structure of a complex consisting of daunomycin molecules bound to the tetrameric qDNA molecule $d(TGGGGT)_4$.[100] The crystal structure shows two quadruplexes stacked end-to-end in a 5' to 5' fashion, with the interface between the two quadruplexes filled by two layers of daunomycin molecules. The latter are arranged into two dyad-related sets of three coplanar molecules. Each trio of daunomycin molecules is held together in one layer by a cluster of van der Waals contacts. The daunosamine sugar moieties bind with all four quadruplex grooves through H-bonding and/or van der Waals interactions.

Reaction mixtures were prepared in which Q5 was first mixed with 30 equivalents of daunomycin, and subsequently 3, 6 or 10 equivalents of either the ruthenium or platinum complex were added. Other mixtures were prepared by first allowing the metal complex to interact with the qDNA, and then the daunomycin was added. ESI mass spectra of solutions with the same final ratios of all three components prepared by the two different approaches were almost identical.

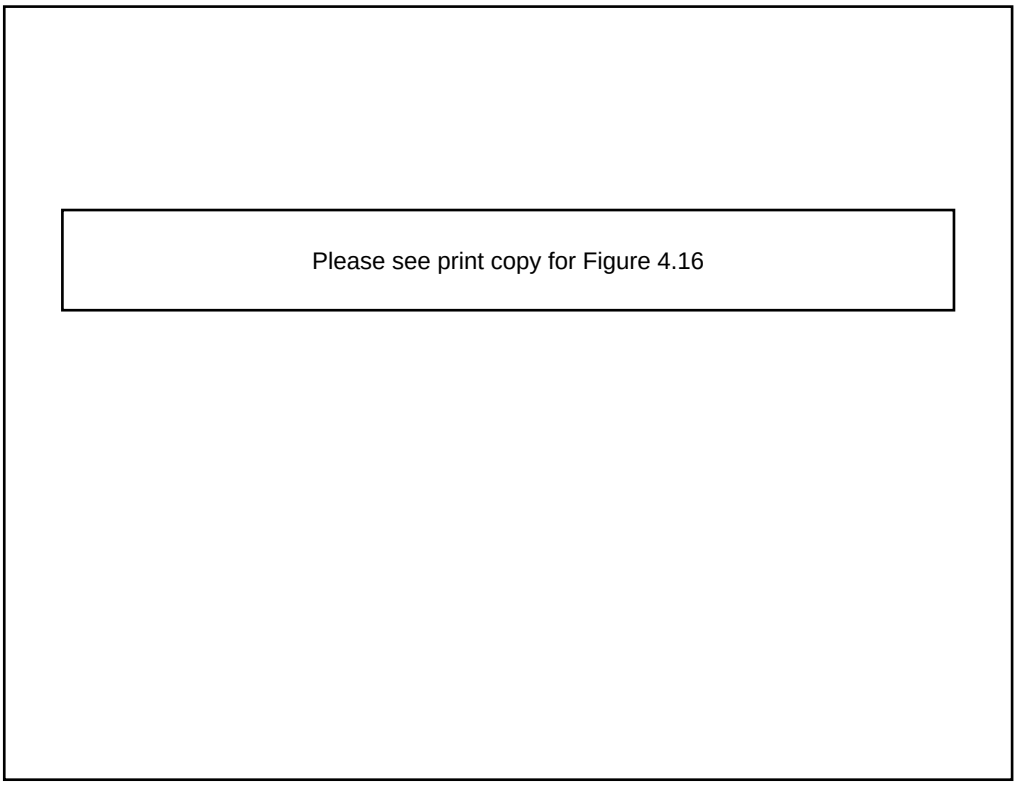

Figure 4.16: Crystal structure showing two d(TGGGGT)$_4$ quadruplexes are stacked at their 5'-ends.Two sets of three daunomycin molecules are stacked at the interface of the quadruplexes (shown in green ball and stick form). Several thymines have been removed to enhance clarity.[100]

Competition between daunomycin and [Ru(phen)$_2$(dppz)]$^{2+}$

A preliminary experiment was conducted in which ESI-MS was used to monitor the titration of Q5 with increasing amounts of daunomycin. This was performed in order to determine how much of the organic drug needed to be added to saturate the quadruplex DNA molecule. The results of this experiment showed that after addition of 30 equivalents of daunomycin the appearance of the spectrum no longer changed, and no ions attributable to free Q5 were present. This indicates that all the daunomycin binding sites on Q5 were now occupied.

Figure 4.17a shows the ESI mass spectrum of a solution containing a 30:1 ratio of daunomycin and Q5. Both 6- and 5- ions are present with the ions of highest abundance being attributable to non-covalent complexes containing 1 and 2 daunomycin molecules bound to Q5. Ions corresponding to non-covalent complexes containing 3 and 4 daunomycin molecules bound to Q5 were also present in medium to high abundance, but only for the 6- charge state. The results show that the abundances of 6- ions attributable to non-covalent complexes containing daunomycin molecules bound to Q5 is greater than that of the corresponding 5- ions. In contrast, in sections 4.3 and 4.4 ESI mass spectra are presented which show that when Q5 is mixed with metal complexes the most abundant ions assigned to non-covalent complexes were those with a 5- overall charge. **Figure 4.17a** suggests that a maximum of four daunomycin molecules can bind to Q5. This is consistent with the crystal structure described above, which revealed 3 daunomycin molecules could stack onto the 5'-terminal end of the closely related quadruplex $d(TGGGGT)_4$. Therefore it appears likely that the majority of ions present in **Figure 4.17a** also contain daunomycin molecules bound at the 5' end of the quadruplex. In the case of the ions containing four bound daunomycin molecules it is likely that three are bound as described above, while the fourth is weakly and/or non-specifically bound somewhere else on the quadruplex.

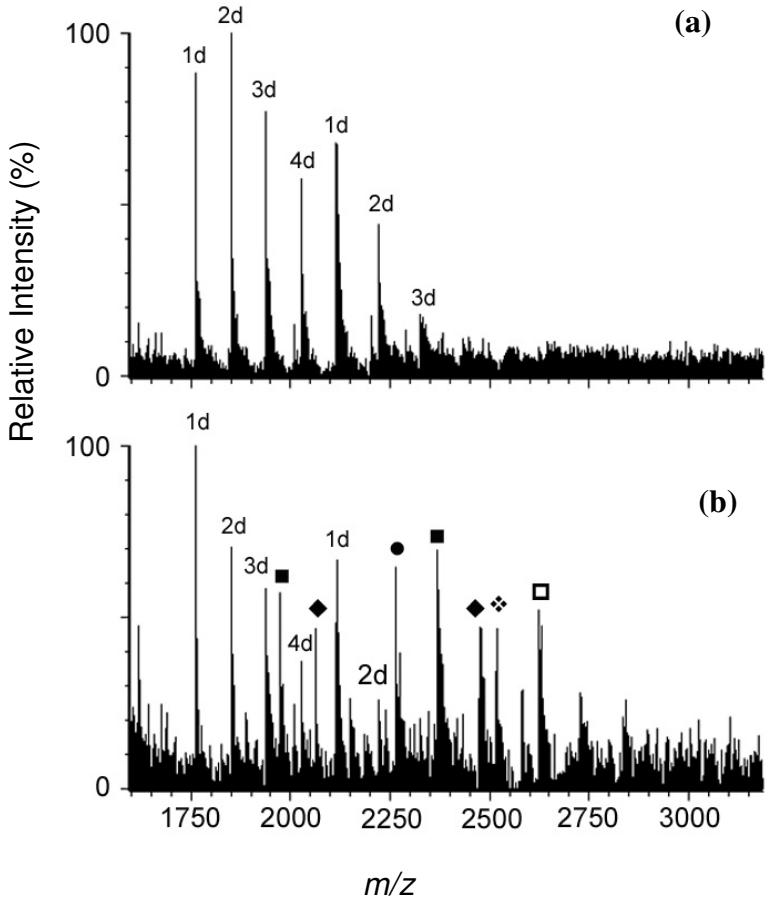

Figure 4.17: Negative ion ESI mass spectra of solutions containing Q5 and: (a) 30 equivalents of daunomycin; (b) 30 equivalents of daunomycin and 6 equivalents of $[Ru(phen)_2(dppz)]^{2+}$. 1d = Q5 + 1daunomycin; 2d = Q5 + 2daunomycin; 3d = Q5 + 3daunomycin; 4d = Q5 + 4daunomycin; ■ Q5 + 2daunomycin + 1$[Ru(phen)_2(dppz)]^{2+}$; ◆ Q5 + 3daunomycin + 1$[Ru(phen)_2(dppz)]^{2+}$; ● Q5 + 1daunomycin + 1$[Ru(phen)_2(dppz)]^{2+}$; ❖ Q5 + 2daunomycin + 2$[Ru(phen)_2(dppz)]^{2+}$; □ Q5 + 3daunomycin + 2$[Ru(phen)_2(dppz)]^{2+}$.

Figure 4.17b shows the ESI mass spectrum of a solution initially containing a 30:1 ratio of daunomycin and Q5, after it was subsequently treated with 6 equivalents of $[Ru(phen)_2(dppz)]^{2+}$. Ions attributable to non-covalent complexes containing between 1 and 4 daunomycin molecules bound to Q5 are still present. However, the relative abundances of some ions, such as that at *m/z* 1850.6 assigned to $[Q5 + 4NH_4^+ + 2daunomycin - 10H]^{6-}$ are

clearly lower than in **Figure 4.17a**, suggesting that they have interacted with the ruthenium complex. These interactions may account for the appearance of new ions such as those at *m/z* 2264.1 and *m/z* 2369.4, which are assigned to [Q5 + $4NH_4^+$ + 1daunomycin + 1$[Ru(phen)_2(dppz)]^{2+}$- 9H]$^{5-}$ and [Q5 + $4NH_4^+$ + 2daunomycin + 1$[Ru(phen)_2(dppz)]^{2+}$-11H]$^{5-}$, respectively. The observation of these ions, containing both daunomycin and $[Ru(phen)_2(dppz)]^{2+}$ molecules bound to Q5, may indicate that the former molecule does not completely inhibit the binding of the metal complex. However, there are at least two possible explanations for this result. One is that one or more $[Ru(phen)_2(dppz)]^{2+}$ molecules are able to bind to a different region of the quadruplex than the 5' end which is already occupied by 1 or 2 daunomycin molecules. This could still involve a single $[Ru(phen)_2(dppz)]^{2+}$ molecule sharing the G-terminal binding region with 1 or 2 daunomycin molecules, or alternatively it may be a result of weak interactions between the metal complex and other sites such as those on the exterior of the quadruplex. An alternative explanation involves displacement of daunomycin from ions such as [Q5 + $4NH_4^+$ + 2daunomycin - 9H]$^{5-}$ and [Q5 + $4NH_4^+$ + 3daunomycin - 9H]$^{5-}$ by $[Ru(phen)_2(dppz)]^{2+}$. It is difficult to determine the relative contributions of these different processes to the changes in appearance of the spectrum. Instead it is perhaps more profitable to speculate on the origin of ions of medium abundance at *m/z* 2623.8 in **Figure 4.17b**, which are assigned to [Q5 + $4NH_4^+$ + 3daunomycin + 2$[Ru(phen)_2(dppz)]^{2+}$ - 9H]$^{5-}$. This is because there are no ions assigned to Q5 with five bound daunomycin in **Figure 4.17a**. Therefore the 2 ruthenium molecules present in the *m/z* 2623.8 ion are most likely to be found somewhere in the quadruplex molecule other than bound to the 5' end. This is also likely in view of the steric bulk associated with both the ruthenium and daunomycin molecules. It therefore appears at $[Ru(phen)_2(dppz)]^{2+}$ may bind to Q5 in a different region

of the quadruplex and possibly by a different mode to that used by daunomycin. This is perhaps not surprising, since it was noted earlier that the affinity of $[Ru(phen)_2(dppz)]^{2+}$ for Q5 was not significantly greater than that of the other ruthenium complexes, indicating that the intercalating dppz ligand was not playing as great a role as it does in binding to dsDNA.

Competition between daunomycin and $[Pt(en)(4,7\text{-}Me_2phen)]^{2+}$

Figure 4.18 shows the ESI mass spectrum of a solution containing Q5 and 30 equivalents of daunomycin, both before and after the addition of 10 equivalents of $[Pt(en)(4,7\text{-}Me_2phen)]^{2+}$. Once again the addition of the metal complex appears to cause a reduction in relative abundance of ions arising from non-covalent complexes containing two and three daunomycin bound to Q5, compared to that of ions arising from non-covalent complexes containing one or both types of drug molecules bound to Q5. As with the previous competition experiment, it is not possible to unambiguously determine whether most of the ions arise from a mechanism involving replacement of daunomycin molecules by platinum molecules, or in which the metal complex binds to a different region of the DNA molecule to that occupied by daunomycin. However, there are ions which do provide insight into how and/or where some of the platinum molecules are binding. **Figure 4.18b** contains ions of medium abundance at *m/z* 2016.3 and *m/z* 2103.9 attributable to non-covalent complexes containing 3 or 4 daunomycin molecules and one platinum molecule bound to Q5. If it is assumed that the three daunomycin molecules are bound at the 5' end, and completely block all other molecules from binding in this region, then this suggests that the platinum molecules are interacting with other regions of the qDNA molecule.

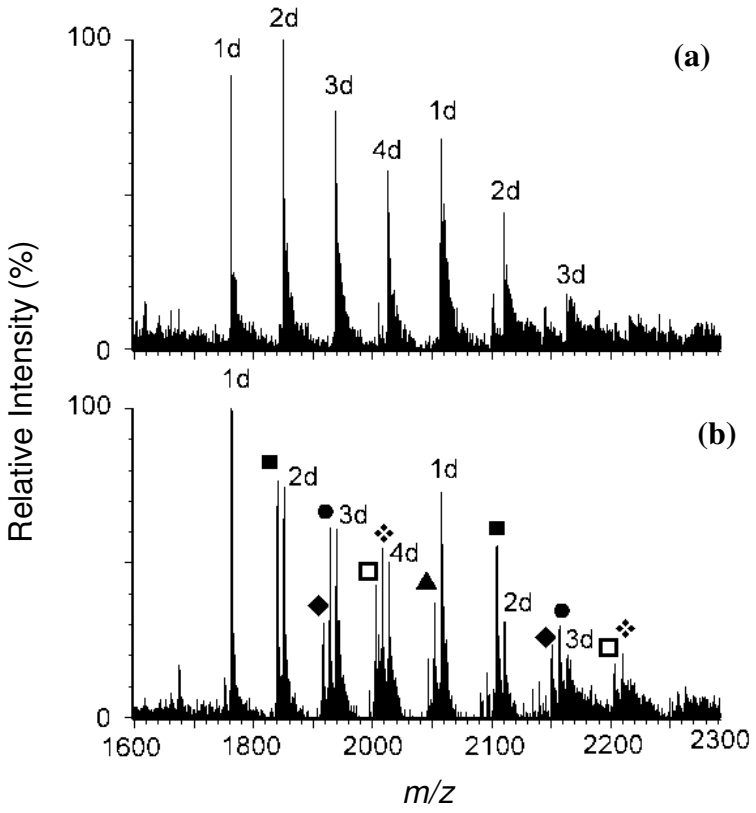

Figure 4.18: Negative ion ESI mass spectra of solutions containing Q5 and: (a) 30 equivalents of daunomycin; (b) 30 equivalents of daunomycin and 10 equivalents of $[Pt(en)(4,7\text{-}Me_2phen)]^{2+}$. 1d = Q5 + 1daunomycin; 2d = Q5 + 2daunomycin; 3d = Q5 + 3daunomycin; 4d = Q5 + 4daunomycin; ■ Q5 + 1daunomycin + 1$[Pt(en)(4,7\text{-}Me_2phen)]^{2+}$; ◆ Q5 + 1daunomycin + 2$[Pt(en)(4,7\text{-}Me_2phen)]^{2+}$;● Q5 + 2daunomycin + 1$[Pt(en)(4,7\text{-}Me_2phen)]^{2+}$; □ Q5 + 2daunomycin + 2$[Pt(en)(4,7\text{-}Me_2phen)]^{2+}$; ❖ Q5 + 3daunomycin + 1$[Pt(en)(4,7\text{-}Me_2phen)]^{2+}$; ▲ Q5 + 4daunomycin + 1$[Pt(en)(4,7\text{-}Me_2phen)]^{2+}$.

4.4.5 Binding of Metal Complexes to Tetrameric Quadruplexes of Different Lengths

Competition experiments involving $[Ru(phen)_2(dppz)]^{2+}$ or $[Pt(en)(4,7\text{-}Me_2Phen)]^{2+}$, and daunomycin suggested that the former complexes may also be able to interact with regions other than the 5'-end of Q5. If this is correct then changing the length of the quadruplex by increasing the number of G-tetrads present might result in increasing numbers of ruthenium

or platinum molecules able to bind to the quadruplex. In order to test this hypothesis, ESI mass spectra were obtained of solutions containing identical ratios of daunomycin, $[Ru(phen)_2(dppz)]^{2+}$ and $[Pt(en)(4,7\text{-}Me_2Phen)]^{2+}$ with three structurally related tetrameric qDNA molecules with different lengths, namely $(TTGGGGT)_4$ (Q4), $(TTGGGGGT)_4$ (Q5) and $(TTGGGGGGGT)_4$ (Q7).

The ESI mass spectra of solutions containing free Q4 and Q7 were obtained using the same instrumental conditions used for solutions containing Q5, and are shown in **Figure 4.19a** and **b**, respectively. The former spectrum shows ions at *m/z* 1452.6 and 1743.4 that are assigned to $[Q4 + 3NH_4^+ - 9H]^{6-}$ and $[Q4 + 3NH_4^+ - 8H]^{5-}$, respectively. This is consistent with the expectation that there will be *n-1* monovalent cations situated in between the G-tetrads, where *n* is the number of G-tetrads. **Figure 4.19b** shows ions at *m/z* 1814.0 and 2119.4 that correspond to $[Q7 + 5NH_4^+ - 12H]^{7-}$ and $[Q7 + 6NH_4^+ - 12H]^{6-}$, respectively. The former ion contains one ammonium ion less than the number expected for this quadruplex in solution. However, its abundance is less than that of the *m/z* 2119.4 ion, which does contain the expected number of ammonium ions. Overall it therefore appears that the ESI process results in minimal changes to the structures of the quadruplex in solution, even for a long quadruplex molecule such as Q7. Such changes should not be totally unexpected and have in fact been seen before. For example, the ESI mass spectrum of the dimeric qDNA Q2 $((GGGGTTTTGGGG)_2)$ showed a 6- ion containing one ammonium ion less bound to the quadruplex compared to other quadruplex ions with a 5- or 4- charge (**Figure 4.2b**).

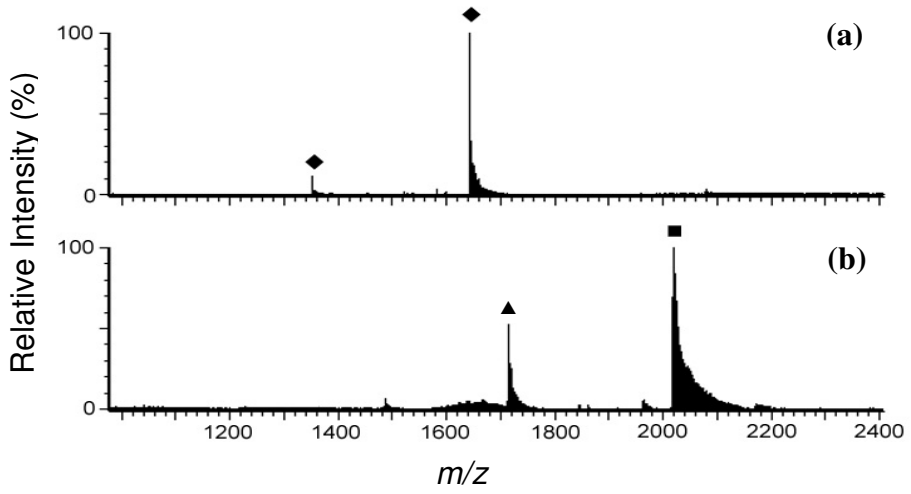

Figure 4.19: Negative ion ESI mass spectra of: (a) Q4 and (b) Q7. ◆ Q4 + 3 NH_4^+; ■ Q7 + 6NH_4^+; ▲ Q7 + 5NH_4^+.

Figure 4.20 compares the results of a large number of experiments in which ESI mass spectra were obtained of solutions containing a 10:1 ratio of daunomycin, $[Pt(en)(4,7\text{-}Me_2phen)]^{2+}$ or $[Ru(phen)_2(dppz)]^{2+}$, and Q5, Q4 or Q7. The results of these experiments are presented graphically as relative abundances of different non-covalent complexes. These were obtained by adding together all the individual ion intensities for signals arising from a specific non-covalent complex (eg. one daunomycin bound to Q5), and dividing by the combined intensities of all signals in the spectrum. The results obtained using solutions containing daunomycin or $[Pt(en)(4,7\text{-}Me_2phen)]^{2+}$ are very similar to each other. First of all there are only small differences, for example, between the relative abundances of ions assigned to non-covalent complexes containing one daunomycin bound to qDNA or one platinum molecule bound to DNA, in the case of all three DNA quadruplexes. Secondly the shapes of the relative abundance profiles in **Figures 4.20a** and **b** are very similar to each other. These observations are consistent with the conclusion that the affinity of daunomycin

and platinum molecules towards tetrameric qDNA is not affected greatly by the length of the quadruplex. Furthermore since it is known from X-ray crystallography studies that daunomycin prefers to bind to the 5'-terminal G-tetrad of tetrameric quadruplexes such as those examined here,[100] these results suggest that $[Pt(en)(4,7\text{-}Me_2phen)]^{2+}$ may also bind to these regions. At first this suggestion may appear at odds with the conclusion presented in section 4.4.4 which was that platinum molecules and daunomycin interact with different regions of Q5. However, it must be remembered that this conclusion was based on results obtained from solutions in which daunomycin and platinum molecules were competing for binding sites on the same qDNA molecule. In the case of the results shown in **Figure 4.20**, these were obtained from spectra of solutions containing only the platinum complex and qDNA, and therefore reflect the preferred binding sites of the former molecules.

The results presented in **Figure 4.20** for $[Ru(phen)_2(dppz)]^{2+}$ vary from those obtained using the other two molecules. For example, in the case of Q7 the complex where one $[Ru(phen)_2(dppz)]^{2+}$ was bound appears highly favoured as it accounted for 60% of all the species in solution. This experiment was repeated another two times with similar results being obtained. Further experiments involving additional platinum and ruthenium molecules, as well as tetrameric DNA molecules of different lengths to those used here, are required to see if these trends are general. However, even if that proves to be the case, the question of where the metal complexes actually bind can only be definitively answered by performing X-ray crystallographic or NMR studies on these systems.

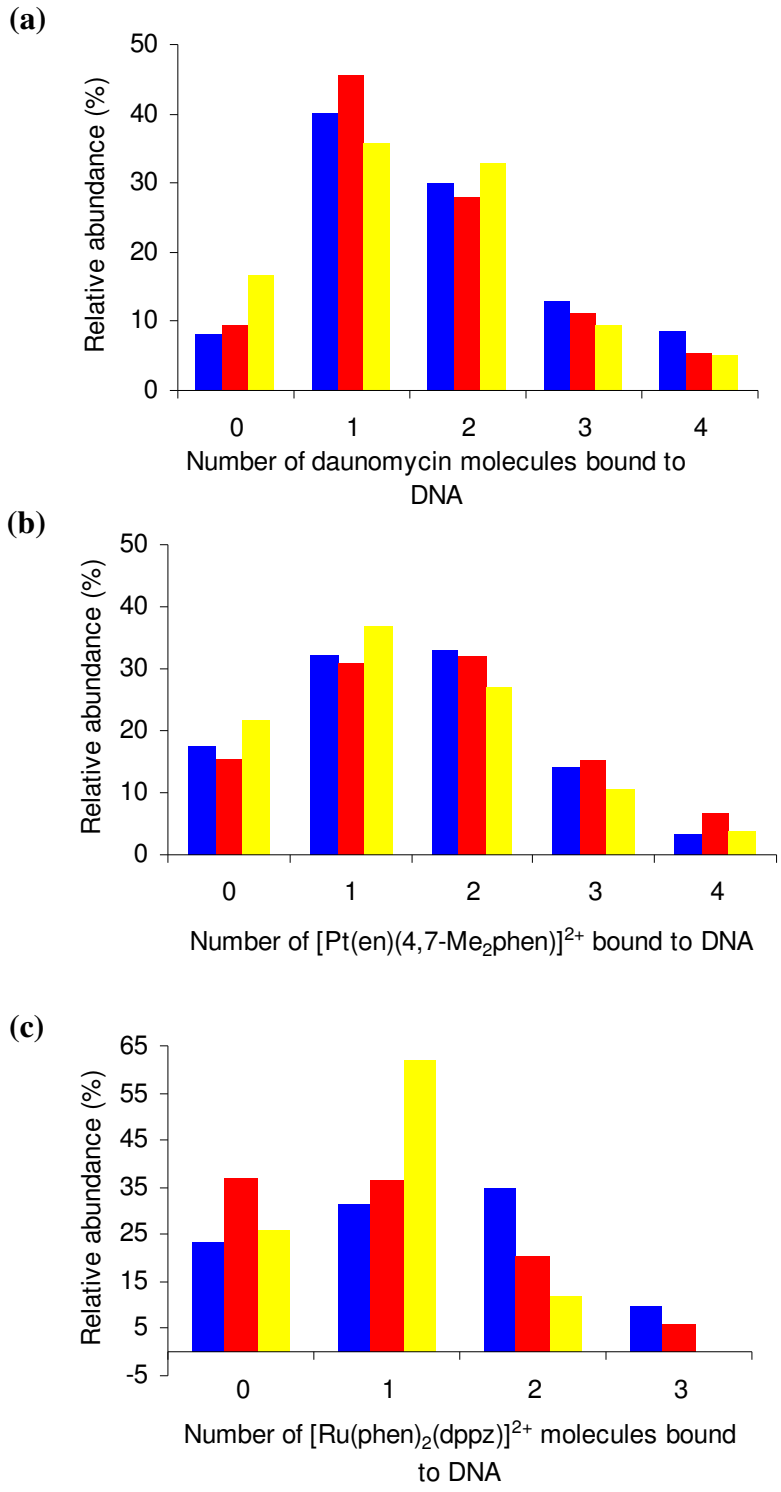

Figure 4.20: Relative abundances (as judged from ESI mass spectra) of different non-covalent complexes present in solutions containing Q4 $(TTGGGGT)_4$ (blue), Q5 $(TTGGGGGT)_4$ (red) or Q7 $(TTGGGGGGGT)_4$ (yellow) and 10-equivalents of: (a) daunomycin, (b) $[Pt(en)(4,7\text{-}Me_2phen)]^{2+}$ and (c) $[Ru(phen)_2(dppz)]^{2+}$.

4.5 CD Studies of the Binding Interactions of Metal Complexes with qDNA

4.5.1 CD Studies of the Binding of Ruthenium Complexes to Q5

The results of ESI-MS studies described in section 4.4.1 led to the following order of increasing DNA binding affinity for the ruthenium complexes: $[Ru(phen)_3]^{2+}$ < $[Ru(phen)_2(dpq)]^{2+}$ < $[Ru(phen)_2(dpqc)]^{2+}$ < $[Ru(phen)_2(dppz)]^{2+}$. In order to provide further support for this order of binding affinities it was decided to obtain CD spectra of solutions containing different ratios of ruthenium complex and Q5. CD spectroscopy has proven useful in the past for providing both qualitative and quantitative measures of the strength of interactions between metal complexes and dsDNA. [13,110-112,234] In addition, it has proven to be a useful technique for diagnosing changes in DNA morphology caused by drug interactions with duplex DNA, as CD signals are very sensitive to the binding mode used by small molecules.[113,234,266] Prior to the current study however, there have been few if any systematic studies into the interactions of metal complexes with qDNA performed using CD spectroscopy.

Figure 4.21 illustrates the CD spectra of solutions containing different ratios of the ruthenium complexes and Q5. The spectrum of Q5 itself is consistent with those previously reported for tetrameric qDNA, which typically have a positive CD band with a maximum near 265 nm and a negative CD band with a minimum near 240 nm.[37,98,167,271,291,292] In addition, the CD spectrum of Q5 contains a second strong positive CD band with a maximum near 210 nm. Addition of increasing amounts of each of the ruthenium complexes was found to result in significant decreases in ellipticity of the two positive CD bands, while only minor changes in ellipticity at 240 nm were observed. The lower energy

positive CD signal also shifted towards shorter wavelengths, and at high Ru:Q5 ratios developed a shoulder at ~ 275 nm. This change was most dramatic for $[Ru(phen)_2(dpqc)]^{2+}$ and $[Ru(phen)_3]^{2+}$, and may indicate the adoption of a second binding mode and/or drug binding inducing further conformational changes to the DNA structure.

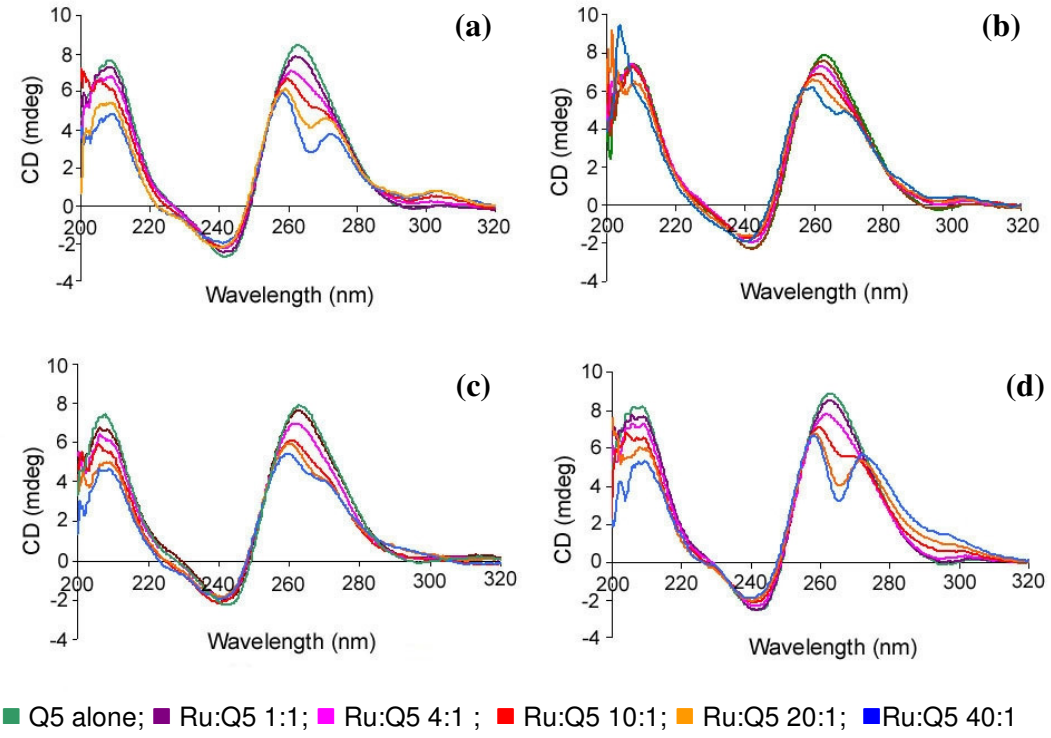

Figure 4.21: Circular dichroism spectra of solutions containing different ratios of ruthenium complexes and Q5: (a) $[Ru(phen)_2(dpqc)]^{2+}$; (b) $[Ru(phen)_2(dpq)]^{2+}$; (c) $[Ru(phen)_2(dppz)]^{2+}$ and (d) $[Ru(phen)_3]^{2+}$.

The magnitude of the change in ellipticity ($\Delta\varepsilon$) of a CD signal at the peak maxima has been used previously to compare the relative binding affinities of ruthenium complexes towards dsDNA.[234] However, for the spectra shown in **Figure 4.21** the ellipticity only changes by a relatively small amount. For example, for the CD signal at 265 nm, maximum $\Delta\varepsilon$ values of

4.3 mdeg, 4.1 mdeg, 2.9 mdeg and 2.4 mdeg were found for $[Ru(phen)_3]^{2+}$, $[Ru(phen)_2(dpqc)]^{2+}$, $[Ru(phen)_2(dppz)]^{2+}$ and $[Ru(phen)_2dpq]^{2+}$, respectively. The similarity between these values probably reflects both the relatively small ellipticities observed for the CD signals of Q5 under the conditions used, and the similar qDNA binding affinities between the ruthenium complexes first revealed by ESI-MS studies. In contrast, $\Delta\varepsilon$ values of 12 mdeg, 21 mdeg, 25 mdeg and 32 mdeg were found for solutions containing D2 and $[Ru(phen)_3]^{2+}$, $[Ru(phen)_2dpq]^{2+}$, $[Ru(phen)_2(dpqc)]^{2+}$ and $[Ru(phen)_2(dppz)]^{2+}$, respectively.[234] These much larger differences in ellipticity parallel trends in binding affinity detected for these complexes by several other techniques, including ESI-MS.[234]

Several studies that have used CD spectroscopy to examine the binding of distamycin, 3,3′-diethyloxadicarbocyanine and porphyrins to Q5 used the appearance of an induced CD signal in the Soret region (~ 450 nm) to distinguish between possible binding modes.[105,278,293,294] For example, White *et al.* found that distamycin bound weakly to qDNA did not produce an induced CD signals at longer wavelengths, and stated this was consistent with an end-stacking binding mode. In contrast, large changes to the magnitude of induced CD signals in this region were believed to indicate a mechanism involving binding to the quadruplex grooves.[105] Other reports have proposed that formation of an induced CD band with a negative sign is an indication of intercalative binding, while an induced CD band with positive ellipticity occurs as a result of groove binding interactions.[98,293] The absence of induced CD signals at wavelengths higher than those shown in **Figure 4.21** therefore suggests that there is only a weak association of the ruthenium complexes with Q5.

4.5.2 CD Studies of the Binding of Nickel Complexes to Q5

Although information about the nature of binding interactions between nickel complexes and Q5 could not be obtained by ESI-MS, it was decided to use CD spectroscopy to investigate these systems. This was done in order to determine if these metal complexes bind to qDNA to a similar extent to their ruthenium analogues, and whether they bind to qDNA more avidly than dsDNA. In addition, it was anticipated that CD spectroscopy might provide information about the effects of metal binding on DNA conformation.

Figure 4.22 shows the CD spectra of solutions containing Q5 as well as 1, 4, 10, 20 and 40 equivalents of different nickel complexes. For each system the ellipticity of the positive CD bands was found to decrease significantly upon addition of increasing amounts of nickel complex. More subtle changes to the negative CD band at 240 nm were observed, with ellipticity generally increasing with increasing drug concentration. At high Ni:Q5 ratios an additional peak (or in the case of $[Ni(phen)_2(dpq)]^{2+}$ a shoulder) appeared at ~ 280 nm. The above changes mirror closely those described earlier for the corresponding solutions containing ruthenium complexes and Q5, suggesting similar non-covalent complexes were being formed in both cases.

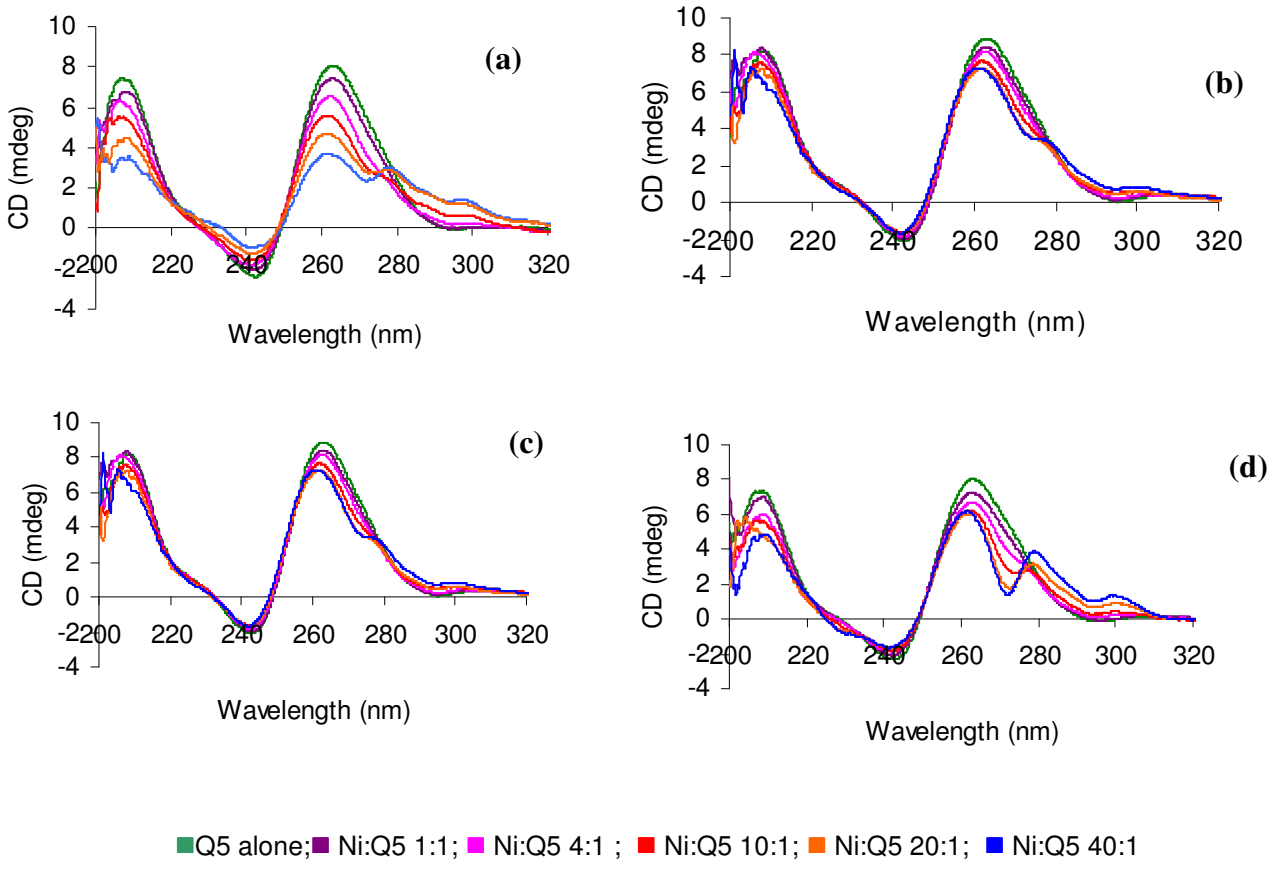

Figure 4.22: Circular dichroism spectra of solutions containing different ratios of nickel(II) complexes and Q5: (a) $[Ni(phen)_2(dppz)]^{2+}$; (b) $[Ni(phen)_2(dpqc)]^{2+}$; (c) $[Ni(phen)_2(dpq)]^{2+}$; and (d) $[Ni(phen)_3]^{2+}$.

The changes in ellipticity at 265 nm ($\triangle\varepsilon$) caused by addition of 40 equivalents of $[Ni(phen)_2(dppz)]^{2+}$, $[Ni(phen)_2(dpqc)]^{2+}$, $[Ni(phen)_2(dpq)]^{2+}$ and $[Ni(phen)_3]^{2+}$ to Q5 are presented in **Table 4.2.** The range of $\triangle\varepsilon$ values is much smaller that what was found for the same complexes in CD studies involving the dsDNA molecule D2, and is more in-keeping with the narrow spread of values found for solutions containing the analogous ruthenium complexes and Q5.

Table 4.2: Differences between the maximum ellipticity observed for the positive CD band at 265 nm in the spectrum of free Q5, and the ellipticity observed at the same wavelength in the spectrum of solutions containing a 40:1 ratio of various metal complexes and Q5.

Metal Complex	CD $\triangle\varepsilon$ (mdeg)
Platinum Complexes	
$[Pt(5,6\text{-}Me_2phen)(S,S\text{-}dach)]^{2+}$	1.6
$[Pt(en)(4,7\text{-}Me_2phen)]^{2+}$	1.7
$[Pt(en)(3,4,7,8\text{-}Me_4phen)]^{2+}$	3.1
$[Pt(en)(phen)]^{2+}$	0.97
Ruthenium Complexes	
$[Ru(phen)_2(dppz)]^{2+}$	2.4
$[Ru(phen)_2(dpqc)]^{2+}$	4.1
$[Ru(phen)_2(dpq)]^{2+}$	2.9
$[Ru(phen)_3]^{2+}$	4.3
Nickel Complexes	
$[Ni(phen)_2(dppz)]^{2+}$	4.4
$[Ni(phen)_2(dpqc)]^{2+}$	2.9
$[Ni(phen)_2(dpq)]^{2+}$	1.7
$[Ni(phen)_3]^{2+}$	1.9

4.5.3 CD studies of the Binding of Platinum Complexes to Q5

CD spectra of solutions containing Q5 with 10, 20, 30 and 40 equivalents of some of the platinum complexes shown in **Figure 4.1** are presented in **Figure 4.23**. In many respects the changes in appearance of the CD spectra caused by addition of increasing amounts of the platinum complexes are similar to those observed with both the ruthenium and nickel complexes. The ellipticities of the positive CD bands were found to decrease once again, whilst there was little change to the negative CD band at ~ 240 nm. In contrast to what was observed with the other two types of complexes, however, no additional CD bands appeared at slightly higher wavelengths than that of the positive CD signal at ~ 265 nm for any of the platinum complexes studied.

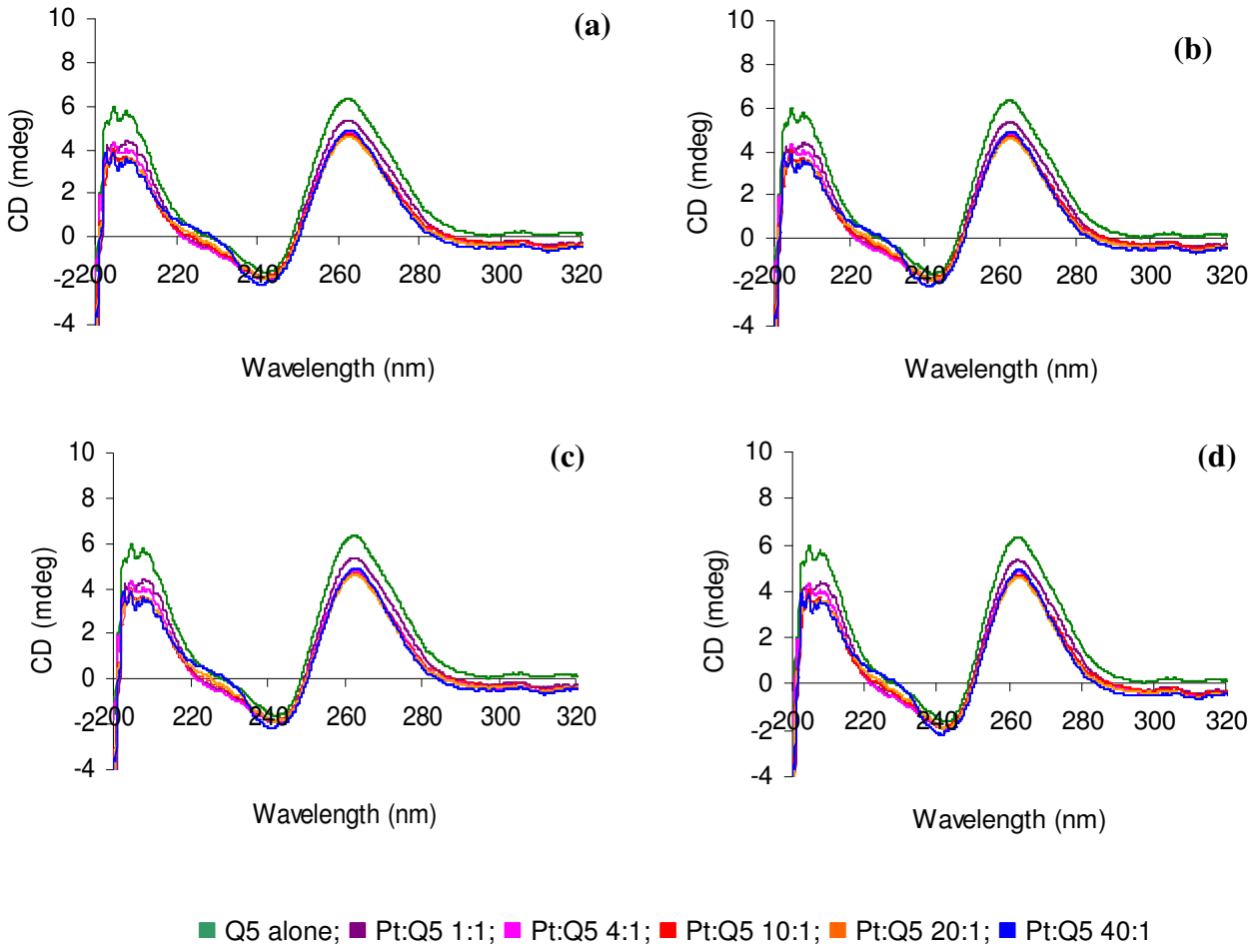

Figure 4.23: Circular dichroism spectra of solutions containing different ratios of platinum complexes and Q5: (a) $[Pt(en)(phen)]^{2+}$; (b) $[Pt(en)(3,4,7,8\text{-}Me_4phen)]^{2+}$; (c) $[Pt(en)(4,7\text{-}Me_2phen)]^{2+}$; and (d) $Pt(5,6\text{-}Me_2phen)(S,S\text{-dach})]^{2+}$.

It should also be noted that the complex $[Pt(5,6\text{-}Me_2phen)(S,S\text{-dach})]^{2+}$ is itself chiral, and produces its own CD spectrum. **Figure 4.24** shows the CD spectrum of $[Pt(5,6\text{-}Me_2phen)(S,S\text{-dach})]^{2+}$ at a concentration equivalent to that in the solution containing a 40:1 ratio of this platinum complex and Q5. None of the CD signals present in **Figure 4.24** are also present in the spectrum of the solutions containing different ratios of $[Pt(5,6\text{-}Me_2phen)(S,S\text{-dach})]^{2+}$ and Q5 (**Figure 4.23d**). This appears to be because the CD signals

of [Pt(5,6-Me_2phen)(*S,S*-dach)]$^{2+}$ are significantly smaller than those of Q5 alone. Therefore the CD signals of this complex do not feature prominently in CD spectra of solutions containing [Pt(5,6-Me_2phen)(*S,S*-dach)]$^{2+}$ and Q5.

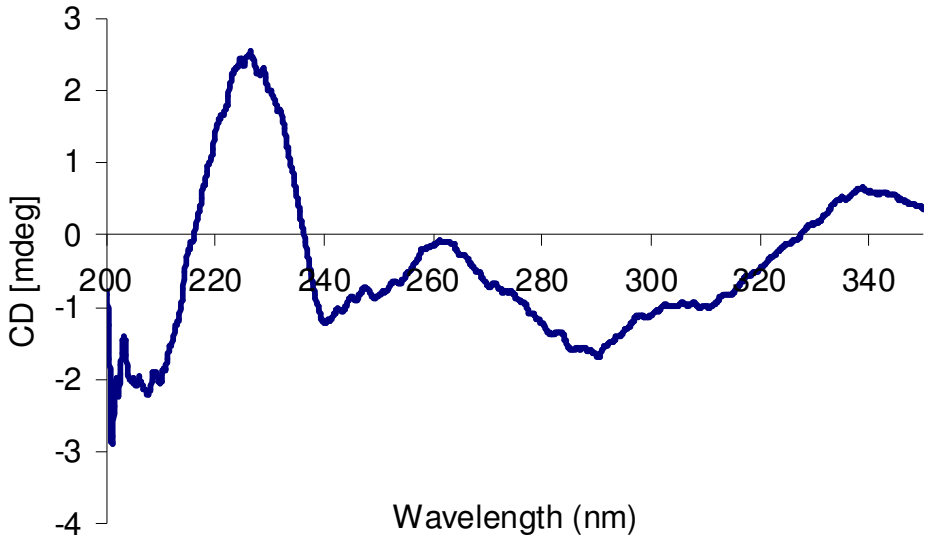

Figure 4.24: Circular dichroism spectrum of a 150 mM NH_4OAc, pH 7 solution containing 0.4 mM [Pt(5,6-Me_2phen)(*S,S*-dach)]$^{2+}$.

The changes in ellipticity (△ε) at 260 nm caused by addition of 40 equivalents of the different platinum complexes to Q5 are compared to each other in **Table 4.2,** as well as to the corresponding values for the ruthenium and nickel complexes. It can be seen that the values obtained for the platinum complexes only span a relatively small range of values, just as found previously with both series of octahedral complexes. Despite this the variations in △ε were found to parallel trends in DNA binding affinity determined previously from ESI-MS results, as the change in ellipticity of the CD band at 265 nm was found to increase according to the following order: [Pt(en)(phen)]$^{2+}$ < Pt(5,6-Me_2phen)(*S,S*-dach)]$^{2+}$ ≤ [Pt(en)(4,7-Me_2phen)]$^{2+}$ < [Pt(en)(3,4,7,8-Me_4phen)]$^{2+}$.

4.5.4 CD Studies of the Binding of Platinum Complexes to D2

The results of ESI-MS studies presented in this chapter showed that overall the platinum complexes examined have greater affinity towards the duplex D2 than the quadruplex Q5. It was therefore of interest to see if this difference in binding affinity was also revealed by another technique. In order to answer this question CD spectra were obtained of solutions containing 1:1, 3:1, 6:1 and 10:1 ratios of all four platinum complexes and D2 (**Figure 4.25**). Addition of increasing amounts of each of the platinum complexes resulted in significant changes to the CD spectra. For example, in all cases the positive CD band at 268 nm was found to shift towards lower energy and decrease in ellipticity. The latter suggests that the base stacking within the DNA molecule was affected by binding of the platinum complexes.[110]

Figure 4.25 also shows that significant changes to the negative CD signal at 240 nm occur upon addition of each of the platinum complexes. Changes in this region of the CD spectrum of DNA has been proposed to indicate unwinding of the double helix, resulting in closer proximity of the two sugar-phosphate backbones in the vicinity of the grooves.[116] The binding of octahedral metal complexes to DNA has generally, as shown here, been found to cause an increase in ellipticity of the positive CD band of DNA at ~ 260 nm. This observation has been attributed to the introduction of negative superhelical turns into the DNA helix,[281] and binding by an intercalative mode of interaction.[113-116,234] In contrast, this study showed that the binding of square planar platinum(II) complexes to dsDNA caused a decrease in ellipticity of this CD band.

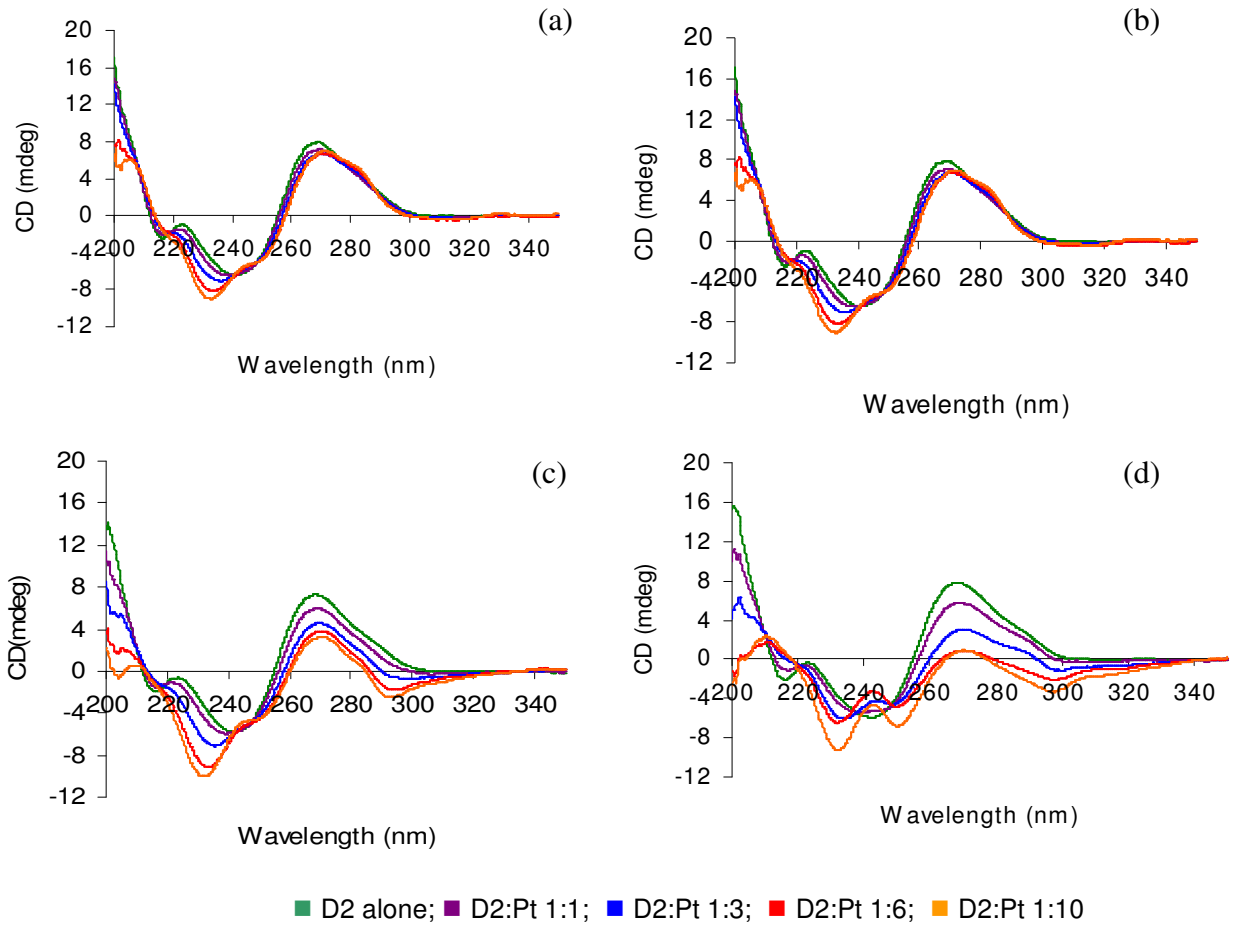

Figure 4.25: Circular dichroism spectra of solutions containing different ratios of platinum complexes and D2: (a) $[Pt(en)(phen)]^{2+}$; (b) $[Pt(en)(3,4,7,8\text{-}Me_4phen)]^{2+}$; (c) $[Pt(en)(4,7\text{-}Me_2phen)]^{2+}$; and (d) $[Pt(5,6\text{-}Me_2phen)(S,S\text{-dach})]^{2+}$.

Studies of DNA binding by square planar platinum complexes containing aromatic ligands such as those used in this study have generally concluded that the mechanism of interaction is *via* intercalation.[76,295-298] It is likely therefore, that the decrease in ellipticity caused by the platinum complexes studied here does not indicate a binding mechanism other than intercalation. Instead the change to the CD spectrum is most likely a result of the dsDNA adopting a different conformation upon platinum binding than that induced by octahedral metal complexes. It should be noted that decreases in ellipticity of this CD band have also

been shown to be caused by dehydration of DNA induced by temperature changes, alcohol or salt.[299-301] These reports proposed that the decrease in ellipticity was attributable to an increase in the unwinding angle of the DNA helix, accompanied by a decrease in twist angle which results in a slight decrease in the number of base pairs per helical turn. The similarity between changes to the CD band at ~ 260 nm caused by addition of platinum complexes, or by the above three factors, suggests that similar changes to DNA conformation may be occurring in all cases.

Table 4.3 presents values of Δε for the CD bands at 265 nm and ~260 nm for platinum complexes with D2 or Q5, respectively. The larger values of Δε found for solutions containing D2 correlate with the higher binding affinities shown by the platinum complexes towards duplex DNA in ESI-MS studies discussed earlier. The values of Δε for the CD band at 260 nm were found to decrease in the following order: $[Pt(5,6\text{-}Me_2phen)(S,S\text{-}dach)]^{2+}$ > $[Pt(en)(4,7\text{-}Me_2phen)]^{2+}$ ~ $[Pt(en)(3,4,7,8\text{-}Me_4phen)]^{2+}$ > $[Pt(en)(phen)]^{2+}$. This sequence is almost identical to the order of binding affinity derived from ESI mass spectra.

Table 4.3: Comparison of △ε values for platinum complexes with qDNA and dsDNA

Platinum Complex	**D2 CD △ε at 265 nm (mdeg)**	**Q5 CD △ε at ~260 nm (mdeg)**
$[Pt(5,6\text{-}Me_2phen)(S,S\text{-}dach)]^{2+}$	7.09	1.6
$[Pt(en)(4,7\text{-}Me_2phen)]^{2+}$	3.68	1.7
$[Pt(en)(3,4,7,8\text{-}Me_4phen)]^{2+}$	2.3	3.1
$[Pt(en)(phen)]^{2+}$	1.41	0.97

4.6 Conclusions

It has been previously reported that ESI-MS can be used to screen non-covalent binding interactions between mononuclear ruthenium(II) complexes and double-stranded DNA, by providing information about the number, relative amounts and stoichiometry of non-covalent complexes present in solution. The current study shows that ESI-MS can also provide detailed information about binding interactions involving ruthenium complexes and quadruplex DNA, or platinum(II) complexes and either duplex or quadruplex DNA. However, ESI mass spectra of solutions containing nickel(II) complexes and Q5 showed ions consisting of only fragments of the original metal complexes bound to the qDNA molecule. This contrasts sharply with what was found previously in studies involving the nickel(II) complexes and double-stranded DNA, where ESI-MS showed that non-covalent complexes were formed consisting of intact nickel molecules bound to D2 (**Figure 3.4**). This difference may be accounted for by proposing that the thermodynamic stability of the nickel(II) complexes, unlike both the platinum(II) and ruthenium(II) complexes, is not sufficient to withstand the more severe instrumental conditions required to acquire spectra of quadruplex DNA. The importance of thermodynamic stability of the metal complexes themselves in studies of this type was further revealed when ESI mass spectra were obtained of solutions containing $[Fe(phen)_3]^{2+}$ or $[Zn(phen)_3]^{2+}$, and D2. In these experiments ESI mass spectra showed little or no ions attributable to non-covalent complexes consisting of intact zinc or iron molecules bound to DNA. Instead virtually all the ions observed were assigned to non-covalent complexes containing fragments of the original metal complexes bound to D2. These observations show that the use of ESI-MS for

probing interactions between metal complexes and DNA may be limited to complexes of only the most thermodynamically stable metal ions.

It is evident from the mass spectra shown here that there is very little difference between the qDNA binding affinities of the ruthenium complexes studied. This conclusion is also supported by the results of CD studies and differs markedly from the distinct differences in binding affinities displayed by the ruthenium complexes towards dsDNA that is evident in previous studies.[77,166,234] Overall these results suggest that the unique ligand L, in the complexes $[Ru(phen)_2(L)]^{2+}$ does not dominate the binding interactions of these metal complexes with qDNA to the same extent that they do in binding interactions with dsDNA. This therefore suggests that classical intercalative interactions are not as important in determining the overall strength of binding interactions between the ruthenium complexes and qDNA.

ESI mass spectral studies of solutions containing platinum(II) complexes and dsDNA showed that the binding affinities of these complexes were just as great or if not greater than those of the ruthenium(II) complexes studied previously. The relative order of binding affinities of the platinum complexes toward dsDNA was found to be: $[Pt(5,6\text{-}Me_2phen)(S,S\text{-dach})]^{2+}$ > $[Pt(en)(4,7\text{-}Me_2phen)]^{2+}$ ≥ $[Pt(en)(3,4,7,8\text{-}Me_4phen)]^{2+}$ > $[Pt(en)(phen)]^{2+}$. These results highlight the significant role hydrophobic interactions may play in determining the strength of binding interactions between metal complexes and dsDNA. Both CD and ESI-MS studies showed that the platinum complexes display lower binding affinities towards qDNA compared to dsDNA. This is again consistent with the idea that metal complexes do not interact with qDNA via exactly the same binding mode(s) they use with dsDNA.

In an attempt to obtain more information about how $[Ru(phen)_2(dppz)]^{2+}$ and $[Pt(5,6\text{-}Me_2phen)(S,S\text{-dach})]^{2+}$ bind to qDNA, ESI-MS was used to analyse competition mixtures containing one of the above metal complexes, as well as the organic drug daunomycin and Q5. The results obtained from these studies provided evidence that the metal complexes can under some circumstances bind qDNA in places other than where daunomycin is present. In contrast, changing the length of the qDNA molecule in solution had very little effect on the binding profile of the above platinum complex, suggesting that it binds to the 5'-terminal end of the quadruplex, which is the same binding region used by daunomycin. The overall extent of binding displayed by $[Ru(phen)_2(dppz)]^{2+}$, however, was surprisingly found to decrease as the length of the qDNA molecule was increased. Therefore the question of where and how these metal complexes bind to qDNA still requires further investigation before it can be answered.

Dissociation profiles for drug/dsDNA complexes have been previously used in order to obtain clues as to where small molecules bind along a length of duplex DNA.[136,164] In order to assess the gas phase dissociation profiles of drug/qDNA complexes, the gas phase dissociation profiles of quadruplex DNA molecules first need to be understood. The dissociation profiles for the teterameric quadruplex Q5 showed an initial loss of ammonium ions, followed by loss of guanine for the higher charge states. For the lower charge states strand separation occurred after the loss of ammonium ions, and before any loss of guanine was observed. The dissociation profile for the dimeric quadruplex Q2 similarly showed initial loss of ammonium ions from the quadruplex, and loss of guanine from the 5- charge state only. Since structural integrity of qudruplex DNA is known to be dependent on the presence of univalent cations situated between their tetrads, in order for CID experiments to

provide credible information on binding interactions between drugs and qDNA, it must be first understood what changes to the structure of qDNA are induced by the loss of these cations.

Chapter 5
Inhibition of DNA Transcription Using Metal Complexes

5.1 Scope of this Chapter

The specific way that proteins and DNA molecules interact is critical for the regulation of many important cellular processes. There are many techniques that have been developed in order to gain information about these binding mechanisms. These techniques include gel mobility shift assays,[302,303] analytical ultracentrifugation,[304] surface plasmon resonance,[305] and expression array technology.[306] A variety of spectroscopic techniques including circular dichroism spectroscopy, light scattering, fluorescence and NMR spectroscopy have also been used, as well as other methods such as X-ray crystallography, differential scanning calorimetry and isothermal titration calorimetry.[304] X-ray crystallography and NMR spectroscopy in particular can provide detailed structural information about non-covalent complexes formed between proteins and nucleic acids. However, both techniques require relatively large quantities of material (multimilligram scale) and relatively long experimental times.[139] The gentleness of ESI allows intact protein/DNA complexes to be directly transferred from solution to the source of a mass spectrometer and detected, and requires relatively small amounts of sample. While ESI-MS does not provide direct structural data as do NMR spectroscopy and X-ray crystallography, it enables the precise stoichiometry of protein/DNA complexes to be determined.

ESI-MS has been used previously to analyse the binding interactions of the transcription factor c-Myb and the replication termination protein Tus, with dsDNA.[307,308] The binding affinity of c-Myb towards different DNA strands, and of mutant forms of the Tus protein

for its specific DNA recognition sequence, were determined and quantitative information on the stability of the DNA/protein complexes also obtained. The interaction of the ETS binding domain of transcription factor PU.1 to dsDNA bearing its recognition sequence, and a dsDNA molecule lacking the consensus sequence, has also been compared previously using ESI mass spectrometry.[309] This study showed that the protein binds to the dsDNA molecule bearing its consensus site with a 1:1 stoichiometry, while no binding to dsDNA lacking the consensus sequence was observed.

The results presented in section 3.2 showed that octahedral metal complexes were capable of inhibiting DNA transcription. However, these experiments did not provide any information about the mechanism of inhibition, which could arise from binding of the metal complex to the enzyme RNA polymerase or, more likely, to the DNA template. The aims of the work described in this chapter were to examine the effects of metal complexes on the binding of transcription factors to DNA. NanoESI-MS was used to examine whether two representative metal complexes, $[Ru(phen)_2(dppz)]^{2+}$ and $[Pt(5,6\text{-}Me_2phen)(S,S\text{-}dach)]^{2+}$, were able to interfere with the binding of the ETS domain of the mouse transcription factor PU.1 to DNA containing its consensus sequence. Both metal complexes have been shown here, and previously,[77,166,234] to have a high affinity towards dsDNA

5.2 NanoESI-MS Mass Spectra of Transcription factor PU.1-DBD

In order to successfully use ESI-MS to analyse DNA/protein interactions it is essential that a number of key experimental parameters are first carefully considered.[138,139] First of all a suitable volatile salt must be selected that will allow the biomolecules to undergo ionisation and also provide an environment where the protein remains folded. Unfortunately most traditional buffers used for studying biomolecular complexes are not suitable for ESI-MS as their lack of volatility interferes with the ionisation process and results in salt adducts (e.g. Na^+) that can reduce sensitivity and make interpretation of mass spectra difficult.[139]

Instrumental parameters must also be carefully selected to ensure that fragile biomolecular complexes are maintained in the gas phase. In preliminary experiments, the optimal conditions required to obtain a standard ESI mass spectrum of the ETS binding domain of the mouse transcription factor PU.1 (hereafter referred to as PU.1-DBD) were determined (spectra not shown). While this was successfully accomplished, too much sample (50 μl of ~ 4 μM solution) of PU.1-DBD was required to obtain a single spectrum given that the goal was to conduct a full study of the effects of metal complexes on the formation of transcription factor/DNA complexes. The use of nanoESI-MS solved this problem, as only 3 μl of a 4 μM solution of protein was required to obtain each spectrum. In nanoESI-MS, the spray comes from a borosilicate capillary through a narrower orifice than for ESI-MS. NanoESI mass spectra of PU.1-DBD were obtained using solutions containing a range of NH_4OAc concentrations (100 mM to 1500 mM). From these experiments an NH_4OAc concentration of 400 mM (pH 7.2) was selected as being optimal for providing both well resolved spectra of the protein with a satisfactory signal-to-noise ratio and a continuous

spray, which was difficult to achieve at higher NH_4OAc concentrations. **Figure 5.1** shows the positive ion nanoESI mass spectrum of PU.1-DBD obtained under these conditions. From this spectrum, the molecular mass of the protein was determined to be 13073.5 Da, which is consistent with the mass of the 113 amino acid residues that make up PU.1-DBD.[241] ESI mass spectra of PU.1-DBD in 50 mM acetic acid (pH 3) have been previously obtained by Cheng *et al.*, using an ESI triple quadrupole mass spectrometer.[309] The greater sensitivity offered by the Waters Q-ToF Ultima used in the current work allowed spectra of PU.1-DBD to be obtained that show a better signal/noise ratio and greater resolution.

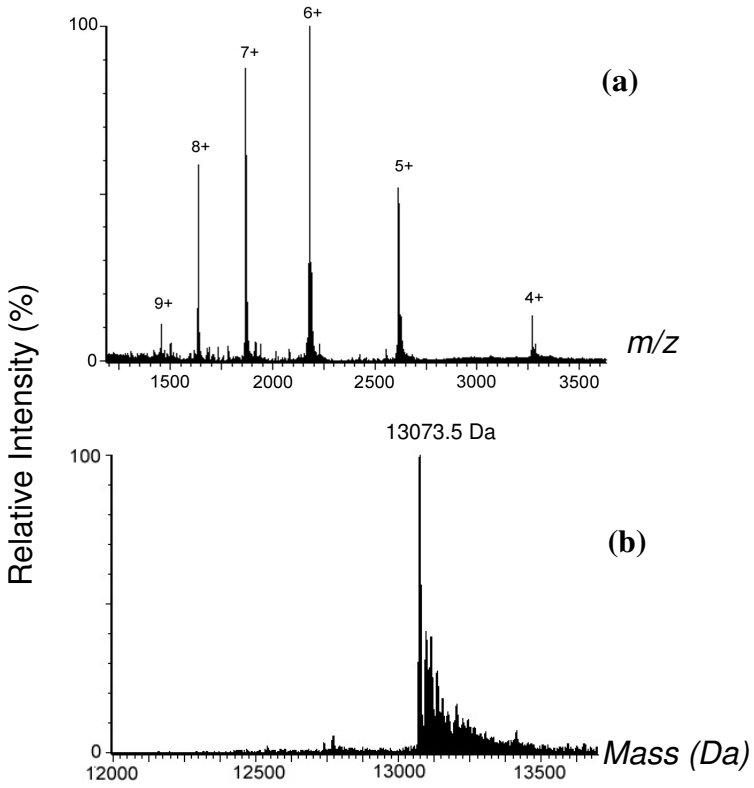

Figure 5.1: Positive ion nanoESI mass spectrum of PU.1-DBD in 400 mM NH_4OAc, pH 7.2. (a) Conventional mass spectrum with charge states of different ions labelled; (b) Transformed mass spectrum obtained using MassLynx software™.

5.3 NanoESI-MS of PU.1-DBD/dsDNA Complex

Prior to conducting experiments also involving metal complexes, it was essential to determine the optimal conditions for obtaining nanoESI mass spectra of non-covalent complexes formed between PU.1-DBD and dsDNA molecules containing the consensus sequence of the transcription factor. Three different dsDNA molecules, called P1, P2 and P3 were used in these experiments. All three dsDNA molecules bear the ETS binding consensus sequence 5'-GGAA/T-3' (shown in bold below) but have different base sequences in flanking positions:

P1 ds(TTGGTTTCAC**TTCC**TTTTATT/AATAAAA**GGAA**GTGAAACCAA)
P2 ds(CTGGTTTCAC**TTCC**TCTCGCG/GCGGAGA**GGAA**GTGAAACCAG)
P3 ds(CAC**TTCC**GCT/AGC**GGAA**GTG)

The specificity of ETS proteins for DNA is critically dependent on the integrity of the central 5'-GGAA/T-3' consensus sequence. However, earlier studies have shown that the flanking base pairs assist in stabilising the ETS/DNA interaction.[213,215,310] Therefore three different dsDNA molecules were used in this study in order to determine which one bound most tightly to the protein, as judged by mass spectra of mixtures containing both DNA and protein. The base sequence in P1 is based on that found in a domain (λB) of a B-cell enhancer sequence (Igλ2-4). PU.1 has been found to be a component of a multiprotein complex which binds to the λB motif of the Igλ2-4 enhancer *in vitro*, and appears to be necessary for the activity of the enhancer *in vivo*.[311] The specific association of the ETS binding domain of murine PU.1 with the enhancer has been characterised previously.[213-215] In addition, it has also been used in studies examining the DNA selectivity of PU.1.[213-215] The shorter dsDNA molecule, P3, was selected because it also is a component of a larger

DNA molecule that was used in a previous study of the DNA binding specificity of the ETS binding domain of murine PU.1, conducted by Poon *et al.*[213,215] Specifically it is also based on the λB motif of the Igλ2-4 enhancer sequence. However, in the study by Poon *et al.*, P3 was shown to bind to the ETS domain with greater affinity compared to the other DNA sequences examined.[213,215] The DNA molecule P2 was selected because it has a larger number of GC base pairs flanking the consensus sequence than either P1 or P3, and because the lower stability of AT rich dsDNA sequences might result in a greater degree of dissociation in the mass spectrometer.

Prior to commencing preliminary experiments to determine the optimal conditions for acquiring a mass spectrum of a PU.1-DBD/DNA complex, the ion mode in which the mass spectra were to be acquired needed consideration. Usually proteins are detected as positive ions whereas oligonucleotides are analysed as negative ions. Whether negative or positive ion mode is best suited for analysis depends on a number of factors including the overall charge on the complex in solution. For example, DNA is negatively charged in solution and its detection as negative ions is likely to preserve the structure in its native form.[312] A number of studies that have used ESI-MS to examine protein/DNA interactions are shown in **Table 5.1**. In earlier work, using lower molecular mass proteins, some protein/DNA complexes were detected in negative ion mode. In more recent work, in particular when large proteins were used, positive ion ESI mass spectra have been acquired. For the work described in this thesis, nanoESI mass spectra of the PU.1-DBD/DNA complex were acquired using positive ion mode, as it was found that this produced better quality spectra .

Table 5.1: DNA/Protein complexes detected by ESI-MS.

Binding Partners	Molecular Mass Protein (Da)	Molecular Mass of the Protein/DNA complex (Da)	Electrospray Solvent	Ion Mode
PU.1-DBD with 17- and 19mer dsDNA.[309]	13500	25148	10 mM NH_4OAc (pH 7.0)	-
DNA binding domain of vitamin D with dsDNA.[313]	12819	47049	Water	-
Binding of XPA binding domain to 20mer dsDNA-cisplatin adduct.[314]	14767	41997	10 mM NH_4OAc (pH 6.7)	-
Tus protein binding to dsDNA with and without its consensus site.[307]	35652	50353	400 mM NH_4OAc (pH 8.0)	+
DNA binding domain of c-Myb with 16- and 22mer dsDNA.[315]	12776	22537	10 mM NH_4OAc (pH 7.0)	+
Thrombin with thrombin-binding aptamer.[316]	36000	40726	acetonitrile/formic acid/ water	+

An initial set of experiments designed to determine the optimal experimental conditions for acquiring mass spectra of protein/DNA complexes was performed using P2. Solutions containing a 1:1 ratio of PU.1-DBD:P2 in 100 mM, 250 mM, 400 mM and 1000 mM NH_4OAc, pH 7.2, were prepared and their positive ion nanoESI mass spectra obtained (**Figure 5.2**). **Figures 5.2a - 5.2c** contain ions at *m/z* 2140.3 and 2568.5 attributable to free P2, and other ions at *m/z* 2885.3 and 3247.2 which correspond to a complex formed from PU.1-DBD and P2. As the concentration of NH_4OAc was increased from 100 mM to 400 mM, ions attributable to the protein/DNA complex increased in abundance relative to those from free P2, and were better resolved.

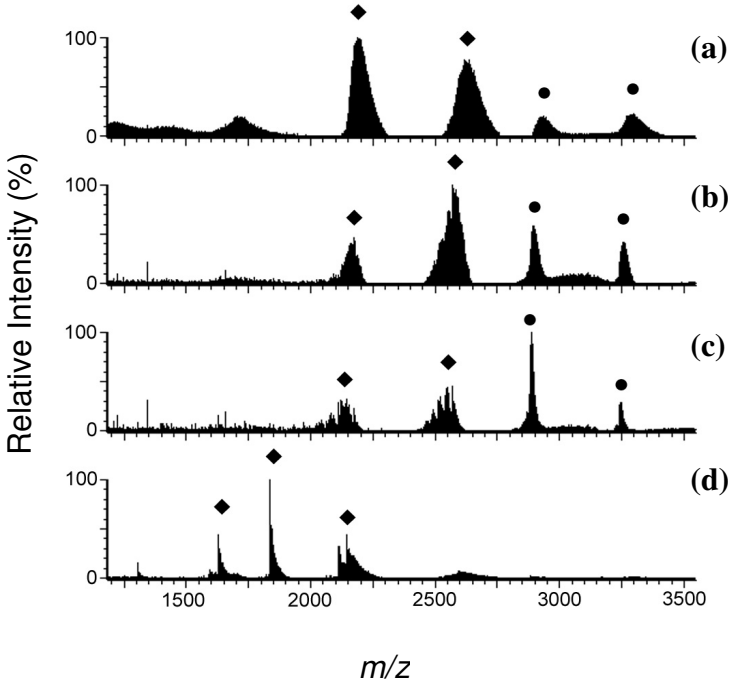

Figure 5.2: Positive ion nanoESI mass spectra of reaction mixtures containing equimolar amounts of PU.1-DBD and P2 in: (a) 100 mM, (b) 250 mM, (c) 400 mM and (d) 1000 mM NH_4OAc, pH 7.2. ◆ Free P2; ● P2 + PU.1-DBD

The above observation is consistent with previous studies that reported that protein aggregation occurs at lower salt concentrations, preventing formation of non-covalent complexes with dsDNA. For example, in one study aggregation of the ETS binding domain of murine PU.1 was reported to occur when the sodium ion concentration was below 150 mM, but complexation between the protein and DNA was detected at concentrations between 150 mM and 250 mM.[215] Furthermore, in an NMR study of the binding of PU.1-DBD to DNA, complex formation was detected at a KCl concentration of 2.5 mM, while at 0.3 mM only free protein could be detected.[317] In the current study increasing the concentration of NH_4OAc further to 1000 mM resulted in ions attributable to the protein/DNA complex completely disappearing (**Figure 5.2d**). This observation is consistent with other ESI-MS studies of protein/DNA interactions, which showed that

increasing the concentration of salt present in solution eventually resulted in complete dissociation of the complexes.[233,315] This occurs because high salt concentrations weaken the electrostatic interactions between protein and DNA molecules. The absence of ions corresponding to free protein may be the result of precipitation of the protein.

Having determined that the optimal solution conditions for obtaining nanoESI mass spectra of the PU.1-DBD/P2 complex involved using 400 mM NH_4OAc, pH 7.2, it was decided to obtain mass spectra of mixtures of PU.1-DBD with either P1 or P3 also using these conditions. **Figure 5.3** shows the positive ion nanoESI mass spectra of solutions containing a 1:1 ratio of PU.1-DBD and P1, P2 and P3 that were obtained.

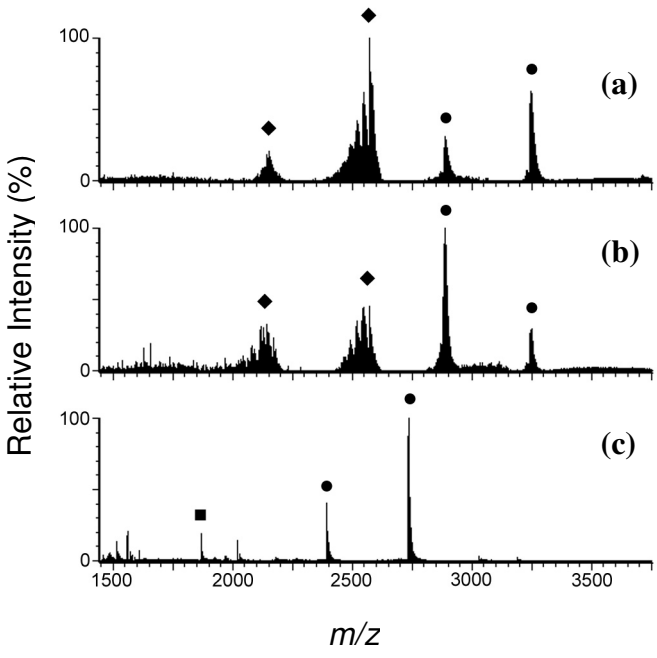

Figure 5.3: Positive ion nanoESI mass spectra of solutions containing a 1:1 ratio of PU.1-DBD and: (a) P1, (b) P2 and (c) P3. ◆ dsDNA ; ●PU.1-DBD/DNA complex ; ■ PU.1-DBD.

Both **Figures 5.3a** and **b** show ions of medium to high abundance attributable to free DNA as well as other ions assigned to the protein/DNA complex. However, in **Figure 5.3c** the

two most abundant ions are due to the complex formed between PU.1-DBD and P3, and there are only ions of low abundance attributable to free DNA or protein. Formation of a protein/DNA complex therefore occurred to the greatest extent with P3, and it was decided to use this DNA molecule in all subsequent studies involving metal complexes.

5.4 NanoESI Mass Spectra of Metal Complexes with P3

The two metal complexes that were selected for this study were $[Ru(phen)_2(dppz)]^{2+}$ and $[Pt(5,6\text{-}Me_2phen)(S,S\text{-dach})]^{2+}$. Both were shown previously using ESI-MS to have high binding affinities towards dsDNA. Prior to examining what effect they have on the formation of the PU.1-DBD/P3 complex, their interactions with the dsDNA molecule P3 were examined.

There have only been a few reports describing the use of positive ion ESI-MS for investigating DNA/drug interactions.[233,312,318] In one study, ESI mass spectra of solutions containing distamycin and dsDNA were obtained, and the extent of complexation was found to be significantly less when the instrument was operated in positive ion mode compared to negative ion mode.[312] The positive ion ESI mass spectra of solutions containing different ratios of either $[Ru(phen)_2(dpqc)]^{2+}$ or $[Ru(phen)_2(dpq)]^{2+}$, and D2, were also significantly different to spectra acquired using negative ion mode.[312] Indeed spectra obtained using positive ion mode showed no ions attributable to non-covalent complexes formed between the metal complex and D2, whereas in negative ion mode the most abundant ions in the spectra obtained were attributable to non-covalent complexes containing 1 and 2 ruthenium molecules bound to D2.[233] The above results are not surprising since DNA is negatively charged in solution, so negative ion spectra are more

likely to provide an accurate picture of the non-covalent complexes present in solution. In contrast, it is expected that non-covalent complexes consisting of positively charged metal complexes bound to DNA will be less stable when the overall complex is forced to adopt a positive charge. For this reason nanoESI mass spectra obtained to test the binding of the metal complexes to P3 were acquired in negative ion mode.

Figure 5.4 illustrates the negative ion nanoESI-mass spectra of solutions containing P3 and 1 or 3 equivalents of either $[Ru(phen)_2(dppz)]^{2+}$ or $[Pt(5,6\text{-}Me_2phen)(S,S\text{-}dach)]^{2+}$. **Figures 5.4a** and **d** show the negative ion ESI mass spectra of P3 alone, which consists only of ions from the free duplex at *m/z* 1512.9 and 2017.5. These ions were still prominent in the spectrum of solutions containing Ru:DNA ratios of 1:1 and 3:1 (**Figures 5.4b** and **c**, respectively), but ions from non-covalent complexes containing either one or two $[Ru(phen)_2(dppz)]^{2+}$ molecules bound to P3 were also present. In the nanoESI mass spectra of the mixtures containing $[Pt(5,6\text{-}Me_2phen)(S,S\text{-}dach)]^{2+}$ and P3 similar observations were made, but examination of these spectra suggested that $[Pt(5,6\text{-}Me_2phen)(S,S\text{-}dach)]^{2+}$ has a greater affinity for P3 than $[Ru(phen)_2(dppz)]^{2+}$. For example, ions attributable to P3 alone are observed in the spectrum of the reaction mixture containing a 3:1 ratio of Ru:P3. Since the ions from free P3 are not present in the spectrum of the reaction mixture containing a 3:1 ratio of Pt:P3, it is evident that all P3 molecules have at least one bound $[Pt(5,6\text{-}Me_2phen)(S,S\text{-}dach)]^{2+}$.

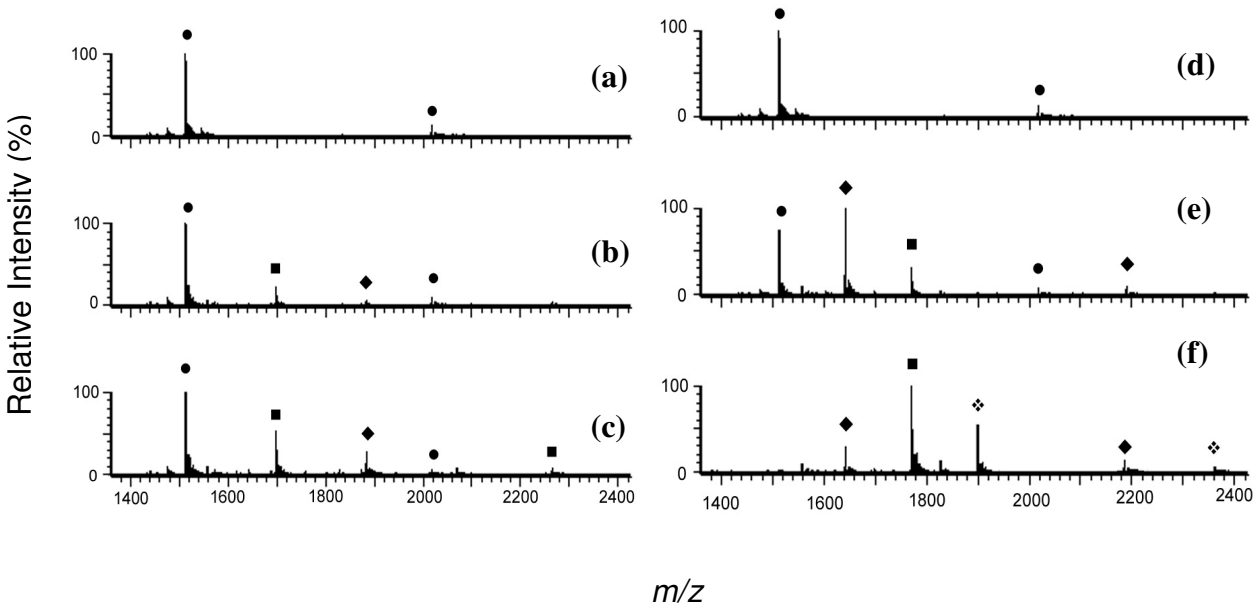

Figure 5.4: Negative ion nanoESI mass spectra of solutions containing P3 with either $[Ru(phen)_2(dppz)]^{2+}$ or $[Pt(5,6\text{-}Me_2phen)(S,S\text{-}dach)]^{2+}$: (a) P3 alone, (b) Ru:P3 = 1:1 (c) Ru:P3 = 3:1, (d) P3 alone, (e) Pt:P3 = 1:1, (f) Pt:P3 = 3:1. ● Free P3; ■ P3 + 1M; ◆ P3 + 2M; ❖ P3 + 3M where M = $[Ru(phen)_2(dppz)]^{2+}$ or $[Pt(5,6\text{-}Me_2phen)(S,S\text{-}dach)]^{2+}$.

The mass spectra of the DNA/metal complex mixtures were also acquired using positive ion nanoESI-MS for comparison. **Figure 5.5** shows the 3+ and 4+ charge states in positive ion nanoESI mass spectra of solutions containing P3 and 1, 3, 6, 10 and 20 equivalents of either $[Ru(phen)_2(dppz)]^{2+}$ or $[Pt(5,6\text{-}Me_2phen)(S,S\text{-}dach)]^{2+}$. For solutions containing $[Ru(phen)_2(dppz)]^{2+}$:P3 ratios of 1:1, 3:1 and 6:1 (**Figures 5.5a** - **c**) the most abundant ions observed were at *m/z* 1515.2 and 2020.8, which correspond to free P3. When the amount of $[Ru(phen)_2(dppz)]^{2+}$ in solution was increased further, the spectra revealed additional ions attributable to non-covalent complexes consisting of P3 with 1 and 2 ruthenium molecules bound. In addition, the nanoESI mass spectra of solutions containing 10:1 and 20:1 ratios of $[Ru(phen)_2(dppz)]^{2+}$ and P3 (**Figures 5.5d** and **5.5e**) both contained ions of very low abundance at *m/z* 2042.5 that may be tentatively assigned to non-covalent complexes of P3

with 3 ruthenium molecules bound. The similarity of the spectra of the 10:1 and 20:1 solutions suggests that equilibrium was being approached in this system at these ratios.

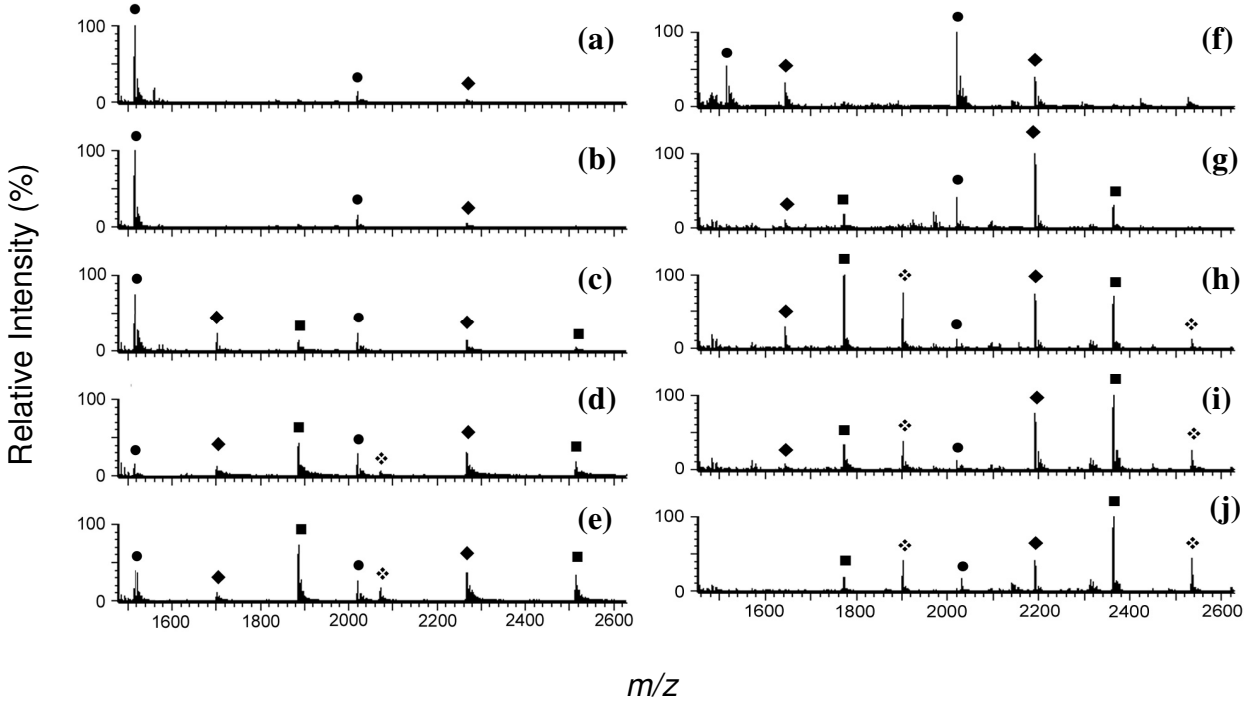

Figure 5.5: Positive ion nanoESI mass spectra of solutions containing P3 with either $[Ru(phen)_2(dppz)]^{2+}$ or $[Pt(5,6\text{-}Me_2phen)(S,S\text{-}dach)]^{2+}$: (a) Ru:P3 = 1:1, (b) Ru:P3 = 3:1, (c) Ru:P3 = 6:1, (d) Ru:P3 = 10:1, (e) Ru:P3 = 20:1, (f) Pt:P3 = 1:1, (g) Pt:P3 = 3:1, (h) Pt:P3 = 6:1, (i) Pt:P3 = 10:1, (j) Pt:P3 = 20:1. ● free P3; ◆ P3+ 1M; ■ P3 + 2M; ❖ P3 + 3M where M = $[Ru(phen)_2(dppz)]^{2+}$ or $[Pt(5,6\text{-}Me_2phen)(S,S\text{-}dach)]^{2+}$.

Comparison of positive ion nanoESI mass spectra of solutions containing identical ratios of $[Pt(5,6\text{-}Me_2phen)(S,S\text{-}dach)]^{2+}$ and P3 on the one hand, and $[Ru(phen)_2(dppz)]^{2+}$ and P3 on the other, suggest that the platinum complex has a higher binding affinity towards P3, in agreement with the results from the negative ion spectra (**Figure 5.4**). For example, when a solution containing a 6:1 ratio of $[Pt(5,6\text{-}Me_2phen)(S,S\text{-}dach)]^{2+}$ and P3 was examined, the most abundant ions present in the nanoESI mass spectrum were those attributable to non-covalent complexes comprised of P3 with 1 or 2 platinum molecules bound. In contrast, the

spectrum of a solution containing a 6:1 ratio of $[Ru(phen)_2(dppz)]^{2+}$ and P3 revealed that the most abundant ions present in solution corresponded to free P3.

Since non-covalent complexes consisting of transition metal complexes bound to DNA have been shown to be less stable in positive ion mode, the spectra in **Figure 5.5** most likely do not fully reflect the range of non-covalent complexes present in solution. Higher concentrations of metal complex were required to (apparently) saturate P3 when the mixtures were analysed using positive ion ESI-MS.[233,312] However, whilst this must be taken into consideration when interpreting **Figure 5.5**, the spectra do indicate that the metal complexes bind to DNA, and that the binding was more extensive in the case of the platinum complex.

5.5 Effect of Metal Complexes on the Binding of a Transcription Factor to DNA

This section describes the results of experiments aimed at determining whether metal complexes can disrupt the formation of the PU.1-DBD/P3 complex. Both positive and negative ion nanoESI mass spectrometry was used initially in these studies. However, negative ion nanoESI-MS resulted in spectra of poor quality, so the mixtures were subsequently analysed using only positive ion nanoESI-MS.

Positive ion nanoESI mass spectra were obtained using solutions containing 1:1:1, 1:1:3, 1:1:6, 1:1:10 and 1:1:20 ratios of PU.1-DBD:P3:metal, in order to determine the effects of the metal complexes on the formation of the PU.1-DBD/P3 complex. Experiments were performed by first allowing P3 to equilibrate with the metal complex for 10 minutes and then adding PU.1-DBD, as well as by first treating P3 with PU.1-DBD for 10 minutes, and

then adding the metal complex. Spectra of solutions prepared by the two different procedures, but with the same final composition, were almost identical. This indicates that regardless of whether the DNA was complexed first with the protein or the metal complex, the same final distribution of complexes was present at equilibrium. Experiments were also conducted to observe if the metal complexes could bind to PU.1-DBD. NanoESI mass spectra of solutions containing metal:protein ratios ranging from 1:1 to 20:1 showed that the metal complexes did not bind to PU.1-DBD.

Figure 5.6 presents positive ion nanoESI mass spectra (transformed to a mass scale) of solutions containing different ratios of protein, DNA and metal complex. The spectrum of a solution containing only PU.1-DBD and P3 (**Figures 5.6a** and **e**) shows the PU.1-DBD/P3 complex at 19130.8 Da (in agreement with the calculated value of 19129.6 Da). Ions assigned to free PU.1-DBD at 13077.4 Da and free P3 at 6057.9 Da are also present. As the amount of $[Pt(5,6\text{-}Me_2phen)(\textit{S,S}\text{-dach})]^{2+}$ present in solution was increased, the spectra shown in **Figures 5.6b - d** were obtained. The abundance of the PU.1-DBD/P3 complex decreased as the amount of platinum was increased. This was accompanied by an increase in abundance of ions assigned to the free protein, and the appearance of ions assignable to non-covalent complexes consisting of one or two intact platinum molecules bound to P3. A similar set of observations was made when increasing amounts $[Ru(phen)_2(dppz)]^{2+}$ were added to a solution containing equimolar amounts of PU.1-DBD and P3 (**Figures 5.6e** - **h**).

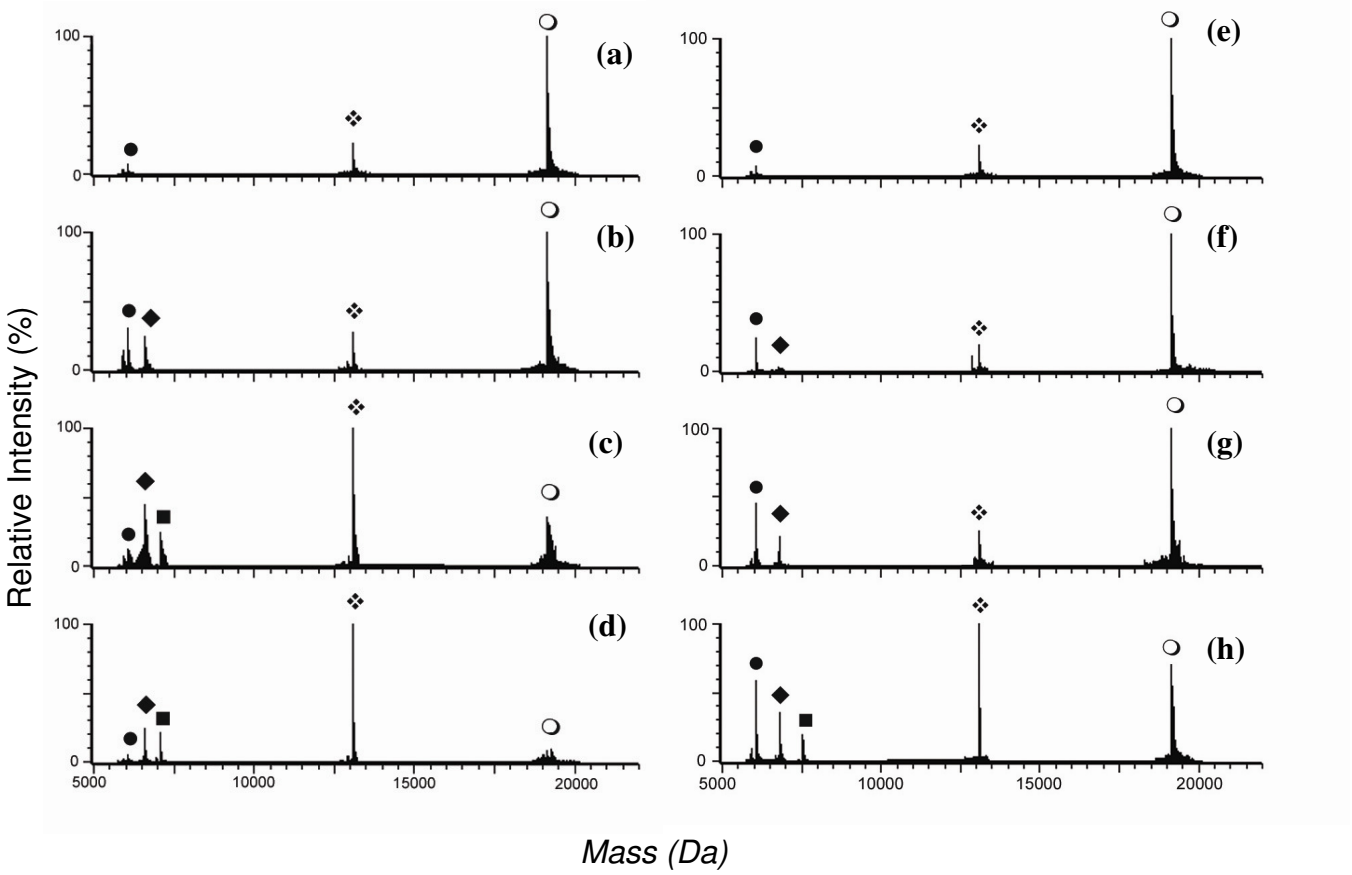

Figure 5.6: Positive ion nanoESI mass spectra (transformed to a mass scale using MassLynx software^{TM}) of solutions containing PU.1-DBD and either [Pt(5,6-Me$_2$phen)(*S,S*-dach)]$^{2+}$ or [Ru(phen)$_2$(dppz)]$^{2+}$: (a) PU.1-DBD:P3 = 1:1 (b) PU.1-DBD:P3:Pt = 1:1:3 (c) PU.1-DBD:P3:Pt = 1:1:6; (d) PU.1-DBD:P3:Pt = 1:1:10; (e) P3:PU.1-DBD = 1:1 (f) PU.1-DBD:P3:Ru = 1:1:3, (g) PU.1-DBD:P3:Ru = 1:1:6, (h) PU.1-DBD:P3:Ru = 1:1:10. ● free P3; ◆ P3 + 1M^{2+}; ■ P3 + 2M^{2+}; ❖ PU.1-DBD and ❍ P3 + PU.1-DBD (M = Ru or Pt complex).

The decrease in abundance of ions assigned to the DNA/protein complex caused by the addition of ruthenium complex was not as dramatic as was observed when the same quantity of platinum complex was present. In addition, the increase in abundance of ions assigned to free protein, free DNA and metal/DNA complexes, was not as dramatic when the ruthenium complex was added compared to when [Pt(5,6-Me$_2$phen)(*S,S*-dach)]$^{2+}$ was added to the PU.1-DBD:P3 complex.

The above changes in solution composition can be seen more clearly in **Figure 5.7,** which shows the variations in relative abundances of the different solution components (PU.1-DBD and PU.1-DBD/P3) as a function of the amount of added metal complex. Relative abundances were determined by first adding together the individual abundances of all ions arising from a particular solution component, and then expressing this as a percentage of the total intensity of ions assigned to PU.1-DBD and PU.1-DBD/P3 present in the spectrum. The abundances of ions assigned to free DNA, and metal/DNA non-covalent complexes, were not included in these calculations as their response factors are not comparable. The response factor takes into account all factors that affect the ability of an ion to be detected under the experimental conditions used, which includes ionisation efficiency and efficiency of transmission through the mass analysers to the detector.[307] The ionisation efficiency will depend on the pH of the solution, the gas phase acidity/basicity of the analyte and other factors. Therefore to compare relative abundances, only molecules with similar ionisation efficiencies (such as PU.1-DBD and its complex with DNA) can be compared.[307]

Figure 5.7 shows that as the amount of either the ruthenium or platinum complex added to the solution was increased, the relative abundances of ions arising from the PU.1-DBD/P3 complex decreased. However, the extent of inhibition of transcription factor/DNA complex formation was greater when $[Pt(5,6\text{-}Me_2phen)(\textit{S,S}\text{-dach})]^{2+}$ was added. For example, the relative abundance of the transcription factor/DNA complex decreased from 80% to just 7% when the PU.1-DBD:P3:Pt ratio was increased from 1:1:1 to 1:1:20. However, when the amount of ruthenium complex present in solution was increased in a similar fashion, the relative abundance of the PU.1-DBD/P3 complex decreased from 85% to 48%. Over the

same range of PU.1-DBD:P3:metal ratios, the relative abundance of free protein increased from 21% to 93% in the case of the platinum complex, while for solutions containing $[Ru(phen)_2(dppz)]^{2+}$ the amount of unbound PU.1-DBD only increased from 15% to 51%.

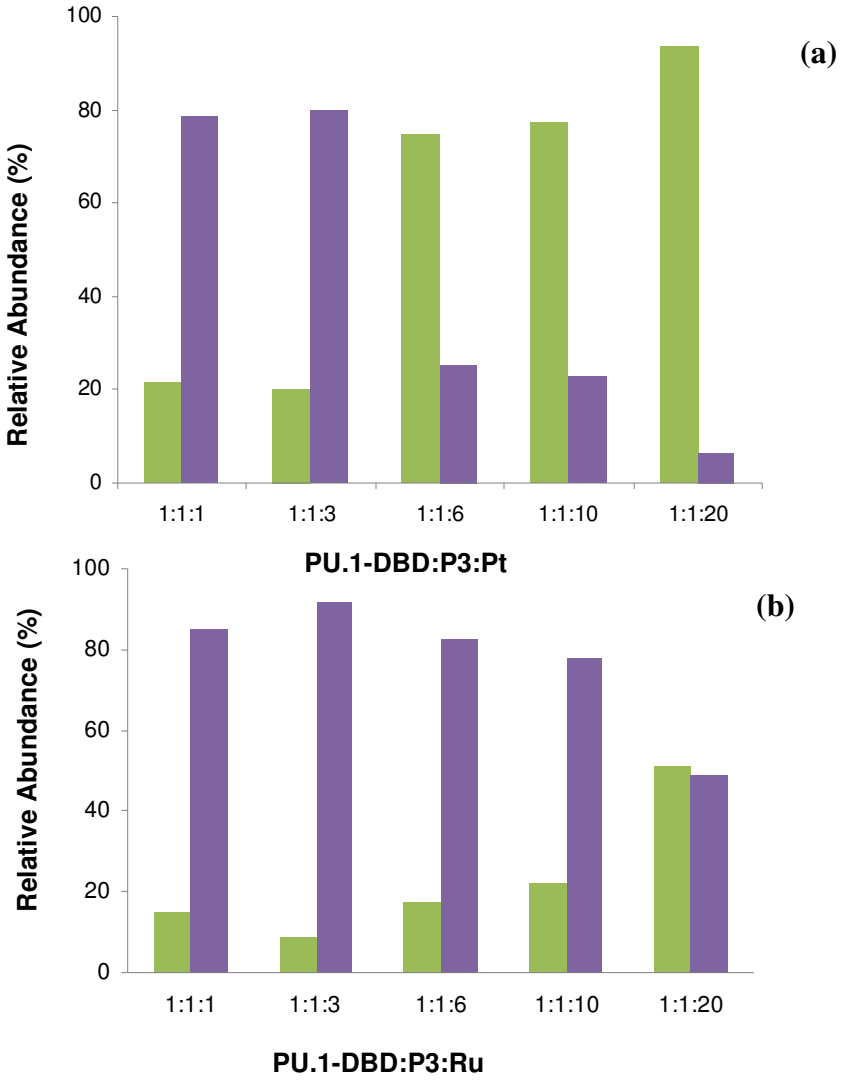

Figure 5.7: Relative abundances of various components present in solutions containing different ratios of the transcription factor PU.1-DBD, the dsDNA molecules P3, and either: (a) $[Pt(5,6\text{-}Me_2phen)(S,S\text{-}dach)]^{2+}$ or (b) $[Ru(phen)_2(dppz)]^{2+}$. ■ PU.1-DBD and ■ PU.1-DBD/P3 complex.

NanoESI mass spectra of solutions containing PU.1-DBD and either of the metal complexes showed that they do not bind to PU.1-DBD (data not shown). This observation implies that the inhibition of formation of a complex between PU.1-DBD and P3 can only be due to binding of the metal complexes to P3. There are several ways that binding of the metal complexes to DNA could inhibit the binding of the transcription factor to P3. First, the metal complexes could be bound at or near the transcription factor consensus sequence, resulting in structural distortions to the dsDNA molecule that inhibits binding of the transcription factor. In addition, DNA bases flanking the consensus sequence might also be involved in binding interactions with the metal complexes that modify the orientation and stability of the ETS binding domain and consequently reduce the binding affinity of PU.1-DBD towards P3. As it is not known where the binding sites are on P3 for either metal complex, the exact mechanism(s) by which the formation of the DNA/transcription factor complex is inhibited cannot be determined, particularly at low protein:DNA:metal ratios. However, at high ratios it is likely that the metal complexes are extensively coordinated to P3, and inhibition of the transcription factor/DNA complex occurs by a combination of the above mechanisms and others.

The greater degree of inhibition of formation of the transcription factor/DNA complex caused by $[Pt(5,6\text{-}Me_2phen)(\textit{S,S}\text{-dach})]^{2+}$, in comparison to $[Ru(phen)_2(dppz)]^{2+}$, is most likely due to the higher binding affinity of the former metal complex towards P3 revealed by the nanoESI mass spectra shown in **Figures 5.4** and **5.5**. A greater level of non-covalent complex formation between the platinum complex and P3 would induce greater structural changes to the DNA molecule, and thereby minimise the ability of the transcription factor to bind in the usual fashion to its DNA consensus sequence.

5.6 Conclusions

The results described in this chapter show that ESI-MS can be used to rapidly screen transcription factor/DNA binding and inhibition of this interaction by metal complexes. ESI mass spectra indicated that $[Ru(phen)_2(dppz)]^{2+}$ and $[Pt(5,6\text{-}Me_2phen)(S,S\text{-}dach)]^{2+}$ can both interfere with the binding of PU.1-DBD to its DNA binding site, but that the platinum complex was a stronger inhibitor of this binding interaction. This can be assumed to be due to the higher binding affinity $[Pt(5,6\text{-}Me_2phen)(S,S\text{-}dach)]^{2+}$ has towards P3, which was evident from ESI mass spectra of solutions containing the metal complex and P3 obtained in both negative and positive ion modes. The higher binding affinity $[Pt(5,6\text{-}Me_2phen)(S,S\text{-}dach)]^{2+}$ has for P3 is most likely due to its square planar geometry, which enables more molecules to non-covalently bind by an intercalative mechanism over a smaller number of base pairs than the bulky octahedral molecule $[Ru(phen)_2(dppz)]^{2+}$.

The nanoESI mass spectra of solutions containing different PU.1-DBD:P3:metal complex ratio revealed that high concentrations of the metal complexes were needed in order to induce a significant reduction in the amount of PU.1-DBD/P3 complex present in solution. In order for complexes of this type to be considered as potential therapeutic agents that act by inhibiting binding of transcription factors to DNA, they will need to demonstrate a higher degree of binding at lower concentrations. To this end, the metal complexes used in the current study should be considered as scaffolds for designing new metal complexes with modified ligands designed to enhance their affinity for the consensus sequence of transcription factors. Future experiments will need to be conducted using different metal complexes with systematically varied structures, in order to understand what features are essential for the inhibition of binding by specific transcription factors to DNA. These

studies should also use DNA molecules with different base sequences in regions flanking the consensus site in order to provide information on how these flanking regions can be used by the metal complexes to inhibit transcription factor binding.

REFERENCES

(1) Matthews, C. K., Van Holde,K. E. and Ahern, K. G. *Biochemistry*; Benjamin Cummings: San Francisco, 2000.

(2) Marty, R.; Ouameur, A. A.; Neault, J. F.; Nafisi, S.; Tajmir-Riahi, H. A. *DNA and Cell Biol.* **2004**, *23*, 135-140.

(3) Lisgarten, J. N.; Coll, M.; Portugal, J.; Wright, C. W.; Aymami, J. *Nature Structural Biology* **2002**, *9*, 57-60.

(4) Kwakye-Berko, F.; R., M. S. *Mol. Biochem. Parasit.* **1989**, *35*, 51-55.

(5) Hewlett, G.; Hallenberger, S.; Rubsamem-Waigmann *Curr. Opin. Parm.* **2004**, *4*, 453-464.

(6) Bischoff, G.; Hoffman, S. *Curr. Med. Chem.* **2002**, *9*, 321-348.

(7) Abeloff, M. D.; Armitage, J. O.; Niederhuber, J. E.; Kastan, M. B.; McKenna, W. G. *Clinical Oncology*; Elsvier, 2003.

(8) Thornsberry, C. *Handbook of Experimental Paramacology* **1998**, *137*, 137-143.

(9) De Backer, M. D.; Van Dijck, P. V. *Trends Microbiol.* **2003**, *11*, 470-478.

(10) Haq, I.; Ladbury, J. *J. Mol. Recognit.* **2000**, *13*, 188-197

(11) Zeglis, B. M.; Pierre, V. C.; Barton, J. K. *Chem. Commun.* **2007**, 4565-4579.

(12) Clarke, M. J.; Sadler, P. J. *Metallopharmaceuticals 1: DNA interactions*; Springer: Berlin, 1999.

(13) Richards, A. D.; Rodger, A. *Chem. Soc. Rev.* **2007**, *36*, 471-483.

(14) Norden, B.; Kurucsev, T. *J. Mol. Recognit.* **1994**, *7*, 141-155.

(15) Tse, W. C.; Boger, D. L. *Acc. Chem. Res.* **2004**, *37*, 61-69.

(16) Demeunynck, M.; Bailly, C.; Wilson, W. D. *DNA and RNA binders: from small molecules to drugs*; Wiley-VCH: Weinhein, 2002.

(17) Haq, I.; Lincoln, P.; Suh, D.; Norden, B.; Z., C. B.; Chaires, J. B. *J. Am. Chem. Soc.* **1995**, *117*, 4788-4796.

(18) Campbell, N. A.; Reece, J. B.; Mitchell, L. G. *Biology*; Benjamin Cummings: Menlo Park, 1999.

(19) Watson, J. D.; Crick, F. H. C. *Nature* **1953**, *171*, 737-738.

(20) Stryer, L. *Biochemistry*; Freeman and Company: New York, 1988.

(21) http://commons.wikimedia.org/wiki/Image:A-DNA, B.-D. a. Z.-D. p.

(22) http://mol-biol4masters.org/Deoxy_Ribonucleic_Acid2-Structure.htm.

(23) Spingler, B. *Inorg. Chem.* **2005**, *44*, 831-833.

(24) Wang, G.; Vasquez, K. M. *Front Biosci* **2007**, *12*, 4424-4438.

(25) Aplan, P. D. *Trends Genet.* **2006**, *22*, 46-55.

(26) Thandla, S. P.; Ploski, J. E.; Raza-Egilmez, S. Z.; Chhalliyil, P. P.; Block, A. W.; de Jong, P. J.; Aplan, P. D. *Blood* **1999**, *93*, 293-299.

(27) Boem, T.; Mengle-Gaw, L.; Kees, U. R.; Spurr, N.; Lavenir, I.; Forster, A.; Rabbitts, T. H. *Embo J.* **1989**, *8*, 2621-2631.

(28) Suram, A.; Rao, K. S.; Latha, K. S.; Viswamitra, M. A. *Neuromolecular Med.* **2002**, *2*, 289-297.

(29) Searle, S.; Blackwell, J. M. *J Med. Genet.* **1999**, *36*, 295-299.

(30) Kim, Y. G.; Muralinath, M.; Brandt, T.; Pearcy, M.; Hauns, K.; Lowenhaupt, K.; Jacobs, B. L. *Proc. Natl. Acad. Sci. U. S. A.* **2003**, *100*, 6974-6979.

(31) Frank-Kamenetskii, M. D.; Mirkin, S. M. *Annu. Rev. Biochem.* **1995**, *64*, 65-96.

(32) Li, H.; Broughton-Head, V. J.; Peng, G.; Powers, V. E. C.; Ovens, M. J.; Fox, K. R.; Brown, T. *Bioconj. Chem.* **2006**, *16*, 1568-1581.

(33) Neidle, S.; Parkinson, G. *Nature Rev.* **2002**, *1*, 383-393.

(34) Kumar, N.; Petersen, M.; Maiti, S. *Chem. Chomm.* **2008**, 1532 -1534.

(35) Neidle, S.; Nunn, C. M. *Natural Products Reports* **1998**, *15*, 1-15.

(36) Kang, C.; Berger, I.; Lockshin, C.; Ratliff, R.; Moyzis, R. K.; Rich, A. *Proc. Natl. Acad. Sci. U. S. A.* **1995**, *92*, 3874-3878.

(37) Baker, E. S.; Bernstien, S. L.; Gabelica, V.; De Pauw, E.; Bowers, M. T. *Int. J. Mass. Spec.* **2006**, *253*, 225-237.

(38) Wang, Y.; Patel, D. J. *J. Mol. Biol.* **1993**, *234*, 1171-1183.

(39) Phan, A. T.; Kuryavyi, V.; Patel, D. J. *Curr. Opin. Struct. Biol.* **2006**, *288*, 288-298.

(40) Williamson, J. R. *Annu. Rev. Biophys. Biomol. Struct.* **1994**, *23*, 703-730.

(41) Hazel, P.; Huppert, J.; Balasubramanian, S.; Neidle, S. *J. Am. Chem. Soc.* **2004**, *126*, 16405-16415.

(42) Kaushik, M.; Bansal, A.; Saxena, S.; Kukreti, S. *Biochemistry* **2007**, *46*, 7119-7131.

(43) Balagurumoorthy, P.; Brahmachari, S. K. *J. Biol. Chem.* **1994**, *269*, 21858 - 21869

(44) He, Y.; Neuman, R. D.; Panyutin, I. G. *Nucleic Acids Res.* **2004**, *32*, 5359-5367.

(45) Parkinson, G. N.; Micheal, P. H. L.; Neidle, S. *Nature* **2002**, *417*, 876-880.

(46) Smith, F. W.; Feigon, J. *Nature* **1992**, *356*, 164-168.

(47) Horvarth, M. P.; Schultz, S. C. *J. Mol. Biol.* **2001**, *310*, 367-377.

(48) Wang, Y.; Patel, D. J. *Structure* **1993**, *1*, 263-282.

(49) Li, J.; Correia, L. W.; Trent, J. O.; Chaires, J. B. *Nucleic Acids Res.* **2005**, *33*, 4649-4659.

(50) Han, H.; Hurley, L. H. *Trends Pharmacol. Sci.* **2000**, *21*, 136.

(51) Castasi, P.; Chen, X.; Moyzis, R. K.; Bradbury, E. M.; Gupta, G. *J. Mol. Biol.* **1996**, *264*, 534-545.

(52) Tang, J.; Kan, Z.; Yao, Y.; Wang, Q.; Hao, Y.; Tan, Z. *Nucleic Acids Res.* **2007**, 1-9.

(53) Strekowski, L.; Wilson, B. *Mutation Research* **2007**, *623*, 3-13.

(54) Blackburn, G. M.; Gait, M. J. *Nucleic Acids in Chemistry and Biology*; Oxford University Press: Oxford, 1990.

(55) Nelson, S. M.; Ferguson, L. R.; Denny, W. A. *Mutation Research* **2007**, *623*, 24-40.

(56) Lah, J.; Vesnaver, G. *J. Mol. Biol.* **2004**, *342*, 73-89.

(57) Tabernero, L.; Verdaguer, N.; Coll, M.; Fita, I.; van der Marel, G. A.; Boom, J. H.; Rich, A.; Aymami, J. *Biochemistry* **1993**, *32*, 8403-8410.

(58) Sharma, S.; Doherty, K. M.; Rosh Jr, R. M. *Curr. Med. Chem. Anticancer Agents* **2005**, *5*, 183-199.

(59) Beerman, T. A.; Woynarowski, J. M.; Sigmund, R. D.; Gawron, L. S.; Rao, K. E.; Lown, J. W. *Biochim. Biophys. Acta* **1991**, *1090*, 52-60.

(60) Cozzi, P. *II Farmaco* **2000**, *55*, 168-173.

(61) Sabatino, M. A.; Colombo, T.; Geroni, C.; Marchini, S.; Brogini, M. *Clin. Cancer. Res.* **2003**, *9*, 5402-5408.

(62) Hageboutros, A.; Mooneyham, A.; De Maria, T.; VonHoff, D.; Vitek, L.; O'Dwyer, P. J.; Weiss, G. R. *Proc. Am. Assoc. Cancer. Res.* **1994**, *35*, 1467.

(63) Broggini, M.; Marchini, S.; Fontana, E.; Moneta, D.; Fowst, C.; Geroni, C. *Anticancer Drugs* **2004**, *15*, 1-16.

(64) Fedier, A.; Fowst, C.; Tursi, J.; Geroni, C.; Haller, U.; Marchini, S.; Fink, D. *British Journal of Cancer* **2003**, *89*, 1559-1565.

(65) Geroni, C.; Marchini, S.; Cozzi, P.; Galliera, E.; Ragg, E.; Colombo, T.; Battaglia, R.; Howard, M.; D'Incalci, M.; Broggini, M. *Cancer Res.* **2002**, *62*, 2332-2336.

(66) Baraldi, P. G.; Bovero, A.; Fruttarolo, F.; Preti, D.; Tabrizi, M. A.; Pavani, M. G.; Ramagnoli, R. *Med Res Rev* **2004**, *24*, 475-528.

(67) Gupta, R.; Wang, H.; Huang, L.; Lown, J. W. *Anti-Cancer Drug Design* **1995**, *10*, 25-41.

(68) Tawar, U.; Jain, A. K.; Chandra, R.; Singh, Y.; Dwawakanath, B. S.; Chaudhury, N. K.; Good, L.; Tandon, V. *Biochemistry* **2003**, *42*, 13339-13346.

(69) Wang, A. H.; Ughetto, G.; Quigley, G. J.; Rich, A. *Biochemistry* **1987**, *26*, 1152-1163.

(70) Wang, A. H. In *Molecular Aspects of Anticancer Drug-DNA Interactions*; Neidle, S., Waring, M., Eds.; The Macmillan press: London, 1993.

(71) Metcalfe, C.; Thomas, J. A. *Chem. Soc. Rev.* **2003**, *32*, 215-224.

(72) Erkkila, K.; Odom, D. T.; Barton, J. K. *Chem. Rev.* **1999**, *99*, 2777-2795.

(73) Sigman, D. S. *Acc. Chem. Res.* **1986**, *19*, 180-186.

(74) Sigman, D. S.; Grahem, D. R.; D'aurora, V.; Stern, A. M. *J. Biol. Chem.* **1979**, *254*, 12269-12272.

(75) Bond, P. J.; Langridge, R.; Jennette, K. W.; Lippard, S. J. *Proc. Natl. Acad. Sci. U. S. A.* **1975**, *72*, 4825-4829.

(76) Howe-Grant, M.; Lippard, S. J. *Biochemistry* **1979**, *18*, 5762-5769.

(77) Urathamakul, T.; Beck, J. L.; Sheil, M. M.; Aldrich-Wright, J. R.; Ralph, S. T. *Dalton Trans* **2004**, 2683-2690.

(78) Arounaguiri, S.; Easwaramoorthy, D.; Ashokkumar, A.; Dattagupta, A.; Maiya, B. G. *Proc. Indian Acad. Sci. (Chem. Sci.)* **2000**, *112*, 1-17.

(79) Terbrueggen, R. H.; Barton, J. K. *Biochemistry* **1995**, *34*, 8227-8234.

(80) Odom, D. T.; Parker, C. S.; Barton, J. K. *Biochemistry* **1999**, *38*, 5155-5154.

(81) Krotz, A. H.; Hudson, B. P.; Barton, J. K. *J. Am. Chem. Soc.* **1993**, *115*, 12577 - 12578.

(82) Kielkopf, C. L.; Erkkila, K. E.; Hudson, B. P.; Barton, J. K.; Rees, D. C. *Nat. Struc. Biol.* **2000**, *7*, 117-121.

(83) Friedman, A. E.; Chambron, J. C.; Sauvage, J. P.; Turro, N. J. *J. Am. Chem. Soc.* **1990**, *112*, 4960-4962.

(84) Turro, C.; Bossmann, S. H.; Jenkins, Y.; Barton, J. K.; Turro, N. J. *J. Am. Chem. Soc.* **1995**, *117*, 9026.

(85) Olson, E. J. C.; Hu, D.; Hormann, A.; Jonkman, A. M.; Arkin, M. R.; Stemp, E. D. A.; Barton, J. K.; Barbara, P. F. *J. Am. Chem. Soc.* **1997**, *119*, 11458.

(86) Arkin, M. R.; Stemp, E. D. A.; Holmlin, R. E.; Barton, J. K.; Hormann, A.; Olson, E. J. C.; Barbara, P. F. *Science* **1996**, *273*, 475.

(87) Hiort, C.; Lincoln, P.; Norden, B. *J. Am. Chem. Soc.* **1993**, *115*, 3448-3454.

(88) Dandliker, P. J.; Holmlin, R. E.; Barton, J. K. *Science* **1997**, *275*, 1465-1468.

(89) Fitzsimons, M. P.; Barton, J. K. *J. Am. Chem. Soc.* **1997**, *119*, 3379-3380.

(90) Arounaguiri, S.; Maiya, B. G. *Inorg. Chem.* **1996**, *35*, 4267-4270.

(91) Bhattacharya, P. K.; Lawson, H. J.; Barton, J. K. *Inorg. Chem.* **2003**, *42*, 8811-8817.

(92) Boer, D. R.; Canals, A.; Coll, M. *Dalton Trans.* **2009**, *3*, 399-414.

(93) Bertrand, H.; Monchaud, D.; De Cian, A.; Guillot, R.; Mergny, J. L.; Teulade-Fichou, M., P. *Org. Biomol. Chem.* **2007**, *5*, 2555-2559.

(94) Neidle, S.; Parkinson, G. N. *Biochimie* **2008**, *90*, 1184-1196.

(95) Haq, I.; Trent, J. O.; Chowdhry, B. Z.; Jenkins, T. C. *J. Am. Chem. Soc.* **1999**, *121*, 1768-1778.

(96) Sun, D.; Thompson, B.; Caters, B. E.; Salazar, M.; Kerwin, S. M.; Trent, J. O.; Jenkins, T. C.; Neidle, S.; Hurley, L. H. *J. Med. Chem.* **1997**, *40*, 2113-2116.

(97) Wheelhouse, R. T.; Sun, D.; Han, H.; Han, F. X.; Hurley, L. H. *J. Am. Chem. Soc.* **1998**, *120*, 3261-3262.

(98) Anantha, N. V.; Azam, M.; Sheardy, R. D. *Biochemistry* **1998**, *37*, 2009-2714.

(99) Maiti, S.; Chaudhury, N. K.; Chowshury, S. *Biochem. Biophys. Res. Commun.* **2003**, *310*, 505-512.

(100) Clark, G. R.; Patrycia, D. P.; Squire, C. J.; Neidle, S. *J. Am. Chem. Soc.* **2003**, *125*, 4066-4067.

(101) Guo, Q.; Lu, M.; Marky, L. A.; Kallenbach, N. R. *biochemistry* **1992**, *31*, 2451-2455.

(102) Beschetnova, I. A.; Kaluzhny, D. M.; Livshits, M. A.; Schyolkina, A. K.; Borisova, O. F. *J. Biomol. Struc. Dyn.* **2003**, *20*, 789-799.

(103) Shchyolkina, A. K.; Ll'icheva, I. A.; Pozmogova, G. E. *Mol. Biol.* **2001**, *35*, 732-739.

(104) Shida, T.; Ikeda, N.; Sekiguchi, J. *Nuleosides and Nucleotides* **1996**, *15*, 599.

(105) White, E. W.; Tanious, F.; A., I. M.; Reszka, A. P.; Neidle, S.; Boykin, D. W.; D., W. W. *Biophys. Chem.* **2007**, *126*, 140-153.

(106) Breuzard, G.; Millot, J.-M.; Riou, J.-F.; Manfait, M. *Anal. Chem.* **2003**, *75*, 4305-4311.

(107) Sun, X.; Cao, E.; He, Y.; Qin, J. *Sci China Ser B-Chem* **1999**, *42*, 62-69.

(108) Reed, J. E.; Arnal, A. A.; Neidle, S.; Vilar, R. *J. Am. Chem. Soc.* **2006**, *128*, 5992-5993.

(109) Rajput, C.; Rutkaite, R.; Swanson, L.; Haq, I.; Thomas, J. A. *Chem. Eur. J.* **2006**, *12*, 4611.

(110) Rodger, A.; Norden, B. *Circular Dichroism and Linear Dichroism*; Oxford University Press: New York, 1997.

(111) Hiort, C.; Norden, B.; Rodger, A. *J. Am. Chem. Soc.* **1990**, *112*, 1971-1982.

(112) Norden, B.; Tjerneld, F. **1982**, *Biopolymers*, 21.

(113) Chen, L. M.; Liu, J.; Chen, J. C.; Tan, C. P.; Shi, S.; Zheng, K. C.; Ji, L. N. *J. Inorg. Biochem.* **2008**, *102*, 330-341.

(114) Ng, C. H.; Kong, K. C.; Von, S. T.; Balraj, P.; Jensen, P.; Thirthagiri, E.; Hamada, H.; Chikira, M. *Dalton Trans* **2008**, 447-454.

(115) Zhang, Q. L.; Liu, J. G.; Xu, H.; Hong, L.; Liu, J. Z.; Zhou, H.; Qu, L. H.; Ji, L. N. *Polyhedron* **2001**, *20*, 3049-3055.

(116) Maheswari, P. U.; Palaniandavar, M. *J. Inorg. Biochem.* **2004**, *98*, 219-230.

(117) Zhao, P.; Xu, L. C.; Huang, J. W.; Zheng, K. C.; Liu, J.; Yu, H. C.; Ji, L. N. *Biophys. Chem.* **2008**, *134*, 72-83.

(118) Rajendiran, V.; Murali, M.; Suresh, E.; Palaniandavar, M.; Periasamy, V. S.; Akbarsha, M. A. *Dalton Trans* **2008**, 2157-2170.

(119) Barton, J. K.; Danishefsky, A. T.; Goldberg, J. M. *J. Am. Chem. Soc.* **1984**, *106*, 2172-2176.

(120) Pyle, A. M.; Rehmann, J. P.; Meshoyrer, R.; Kumar, C. V.; Turro, N. J.; Barton, J. K. *J. Am. Chem. Soc.* **1989**, *111*, 3051-3058.

(121) Cusamano, M.; Di Pietro, M. L.; Gianetto, A.; Vainiglia, P. A. *J. Inorg. Biochem.* **2005**, *99*, 560-565.

(122) Cusamano, M.; Di Pietro, M. L.; Gianetto, A. *Inorg. Chem.* **1999**, *38*, 1754-1758.

(123) Vaidyanathan, V. G.; Nair, B. U. *Eur. J. Inorg. Chem.* **2004**, 1840-1846.

(124) Murali, S.; Sastri, C. V.; Maiya, B. G. *Proc. Indian Acad. Sci. (Chem. Sci.)* **2002**, *114*, 403.

(125) Sastri, C. V.; Easwaramoorthy, D.; Girbabu, L.; Maiya, B. G. *J. Inorg. Biochem.* **2003**, *94*, 138-145.

(126) Scatchard, G.; Ann, N. Y. *Acad. Sci.* **1949**, *51*, 660.

(127) McGee, J. D.; von Hipple, P. H. *J. Mol. Biol.* **1974**, *86*, 469-489.

(128) Norden, B.; Tjerneld, F. *Biophys. Chem.* **1976**, *4*, 191-198.

(129) Rodger, A. *Methods Enzymol* **1992**, *226*, 232-258.

(130) Kumar, C. V.; Asuncion, E. H. *J. Am. Chem. Soc.* **1993**, *115*, 8547-8553.

(131) Stoutman, F. H.; Fisher, D. M.; Rodger, A.; Aldrich-Wright, J. R. *The Analyst* **2006**, *131*, 1145-1151.

(132) Benesi, H. A.; Hildebrand, J. H. *J. Am. Chem. Soc.* **1949**, *71*, 2703-2707.

(133) Wolfe, A.; Shimer, G. H.; Meehan, T. *Biochemistry* **1987**, *26*, 6392-6396.

(134) Chen, H.; Parkinson, J. A.; Novakova, O.; Bella, J.; Wang, F.; Dawson, A.; Gould, R.; Parsons, S.; Brabec, V.; Sadler, P. J. *proc. Natl. Acad. Sci. U. S. A.* **2003**, *100*, 14623-14628.

(135) Keck, M. V.; Lippard, S. J. *J. Am. Chem. Soc.* **1992**, *114*, 3386-3390.

(136) Rosu, F.; E., D. P.; Gabelica, V. *Biochimie* **2008**, 1-14.

(137) Hofstadler, S. A.; Griffey, R. H. *Chem. Rev.* **2001**, *101*, 377-390.

(138) Loo, J. A. *Mass Spectrom Rev* **1997**, *16*, 1-23.

(139) Beck, J. L.; Colgrave, M. L.; Ralph, S. F.; Sheil, M. M. *Mass Spectrom Rev* **2001**, *20*, 61-87.

(140) Smyth, W. F. *Trends Anal Chem* **1999**, *18*, 335-345.

(141) Nordhoff, E.; Kirpekar, F.; Roepstorff, P. *Mass Spectrom Rev* **1998**, *15*, 67-138.

(142) Dempster, A. J. *Phys. Rev.* **1921**, *18*, 415-422.

(143) Munson, M. S. B.; Field, F. H. *J. Am. Chem. Soc.* **1966**, *88*, 2621-2630.

(144) Beckey, H. D. *Int. J. Mass. Spec.* **1969**, *1969*, 500-503.

(145) Hsu, C. S.; Green, M. *Rapid commun mass sp* **2001**, *15*, 236-239.

(146) Torgerson, D. F.; Skowronski, R. P.; Macfarlane, R. D. *Biochem. Biophys. Res. Commun.* **1974**, *60*, 616-621.

(147) Barber, M.; Bordoli, R. S.; Sedgwick, R. D.; Tyler, A. N.; Bycroft, B. W. *Biochem. Biophys. Res. Commun.* **1981**, *101*, 632-638.

(148) Tanaka, K.; Waki, H.; Ido, Y.; Akita, S.; Yoshida, Y.; Yohida, T. *Rapid commun mass sp* **1981**, *2*, 151-153.

(149) Karas, M.; Hillenkamp, F. *Anal. Chem.* **1988**, *60*, 2299-2301.

(150) Yamashita, M.; Fenn, J. B. *J. phys. chem.* **1984**, *88*, 4451-4459.

(151) Yamashita, M.; Fenn, J. B. *J. phys. chem.* **1984**, *88*, 4671-4675.

(152) http://www.chm.bris.ac.uk/ms/theory/esi-ionisation.html.

(153) Iribarne, J. V.; Thomson, B. A. *J chem phys* **1976**, *64*, 2287-2294.

(154) Thomson, B. A.; Iribarne, J. V. *J chem phys* **1979**, *64*, 2287-2294.

(155) Mann, M.; Fenn, J. B. *Mass spectrometry clinical and biomedical applications*; Plenum Press: New York, 1992.

(156) Ganem, B. *Tetrahedron Lett.* **1993**, *34*, 1445-1448.

(157) Light-Wahl, K. J.; Springer, D. L.; Winger, B. E.; Edmonds, C. G.; Camp, I., D. G.; Thrall, B. D.; Smith, R. D. *J. Am. Chem. Soc.* **1993**, *115*, 803-804.

(158) Gale, D. C.; Goodlett, D. R.; Light-Wahl, K. J.; D., S. R. *j. Am. Chem. Soc.* **1994**, *116*, 6027-6028.

(159) Rosu, F.; Gabelica, V.; Houssier, C.; De Pauw, E. *Nucleic Acids Res.* **2002**, *30*, e82.

(160) Wan, K. X.; Shibue, T.; Gross, M. L. *J. Am. Chem. Soc.* **2000**, *122*, 300-307.

(161) Kapur, A.; Beck, J. L.; Sheil, M. M. *Rapid commun mass sp* **1999**, *13*, 2489-2497.

(162) Reyzer, M. L.; Brodbelt, J. S.; Kerwin, S. M.; Kumar, D. *Nucleic Acids Res.* **2001**, *29*, e103.

(163) Sherman, S. E.; Gibson, D.; Wang, A. H. J.; Lippard, S. J. *J. Am. Chem. Soc.* **1988**, *110*, 7368-7381.

(164) Gale, D. C.; Smith, R. D. *J Am Mass Spectrom* **1995**, *6*, 1154-1164.

(165) Gabelica, V.; De Pauw, E.; Rosu, F. *J Mass Spectrom* **1999**, *34*, 1328.

(166) Beck, J. L.; Gupta, R.; Urathamakul, T.; Williamson, N. L.; Sheil, M. M.; Aldrich-Wright, J. R.; Ralph, S. F. *Chem. Commun.* **2003**, 626-627.

(167) Rosu, F.; Gabelica, V.; Houssier, C.; Colson, P.; De Pauw, E. *Rapid commun mass sp* **2002**, *16*, 1729-1736.

(168) Vairamani, M.; Gross, M. L. *J. Am. Chem. Soc.* **2002**, *125*, 42-43.

(169) David, W. M.; Brodbelt, J. S.; Kerwin, S. M.; Thomas, P. W. *Anal. Chem.* **2002**, *74*, 2029-2033.

(170) Talib, J.; Green, C.; Davis, K. J.; Urathamakul, T.; Beck, J. L.; Aldrich-Wright, J. R.; Ralph, S. F. *Dalton Trans* **2008**, 1018-1026.

(171) Gornall, K. C.; Samosorn, S.; Talib, J.; Bremner, J. B.; Beck, J. L. *Rapid commun mass spectrom* **2007**, *21*, 1759-1766.

(172) Pandolfi, P. P. *Oncogene* **2001**, *20*, 3116-3127.

(173) Schwarz, E.; Firestein, G. S. *Q. rev. biol* **2000**, *75*, 310-311.

(174) Dittmer, J.; Nordheim, A. *Biochim. biophys. acta* **1998**, *1377*, F1- F11.

(175) Redell, M. S.; Tweardy, D. J. *Drug discovery today. Technologies* **2006**, *3*, 261-267.

(176) http://www.phschool.com/science/biology_place/biocoach/transcription/tctlpreu.html.

(177) Karin, M. *Nature* **2006**, *441*, 431-436.

(178) Huang, Y.-T.; Pan, S.-L.; Guh, J.-H.; Chang, Y.-L.; Lee, F.-Y.; Kuo, S.-C.; Teng, C.-M. *Mol. Cancer Ther* **2005**, *4*, 1628-1635.

(179) Mutsumoto, G.; Namekawa, J.; Mariko, M.; Nakamura, T.; Tohyama, K.; Toi, M.; Umezawa, K. *Clin. Cancer Res.* **2005**, *11*, 1287-1293.

(180) Olsen, L. S.; Vig Hjarnaa, P.-J.; Latini, S.; Holm, P. K.; Larsson, R.; Bramm, E.; Binderup, L.; Madsen, M. W. *Int. J. Cancer* **2004**, *111*, 198-205.

(181) Zirong, L.; Van Calcar, S.; Chunxu, Q.; Cavenee, W. K.; Zhang, M. Q.; Bing, R. *Proc. Natl. Acad. Sci. U. S. A.* **2003**, *100*, 8164-8169.

(182) Rothberg, P. G.; Erisman, M. D.; Diehl, R. E.; Rovigatti, U. G.; Astrin, S. M. *Mol Cell Biol.* **1984**, *4*, 1096-11031096.

(183) Inversen, P. L.; Arora, V.; Acker, A. J.; Mason, D. H.; Devi, G. R. *Clin. Cancer Res.* **2003**, *9*, 2510-2519.

(184) Leonetti, C.; Biroccio, A.; Benassi, B.; Stringaro, A. *Cancer Gene Ther.* **2001**, *9*, 4595.

(185) Pastorino, F.; Brignole, C.; Marimpietri, D.; Pagnan, G.; Morando, A.; Ribatti, D.; Semple, S. C.; Gambini, C.; Allen, T. M.; Pozoni, M. *Clin. Cancer Res.* **2003**, *9*, 4595-4605.

(186) O'Donnell, K. A.; Wentzel, E. A.; Zeller, K. I.; Dang, C. V.; Mendell, J. T. *Nature* **2005**, *435*, 839-843.

(187) Scott, E. W.; Simon, M. C.; Anastasi, J.; Singh, H. *Science* **1994**, *265*, 1573-1577.

(188) Sharrocks, A. D. *Nat. Rev.* **2001**, *2*, 827-837.

(189) Barton, B. E.; Murphy, T. F.; Shu, P.; Huang, H. F.; Meyenhofen, M.; Barton, A. *Mol. Cancer Ther* **2004**, *3*, 1183-1191.

(190) Kortylewski, M.; Kujawski, M.; Wang, T.; Wei, S.; Zhang, S.; Pilon-Thomas, S.; Niu, G.; Kay, H.; Mule, J.; Kerr, W. G.; Jove, R.; Pardoll, D.; Yu, H. *Nat. Med.* **2005**, *11*, 1314.

(191) Blaskovich, M. A.; Sun, J.; Cantor, A.; Turkson, J.; Jove, R.; Sebti, S. M. *Cancer Res.* **2003**, *63*, 1270-1279.

(192) Dery, M. A.; Michaud, M. D.; Richard, D. E. *Int J Biochem Cell Biol* **2005**, *37*, 535-540.

(193) Grimshaw, M. J. *Endocr Relat Cancer* **2007**, *14*, 233-244.

(194) Bryden, A. A. G.; Hoyland, J. A.; Freemont, N. W.; Clarke, N. W.; Schembri Wismayer, D.; George, N. J. R. *Brit J Urol* **2002**, *89*, 400-403.

(195) Levine, A. J. *Cell* **1997**, *88*, 323-331.

(196) Wang, N. P.; To, H.; Lee, W. H.; Lee, E. Y. *Oncogene* **1993**, *8*, 279-288.

(197) Hollstein, M.; Sidransky, D.; Vogelstein, B.; Harris, C. C. *Proc. Natl. Acad. Sci. U. S. A.* **1990**, *87*, 9958-9961.

(198) Hollstein, M.; Metcalf, R. A.; Welsh, J. A.; Montesano, R.; Harris, C. C. *Proc. Natl. Acad. Sci. U. S. A.* **1990**, *87*, 9958-9961.

(199) Baker, S. J.; Fearon, E. R.; Nigro, J. M.; Hamilton, S. R.; Preisinger, A. C.; Jessup, J. M.; vanTuinen, P.; Ledbetter, D. H.; Barker, D. F.; Nakamura, Y.; White, R.; Vogelstein, B. *Science* **1989**, *244*, 217-221.

(200) Takahashi, T.; Nau, M. M.; Chiba, I.; Birrer, M. J.; Rosenberg, R. K.; Vinocour, M.; Levitt, M.; Pass, H.; Gazdar, A. F.; Minna, J. D. *Science* **1989**, *246*, 491-494.

(201) Mulligan, L. M.; Matlashewski, G. J.; Scrable, H. J.; Cavenee, W. K. *Proc. Natl. Acad. Sci. U. S. A.* **1990**, *87*, 5863-5867.

(202) Watanabe, T.; Hotta, T.; Ichikawa, A.; Kinoshita, T.; Nagai, H.; Uchida, T.; Murate, T.; Saito, H. *Blood* **1994**, *84*, 3158-3165.

(203) Vogt, P. K. *Oncogene* **2001**, *20*, 2365-2377.

(204) Xiao, L.; Lang, W. *Cancer Res.* **2000**, *60*, 400-408.

(205) Raitano, A. B.; Halpern, J. R.; Hambuch, T. M.; Sawyers, C. L. *Proc. Natl. Acad. Sci. U. S. A.* **1995**, *92*, 11746-11750.

(206) Dalla-Fevera, R.; Bregni, M.; Erikson, J.; Patterson, D.; Gallo, R. C.; Croce, C. M. *Proc. Natl. Acad. Sci. U. S. A.* **1982**, *79*, 7824-7827.

(207) Malempati, S.; Tibbitts, d.; Cunnigham, M.; Akkari, Y.; Olson, S.; Fan, G.; Sears, R. C. *Leukemia* **2006**, *20*, 1572-1581.

(208) Liao, D. J.; Dickson, R. B. *Endor. Relat. Cancer* **2000**, *7*, 143-164.

(209) Harbour, J. W.; Dean, D. C. *Genes Dev.* **2000**, *14*, 2393-2409.

(210) Friend, S. H.; Bernards, R.; Rogeli, S.; Weinberg, R. A.; Rapaport, J. M.; Albert, D. M.; Dryja, T. P. *Nature* **1986**, *323*, 643-646.

(211) Nevins, J. R. *Human. Mol. Genet.* **2001**, *10*, 699-703.

(212) Kodandapani, R.; Pio, F.; Ni, C. Z.; Piccialli, G.; Klemsz, M.; McKercher, S.; Maki, R. A.; Ely, K. R. *Nature* **1996**, *830*, 456-460.

(213) Poon, G. M. K.; Macgregor, R. B. *J. Mol. Biol.* **2003**, *328*, 805-819.

(214) Poon, G. M. K.; Gross, M. L.; Macgregor, R. B. *Biochemistry* **2002**, *41*, 2361-2371.

(215) Poon, G. M. K.; Macgregor, R. B. *J. Mol. Biol.* **2004**, *335*, 113-127.

(216) Gupta, P.; Guradutta, G. U.; K., V. Y.; Kishore, V.; S., G.; K., S. R.; Chandra, R.; Saluja, D. *Stem Cells and Dev.* **2006**, *15*, 609-617.

(217) Mueller, B. U.; Pabst, T.; Osato, M.; Asou, N.; Johansen, L. M.; Minden, M. D.; Behre, G.; Hiddemann, W.; Ito, Y.; Tenen, D. G. *Blood* **2008**, *100*, 998-1007.

(218) Rao, G.; Rekhtman, N.; Cheng, G.; Krasikov, T.; Skoultchi, A. I. *Oncogene* **1997**, *14*, 123-131.

(219) Darnell, J. E. *Nat. Rev.* **2002**, *2*, 740-749.

(220) Gniazdowski, M.; Denny, W. A.; Nelson, S. M.; Czyz, M. *Curr. Med. Chem.* **2003**, *10*, 909-924.

(221) Welch, J. J.; Rauscher, I. F. J.; Beerman, T. A. *J. Biol. Chem.* **1994**, *269*, 31051.

(222) Essigmann, J. M.; Rink, S. M.; Park, H.-J.; Croy, R. G. In *Biological Reactive Intermediates VI: Chemical and Biological Mechanisms in Susceptibility to and Prevention of Environmental Diseases*; Dansette, P. M., Ed.; Springer: New York, 2001.

(223) Wemmer, D. E.; Dervan, P. B. *Curr. Opinion. Struct. Biol.* **1997**, *7*, 355-361.

(224) Gottesfeld, J. M.; Neely, L.; Trauger, J. W.; Baird, E. E.; Dervan, P. B. *Nature* **1997**, *387*, 282.

(225) Nicholas, G.; Dervan, P. B. *Proc. Natl. Acad. Sci. U. S. A.* **2007**, *104*, 10418-10423.

(226) Holmlin, R. E.; Stemp, E. D. A.; Barton, J. K. *Inorg. Chem.* **1998**, *37*, 29-34.

(227) Dupureur, C. M.; Barton, J. K. *J. Am. Chem. Soc.* **1994**, *116*, 10286-10287.

(228) Xiong, X.-O.; Liang, F.; Yang, L.; Wang, X.-L.; Zhou, X.; Zheng, C.-Y.; Cao, X.-P. *Chem. Biodiversity* **2007**, *4*, 2791-2797.

(229) Fu, P. K.-L.; Bradley, P. M.; Turro, C. *Inorg. Chem.* **2003**, *42*, 878-884.

(230) Sorasaenee, K.; Fu, P. K.-L.; Angeles-Boza, A. M.; Dunbar, K. R.; Turro, C. *Inorg. Chem.* **2003**, *42*, 1267-1271.

(231) Fu, P. K.-L.; Turro, C. *Chem. Commun.* **2001**, 279-280.

(232) Campisi, D.; Morii, T.; Barton, J. K. *Biochemistry* **1994**, *33*, 4130-4139.

(233) Gupta, R.; Beck, J. L.; Ralph, S. F.; Sheil, M. M. *J Am Soc Mass Spectrom* **2004**, *15*, 1382-1391.

(234) Urathamakul, T.; Waller, D. J.; Beck, J. L.; Aldrich-Wright, J. R.; Ralph, S. F. *Inorg. Chem.* **2008**.

(235) Dupureur, C. M.; Barton, J. K. *Inorg. Chem.* **1997**, *36*, 33-43.

(236) Collins, J. G.; Sleeman, A. D.; Aldrich-Wright, J. R.; Hambley, T. W. *Inorg. Chem.* **1998**, *37*, 3133-3141.

(237) Liu, H.; Liu, L.; Zhong, B. *Anal. Sci.* **2004**, *20*, x63-x64.

(238) Wickham, G.; Iannitti, P.; Boschenok, J.; Sheil, M. M. *J. Mass Spectrom.* **1995**, *30*.

(239) http://www.basic.northwestern.edu/biotools/oligocalc.html.

(240) Liew, C. W.; Rand, K. D.; Simpson, R. J. Y.; Yung, W. Y.; Mansfield, R. E.; Crossley, M.; Proetorius-Ibba, M.; Nerlov, C.; Poulson, F. M.; Mackay, J. P. *J. Biol. Chem.* **2006**, *281*, 28296-28306.

(241) http://ca.expasy.org/cgi-bin/proparam.

(242) Ramakrishnan, S.; Palanianadavar, M. *Dalton Trans* **2008**, 3866-3878.

(243) Jackson, B. A.; Barton, J. K. *J. Am. Chem. Soc.* **1997**, *119*, 12986-12987.

(244) Harris, C. M.; McKenzie, E. D. *J. Inorg. Nucl. Chem.* **1967**, *29*, 1047-1068.

(245) Hard, T.; Norden, B. *Biopolymers* **1986**, *25*, 1209-1228.

(246) Coggan, D. Z. M.; Howarth, I. S.; Bates, P. J.; Robinson, A.; Rodger, A. *Inorg. Chem.* **1999**, *38*, 4486-4497.

(247) Patel, K. K.; Plummer, E. A.; Darwish, M.; Rodger, A.; Hannon, M. J. *J. Inorg. Biochem.* **2002**, *91*, 220-229.

(248) Mudasir, K. W.; Tjahjono, D. H.; Yoshioka, N.; Inoue, H. *Z. Naturforsch* **2004**, *59b*, 310-318.

(249) Meehan, T.; Gamper, H.; Becker, J. F. *Biochemistry* **1982**, *257*, 10479-10485.

(250) Vaidyanathan, V. G.; Nair, B. U. *J. Inorg. Biochem.* **2003**, *95*, 334-342.

(251) Mudasir, K. W.; Wijaya, N.; Wahyuni, H.; Yoshioka, N.; Inoue, H. *Spectrochim. Acta.* **2007**, *66*, 163-170.

(252) Mudasir, K. W.; N., W.; Yoshioka, N.; Inoue, H. *J. Inorg. Biochem.* **2003**, *94*, 263-271.

(253) Liu, J.; Mei, W. J.; Lin, K. C.; Zeng, K. C.; Chao, H.; Yun, F. C.; Ji, L. N. *Inorg Chim Acta* **2004**, *357*, 285-290.

(254) Nakabayashi, Y.; Watanabe, T.; Nakao, T.; Yamauchi, O. *Inorg. Biochem.* **2004**, *98*, 2553-2560.

(255) Wang, X.-L.; Chao, H.; Li, H.; Hong, X.-L.; Liu, Y.-J.; Tan, L.-F.; Ji, L.-N. *J. Inorg. Biochem.* **2004**, *98*, 1143-1150.

(256) Mahadevan, S.; Palanianadavar, M. *Inorg. Chem.* **1998**, *37*, 693-700.

(257) Lippard, S. J.; Bond, P. J.; Wu, K. C.; Bauer, W. R. *Science* **1976**, *194*, 726-728.

(258) Pellegrini, P.; Aldrich-Wright, J. R. *Dalton Trans* **2003**, 176-183.

(259) Yam, V. W.-W.; Lo, K.-K.; Cheung, K.-K.; Kong, R. Y.-C. *J. Chem. Soc., Dalton Trans.,* **1997**, 2067-2072.

(260) Maheswari, P. U.; Palanianadavar, M. *Inorg Chim Acta* **2004**, *357*, 901-912.

(261) Ghosh, S.; Barve, A. C.; Kumbhar, A. A.; Kumbar, A. S.; Puranik, V. G.; Datar, P. A.; Sonawane, U. B.; Joshi, R. R. *J. Inorg. Biochem.* **2006**, *100*, 331-343.

(262) Breu, J.; Stoll, A. J. *Acta Cryst. C* **1996**, *52*, 1174-1177.

(263) Maheswari, P. U.; Rajendiran, V.; Palaniandavar, M.; Thomas, R.; Kulkarni, G. U. *Inorg Chim Acta* **2006**, *359*, 4601-4612.

(264) Suescun, L.; Mombrú, A. W.; Mariezcurrena, R. A. *Acta Cryst. C* **1999**, *55*, 1991-1993.

(265) Abdel-Rahman, L.; Battaglia, L. P.; Rizzoli, C.; Sgarabotto, P. *J. Chem. Crystallog.* **1995**, *25*, 629-632.

(266) Lincoln, P.; Tuite, E.; Norden, B. *Short-Circuiting the Molecular Wire: Cooperative Binding of -[Ru(phen)2dppz]2+ and -[Rh(phi)2bipy]3+ to DNA*, *119*, 1454-1455.

(267) Lincoln, P.; Tuite, E.; Norden, B. *J. Am. Chem. Soc.* **1997**, *119*, 1454-1455.

(268) Siegal, M. M. *Curr. Top. Med. Chem.* **2002**, *2*, 13-33.

(269) Franceschin, M.; Rosetti, L.; D' Ambrosio, A.; Schirripa, S.; Bianco, A.; Ortaggi, G.; Savino, M.; Schultes, C.; Neidle, S. *Bioorg. Med. Chem. Lett.* **2006**, *16*, 1707-1711.

(270) Moore, M. J. B.; Cuenca, F.; Searcey, M.; Neidle, S. *Org. Biomol. Chem.* **2006**, *4*, 3479-3488.

(271) Mazzitelli, C. L.; Wang, J.; Smith, S. I.; Brodbelt, J. S. *J Am Soc Mass Spectrom* **2007**, *18*, 1760-1773.

(272) Pan, S.; Sun, X. J.; Lee, J. K. *J. Mass Spectrom.* **2006**, *253*, 238-248.

(273) Gabelica, V.; Rosu, F.; Witt, M.; Baykut, G.; De Pauw, E. *Rapid commun mass sp* **2005**, *19*, 201-208.

(274) Gabelica, V.; De Pauw, E. *Int. J. Mass. Spec.* **2002**, *219*, 151-159.

(275) Gabelica, V.; De Pauw, E. *J. Mass Spectrom.* **2001**, *36*, 397-402.

(276) Wan, K. X.; Gross, M. L.; Shibue, T. *J Am Soc Mass Spectrom* **2000**, *11*, 450-457.

(277) Ni, J.; Mathews, M. A.; McCloskey, J. A. *Rapid Commun. Mass Spectrom* **1997**, *11*, 535.

(278) Rodgers, M. T.; Campbell, S.; Marzluff, E. M.; Beauchamp, J. L. *Int. J. Mass. Spectrom. Ion Process* **1995**, *148*, 1.

(279) Weimann, A.; Iannitti-Tito, P.; Sheil, M. M. *Int. J. Mass. Spec.* **2000**, *194*, 269-288.

(280) Keniry, M. A. *Biopoly (Nucleic Acid Sci)* **2001**, *56*, 123-146.

(281) Maestre, M. F.; Wang, J. C. *Biopolymers* **1971**, *10*, 1021-1030.

(282) Pashynska, V. A.; Kosevich, M. V.; Van den Heuvel, H.; Claeys, M. *Rapid commun mass sp* **2006**, *20*, 755-763.

(283) Mouchaud, D.; Teulade-Fichou, M.-P. *Org. Biomol. Chem.* **2008**, *6*, 627-636.

(284) Teixeira, S. C.; Thorpe, J. H.; Todd, A. K.; Powell, H. R.; Adams, A.; Wakelin, L. P. G.; Denny, W. A.; Cardin, C. J. *J. Mol. Biol.* **2002**, *323*, 167-171.

(285) Parkinson, G. N.; Ghosh, R.; Neidle, S. *Biochemistry* **2007**, *46*, 2390-2397.

(286) Mita, H.; Ohyama, T.; Tanaka, Y.; Yamamoto, Y. *Biochemistry* **2006**, *43*, 6765-6772.

(287) Wei, C.; Jia, G.; Yuan, J.; Feng, Z.; Li, C. *Biochemistry* **2006**, *45*, 6681-6691.

(288) Han, H.; Langely, D. R.; Rangan, A.; Hurley, L. H. *J. Am. Chem. Soc.* **2001**, *123*, 8902-8913.

(289) Brodie, C.; Collins, G. J.; Aldrich-Wright, J. R. *Dalton Trans* **2004**, 1145-1152.

(290) McFadyen, W. D.; Wakelin, L. P. G.; Roos, I. A. G.; Leopold, V. A. *J. Med. Chem.* **1985**, *28*, 1113-1116.

(291) Giraldo, R.; Suzuki, M.; Chapman, L.; Rhodes, D. *Proc. Natl. Acad. Sci. U. S. A.* **1994**, *91*, 7658-7662.

(292) Paramasivan, S.; Rajun, I.; Bolton, P. H. *Methods* **2007**, *43*, 324-331.

(293) Yamashita, T.; Uno, T.; Ishikawa, Y. *Bioorg. med. chem* **2005**, *13*, 2423-2430.

(294) Ishikawa, Y.; Yamashita, T.; Tomisugi, Y.; Uno, T. *Nucleic Acids Res.* **2001**.

(295) Jennette, K. W.; Gill, J. T.; Sadownick, J. A.; Lippard, S. J. *J. Am. Chem. Soc.* **1976**, *98*, 6159.

(296) Howe-Grant, M.; Wu, K. C.; Bauer, W. R.; Lippard, S. J. *Biochemistry* **1976**, *15*, 4339.

(297) Norden, B. *Inorg. Chim. Acta* **1978**, *31*, 83.

(298) Lippard, S. J. *Acc. Chem. Res.* **1978**, *11*, 211.

(299) Kilkulskie, R.; Wood, N.; Ringquist, S.; Shinn, R.; Hanlon, S. *Biochemistry* **1988**, *27*, 4377.

(300) Johnson, B. B.; Dahl, K. S.; Tinoco, I. J.; Ivanov, V., I.; Zhurkin, V. B. *Biochemistry* **1981**, *20*, 73.

(301) Sheardy, R. D.; Suh, D.; Kurzinsky, R.; Doktycz, M. J.; Benight, A. S.; Chaires, J. B. *J. Mol. Biol.* **1993**, *231*, 475.

(302) Broggini, M.; Ponti, M.; Ottolenghi, S.; D'Incalci, M.; Moongelli, N.; Mantovani, R. *Nucleic Acids Res.* **1989**, *17*, 1051.

(303) Ray, R.; Snyder, R. C.; Thomas, S.; Koller, C. A.; Miller, D. M. *J. Clin. Invest.* **1989**, *83*, 2003.

(304) Hensley, P. *Structure* **1996**, *4*, 367-373.

(305) Szabo, A.; Stolz, L.; Granzow, R. *Curr. Opin. Struct. Biol.* **1995**, *5*, 699-705.

(306) Burgess, J. K. *Clin. Exp. Pharmacol. Physiol.* **2001**, *28*, 321.

(307) Kapur, A.; Beck, J. L.; Brown, S. E.; Dixon, N. E.; Sheil, M. M. *Protein Science* **2002**, *11*, 147-157.

(308) Askashi, S.; Osawa, R.; Nishimura, Y. *2005* **2004**, *16*, 116-125.

(309) Cheng, X.; Morin, P. E.; C., H. A.; Bruce, J. E.; Ben-David, Y.; Smith, R. D. *Anal. Biochem.* **1996**, *239*, 35-40.

(310) Szymczyna, B. R.; Arrowsmith, C. H. *J. Mol. Biol.* **2000**, *275*, 28363-28370.

(311) Eisenbeis, C. F.; Singh, H.; Storb, U. *Mol. Cell. Biol.* **1993**, *13*, 6452-6461.

(312) Gupta, R.; Kapur, A.; Beck, J. L.; Sheil, M. M. *Rapid commun mass spectrom* **2001**, *15*, 2472-2480.

(313) Veenstra, T. D.; Johnson, K. L.; Tomlinson, A. J.; Craig, T. A.; Kumar, R.; Naylor, S. *J Am Soc Mass Spectrom* **1998**, *9*, 8-14.

(314) Xu, N.; Pasa-Tollic, L.; D., S. R.; Ni, S.; Thrall, B. D. *Anal. Biochem.* **1999**, *272*, 26-33.

(315) Akashi, S.; Osawa, R.; Nishimura, Y. *J Am Soc Mass Spectrom* **2004**, *16*, 113-125.

(316) Sperry, J. B.; Wilcox, J. M.; Gross, M. L. *J Am Soc Mass Spectrom* **2008**, *19*, 887-890.

(317) Jia, X.; Lee, L. K.; Light, J.; Palmer, A. G.; Assa-Munt, N. *J. Mol. Biol.* **1999**, *292*, 1093-1093.

(318) Rosu, F.; Pirotte, S.; D., P. E.; Gabelica, V. *Int. J. Mass. Spec.* **2006**, *253* 153-171.